IGNEOUS ROCKS AND STRUCTURES OF THE NIXON FORK MINE, ALASKA, AND THEIR RELATIONS TO ORES

By

Brian Perttu

RECOMMENDED:

Dr. Wesley K. Wallace

Dr. Paul W. Layer

Dr. Rainer J. Newberry
Advisory Committee Chair

Dr. Paul J. McCarthy
Chair, Department of Geology and Geophysics

APPROVED:

Dr. Paul W. Layer
Dean, College of Natural Science and Mathematics

Dr. John C. Eichelberger
Dean of the Graduate School

16 December 2013
Date

IGNEOUS ROCKS AND STRUCTURES OF THE NIXON FORK MINE, ALASKA, AND THEIR RELATIONS TO ORES

A

THESIS

Presented to the Faculty

of the University of Alaska Fairbanks

in Partial Fulllment of the Requirements

for the Degree of

MASTER OF SCIENCE

By

Brian Perttu, B.S.

Fairbanks, Alaska

December 2013

Abstract

The Nixon Fork Mine is a high-grade Cu-Au skarn deposit located near the western contact of the 5 square km Late Cretaceous Mystery pluton with marble, 7 km southeast of the Iditarod-Nixon Fork (I-NF) fault. This fault strikes at ~060°, and can be traced for ~400 km, with a minimum dextral displacement of ~90 km. Close proximity suggests that the Nixon Fork deposit should have been affected by the I-NF fault. In order to assess the structural evolution, I analyzed the orientations of geologic structures. I transcribed 1172 structures from previous mapping (to assess structures) and converted 186 maps into Vulcan CAD software (to create a three-dimensional model). I also acquired $^{40}Ar/^{39}Ar$ dates for eleven representative potassium-bearing minerals and rocks. I identified six different episodes of deformation, including intrusion of felsic dikes, intrusion of mafic dikes, two episodes likely related to the I-NF fault, and two other poorly constrained episodes. $^{40}Ar/^{39}Ar$ dates show the skarn is significantly younger than the Mystery Creek pluton, indicating it was likely sourced from an unexposed pluton. The main skarn pipe can be approximated as a line oriented ~ 210°/65°, which is approximately the intersection of planes defined by felsic dikes and major veins.

Table of Contents

Page

List of Figures

Page

List of Tables

Page

Acknowledgements

First, this project wouldn't have existed without the support of Pacific Northwest Capital Corporation, now Fire River Gold. Toward the end of my first year Greg Myers (then VP of Business Development) not only offered me employment for the following summer, but also funds for XRF, thin sections and geochronology, as well as access to their previous files and databases. I had no idea how vital those files would be.

For help throughout, but especially toward the end: Rainer Newberry, Paul Layer and Wes Wallace.

Rainer arranged everything. Rainer got me a field area and outlined a project. Rainer is one of the best and most dedicated instructors I've ever had, and moreover, such is his geologic insight that I suspect he knew my conclusions before I knew my project.

Paul helped with the geochronology, which was invaluable, but I am equally thankful that he was always open for a chat at the pub which kept the stress level low.

Wes (kiitoksia) took a lot of time to help me sort out my structural problems, and I am quite thankful that he provided me with so many thorough and deeply considered explanations.

Before I went out to Nixon Fork I received advice from Lawrence Freeman and David Szumigala on the peculiar nature of the skarn and intrusive rocks at the site, which was

helpful in preventing complete confusion when confronted with the on-site geology for the first time.

During my stint at the mine I ended up spending most of my spare time with Ted Howard, the camp cook, whom I credit with keeping me sane. He remains affable and larger than life. He also makes a damn fine shepherd's pie.

Upon my return I had to start working with samples. I am grateful to Jeff Benowitz, who helped me with sample preparation, mineral picking, and providing me with copies of my geochronology data. Similarly, Ken Severin was enormously helpful whenever my samples took me into the domain of the Advanced Instrumentation Lab (which was often). And thank you, Mary Keskinen, because you can never have the advice of too many petrologists.

And Anna. She is my guide and motivator. She is the force that surrounds and binds this all together.

Thank you.

1 Introduction

1.1 The Nixon Fork skarn

A skarn is a mineral deposit identified by a coarse grained, generally iron-rich mixture of ores and Ca-Mg-Fe-Al silicates, formed from carbonate rocks by metasomatic processes at relatively high temperatures (Einaudi and Burt, 1982). In the case of the Nixon Fork skarn, past workers have assumed that the metasomatic fluids were derived from the nearby Mystery pluton (e.g. Martin, 1922; Cutler, 1994; Power and others, 2003).

The Nixon Fork deposit is a high-grade Cu-Au skarn located in west-central Alaska (**Figure 1.1**). It is one of a few economically significant lode occurrences in the region (Szumigala, 1996). It has been intermittently mined since 1920, most recently from 1995 to 2007 and 2011 to 2013. The attraction of Nixon Fork is the very high Au and Cu grades. The unattractive features are the remote location (**Figure 1.1**) and the irregular distribution of ore bodies.

Nixon Fork is located in an area never glaciated (Hamilton, 1994), hence, extremely weathered. Surface exposures are poor and historic production (approximately 42,000 oz Au, 11,282 oz Ag, and 41,440 lbs. Cu) was from highly oxidized material. Historic production (1920-1961) focused on very high grade Fe- and Cu-oxide material, with average head grades of 1.5 opt (ounces per ton) Au, 3.0 opt Ag, and 2% Cu (Wallis and others, 2003; Freeman and Giroux, 2012).

Ultimately, the size, shape, and distribution of ores are related to host-rock types and the structural features of the rocks—both to older faults that controlled hydrothermal fluid flow and to younger faults that displaced ore bodies. However, due to the extensive weathering present in west-central Alaska, the surface exposures are poor and weathering to more than 300 m below the surface makes rock identification difficult.

Consequently, although the Nixon Fork skarn has been studied by previous workers (e.g., Cutler, 1994; Burnett and Grady, 2005), the geology—the timing and character of the structures and rock units present—remains poorly understood. In this thesis, I re-examine the published geologic data from Nixon Fork and integrate that with new petrographic, geochemical, geochronologic and structural data to construct a model of the origin and distribution of the Nixon Fork deposit.

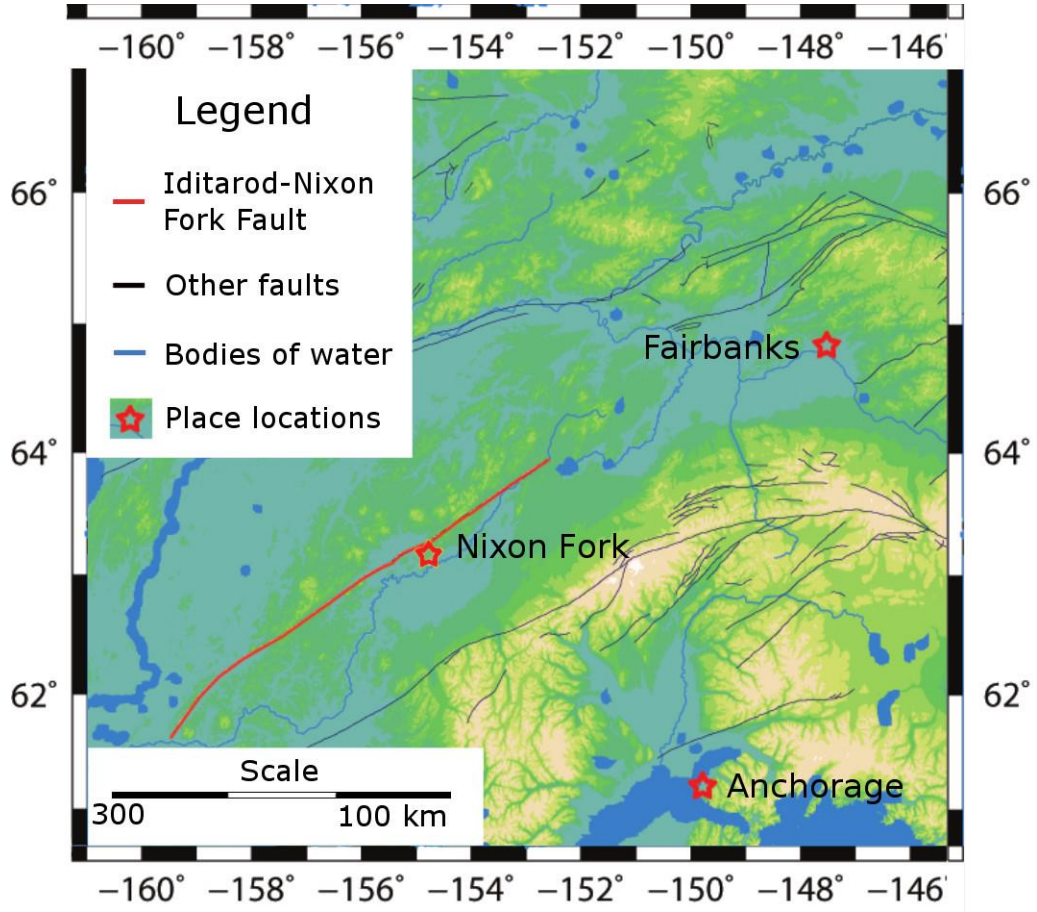

Figure 1.1 The Nixon Fork deposit's location in west-central Alaska is within five km of the Iditarod-Nixon Fork fault.

1.2 Geologic setting

1.2.1 Regional Geology

The Nixon Fork deposit is situated in Proterozoic through Lower Cretaceous rocks of the Nixon Fork terrane (Patton and others, 1994; Silberling and others, 1994). The Nixon Fork terrane, along with Dillinger terrane and Mystic terrane (Decker and others, 1994), are part of the Farewell composite terrane (specifically the Nixon Fork subterrane (Bundtzen and Miller, 1997; Blodgett, 1998)). Paleozoic rocks are predominantly shallow

marine platform facies (Decker and others, 1994) likely originally from Siberia (Blodgett, 1998).

Paleomagnetic studies suggest the Farewell terrane became part of Alaska before the middle Cretaceous (Coe and others, 1985), forming part of the basement for the Kuskokwim basin (Decker and others, 1994; Nokleberg and others, 1994; Patton and others, 1994). The basin was filled in mid-to-Late Cretaceous time with a thick terrigenous clastic sequence, the Kuskokwim Group (Patton and others, 1984; Wallace and others, 1989; Bundtzen and Miller, 1997).

Plutons intruded the Kuskokwim Group during the Late Cretaceous and Early Tertiary (Bundtzen and Miller, 1997). The Late Cretaceous and Early Tertiary plutonic rocks are primarily granodiorite to quartz monzonite and are associated with mineral deposits hosted in the Kuskokwim Group, referred to as the Kuskokwim Mineral Belt (Patton and others, 1984; Szumigala, 1996). The Kuskokwim Mineral Belt, formed during an approximately 70 Ma episode of magmatism and associated mineralization, is roughly fault bounded to the southeast by the Denali-Farewell fault system and to the northwest by the Iditarod-Nixon Fork fault system (Miller and others, 2002). Both the Denali-Farewell fault system and the Iditarod-Nixon Fork fault system (**Figure 1.1**) strike NE-NNE (Decker and others, 1994; Miller and others, 2002). The Denali-Farewell fault system has a displacement of approximately 130 to 140 km in western Alaska, while the Iditarod-Nixon Fork fault has greater than 90 km displacement. Both systems display dominantly dextral motion, although there is some speculation about sinistral motion as well (Decker and others, 1994; Miller and others, 2002).

1.2.2 Local Geology

Due to extensive weathering and vegetation in the immediate Nixon Fork area, the geology is poorly exposed (Martin, 1922; Jasper, 1961; Szumigala, 1996; Cutler, 1994). Publicly available geologic mapping is limited to sketch maps (e.g., (Herreid, 1966)) and a 1:250,000 regional scale map (Patton and others, 1980) (**Figure 1.2**).

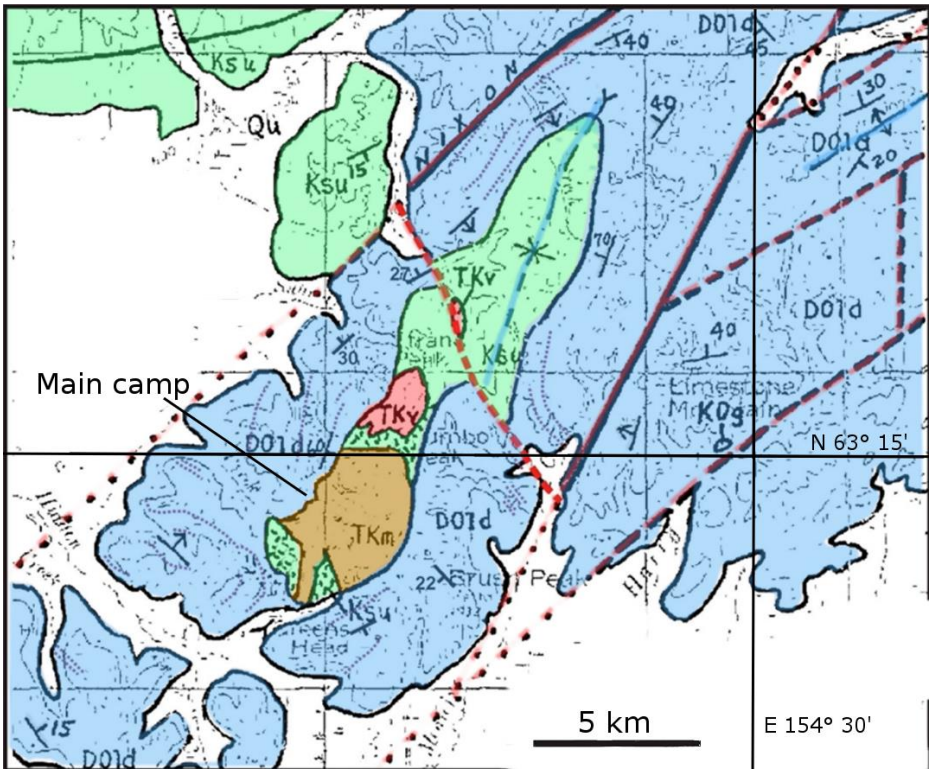

Figure 1.2 Generalized geology of the Nixon Fork area, modified from Herreid (1966) and Patton and others (1980). DOld is the carbonate unit hosting the skarn, TKm is the Late Cretaceous Mystery Creek pluton, KSu is mid- to Early Cretaceous sedimentary rocks (Kuskokwim Group) and the stippled pattern indicates hornfels. The dotted lines in DOld are apparent bedding traces from Herreid (1966). The main camp is situated near skarn occurrences examined in this work.

The Nixon Fork deposits are primarily hosted in a 2,000 m thick Middle Ordovician to Upper Ordovician carbonate unit (Herreid, 1966). The deposits (**Figure 1.3**) are near the

~68-69 Ma Mystery Creek pluton (Brooks and Martin, 1921; Brown, 1925; Moll and others, 1981; Cutler, 1994). The host limestone varies from thick-bedded and fine-grained to thin-bedded, silty and micritic, with fine-grained blue-gray dolomite interbeds (Szumigala, 1996), which are moderately recrystallized and cut by joints and thin calcite veins (Martin, 1922; Brown, 1925). Carbonate rocks near the Mystery Creek pluton are contact metamorphosed and slightly coarser-grained than elsewhere in the carbonate unit (Szumigala, 1996).

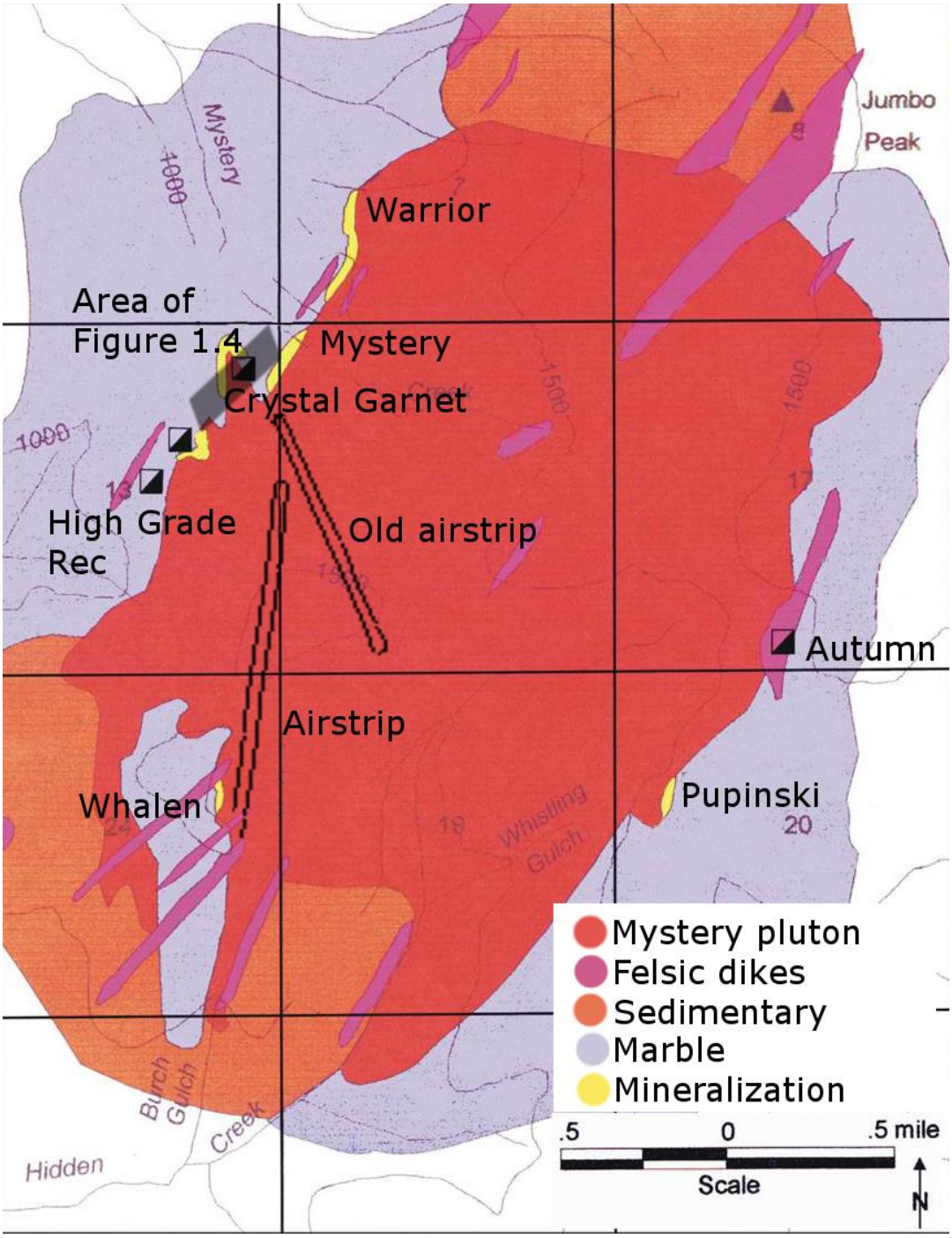

Figure 1.3 Location map showing mineral deposits and anthropogenic features in relation to the Mystery Creek pluton. Area of Figure 1.4 indicated by shaded area. After (Cutler, 1994).

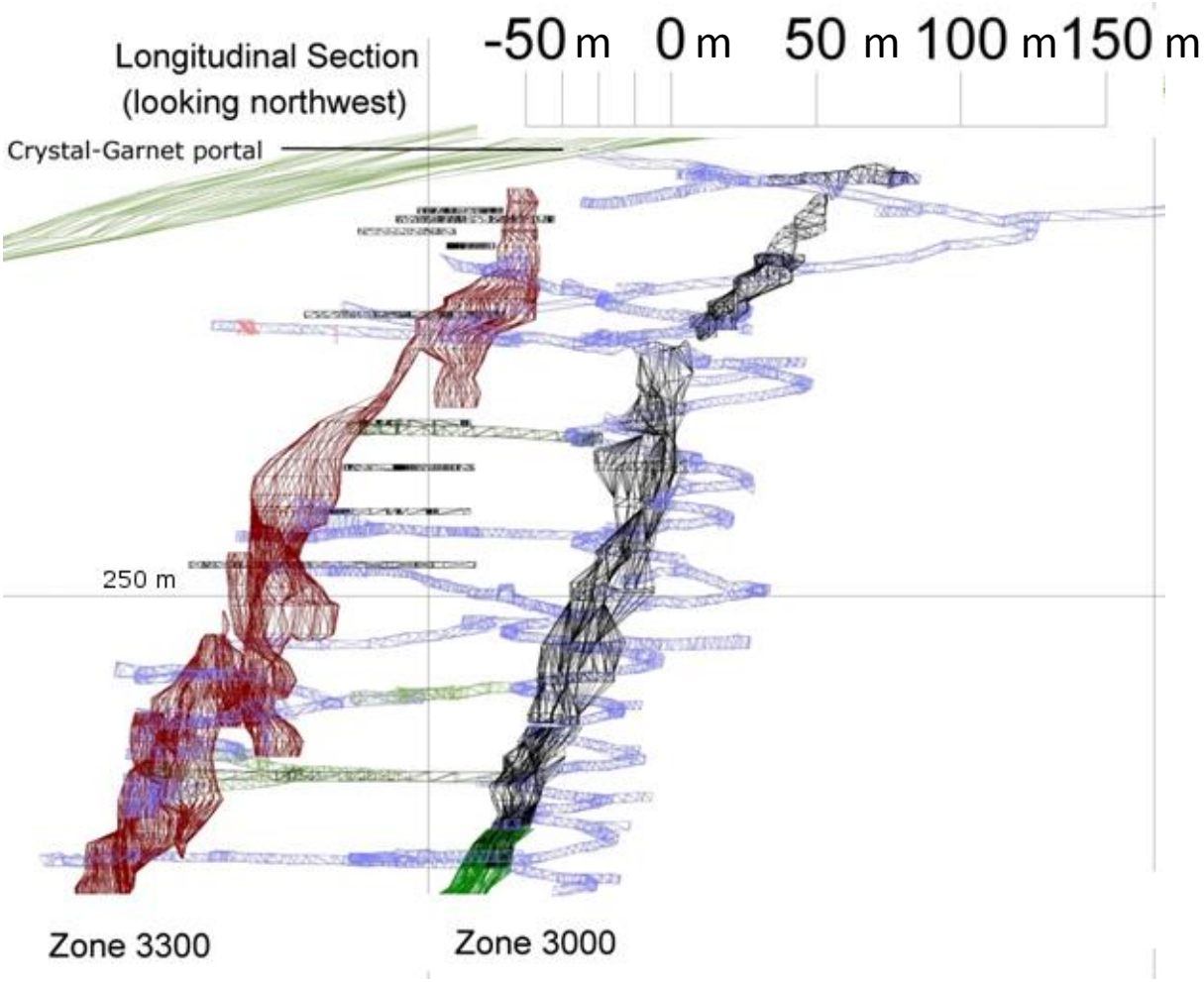

Figure 1.4 Southwest-northeast cross section through the Nixon Fork main working, looking northwest. Ore is enclosed by red and black wireframe models extending downward from the green wireframe model ground surface, surrounded by the blue wireframe model decline (unpublished Mystery Creek internal document). Elevation is in m above sea level.Zone 3000 is the Crystal-Garnet orebody, zone 3300 is an adjacent mineralized body. Modified from unpublished Mystery Creek sources.

The Mystery pluton is roughly elliptical in shape, approximately 4.5 by 8 km, with a major axis that trends approximately 35 degrees (**Figure 1.2, Figure 1.3**). The western margin is irregular and dips steeply (Martin, 1922). The pluton consists of medium to

coarse grained monzodiorite, quartz monzonite, quartz monzodiorite and monzonite (Cutler, 1994). Variable biotite, amphibole, hypersthene (almost wholly replaced), and clinopyroxene occur in these units (Cutler, 1994). Within the pluton, hornblende and clinopyroxene are not present as discrete crystals, but rather as clots, typically with clinopyroxene centers and hornblende (±biotite) rims (Cutler, 1994). Portions of the pluton display sericitic alteration; near-surface exposures are moderately to strongly weathered (Herreid, 1966; Cutler, 1994).

The Mystery pluton and adjacent carbonate rocks(Brown, 1925; Cutler, 1994) are intruded by felsic, sericitic altered dikes (Herreid, 1966; Moll and others, 1981; Cutler, 1994). Herreid (1966) claims these constitute approximately one third to one half the volume of the Mystery Creek pluton. The dikes are composed of fine to medium grained subhedral alkali feldspar and anhedral quartz, plagioclase and biotite with secondary minerals including fine-grained white mica ("sericite") chlorite, rutile, and hematite (Cutler, 1994). The dikes are variously described as "dacite", "quartz latite", and "granite" by different workers (Brown, 1925; Herreid, 1966; Cutler, 1994). The original dike compositions are unknown, as abundant secondary calcite, sericite, clay, and silica replaced both matrix and phenocrysts, and also destroyed original ferromagnesian minerals (Brown, 1925). Herreid (1966) interpreted the felsic dikes as slightly younger and more silicic differentiates from a deeper magmatic source than the main host pluton.

Moll and others (1981) published two K-Ar ages for the pluton (68.6 ± 2.0 Ma and 70.4 ± 2.1 Ma) and one for sericitic alteration (69.1 ± 2.1) and concluded that the mineralization was associated with nearby plutonism. Unpublished $^{40}Ar/^{39}Ar$ ages (P. Layer, pers. comm.) indicate a similar age for phlogopite from a Mg skarn, but a younger (but imprecise) age for retrograde hornblende.

Skarns occur as discontinuous bodies primarily near (within 60 m; **Figure 1.3**) the western edge of the Mystery Creek pluton (Martin, 1922; Mertie, 1936; Cutler, 1994; Szumigala, 1996). Several skarns occur as sub-vertical pipes (**Figure 1.4**), and some possess garnet-rich cores, garnet-pyroxene margins, and wollastonite-idocrase-scapolite rims (Newberry and others, 1997). Calcic and magnesian skarns are both present at Nixon Fork (Cutler, 1994; Szumigala, 1996; Newberry and others, 1997; Power and others, 2003), although calcic skarn is dominant, accounting for over ninety percent of the total skarn volume (Szumigala, 1996). Oxidized calcic skarn has the highest gold grades at Nixon Fork (Szumigala, 1996) and has been mined to the 460 foot depth at the Garnet shaft as "chimney" deposits, in these weathering-induced calcite dissolution created caverns into which slabs of ore dropped (Jasper, 1961; Szumigala, 1996).

1.2.3 Geology and Geography of the Current Nixon Fork Orebody

The Crystal Garnet (**Figure 1.3**) body is accessed by a 1,600 m decline (**Figure 1.5**) and 3,305 m of development. The decline bottom is at 145 m above sea level (ASL) and the portal is at 400 m ASL. The water table varies from 140 to 168 m ASL. The High Grade/Rec body (southwest of the Crystal-Garnet portal (**Figure 1.3**)) was accessed from

the 335 drift of the Crystal decline, but mining was largely confined to the Crystal Garnet bodies (Freeman and Giroux, 2012).

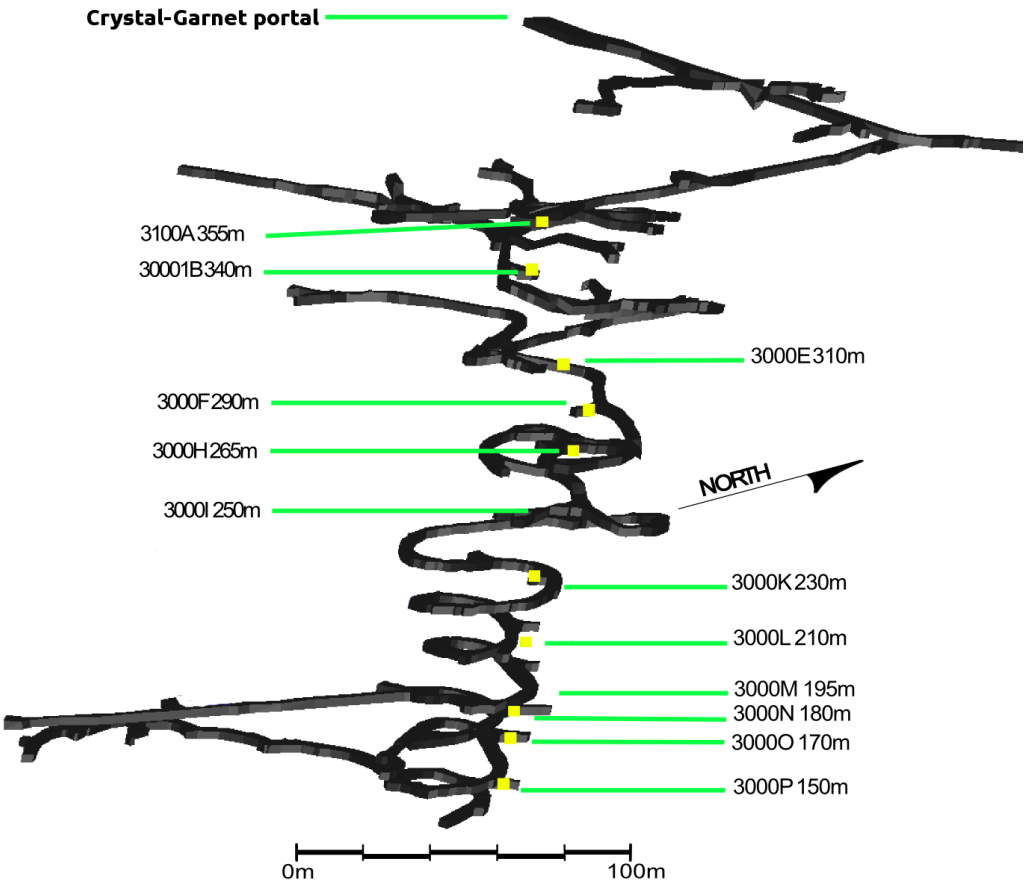

Figure 1.5 Three dimensional representation of the Crystal Garnet decline. First number is the level, second is the elevation above sea level. Image modified from unpublished 2007 Nixon Fork internal document

I acquired 1:200 scale maps of the Crystal-Garnet Decline area (e.g., **Figure 1.6**), totaling 56 sheets, these covered levels 70, 85, 100, 115, 130, 145, 160, 175, 190, 205, 220, 235, 250, 265, 280, 295, 310, 325, 340, 355, 370, 385, and 400 of the Crystal Garnet mine. These were scanned and digitized in May, 2003 and I converted and imported them into

Vulcan (**Chapter 4.3**) in 2010. I also recorded structural measurements shown on the maps (e.g., **Figure 1.6**) as well as dike orientations from MapInfo files and maps in Burnett and Grady (2005). Structural measurements are also given on the maps that I digitized (e.g., **Figure 1.6**, **Appendix 1**).

Steeply dipping, north-south striking (**Figure 1.7**) mafic dikes of presumed Late Cretaceous age cut the deposit (Burnett and Grady, 2005; Power and others, 2003; Wallis and others, 2003).

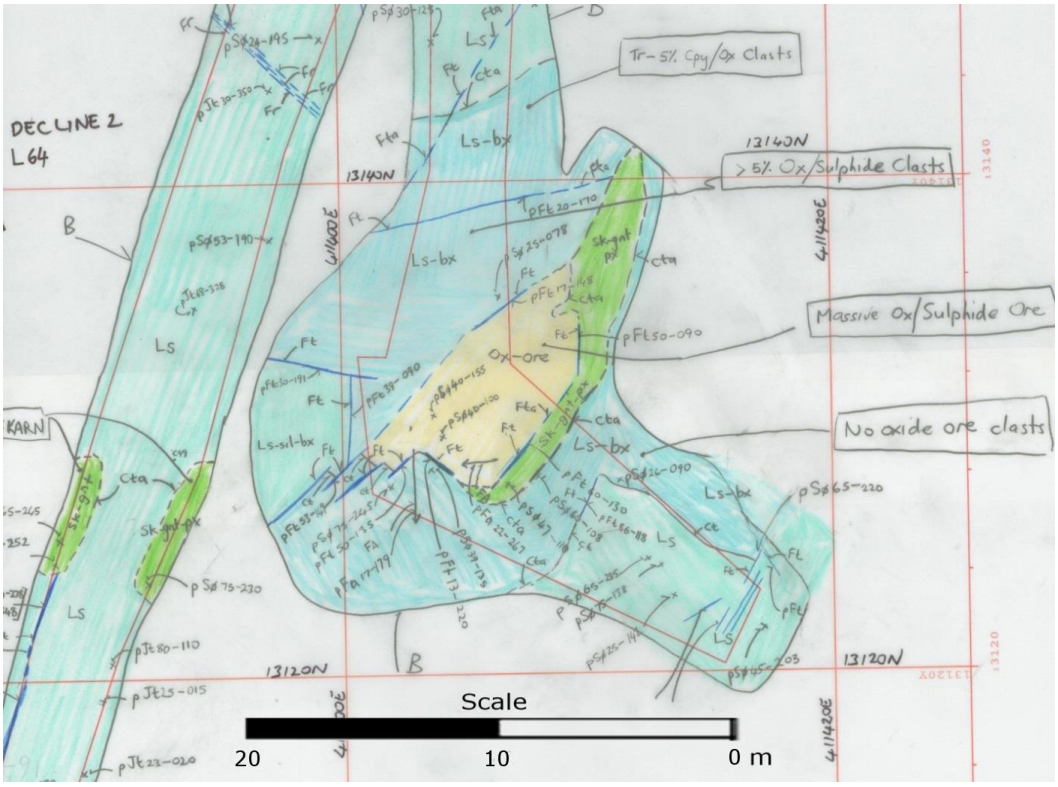

Figure 1.6 Geologic map of 210 level underground workings. Yellow is strongly oxidized skarn, green is garnet-pyroxene skarn, darker blue is limestone breccia and lighter blue is limestone. Red outline is CAD outline of the mine level. Measurements are in dip-dip direction. pSø = layering, pJt = joint plane, pFa = fold axis, pFt = fault plane, Ct = contact, Ft = minor fault, Fr = minor fracture. Map image from unpublished Mystery Creek database.

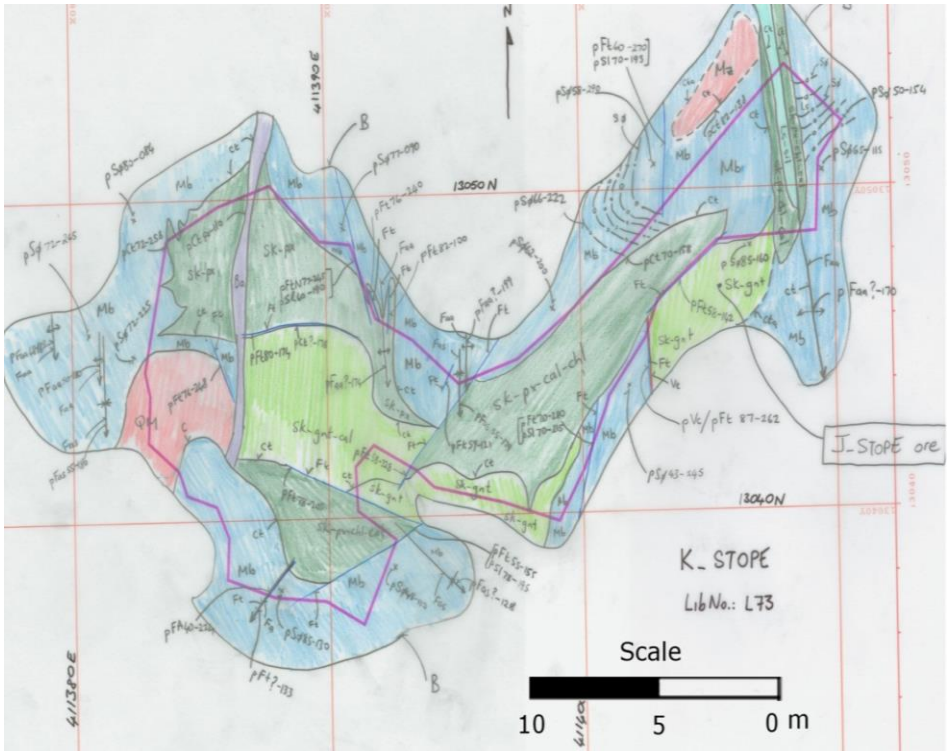

Figure 1.7 Geologic map of 230 level underground workings. Light green is garnet skarn, dark green is pyroxene skarn, blue is limestone, orange is Mystery pluton and purple is mafic dike. Purple like is CAD outline of the level. .pSø = layering, pJt = joint plane, pFa = fold axis, pFaa = fold axis-anticline, pFas = fold axis-syncline, pSl = slickenlines, pFtN = normal fault, pFt = fault plane, pVc = calcite vein, pCt = contact plane, Ct = contact, Ft = minor fault, Fr = minor fracture. Map image from unpublished Mystery Creek database.

1.3 Structural setting of the Nixon Fork deposit

1.3.1 Structures at Nixon Fork

Past workers have described a variety of structural features, including bedding, dikes, pluton embayments, breccia zones, and NE-striking faults and localized skarns, although none explained the skarn pipes. Skarn zoning is further complicated by post-ore faults (Brown, 1925; Newberry and others, 1997).

The Nixon Fork deposit is approximately 5 kilometers east of the Iditarod-Nixon Fork fault (**Figure 1.2**). Strands of the Iditarod-Nixon Fork fault have been active since approximately 90 Ma (Miller and others, 2002), and the strand closest to the Nixon Fork deposit has had 88-94 km right lateral offset since 65 Ma (Miller and others, 2002). Power and others (2003), primarily using detailed aeromagnetic maps, interpreted a large number of steeply dipping faults in the Nixon Fork area. **Figure 1.8** is based on aeromagnetic data and the pluton outline of Cutler (1994). Faults in the immediate vicinity of the Mystery Creek pluton were not shown due to fault density potentially obscuring the pluton (Power and others, 2003). **Figure 1.9** is a more detailed depiction of faults in the immediate vicinity of the Mystery Creek pluton, including faults that cut the pluton. The revised pluton shape is based mostly on the aeromagnetic survey and the assumption that linear or permissibly linear pluton contacts are faults.

However, due to poor exposures, few faults have been documented on the surface in the immediate mine area. Faults shown on **Figure 1.9** must be treated as highly interpretive. Note that only a few of the faults on **Figure 1.9** correspond to those (**Figure 1.2**) mapped by Patton and others (1980); further, faults shown >2 km from the pluton on **Figure 1.9** do not correspond well to what should be the same faults shown 3-5 km from the pluton on **Figure 1.8**. Additionally, if the faults bounding the west side of the intrusion (**Figure 1.9**) are correct, then the skarns on the northwest side of the pluton (**Figure 1.3**) are separated from the intrusion by faults.

In sum, due to poor natural exposures and limited artificial exposures in the Nixon Fork Mine area, not much is known about the structural geology of the immediate region. In

particular, the degree to which the pluton and skarns are displaced by post-ore faults (as depicted on **Figure 1.9**) is uncertain.

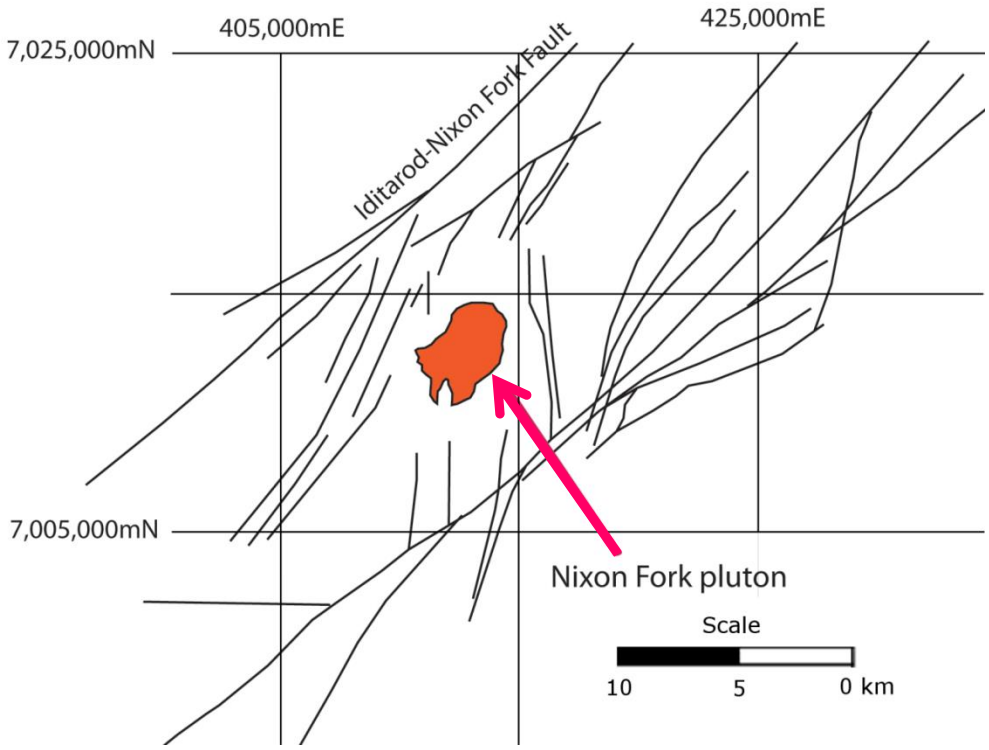

Figure 1.8 Generalized structural map of the Nixon Fork region, emphasizing steeply dipping faults, modified from (Power and others, 2003). The Mystery Creek pluton is depicted as surrounded by a population of north-northeast-south-southwest and north-south striking faults. Faults are deliberately not depicted within 2 km of the pluton. Grid is 5 km spacing, Zone 5 NAD 27 UTM.

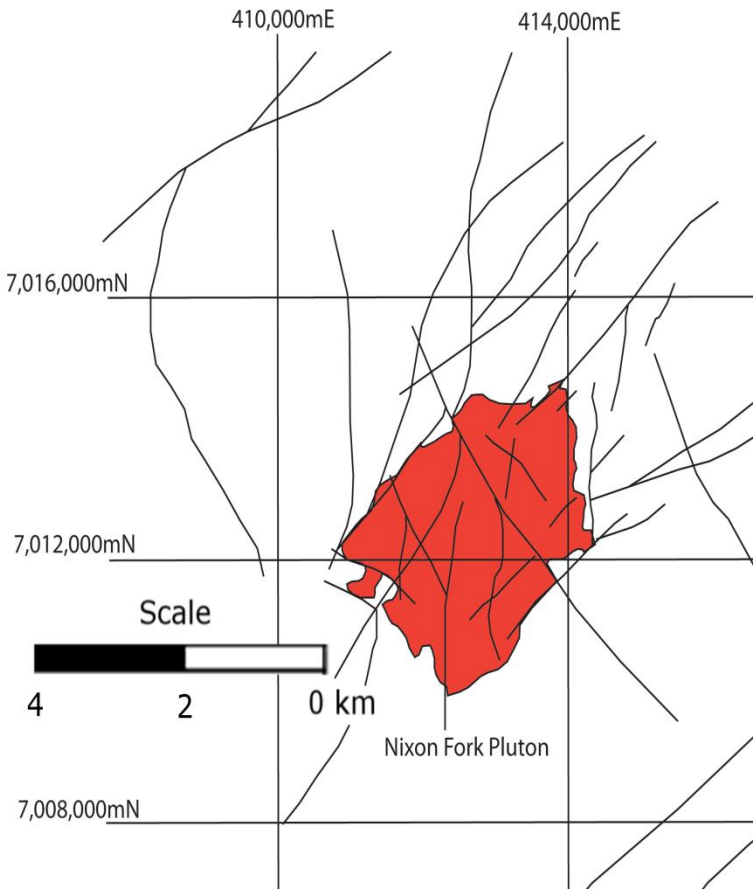

Figure 1.9 Interpretive structural geologic map of the immediate Nixon Fork area, emphasizing steeply dipping faults, from Power and others (2003). Faults are shown bounding the west and east contacts of the pluton. Grid is 4 km spacing, Zone 5 NAD 27 UTM.

1.3.2 The Basis for Structural Analysis

Given the complex structural setting of the deposit, and some inconsistencies in fault and lineation mapping, a significant part of this thesis will be to re-examine the structural setting of the deposit on both broad and small scales. This will be discussed in more detail in Chapter 5, but a brief introduction is included here to illustrate the complexities of the problem at Nixon Fork. In order to compare sets of structures, I defined the

orientations of structures that would be expected to form from given directions of maximum horizontal shortening and extension.

I consider two structural end-member cases and two ways of looking at the structures. For case (a) all the structures at the Nixon Fork mine are hypothesized as caused by the same stresses that produced the Nixon Fork-Iditarod fault. For case (b) all the structures at the mine are hypothesized as caused by local stresses induced by movement on the Nixon Fork-Iditarod fault system. These two are simply rotated by 15 degrees relative to each other. The two ways of viewing the data are in map view and stereographic projection.

Figures 1.10 and **1.11** represent the same relative orientations of structures in map view and stereographic projection, respectively. **Figure 1.10a** and **Figure 1.11**a are idealized representations of primary structures that could be expected to form with the directions of maximum horizontal shortening and extension in the regional stress/strain field in which the Iditarod-Nixon Fork fault formed. **Figure 1.10**b and **Figure 1.11**b are idealized representations of secondary structures that could be expected to form with the directions of maximum horizontal shortening and extension within a local stress/strain field in the Iditarod-Nixon Fork fault zone. If shear is horizontal and parallel with the Iditarod-Nixon Fork fault, structural features shown in **Figure 1.10b** and **Figure 1.11**b could form. Dikes, veins and normal faults that could (although not necessarily would) form in the local shear/strain field are depicted by this diagram and would strike approximately east-west. This representation only considers strain in the horizontal plane (the surface of the

Earth) and the types of structures that actually form depend on the strain in three dimensions. This means that not all types of structures shown (such as the normal, thrust and strike slip faults) would form given the same directions of maximum horizontal shortening and extension.

Maps depicted in Patton and others (1980) **(Figure 1.2)** and Power and others (2003) **(Figure 1.9)** suggest that the Mystery Creek pluton and hosted mineral deposits are surrounded by a shear zone. This may or may not be the case, but it provides a testable hypothesis. I will test the hypothesis that the structures in the Nixon Fork mine area can be directly or indirectly related to the Iditarod-Nixon Fork fault.

As part of this thesis, I will use **Figure 1.11** to identify compatibly oriented sets of structures, since once I locate a structure of known type, I can rotate the figure to match the orientation of the known structure type and I can then assess whether other observed structures are appropriately oriented to be compatible structures. For example, if I identify a mafic dike with approximately north-south strike (e.g. **Figure 1.7**), I rotate the stereonet in **Figure 1.11**b roughly 85 degrees counter-clockwise so the vein/dike orientation is north-south and then use the figure in that orientation to attempt to find matching sets of structures (i.e. north-south striking normal faults and veins, east-west striking thrust faults and folds, and right and left lateral strike slip faults at approximately 150 and 30 degrees respectively).

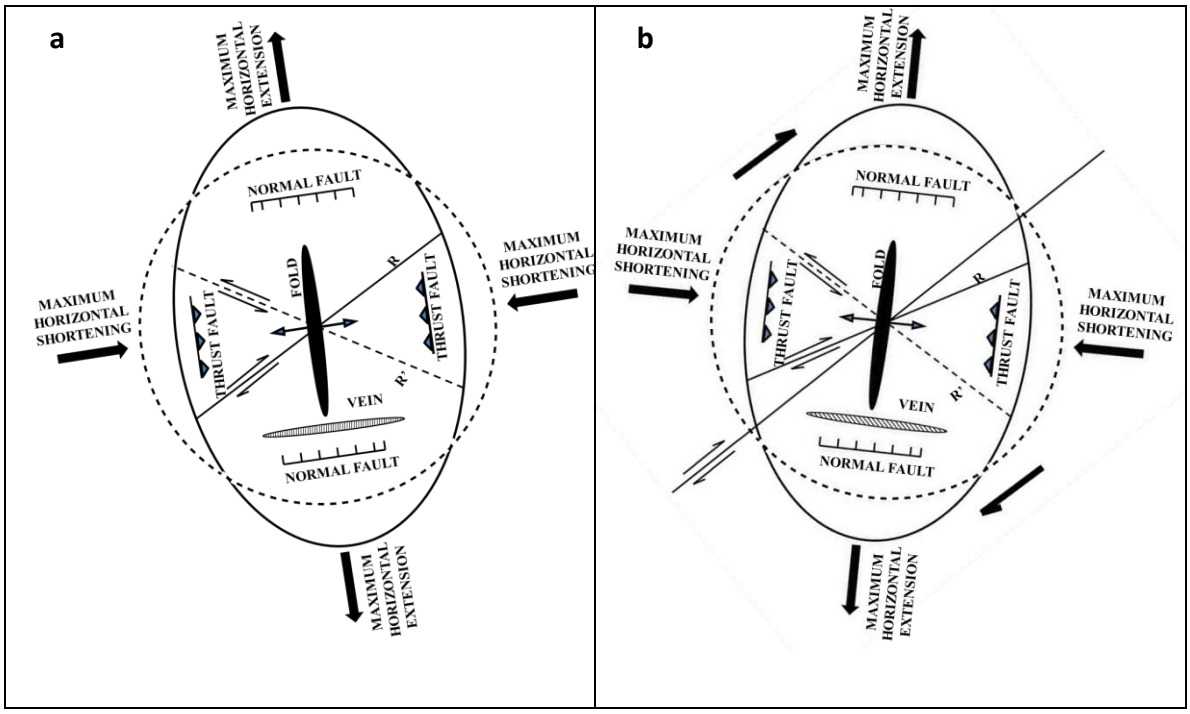

Figure 1.10 Regional primary (a) structures expected from the stress/strain field within which the Iditarod-Nixon Fork fault system formed and local secondary (b) structures expected within a northeast-striking right-lateral shear zone. If the Iditarod-Nixon Fork fault had the strike of the right-lateral shear zone in figure b, any secondary structures related to the axes of shortening and extension within the shear zone would be expected to have orientations relative to the right-lateral shear zone as shown in figure b. For example, one would expect related dikes, veins, and normal faults to strike approximately east-west and secondary left-lateral faults to strike northwest-southeast. Similarly, if the regional stress/strain field has created structures in the Nixon Fork mine locality, they would have the primary structure orientations in figure a.

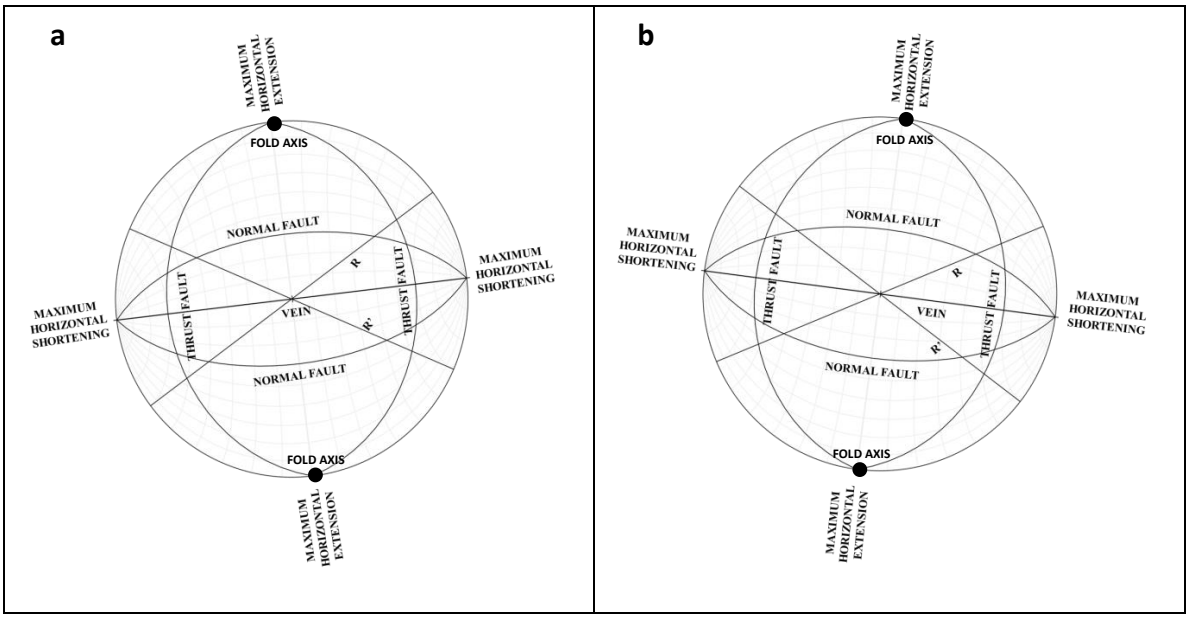

Figure 1.11 Stereonet diagrams of idealized original orientation of structures expected from a given orientation of orthogonal axes of maximum horizontal contraction and extension, as in Figure 1.10. R = right lateral, R' = left lateral.

1.4 Definition of problem

Three questions constitute the major focus of this thesis.

1. Is the Mystery pluton the source of the Nixon Fork gold skarn? That the Mystery pluton is the source of the skarn forming fluids is the historic assumption, but the discontinuous nature of the skarn (e.g. **Figure 1.3**) and pipe-like nature of the skarn (**Figure 1.4**) call this into question.

2. What structures control the pipe-like shape and distribution of the skarn? Whatever the source of the skarn might be, its shape does not simply reflect the intrusive contact. The most likely reason for a pipe shape is the intersection of two planar features, neither of which has yet been identified.

3. What types of deformation at Nixon Fork might affect the skarn, disrupting it? Numerous faults have been mapped at Nixon Fork, so presumably some faulting offsets the skarn. How would I go about finding structures that offset skarn?

1.5 Methods

To address this problem, I have compiled the existing geologic information from the Nixon Fork ore body and surrounding lithologies. I have also obtained new petrologic, geochemical, geochronological and structural data to help constrain the origin and structure of the deposit.

I collected twenty igneous rock samples, six of which I analyzed by polished slab and pressed powder pellet XRF for major and minor elements. For fine grained igneous rocks, polished slabs and pressed pellets yield similar compositions, and disparities in elemental composition (chiefly in Na, Mg and Al) contribute insignificant error in calculations of normative mineralogy (Deal, 2012). However, Deal (2012) also reported that polished slab XRF under-reports FeO and MgO by 15-20% and under-reports some minor elements. Consequently, I also compared the accuracy of slab vs. pressed pellet XRF for my rocks. I analyzed an additional five mafic dike samples by polished slab XRF.

To create polished slabs I cut rock into disks approximately 35 mm in diameter and 15-35 mm thick and polished them with increasingly fine lapidary wheels producing a uniformly reflective surface. I ground samples for pressed powder pellets by crushing them to sub-centimeter size, pulverizing for 10 minutes in a SPEX Dual Mixer/Mill. I

then added 7 g of sample powder to a pre-rinsed mortar along with 7 drops of 5% polyvinyl alcohol and mixed in a pre-rinsed pestle until homogenous. I then added the sample mixture to a 35 mm XRF cup inside a stainless steel die set and compressed the pellet to 10 metric tons of pressure. I analyzed the samples using the IQ+ routine on the PanAlyticalAxios four-kilowatt wavelength-dispersive XRF.

I collected eleven geochronology samples from a combination of drill core, surface samples and previous field work. Samples selected for dating were crushed and washed in deionized water. Mineral separates were prepared through handpicking. The samples were irradiated at the McMaster University nuclear reactor in Hamilton, Ontario. The 6W argon ion laser in the Geochronology Lab at the University of Alaska Fairbanks was used to step-heat the samples (Layer, 2000). During the heating process, a liquid nitrogen cold finger and a Zr-Al getter at 400°C purified the gas, which was then measured with a VG3600 mass spectrometer. The monitor mineral MMhb-1 (Samson and Alexander, 1987) with an age of 513.9 Ma (Lanphere and Dalrymple, 2000) was used to monitor neutron flux (and calculate the irradiation parameter, J).

I sorted through digitized data (30,994 files) from existing Nixon Fork electronic files in an attempt to determine spatial relationships between the ore body and bodies that could have been the source or control for mineralization. I converted 186 AutoCAD, CSV, and triangulation files into a format readable by Vulcan software, which resulted in plan maps of mine levels. I then used the plan maps to triangulate between levels to define ore bodies as well as dikes and altered zones.

I examined forty petrographic thin sections of brecciated rocks from Nixon Fork in transmitted light for micro-structures and, with the help of Dr. Elizabeth Nadin, University of Alaska Fairbanks, identified and photographed tectonic micro-structures.

I examined and recorded structural orientations taken from 1500 m of previous underground mapping, as well as measurements I made of orientations of dikes and faults at underground and limited surface exposures in the mine vicinity. I used these data to plot structural orientations on lower hemisphere stereographic projections so I could define structural sets.

1.6 Organization of thesis

This thesis contains five chapters. This introductory chapter (**Chapter 1**) has provided background on the Nixon Fork deposit and geology, the main issues that have impeded understanding of the deposit, and the methods that I will use to address the problem. **Chapter 2** presents compositional data on igneous rocks from the deposit. **Chapter 3** consists of a radiometric dating study of the deposit. **Chapter 4** broadly covers the structures present at Nixon Fork and is broken into three **sub-chapters**: (**1**) Structural orientations derived from previous mapping; (**2**) character and origins of breccias; and (**3**) the three-dimensional shape of the Crystal-Garnet ore body and associated units. In the final chapter (**Chapter 5**), I combine the various data sets and present a model of the structural history of the deposit.

2 Igneous rock composition

2.1 Introduction

A variety of names have been, and continue to be, applied to the igneous rocks at Nixon Fork (Brown, 1925; Herreid, 1966; Cutler, 1994)**.** For example, recent logging codes at the deposit (**Table 2.1**) allow for 14 igneous units. In addition, igneous dikes provide major structural-temporal data, as their orientations give extensional directions and their ages give the time of that extension. Trace element compositions of the igneous rocks also provide clues about their overall tectonic settings (Pearce and Cann, 1973).

Table 2.1 Mystery Creek 2003 Codes for Igneous Rocks

Code	Rock type
110	Undifferentiated phaneritic/feldspathic rocks
111	Equigranular diorite/granodiorite/quartz monzonite
112	Porphyritic quartz monzonite
113	"Latite" dike
114	Marginal phase monzonite
120	Undifferentiated aphaniticfeldspathic rocks
121	Feldspar porphyry
122	Quartz-eye (rhyolite) porphyry
123	Silicified/siliceous chlorite- spotted porphyry
124	Vesicular, tourmaline filled porphyry
125	Green sericite porphyry
130	Undifferentiated aphanitic mafic rocks (probably intrusives)
131	Pyroxenite
132	Mafic dike "Basalt" is field term - approx andesite/basalt composition

Three major types of igneous rocks--felsic dikes, main phase, and mafic dikes--(Power and others, 2003; Burnett and Grady, 2005) are known at Nixon Fork. In order to better

understand their relationships among and between each other I embarked on a small study of compositions using representative, least-altered examples of each.

Additionally, I tested the use of polished fine-grained igneous slabs versus pressed pellets for elemental analysis. The key advantages of polished slabs are sample preparation in a tenth of the time and the impossibility of elemental contamination. Deal (2012) showed that for a restricted compositional range polished slabs yielded acceptable data. My study however, encompasses the range from felsic to mafic and provides a wider compositional test.

Plutonic rocks are officially classified using the International Union of Geological Sciences modal mineralogy scheme: percentages of quartz, plagioclase, alkali feldspar, and feldspathoid minerals (Bateman and others, 1989). Due to uniformly white feldspars and variable hydrothermal alteration at Nixon Fork, however, distinction between the two feldspars is not always possible. Consequently I have resorted to various (non-official) schemes that rely on some variety of major element composition. In addition, Winchester and Floyd (1977) proposed classification schemes based on immobile minor and trace elements that I also employ, given the variable hydrothermal alteration present.

I employed sample preparation and XRF analytical routines as described in **Chapter 1**, with pressed pellets and polished slabs each made from the same rock sample. R. Newberry (written communication, 2012) supplied additional slab XRF analyses of trace elements in mafic dikes.

2.2 Results

Table 2.2 gives major and minor element compositions for the 5 samples studied. Values appear broadly comparable; some elements appear more closely correlated than others, however. **Figure 2.1** compares major element concentrations in polished slabs and pressed pellets of the same rocks using a log scale to show a wide range of concentrations. Most of the values for most elements agree within ±20%.

Table 2.2 Major and Trace element data for Nixon Fork Igneous Rocks comparing pressed pellets to polished slabs. Pressed pellets are bold.

wt %	**Main1-PP**	Main1	**Main2-PP**	Main2	**Main3-PP**	Main3	**Felsic PP**	Felsic	**Mafic1 PP**	Mafic1	**Mafic2 PP**	Mafic2
SiO_2	**59.9**	62.5	**59.8**	62.5	**61.1**	62.4	**73.5**	73.8	**46.1**	47.1	**46.5**	47.5
TiO_2	**1.1**	1.1	**1.1**	0.96	**1.0**	0.97	**0.12**	0.11	**2.5**	2.3	**2.5**	2.3
$Al2O_3$	**16.7**	15.9	**16.8**	16.3	**16.9**	16.8	**14.6**	13.9	**15.1**	16	**15.6**	15.8
$Fe2O_3$	**6.7**	5.4	**6.7**	4.7	**5.92**	4.41	**1.44**	0.89	**11.6**	10.4	**11.4**	10.9
MnO	**0.09**	0.07	**0.09**	0.07	**0.07**	0.06	**0.05**	0.04	**0.21**	0.19	**0.18**	0.15
MgO	**2.3**	2.0	**2.4**	1.9	**2.2**	2.0	**0.3**	0.9	**6.4**	5.6	**6.2**	6.3
CaO	**4.1**	4.0	**4.4**	4.4	**4.1**	4.3	**1.1**	1.5	**10.1**	10.2	**9.8**	8.8
Na2O	**3.1**	3.2	**3.4**	3.3	**3.4**	3.3	**2.8**	3.0	**1.8**	2.19	**2.43**	3.13
K2O	**4.3**	4.0	**3.4**	3.7	**3.8**	3.9	**5.3**	4.7	**4.1**	3.9	**3.2**	2.9
P2O5	**0.39**	0.4	**0.4**	0.4	**0.34**	0.31	**0.04**	0.05	**0.95**	0.82	**0.87**	0.79
SO3	**0.02**	0.06	**0.04**	0.07	**0.02**	0.06	**0.01**	0.12	**0.16**	0.19	**0.21**	0.26
Cl	**0.1**	0.09	**0.07**	0.05	**0.1**	0.08	**0.00**	0.06	**0.02**	0.02	**0.02**	0.03
BaO	**0.14**	0.13	**0.11**	0.14	**0.12**	0.12	**0.08**	0.08	**0.16**	0.16	**0.13**	0.18
$Cr2O_3$	**0.01**	0.01	**0.01**	0.01	**0.01**	0	**0.02**	0	**0.06**	0.04	**0.04**	0.05
Ppm												
Rb	**203**	191	**178**	169	**193**	176	**251**	238	**130**	138	**95**	103
Sr	**327**	376	**319**	405	**346**	420	**72**	78	**678**	824	**737**	826
Y	**38**	30	**37**	28	**38**	28	**23**	17	**23**	25	**23**	25
Zr	**416**	259	**349**	256	**349**	177	**78**	67	**155**	161	**165**	176
Nb	**19**	14	**19**	12	**17**	12	**15**	13	**51**	52	**57**	59

Obvious exceptions are Fe_2O_3, for which the slabs gave significantly lower values than the pressed pellets (felsic and intermediate rocks) and MgO, for which the felsic dike slab and pellet (very low MgO) are radically different.

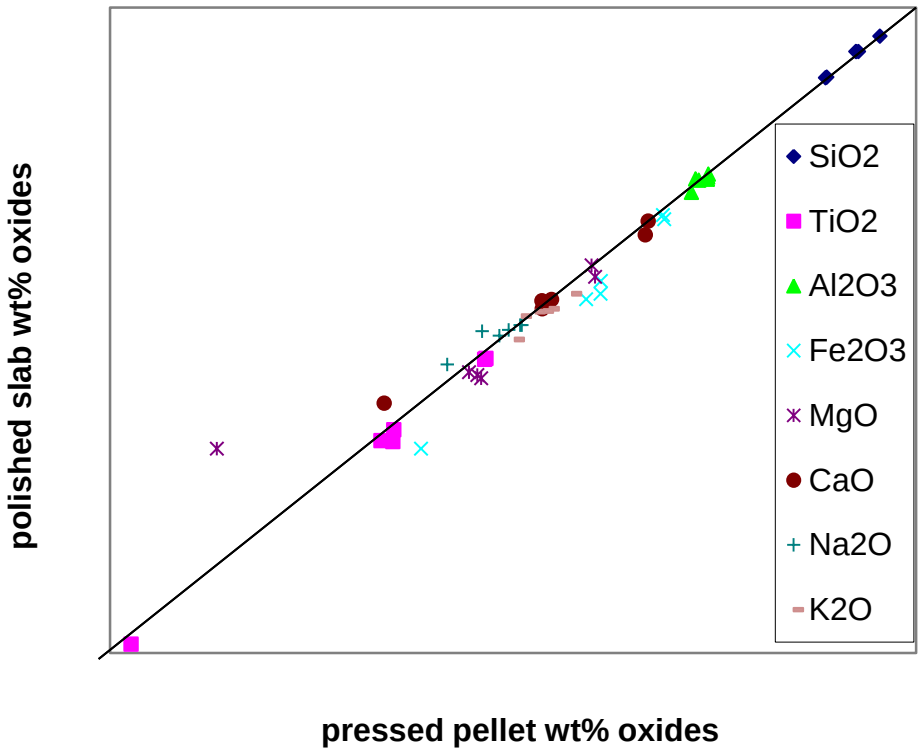

Figure 2.1 Major element composition comparisons for pressed powder pellet vs. polished slab XRF. Reasonable agreement is shown for the two analytical methods except MgO in the felsic dike.

Table 2.3 gives numeric comparisons of the slab and pressed pellet data, expressed as percent deviation of slab from pellet. Here the felsic dike sample stands out as showing the greatest deviations between slab and pellet for a variety of major elements. Mafic dike samples also stand out, however, in that pellet-slab concordance varies by element in

a manner different from the other samples. For example, Na_2O shows little systematic deviation for the non-mafic samples, but the mafic pellets yielded 20-30% less Na_2O than the slabs (**Table 2.3).**

Table 2.3 Comparison of Pressed Pellet and Polished slab XRF data. Values are 100*(PP-Slab)/PP value, i.e., % deviation of slab XRF from Pressed Pellet values

	Main1	**Main2**	**Main3**	**Felsic**	**Mafic 1**	**Mafic 2**
%						
SiO2	-4	-4	-2	-0.4	-2	-2
TiO2	4	15	5	8	6	7
Al2O3	5	3	0	5	-6	-2
Fe2O3	20	30	26	38	10	5
MnO	22	22	14	20	9	17
MgO	16	22	7	-256	12	-2
CaO	2	0	-7	-38	-1	11
Na2O	-4	2	1	-6	-22	-29
K2O	8	-8	0	11	6	11
P2O5	-3	0	9	-25	13	9
BaO	7	-27	0.0	0.0	-0.2	-39
Cr2O3	0.0	0.0	60	85	33	-25
Ppm						
Rb	6	5	9	5	-6	-8
Sr	-15	-27	-21	-9	-22	-12
Y	21	26	26	28	-5	-12
Zr	38	27	49	14	-4	-7
Nb	23	35	31	14	-3	-5

Across all analyses, pressed powder samples yielded 0.5-4 relative percent less SiO2 than the polished slabs of the same rock. Because the results are normalized to 100%, the other elements must—in general—be higher in the pressed pellets. The pellets generally yielded lower Na_2O and variable CaO relative to the slabs, however. TiO_2 values are very similar for the two types of analyses, as are P_2O5, Al_2O_3, SiO_2, CaO, and K_2O

Comparison of values for minor elements (**Figure 2.2**) shows much higher percent variation between polished slabs and pressed pellets than major element measurements. Here again, however, the deviations between pressed pellet and slab vary with rock type. For example, Zr, Nb, and Y are only slightly (5-10%) higher in mafic slabs than pellets (**Table 2.3**). Concentrations of these same elements in the felsic-intermediate composition rocks are 20-50% higher for pellets than slabs. Rb displays a similar (but not as extreme) pattern: felsic-intermediate slabs yielded slightly lower concentrations than the pellets and vice-versa for the mafic rocks.

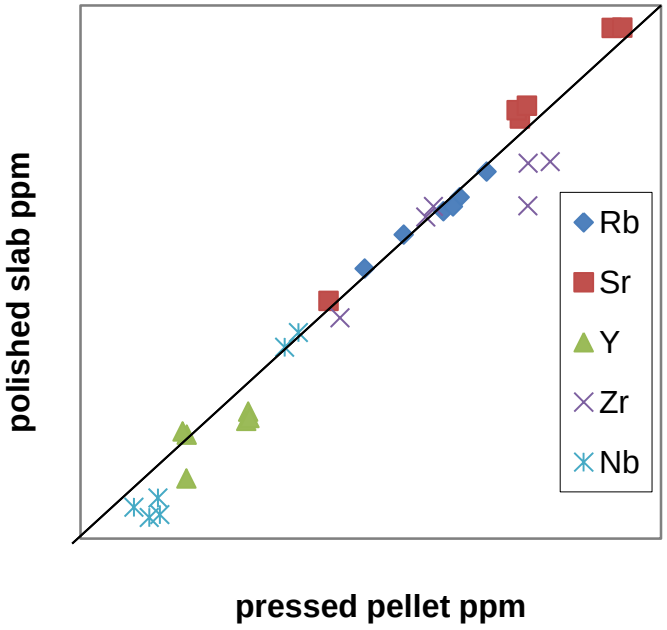

Figure 2.2 Minor element composition comparisons for pressed powder pellet vs. polished slab XRF. Reasonable agreement is show for the two techniques, although Nb, Zr, and Y concentrations are commonly higher and Sr commonly lower for pressed pellets than polished slabs.

CIPW norms for the various igneous rocks (**Table 2.4**) show considerably lower normative quartz for rocks from the main body than the felsic dike. Classification (**Figure 2.3**) of the felsic-intermediate samples based on the normative classification scheme of Streckeisen and Le Maitre (1979) yields quartz-monzonite and quartz-monzodiorite for the main intrusion and granite for the felsic dike.

Table 2.4 CIPW normative mineralogy for igneous Nixon Fork rocks

	Main1-PP	Main2-PP	Main3-PP	Felsic PP	Mafic1 PP	Mafic2 PP
Quartz	11.9	12.5	13.7	33.6	0	0
Albite	25.3	28.3	27.8	23.9	6.2	13.1
Anorthite	18.4	19.8	18.6	5.4	21.6	22.8
Orthoclase	25.9	20.5	22.8	31.6	24.8	19.3
Nepheline	0	0	0	0	4.9	4.1
Corundum	0.6	0.6	0.8	2.3	0	0
Diopside	0	0	0	0	19.3	17.5
Hypersthene	13.7	14	12.4	2.7	0	0
Olivine	0	0	0	0	14.2	14.2
Ilmenite	2.1	2.1	1.9	0.2	4.8	4.9
Magnetite	0.99	0.99	0.87	0.22	1.71	1.7
Apatite	0.93	0.95	0.81	0.09	2.3	2.1
Pyrite	0.02	0.04	0.02	0.02	0.17	0.23
Halite	0.19	0.13	0.19	0	0.04	0.04
Chromite	0.01	0.01	0.01	0	0.09	0.06
Sum	100	100	100	100	100	100

In contrast, classification based on the R1-R2 scheme (**Figure 2.4**) of La Roche and others (1980) yields alkali gabbro for the mafic dikes, tonalite for the main body and granite for the felsic dike. Finally, classification via the total alkali-silica diagram (**Figure 2.5**) which is the official classification for volcanic (very fine-grained) igneous

rocks, yields trachy –basalt for the mafic dikes, trachy-andesite for the Mystery pluton and rhyolite for the felsic dike.

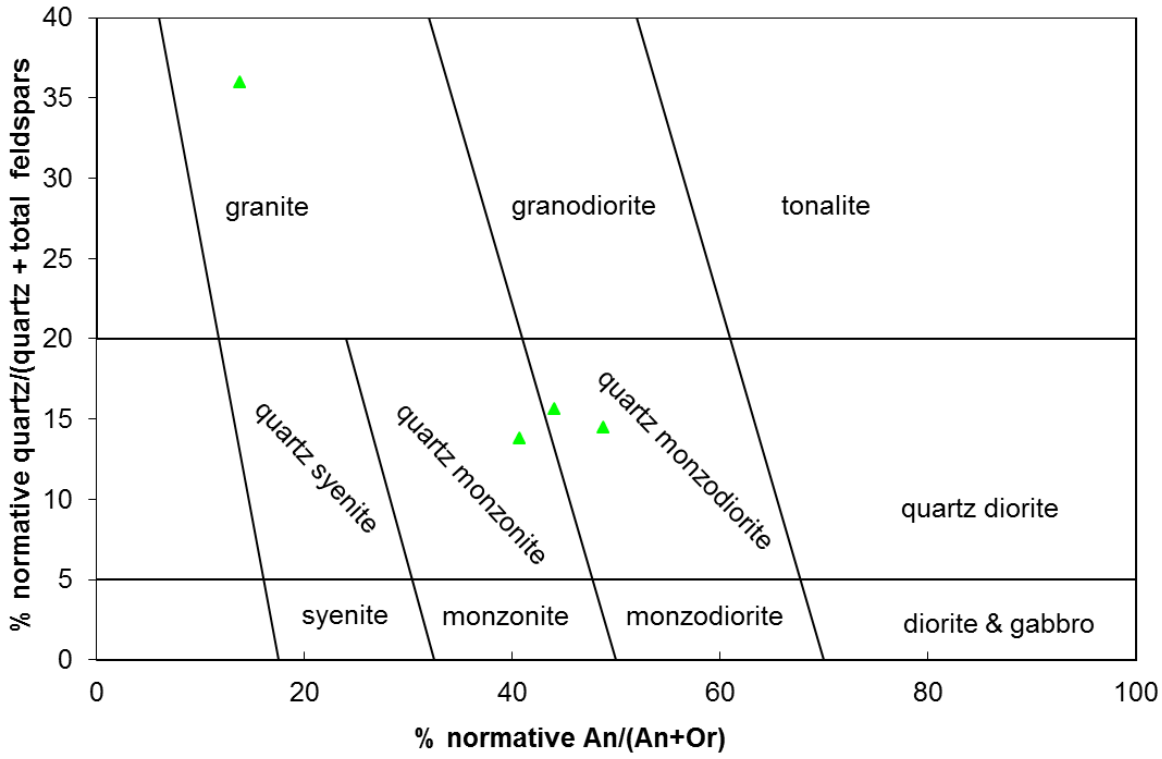

Figure 2.3 Classification of pressed powder samples of igneous rock from Nixon Fork using the normative scheme of (Streckeisen and Le Maitre, 1979). Felsic sample plots as granite; Main intrusion as quartz monzonite and quartz monzodiorite.

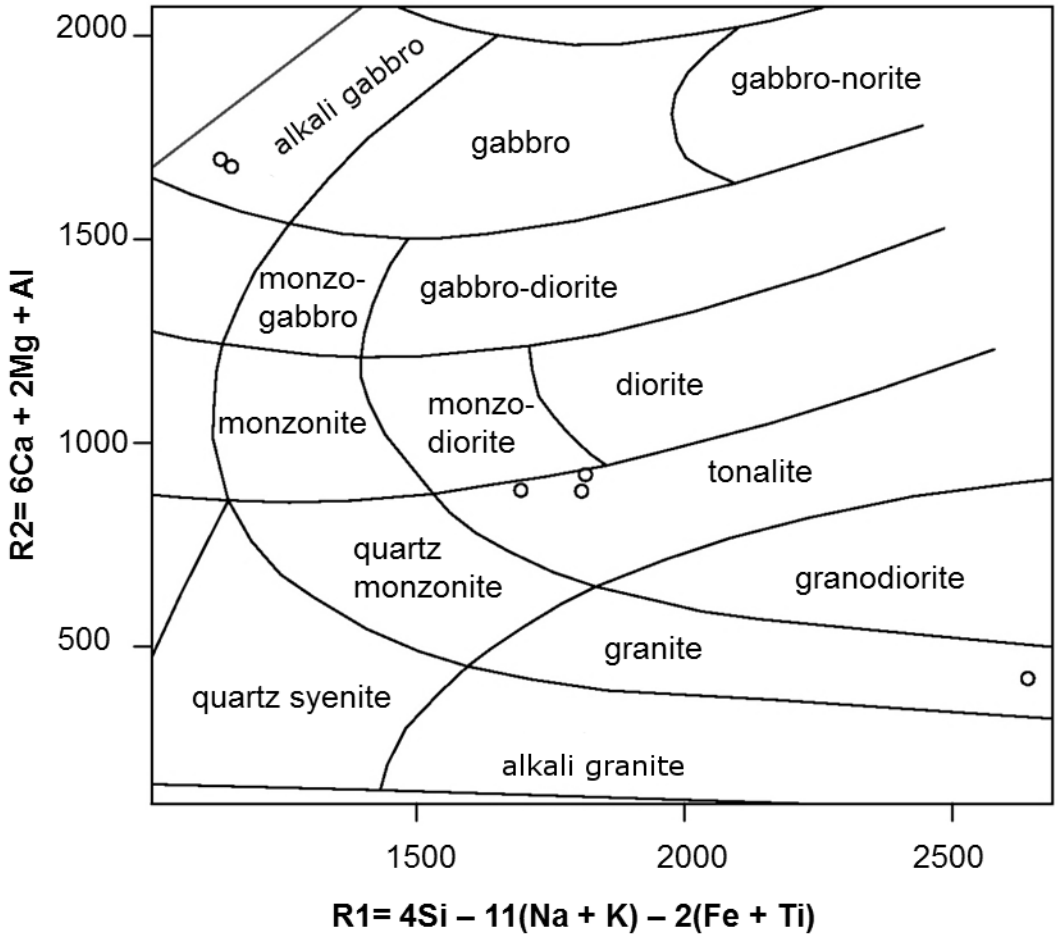

Figure 2.4 Classification of igneous pressed powder samples based on the R1-R2 plutonic rock scheme of (La Roche and others, 1980). Mystery pluton samples plot as tonalite, but near the boundary with monzodiorite; mafic samples as alkalai gabbro; and the felsic dike sample as granite.

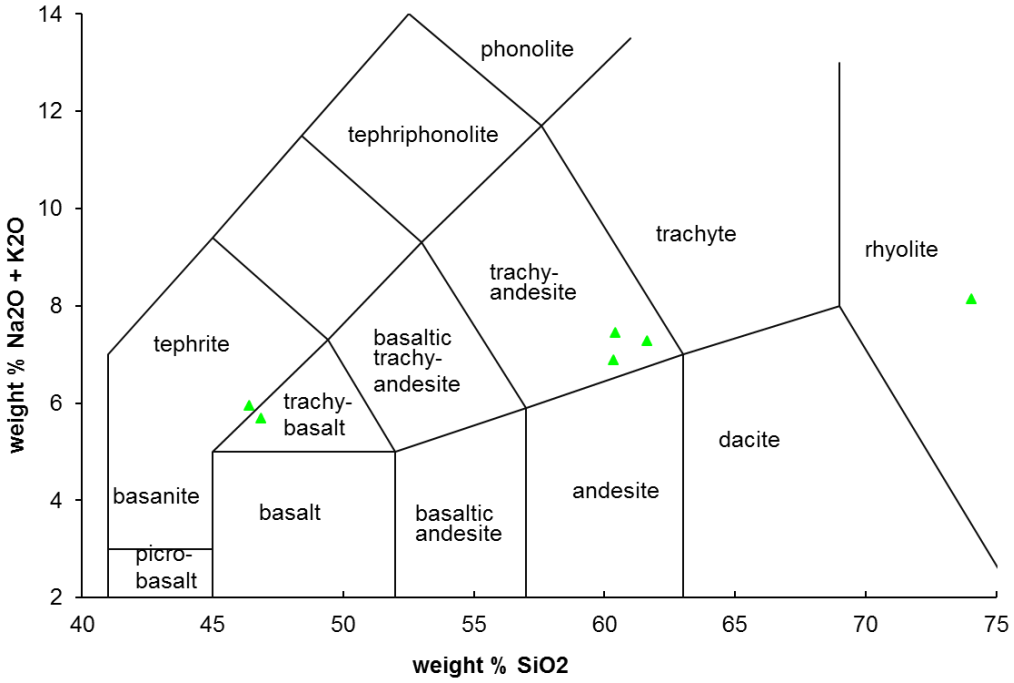

Figure 2.5 SiO2 vs. Na2O + K2O classification scheme for volcanic rock classification from LeBas and others (1986). Pressed powder XRF results are plotted. The felsic dike sample plots as rhyolite; the Mystery pluton samples as trachy-andesite; and the mafic dike samples as trachy-basalt/tephrite.

The 'immobile' element classification diagrams of Winchester and Floyd (1977) (**Figure 2.6** and **Figure 2.7**) yield different results for the two different schemes. On one the mafic rocks plot as alkalic, on the other as sub-alkalic. Conversely, samples from the Mystery pluton plot as either alkalic or 'normal' intermediate-felsic rocks depending on the diagram employed.

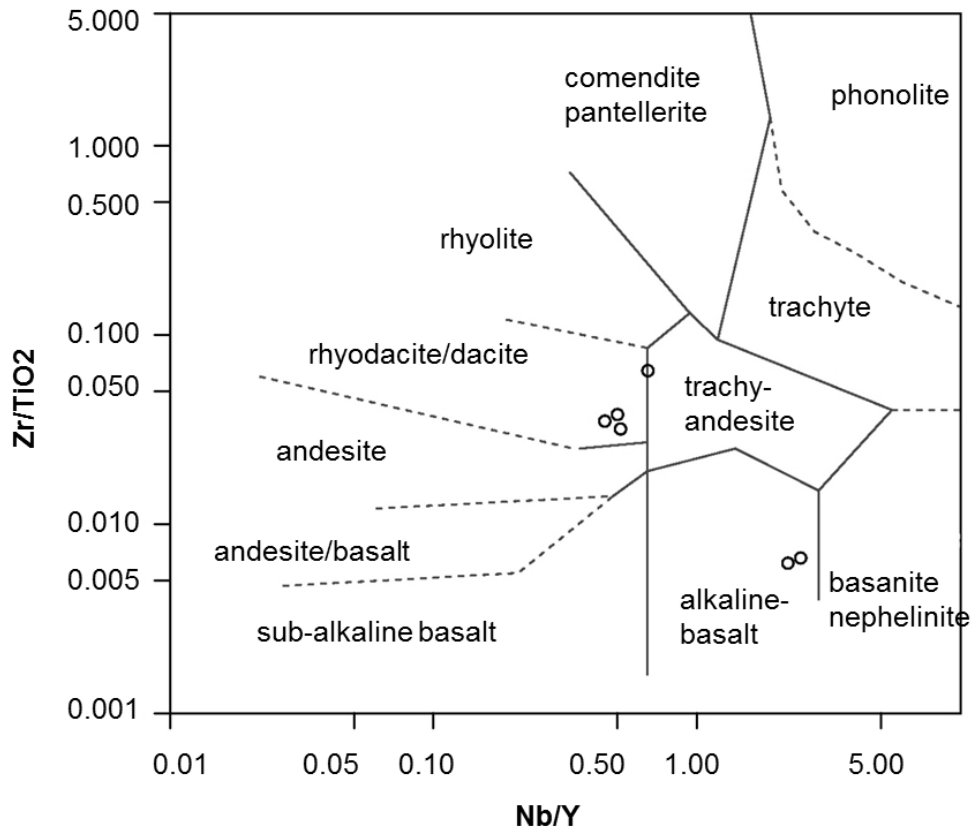

Figure 2.6 Nb/Y vs. Zr/TiO2 classification diagram for volcanic rocks (Winchester and Floyd, 1977) using pressed pellet analyses. The mafic dike samples plot as alkali basalt, Mystery pluton and felsic dikes as rhyodacite/dacite.

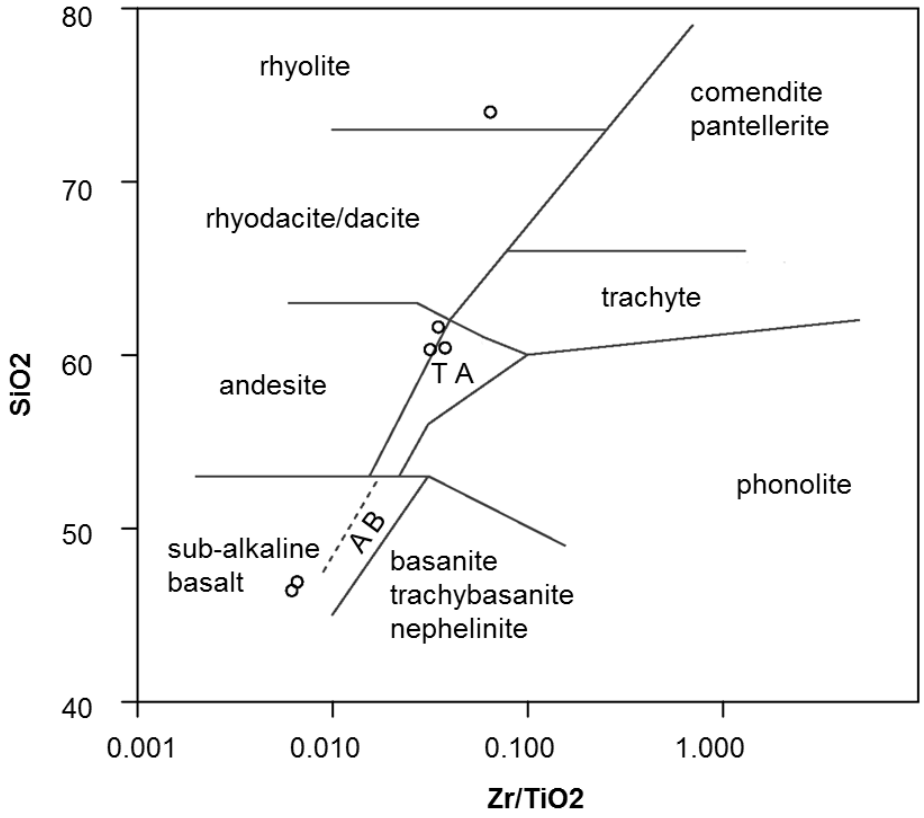

Figure 2.7 Zr/TiO2 vs. SiO2 classification diagram for volcanic rocks (Winchester and Floyd, 1977) using the pressed powder analyses. TA = trachy-andesite, AB = alkali basalt. The mafic samples plot as sub-alkalic basalt; Mystery pluton as andesite/trachy-andesite; and the felsic dike as rhyolite.

Tectonic setting diagrams for the felsic-intermediate rocks seemingly indicate different tectonic origins for the two types at Nixon Fork (**Figure 2.8** and **Figure 2.9**). Using both Rb vs. Y + Nb and Nb vs. Y schemes the Mystery pluton (barely) plots in the 'within-plate granite' field whereas the felsic dike sample plots (barely) in the 'volcanic arc granite' field.

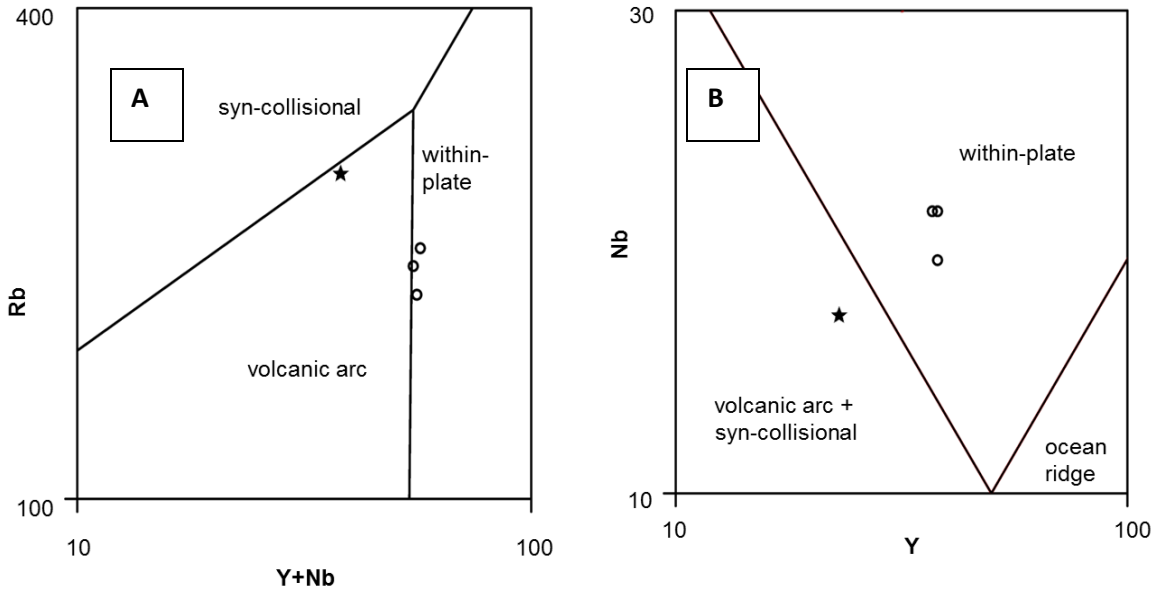

Figure 2.8 Felsic rock tectonic discrimination diagrams from Pearce and others (1984) using pressed pellet XRF data. Circle = Mystery pluton, star = felsic dike. In both cases the Mystery pluton plots as 'within plate' and the felsic dike as 'volcanic arc.' 2.8A: Y+Nb vs. Rb 2.8B. Y vs. Nb

Tectonic setting diagrams based on immobile elements for mafic rocks (**Figure 2.9** and **Figure 2.10**) consistently yield a 'within-plate' classification for the mafic dikes. I have added data from Newberry (written communication, 2012)(**Table 2.5**) for slab XRF Nb-Y-Zr-TiO_2 and Szumigala (1993) for conventional XRF Y-Zr-TiO_2 data to my data on these diagrams. They clearly show that the tectonic setting for the more mafic rocks of the Mystery pluton (Volcanic arc) is quite different from that of the mafic dikes.

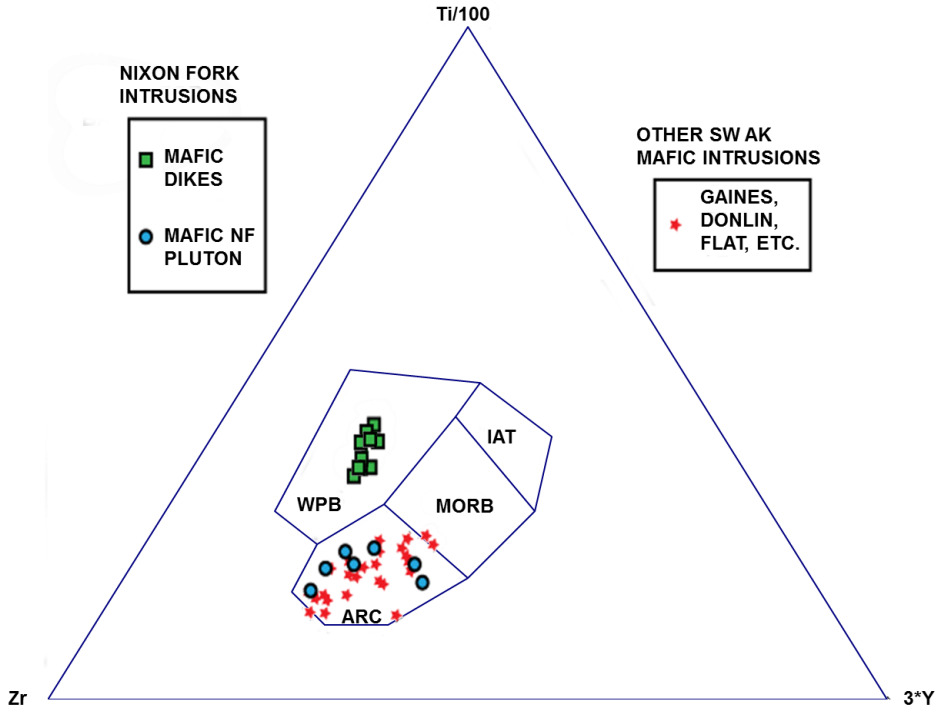

Figure 2.9 Pearce and Cann (1973) tectonic discrimination diagram showing the composition of the mafic portions of the Mystery pluton versus the composition of mafic dikes present at Nixon Fork and elsewhere in southwest Alaska. WPB= within-plate basalt, IAT= island arc tholeiite, MORB= mid-ocean ridge basalt, ARC =volcanic arc basalt. The mafic dikes plot in a completely different field from the mafic portions of the Mystery pluton. Data from (Szumigala, 1993); Newberry, written communication (2011), and this study.

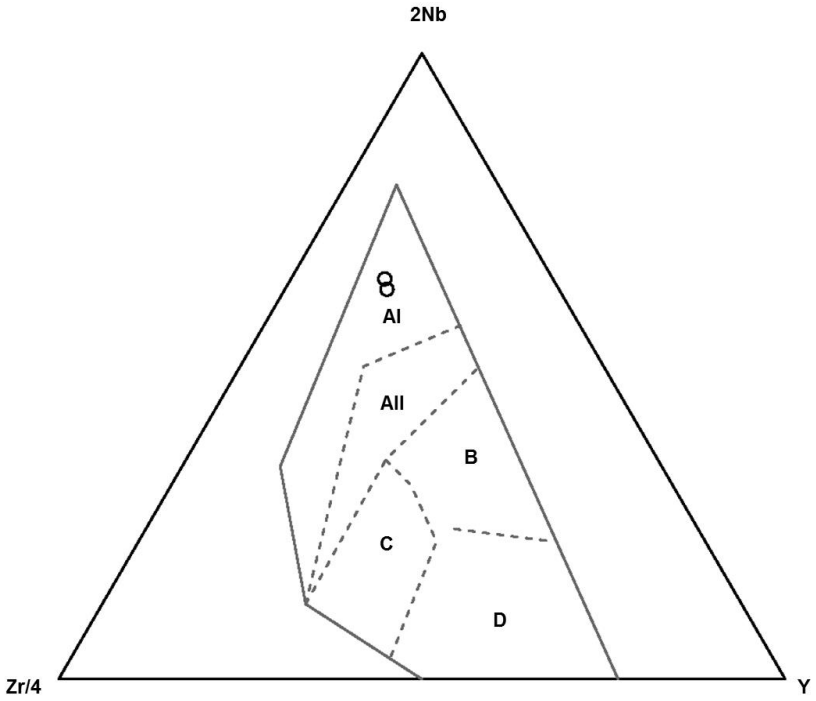

Figure 2.10 Mafic tectonic discrimination diagram (Meschede, 1986) with pressed pellet XRF data from the mafic dikes. AI =within-plate alkali basalt, AII =within-plate alkalai basalt + within-plate tholeiite B= E-type MORB; C =within-plate tholeiite + island-arc basalt, D =N-type MORB + island-arc basalt. The dike samples plot in the within-plate alkali basalt field.

Table 2.5 Additional mafic dike polished slab measurements (Newberry, written communication, 2011).

wt%	U12-3.4MF_DK	07U-88-4.5	09SM-U03-ALTD	09SM-U03-UN	BP-FLOODED	BP-RAMP	09SM-056-altd	09SM-56#2
SiO2	48.2	49.2	46.3	48.0	48.6	47.6	47.4	47.2
TiO2	2.5	2.5	2.7	2.5	2.4	2.5	2.6	2.7
ppm								
Nb	66	56	56	59	63	63	52	53
Zr	193	177	163	182	187	184	148	146
Y	27	26	26	29	26	27	21	22

2.3 Discussion

XRF chemical analyses of the polished slabs and the pressed pellets give broadly similar results (**Figure 2.1** and **Figure 2.2**, **Table 2.3**) for most elements and most samples. Among the major elements the lighter elements Na and Mg appear to yield the most discordance, especially where either is present in small abundance (**Table 2.3**). This is likely due to the extremely small penetration distance for the lighter X-rays (microns), and consequently their extreme sensitivity to the micro-topography of the analyzed surfaces. The exception to this generalization is Fe, which was consistently 5-40% higher in the pressed pellets than the associated polished slabs. I don't understand this discordance. However, because Fe is not employed (except in an indirect way) in any of the classification schemes, this discrepancy does not affect the rock classification.

More puzzling is the discordance in trace element analyses between the slabs and pressed pellets for the intermediate-composition rocks (**Table 2.3**). Measured concentrations of Y, Zr, and Nb in the pressed pellets are 20-50% higher than the associated polished slabs. These are enormous and basically inexplicable. Conversely, measured concentrations of these elements for the mafic pellets are only about 5% lower than in the polished slabs. These differences are sufficiently small to be considered negligible.

In sum, polished slabs, especially for fine-grained rocks and major elements, appear to be suitable for semi-quantitative XRF analyses. Such are sufficiently accurate to provide at least rock classification. Trace element analyses appear to be more sensitive to grain size

and (or) rock major element composition: they are certainly suitable for fine-grained, mafic rocks.

Table 2.6 Names and classifications of Nixon Fork rocks using various schemes. Italicized schemes are for volcanic rocks; normal font for plutonic rocks.

Rock Classification	**Figure**	Main1-PP	Main2-PP	Main3-PP	Felsic-PP	Mafic1-PP	Mafic2-PP
Streckeisen and Le Maitre (1979)	3	quartz monzonite	quartz monzodiorite		Granite		
De la Roche and others (1980)	4	Tonalite			Granite	alkali gabbro	
Total Alkalai vs. Silica	*5*	*trachy-andesite*			*Rhyolite*	*tephrite*	*trachy-basalt*
Winchester and Floyd (1977)	*6*	*rhyodacite /dacite*			*rhyodacite dacite*	*alkali basalt*	
Winchester and Floyd (1977)	*7*	*trachy-andesite*	*andesite*		*Rhyolite*	*sub-alkalic basalt*	
Geotectonic Classification	**Figure**	Main1-PP	Main2-PP	Main3-PP	Felsic-PP	Mafic1-PP	Mafic2-PP
Pearce and others (1984)	8	arc/within plate boundary			volcanic arc		
Pearce and others (1984)	9	within plate			arc/syn-collision		
Pearce and Cann (1993)	10					within-plate	
Meschede (1986)	11					within-plate alkali	

The various major and minor element schemes for igneous rock identification give at best overlapping names for the three Mystery Creek pluton samples (**Table 2.6**). In large part this is due to different names for volcanic rocks and plutonic rocks of the same composition. Two of the 3 schemes that give volcanic rock names identify the samples as intermediate alkalic, i.e., quartz-poor. Similarly, via the normative scheme the pluton samples are classified as quartz monzonite and quartz monzodiorite. In contrast, the R1-R2 scheme classifies the samples as tonalite, i.e., non-alkalic. The differences highlight the lack of a generally accepted compositional-based classification for plutonic rocks.

CIPW normative mineralogy can approximate the actual modal mineralogy for rocks that lack amphibole, biotite, and alkali feldspar. This is because (a) the norm calculation assumes all mafic minerals are anhydrous and (b) albite component in real rocks is divided between plagioclase and alkalai feldspar in a manner that cannot be predicted. The mafic mineral problem is illustrated by the reaction:

$2CaMgSi_2O_6$ + $3MgSiO_3$ + SiO_2 + H2O = $Ca_2Mg_5Si_8O_{22}(OH)_2$

(clinopyroxene) (orthopyroxene) (quartz) (amphibole)

That is, depending on its precise composition a normative amphibole could be constructed from a combination of normative pyroxenes plus quartz. Similarly, the CIPW norm takes all Fe_2O_3 and turns it into normative magnetite, instead of combining the iron with SiO_2 to make an iron silicate. In other words, for an amphibole-bearing and magnetite absent igneous rock (such as the Nixon Fork main phase) the calculated normative quartz content is higher than the actual amount of quartz in the rock.

Consequently, the normative scheme can only prove an approximate name for a typical intermediate or felsic composition igneous rock.

On the other hand, the R1-R2 scheme is entirely empirical, built around a linear combination of compositional variables that appear to best predict modal-based igneous rock names for a large dataset. It is presumably more useful for discriminating varieties of mafic and extremely alkalic than 'normal' felsic rocks, which occupy only a small portion of the diagram.

Previous workers have (based on some combination of thin section and hand specimen examination) described the pluton at Nixon Fork as monzonite (Brown, 1925, Cutler, 1994), quartz monzonite (Herreid, 1966, Cutler 1994), monzodiorite, and quartz monzodiorite (Cutler, 1994). Such indicates that the R1-R2 scheme—at least in this case—does not yield an appropriate rock name whereas the CIPW normative one does. However, an appreciable fraction of the 21 plutonic samples analyzed by Cutler (1994) contained low modal quartz and were classified as monzonite or monzodiorite, whereas all of my samples contained appreciable (> 10%) normative quartz. Likely reasons for this discordance include the norm calculation problems outlined above, the possibility that some fine-grained quartz was overlooked during examination, and possibility that my 3 samples were not representative of the pluton's compositional range.

2.4 Conclusions

Correspondence between pressed powder pellets and polished slabs is generally better for the mafic dike than for other rocks, presumably due to the fine grain size in the mafic

rock more closely approximating the pressed powder pellets. Felsic polished slabs don't match pressed powder pellets on Zr, Nb, and Y very closely, possibly due to these elements concentrating in minerals that might not be exposed on a polished slab.

The Mystery pluton and the felsic dikes plot in distinct separate groups on normative, TAS and Nb/Y vs. Zr/TiO_2 diagrams, indicating truly different compositions and possibly different origins. The appropriate name for the plutonic rocks varies with the classification scheme, however the felsic dike always plots as granite or rhyolite. Based on my limited samples, the bulk of the Mystery pluton is probably quartz monzonite and quartz monzodiorite and likely contains less than 20% quartz.

The mafic dikes are best classified as alkali basalt and appear to represent a different magmatic setting from that of the pluton. Data plotted on the Pearce and Cann (1973) geotectonic diagram suggests the Mystery pluton is due to convergent subduction magmatism, while the mafic dikes are the result of within-plate extensional magmatism. That is, rather than representing bi-modal magmatism, the mafic and felsic dikes simply represent different tectonic settings and origins.

The Mystery pluton has been described with a range of compositions, confirmed by my samples. The felsic dikes are consistently more felsic than the Mystery pluton, but usually within the compositional range of granite or rhyolite, and the mafic dikes are different varieties of basalt. Given these variations, I employ generalized (e.g., 'pluton') instead of specific (e.g., 'quartz monzonite') terms in referring to the igneous rocks.

3 Radiometric Dating

3.1 Introduction

Is the Mystery pluton the source of the Nixon Fork skarn? While this has long been the assumption, skarn is restricted to one small part of the pluton/marble contact (e.g. **Figure 1.3**) which is odd if the pluton was the source. However, if the skarn formed due to fluids derived from the Mystery pluton, the skarn and Mystery pluton should yield the same radiometric age. I tested the hypothesis of similar age using $^{40}Ar/^{39}Ar$ geochronology Most samples were located in the general area of the Crystal Garnet decline, broadly associated with mineralization (**Figure 3.1**).

3.2 The $^{40}Ar/^{39}Ar$ Dating System

The $^{40}Ar/^{39}Ar$ dating system is an extension of the K-Ar dating system. The $^{40}Ar/^{39}Ar$ dating technique requires converting ^{39}K to ^{39}Ar in a nuclear reactor, and then using a mass spectrometer to determine the relative abundances of the different Argon isotopes (Mitchell, 1968; Dickin, 2005). The age is determined using the equation $t = \frac{1}{\lambda}\ln(J \times R + 1)$ where J is the irradiation parameter, R is the $^{40}Ar/^{39}Ar$ ratio and λ is the decay constant of ^{40}Ar (Mitchell, 1968). Corrections are made for interferences from isotopes produced in the reactor (McDougall and Harrison, 1999).

The sample is step-heated in the laboratory, a process in which incrementally more argon migrates out of the mineral (Merrihue and Turner, 1966). A plateau age represents three or more consecutive step-heat fractions constituting 50% or more of the argon released

and is generally considered the mineral 'age'. Deviations from a plateau are interpreted as either due to to argon loss or gain or to multiple minerals in the sample. Isochron analysis can also identify cooling ages of mineral phases. The initial argon ratio is used to identify excess argon or argon loss events (Dickin, 2005), thus recording a variation in age.

Mineral irradiation also produces ^{38}Ar and ^{37}Ar from ^{37}Cl and ^{40}Ca, respectively. $^{37}Ar_{Ca}/^{39}Ar_K$ and $^{38}Ar_{Cl}/^{39}Ar_K$ can be used as a proxy for the relative calcium and chlorine concentrations in a mineral, and I use them as clues to the mineralogy of the samples and to identify different mineral phases.

3.3 Sample selection

In all, 11 samples were chosen for dating (**Table 3.1, Figure 3.**1). The chosen minerals have a range of closure temperatures to allow for a better assessment of the thermal history of the deposit. For this study, the following closure temperatures were used: hornblende; 450-500 °C (Harrison, 1981), biotite; 350-400 °C (Reiners and others, 2005), phlogopite; ~ 450 °C (Reiners and Brandon, 2006), sericite; 350 °C (McDougall and Harrison, 1999); scapolite 300 to 150 °C (McDougall and Harrison, 1999; Kendrick and Phillips, 2009). A “whole rock” sample was dated from a mafic dike. This consists of small chips of phenocryst-poor microcrystalline groundmass. Because the sample is polyphase and the K-bearing phases are not known, no specific closure temperature for this sample could be assigned.

Table 3.1 $^{40}Ar/^{39}Ar$ and K-Ar ages for the Nixon Fork Deposit, including those from previous studies

Sample Number	Rock Type[1]	Mineral[2]	Plateau age ± one sigma	Integrated age ± one sigma	Comments
11BP03HO	Skarn	hornblende	68.7 ± 1.1 Ma		N04U109
11BP02PHLOG	Skarn	phlogopite	67.4 ± 0.6 Ma		Whalen Prospect
11BP01SER	QSP altered Mystery pluton	Sericite	68.0 ± 0.5 Ma		N04U080 20.30
09BP-SCAP	Skarn	scapolite	72.6 ± 0.5 Ma		07 Drill hole
09NF-FL	Mafic dike	whole rock	62 ± 0.2 Ma		170 level
09NF-PHL	Skarn	phlogopite	67.6 ± 0.3 Ma		Mystery Prospect
09BPSkar Hb	Skarn	hornblende	68.9 ± 0.4 Ma		Mystery Prospect
N07U33 11.2 Hb	Mystery pluton	hornblende	68.1 ± 0.3 Ma		DH N07U33
N07U33 11.2 Hb	Mystery pluton	hornblende	68.3 ± 0.4 Ma		DH N07U33
N07U33 11.2 Bi	Mystery pluton	biotite		68.7± 0.3 Ma	DH N07U33
09 RN 050 A Bi	Felsic dike	biotite		68.6 ± 0.3 Ma	Runway dikes
09NFBPSER	QSP altered Mystery pluton	sericite	70.3 ± 0.3 Ma		DH N05-17
Moll and others (1981)	Mystery pluton	biotite		68.6 ± 2.0 Ma	K-Ar age
Moll and others (1981)	Mystery pluton	biotite		70.4 ± 2.1 Ma	K-Ar age
Moll and others (1981)	QSP altered Mystery pluton	sericite		69.1 ± 2.1 Ma	K-Ar age
Unpublished	Skarn	phlogopite	68.1 ± 0.3 Ma		
Unpublished	Skarn	hornblende	67.6 ± 0.3 Ma		

Notes: [1] QSP = quartz-sericite-pyrite; [2] sericite = fine-grained white mica

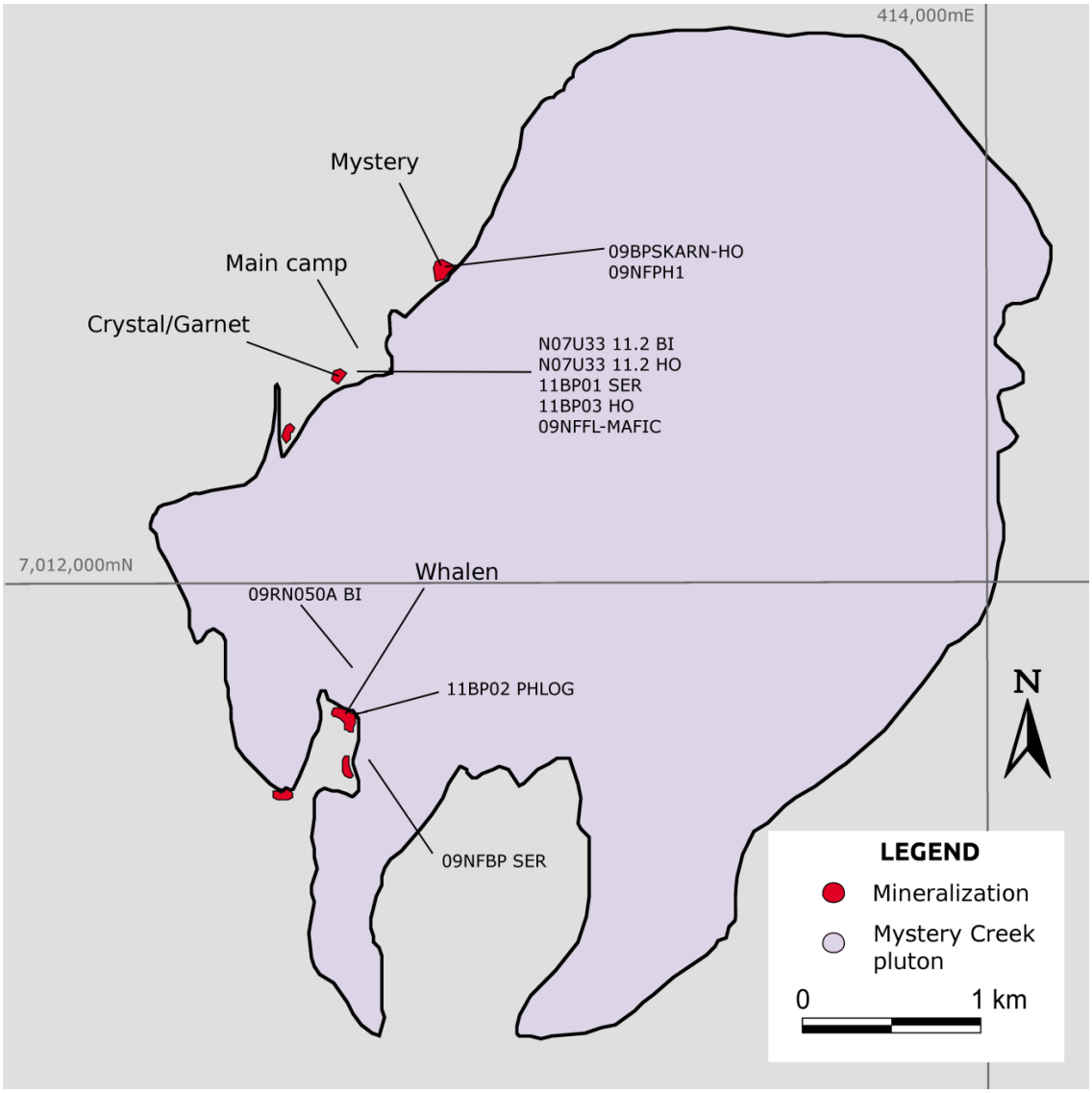

Figure 3.1 Approximate locations of samples submitted for radiometric dating from Nixon Fork. Locations are accurate within 100 m and include both surface and sub-surface samples. NAD 27, zone 5 UTM coordinates.

Although geochronologists prefer to use plateau ages to characterize cooling ages, plateau ages from biotite can be unreliable due to variable instability during heating in vacuo (Gaber and others, 1988). Some workers consider biotite $^{40}Ar/^{39}Ar$ integrated ages

as more reliable indicators of time elapsed since Ar closure (Tc; ~350 °C to ~400 °C; Reiners and others, 2005). The integrated age is the mean of all steps weighted by the amount of ^{39}Ar released per step.

In addition to problems associated with individual phases, mineral separation has proven problematic. For example, complex pyroxene-hornblende-biotite intergrowths (**Figure 3.2**) characterize much of the Mystery pluton, making it impossible to create pure igneous biotite and hornblende separates. **Figure 3.2** shows magmatic pyroxene surrounded by biotite and a later rim of amphibole, indicating initially water-undersaturated mineral growth with increasing H_2O fugacity during crystallization. Similarly, a skarn hornblende separate invariably contains at least a small amount of precursor clinopyroxene.

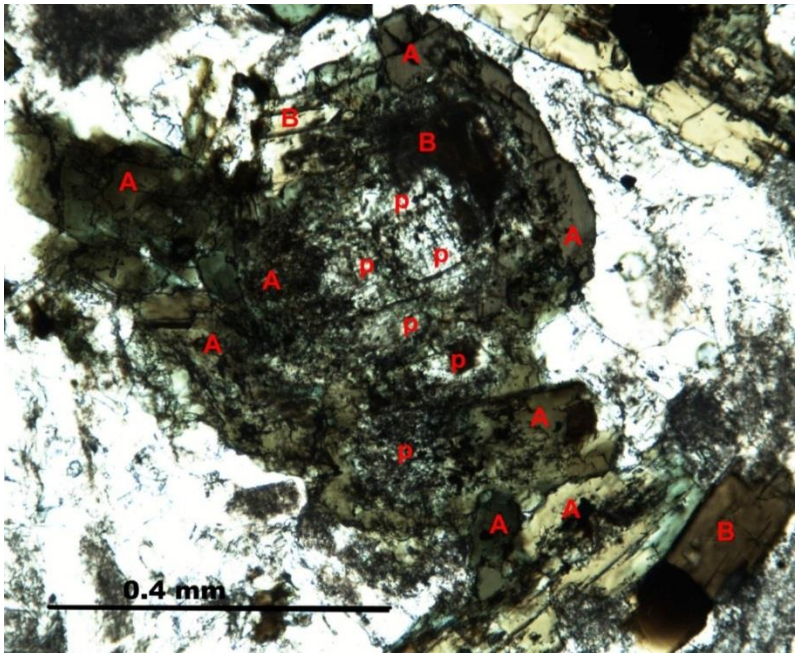

Figure 3.2 Plane polarized light photomicrograph of a mafic clot in the Mystery pluton. P = pyroxene, A = hornblende, B = biotite.

3.4 Results

3.4.1 Skarn ages

Sample 09BP SkarHb (**Figure 3.3**) yields a plateau (5 fractions representing 83.6% of ^{39}Ar released) at 68.9 $\pm$ 0.4 Ma. The initial fractions have very high Ca values, probably the result of calcite in the sample. The third from last fraction in all the spectra shows a drop, followed by a rise in age and Ca/K and eventually a small drop in Cl/K. The drop in age is correlated with lower Ca/K and Cl/K values and may reflect degassing of a non-hornblende inclusion.

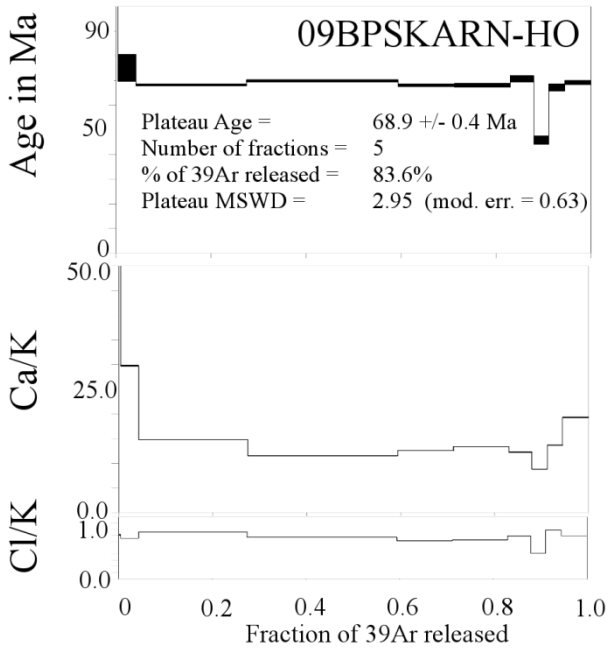

Figure 3.3 09BPSkarHb ^{40}Ar/^{39}Ar age, Cl/K, and Ca/K spectra

Sample 11BP03HO (**Figure 3.4**) yields a good plateau (3 fractions representing 85.1% of ^{39}Ar released) at 68.7 $\pm$ 1.1 Ma. The Ca/K spectrum has an initial spike, most likely from calcite inclusions, and a final spike that is likely due to admixed pyroxene.

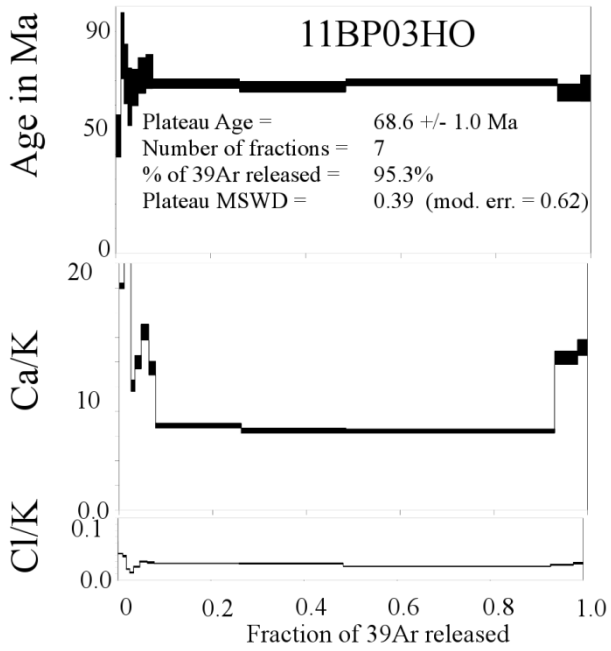

Figure 3.4 11BP03HO $^{40}Ar/^{39}Ar$ age, Cl/K, and Ca/K spectra.

Sample 09NFPH1 (**Figure 3.5**) displays a plateau (4 fractions representing 79.8% of ^{39}Ar released) at 67.6 $\pm$ 0.3 Ma. The high initial Ca/K fractions are likely the result of calcite contamination in the sample. The straightforward age spectrum suggests that the age is a highly reliable one.

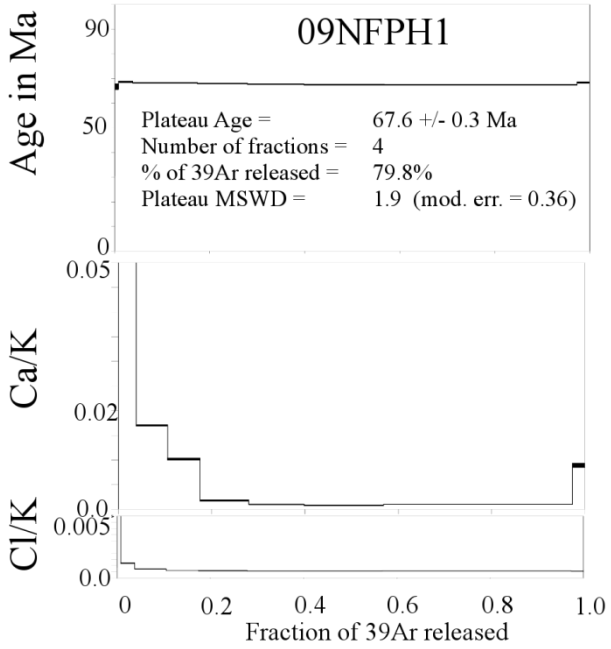

Figure 3.5 09NFPH1 $^{40}Ar/^{39}Ar$ age, Cl/K, and Ca/K spectra.

Sample 11BP02PHLOG (**Figure 3.6**) yields a well-defined plateau (5 fractions representing 89.8% of ^{39}Ar released) at 67.4 $\pm$ 0.6 Ma. The second half of the Ca/K spectrum shows a slight increase in Ca/K (~0.01 to ~0.03), most likely due to contamination with a small amount of a high-Ca silicate mineral.

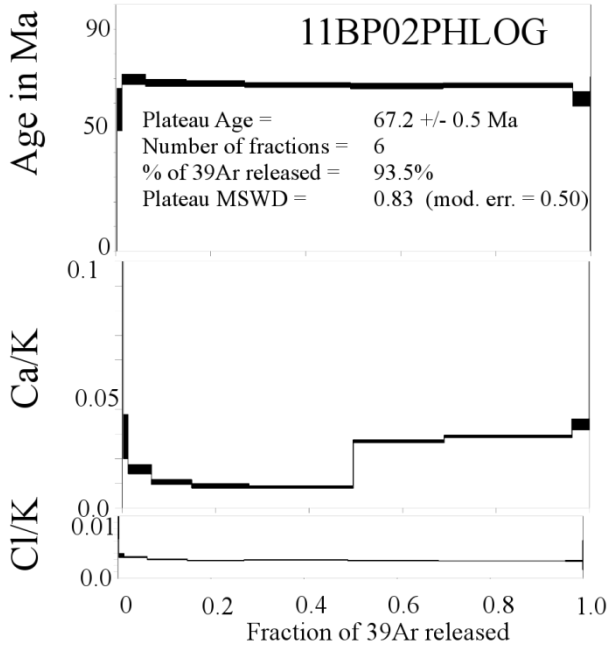

Figure 3.6 11BP02PHLOG $^{40}Ar/^{39}Ar$ age, Cl/K, and Ca/K spectra.

Sample BP Scap (**Figure 3.7**) yields an apparent plateau age of 72.6 ± 0.5 Ma (6 fractions representing 68.3% of ^{39}Ar released). Isochron analysis shows some evidence of excess argon with an 8-fraction initial $^{40}Ar/^{36}Ar$ ratio of 311 ± 7 and an isochron age of 72.5 ± 0.5 Ma. The $^{40}Ar/^{36}Ar$ ratio for atmosphere is approximately 295.5, and while ^{40}Ar in excess of this is used to calculate radiogenic argon, too high of a ratio can indicate argon inherited from another source. Of note are the high Ca/K and Cl/K ratios associated with the high temperature fractions, approximately 40% of the Ar released (**Figure 3.7**).

The ratios from the lower-temperate fractions are not compatible with scapolite, a high Ca- and Cl- mineral, and indicate that approximately 40% of the Ar released from this sample was not derived from scapolite. A candidate contaminant is alkali feldspar, which has a lower Ar release temperature than scapolite, very low Ca/K and Cl/K ratios, and a

similar appearance to scapolite. That is, scapolite containing a few percent feldspar inclusions would not be readily recognized. A plausible alternative explanation is that the low Ca/K and Cl/K phase is muscovite, a potential alteration product of the scapolite, although muscovite has a higher Ar-release temperature than scapolite. Whatever the contaminant, Ar released from it yields apparent ages older than the plateau (**Figure 3.7**) suggesting that this phase is responsible for an incorrectly 'old' apparent age for the sample.

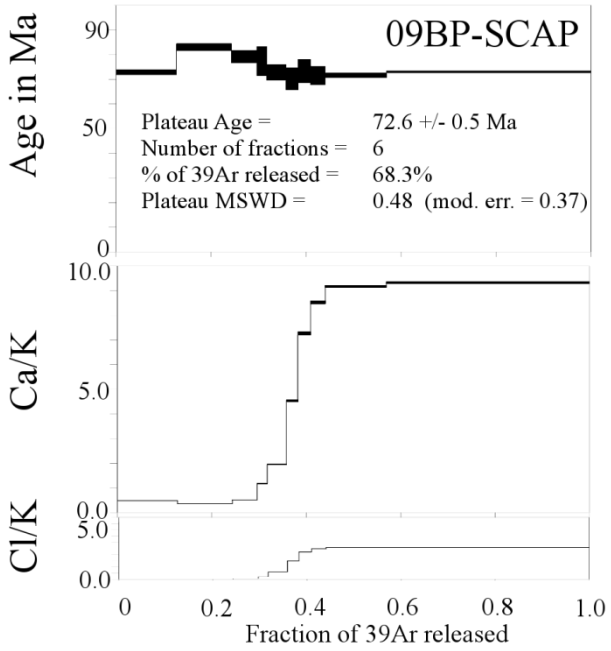

Figure 3.7 BPScap $^{40}Ar/^{39}Ar$ age, Cl/K, and Ca/K spectra.

In contrast, Mrozek (2012) after treating her skarn scapolite samples with mild acid to remove calcite, obtained Ar spectra with more than 90% of the Ar exhibiting the high Ca/K and Cl/K ratios indicative of scapolite. Isochrons for these samples did not yield anomalous $^{40}Ar/^{36}Ar$ initial ratios and the Ar age spectra did not display an increase in apparent age in the lower temperature fractions (Mrozek, 2012).

In sum, the anomalous $^{40}Ar/^{36}Ar$ ratio derived from the isochron, the fact that nearly half of the Ar released from the sample was derived from an unknown K-rich mineral, and the anomalously old apparent ages derived from this phase makes me suspicious of the calculated age for the sample. Most likely it contains "excess" argon and the plateau age is older than the true geologic age.

3.4.2 Pluton ages

Sample N07U33 11.2 Hb 1st run (**Figure 3.8a**) yields some variability in the first five heating steps (10.6% cumulative ^{39}Ar) and a plateau (9 fractions representing 89.5% of ^{39}Ar released) at 68.1 $\pm$0.3 Ma. The Ca/K and Cl/K spectra are similar, with highest values associated with moderate temperature fractions. The plateau is very flat and the uncertainty in this and the second run is quite low ($\pm$ 0.3-0.4 Ma, **Figure 3.8**).

Sample N07U33 11.2 Hb 2nd run (**Figure 3.8b**) yields some variability in the first five heating steps (18.9% cumulative ^{39}Ar) and a plateau (8 fractions representing 81.1% of ^{39}Ar released) at 68.3 $\pm$0.4 Ma. The Ca/K and Cl/K spectra for this sample do not exhibit the pronounced low K 'peaks' at intermediate release temperatures exhibited by the 1st run, making a consistent interpretation problematic. One possibility, suggested by the anomalous apparent ages from the low-temperature fractions, is that the lower-temperature fractions are contaminated by a small amount of biotite. Such seems feasible, given the complex biotite-hornblende intergrowths commonly present in the pluton, e.g., **Figure 3.2**. In contrast, the hornblende might possess compositional zoning, with higher-

K portions releasing Ar at the highest temperatures. Whatever the cause, these variations have minor impact on the calculated age. The ages given by the two runs are basically identical.

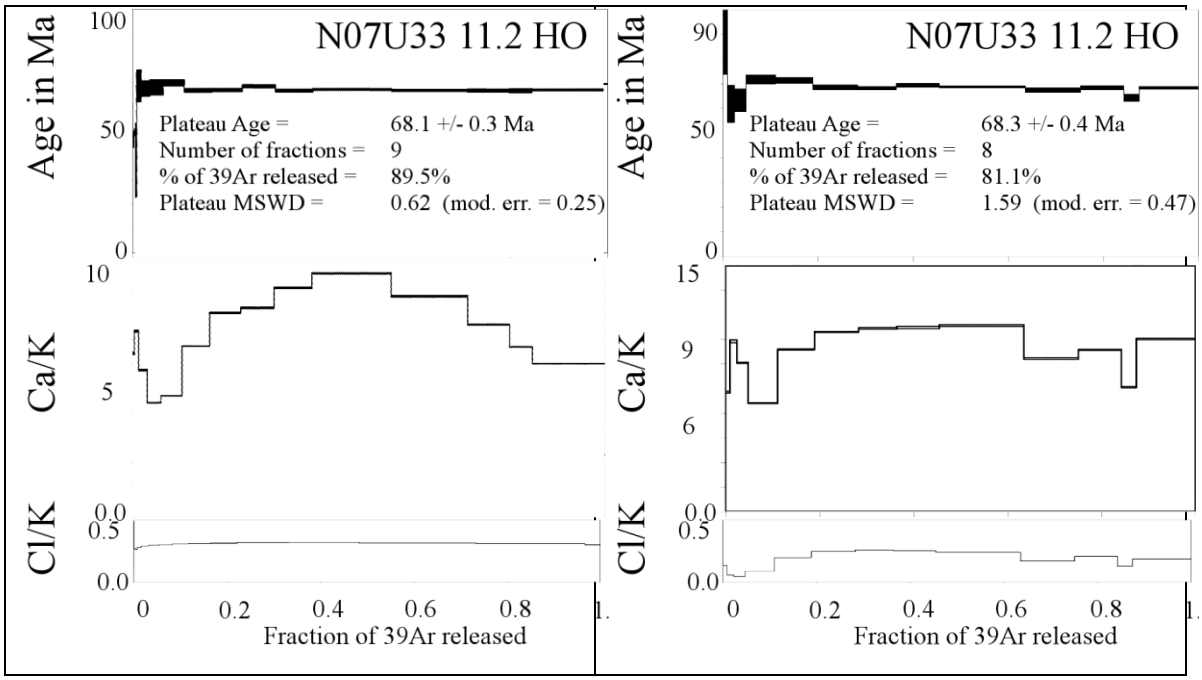

Figure 3.8 N07U33 11.2Hb 2 runs $^{40}Ar/^{39}Ar$ age, Cl/K, and Ca/K spectra.

Sample N07U33 11.2 Bi (**Figure 3.9**) shows an age spectrum with an integrated age of 68.7 $\pm$ 0.3 Ma. Because there is some evidence of Ar loss, this integrated age is probably a minimum age for the mineral. The Ca/K ratio of approximately 0.3 indicates significant mineral contamination because biotite does not contain appreciable Ca (c.f., spectra from the skarn phlogopite, **Figure 3.5**, **Figure 3.6**). For hornblende with atomic Ca/K of about 9 (1% K_2O, 11% CaO) and biotite with 10% K_2O, a mixture of 25% hornblende and 75% biotite would give rise to an atomic Ca/K of 0.3. Again, such seems reasonable given the

complex igneous biotite-hornblende intergrowths (**Figure 3.2**). Because both biotite and hornblende contain Cl, the relatively flat Cl/K spectrum gives no information about the mineral mix.

The biotite age (68.7 $\pm$ 0.3) is older than the hornblende age (68.3 $\pm$ 0.4) from the same sample, but not significantly older. Because biotite has a lower Ar-closure temperature than hornblende it ought to yield a younger age than hornblende from the same sample—as shown for the skarn phlogopite and hornblende (**Table 3.1**). The situation is complicated by the presence of significant hornblende in this sample. At face value, however, either the hornblende age is anomalously young or the pluton cooled sufficiently quickly that the time required to cool from hornblende to biotite closure temperatures was within the analytical uncertainties.

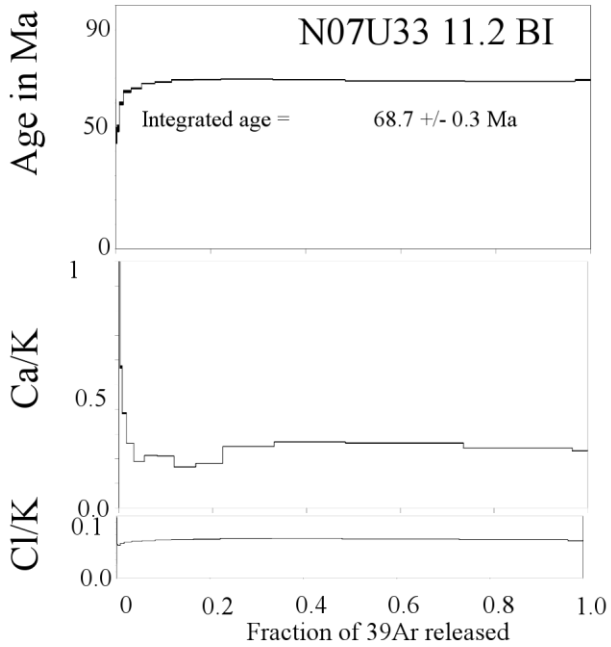

Figure 3.9 N07U33 11.2Bi $^{40}Ar/^{39}Ar$ age, Cl/K, and Ca/K spectra

Sample 11BP01SER (**Figure 3.10**) yielded younger ages in the initial fraction and a plateau (6 fractions representing 73.5% of ^{39}Ar released) of 68.0 $\pm$ 0.5 Ma. The isochron age of 67.3$\pm$ 0.6 Ma is younger, but not significantly so. The Cl/K ratio is mostly below 0.001, a reasonable value for white mica. The Ca/K ratios rise from 0.1 on the first fraction to 19 on the third fraction and irregularly declines for the rest of the run. Because white mica contains essentially no Ca, these results require that the material dated is a mix of white mica with a Ca-rich phase. The logical mineral is calcite, which is commonly associated with sericite at Nixon Fork. Given the average Ca/K ratio of about 5, the mixture dated is approximately 50% calcite.

A disturbing aspect of this spectrum is that, neglecting the two lowest-temperature fractions, the apparent ages generally decrease with fraction temperature and with Ca/K ratio. That is, the higher the Ar release temperature, the smaller the amount of Ar released from calcite and the younger the calculated age (**Figure 3.11**). In fact, the highest-temperature fraction yielded one of the younger ages and was not used in calculating the plateau age. Since the reliability of an age should increase with decreasing contamination, the highest-temperature, lowest-Ca/K fractions aught to yield the most reliable age: one closer to 66 Ma than to the plateau age of 68 Ma. Thus, due to the extensive mineral contamination and to the odd age spectrum, the plateau age is not terribly reliable.

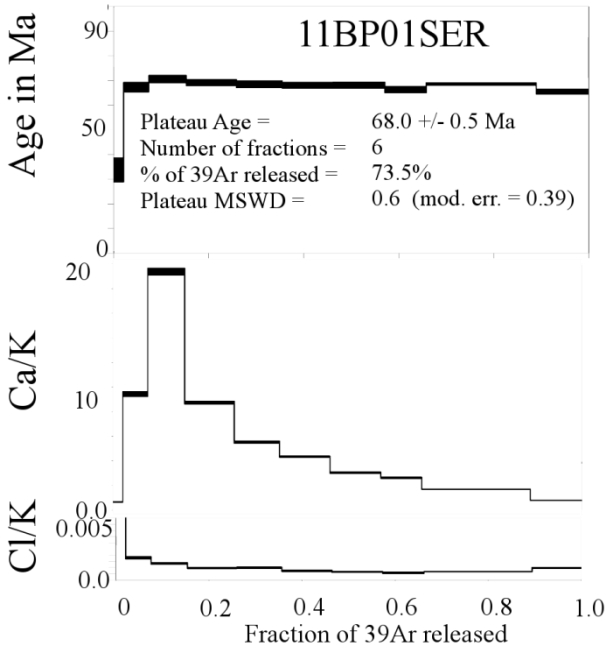

Figure 3.10 11BP01SER $^{40}Ar/^{39}Ar$ age, ClCa/K, and Ca/K spectra.

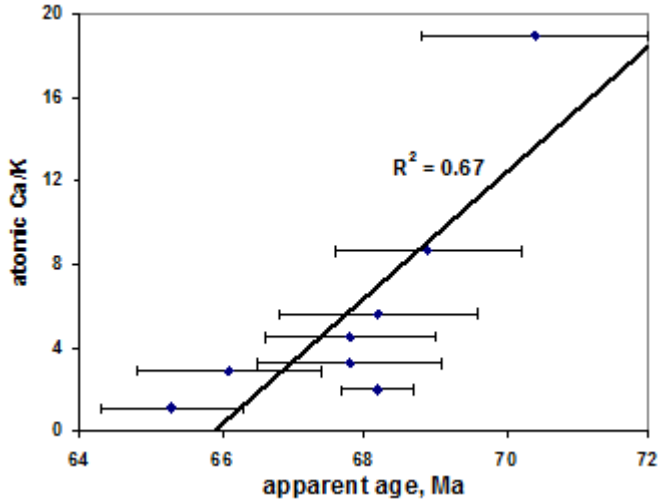

Figure 3.11 Apparent age vs. atomic Ca/K for all but the two lowest-temperature fractions of 11BP01Ser

Sample 09NFBPSER (**Figure 3.12**) yields Ar loss and a plateau (10 fractions representing 91.4% of ^{39}Ar released) at 70.3 $\pm$ 0.3 Ma. The Ca/K, Cl/K, and age spectrum plots all show an Argon loss event in the first three steps.

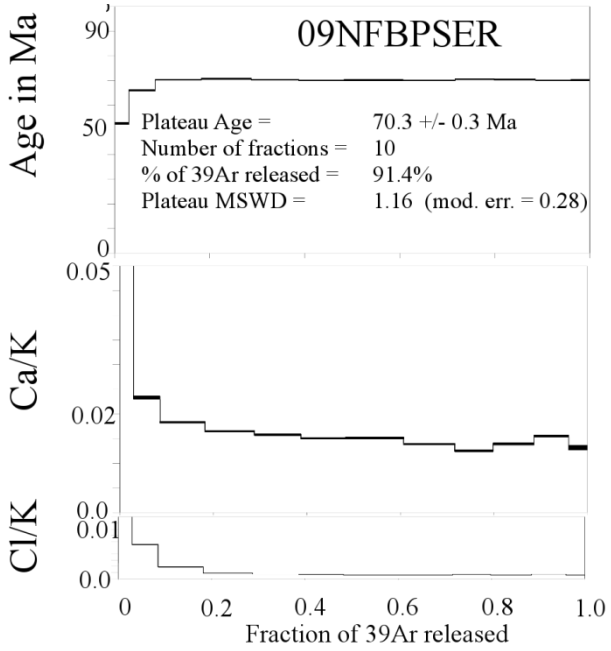

Figure 3.12 09NFBPSER ^{40}Ar/^{39}Ar age, Cl/K, and Ca/K spectra.

Unfortunately, although this appears to be one of the 'cleanest' spectra, showing essentially no mineral contamination, and no systematic change in age with Ar release temperature, the plateau age is significantly older than any of the ^{40}Ar/^{39}Ar ages for the host pluton (**Table 3.1**). That is, the alteration happened before the host pluton crystallized. The geologic impossibility of such indicates that either this age is anomalously old (of unknown reasons) or that the pluton hornblende and biotite ages are

anomalously young. The latter possibility is consistent with the anomalously young hornblende versus biotite ages from the pluton.

3.4.3 Mafic dike age

Sample 09NF FL (**Figure 3.13**) yields an argon loss event and a plateau (4 fractions representing 45.3% of ^{39}Ar released) at 62.2 $\pm$ 0.2 Ma. The whole rock Ca/K spectrum shows a high initial Ca value, most likely due to alteration related calcite. The Ca/K graph stair steps up, likely due to Ca-pyroxene in the sample.

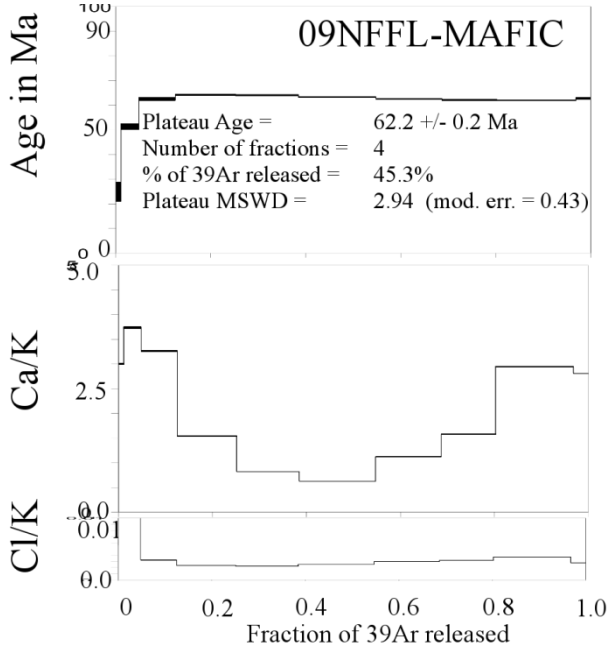

Figure 3.13 09NFFL ^{40}Ar/^{39}Ar age, Cl/K, and Ca/K spectra

3.4.4 Felsic dike age

Biotite sample 09RN050A (**Figure 3.14**) yielded a problematic age spectrum which displays Ar loss at low temperatures and no plateau. The integrated age of 68.6± 0.3 Ma is consequently a minimum age for the sample. The Ca/K ratios for this sample mostly climb from essentially zero to about 0.12; the Cl/K ratios remain constant at very low values. Since biotite contains no Ca, the upward-stepping Ca/K ratios indicate a very small amount of contamination from a Ca-bearing phase with a high-temperature release. Possible candidates are apatite and plagioclase, either or both of which could be present as micro-inclusions in the magmatic biotite.

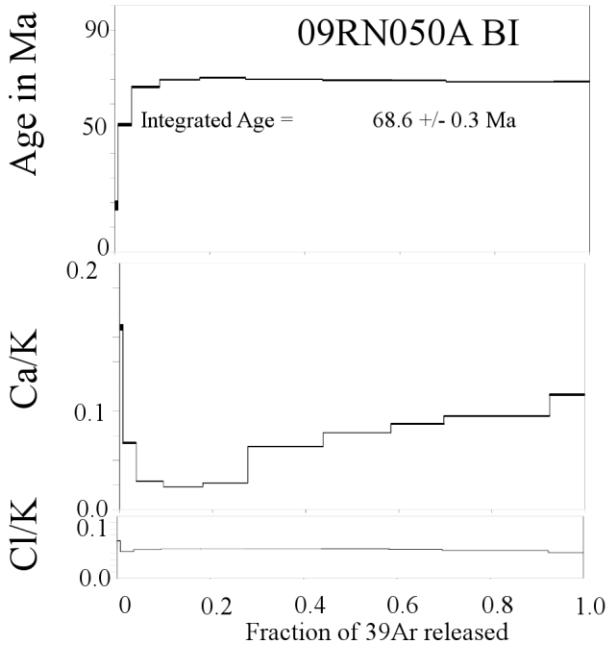

Figure 3.14 09RN050A $^{40}Ar/^{39}Ar$ age, Cl/K, and Ca/K spectra.

Close examination of the age spectrum (**Figure 3.15**) for biotite 09RN50A shows that ages step down with increasing temperature of heating past the fourth fraction (20% of the Ar released), making the resulting spectrum a 'pseudo-plateau'. The integrated age for this 78% of the Ar release is 69.6 ± 0.2 Ma, 1 Ma older then the integrated age. Although interpreting biotite Ar spectra is problematic, this older age (and a similar plateau age for biotite from the pluton main phase) is closer to that of the sericite 09NFBP-SER than is the integrated age.

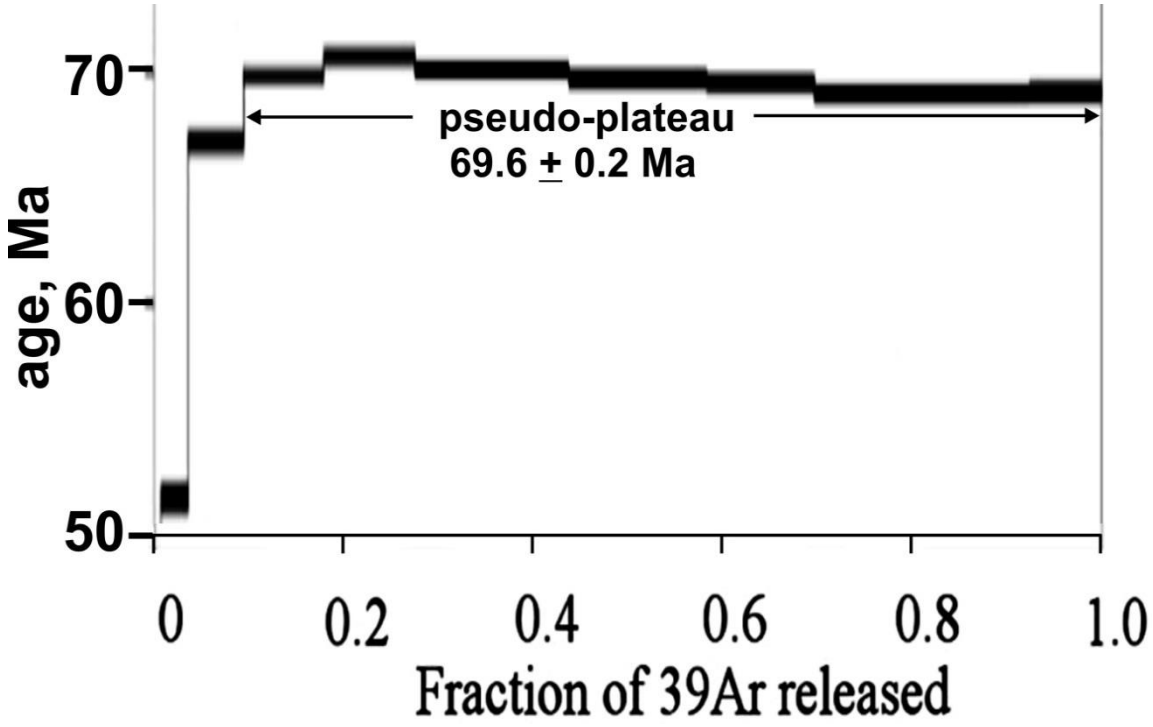

Figure 3.15 Expanded-scale age spectrum for biotite 09RN050A, showing peculiar pattern of apparent age vs. Ar release steps.

3.5 Discussion

A simple tabulation (**Table 3.1**) of radiometric ages from the various samples does not adequately allow for comparisons. The various minerals have different 'age retention temperatures' (**Figure 3.16**) and thus yield different radiometric ages, even where from the same rock. Ages of the 17 samples from the Nixon Fork deposit plotted in terms of likely age retention temperature, yield a surprising chronology (**Figure 3.16**). Biotite and hornblende from the Mystery pluton, felsic dike biotite, and mica from quartz-sericite-pyrite alteration yield a cluster of ages averaging 69.3 $\pm$ 0.8 Ma. Considering that the biotite ages are probably minimum ages, the average 'igneous' age is still older. In contrast, hornblende and phlogopite from skarn yield an average age of 68 $\pm$ 0.6, i.e., 1.5 Ma younger than the nearby pluton. In particular, the skarn phlogopite ages are significantly younger than the plutonic biotite ages, even though biotite has a lower Ar retention temperature (**Figure 3.16**) Finally, the mafic dike yields a considerably younger age of 62 $\pm$ 0.2 Ma. (**Figure 3.16**, **Table 3.2**).

That said, there are considerable uncertainties in the above conclusions. For example, alteration muscovite (**Figure 3.16** point 2) is significantly older than any of the ages from the host pluton. Either this age is anomalously old (for unknown reasons) or the other plutonic ages have been slightly reset to anomalously young ones. Points 10 and 11 (**Figure 3.16**) are from "hornblende" concentrates of the Mystery pluton and contain inclusions of biotite and clinopyroxene, as documented from their Ca/K spectra (**Figure 3.8**). These ages thus have considerable uncertainty and probably represent lower-than-typical age retention temperatures for pure hornblende (**Figure 3.16**,**Figure 3.8**).

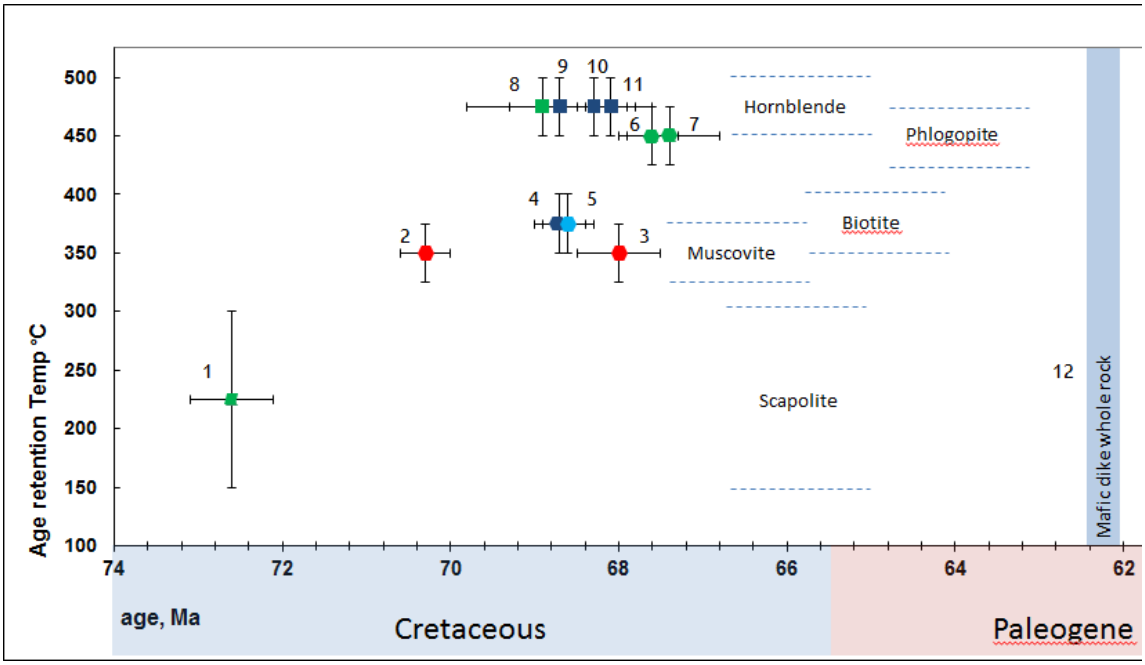

Figure 3.16 Argon ages vs. age retention T as recorded by minerals from the Nixon Fork mine. All data are Ar-Ar unless specified otherwise. Dark blue points = Mystery pluton, light blue points = felsic dike, light green points = skarn, red points = sericitic alteration 1 = scapolite plateau age (09BP-SCAP) 2 & 3 = sericite plateau ages (09NFBP-SER & 11BP01SER), 4 & 5 = biotite integrated ages (N07u33 11.2 Bi & 09RN050 A Bi), 6 & 7 = phlogopite plateau age (09NF-Phl & 11BP02Phlog), 8 = hornblende plateau age (09BP-Skar Hb), 9 = hornblende mixed spectrum plateau age (11BP03HO), 10 & 11 = hornblende plateau ages (N07U33 11.2 Hb runs 1 & 2), 12 = whole rock plateau age (09NF-FL), Most of the ages were determined over 4 days and under similar conditions at UAF; thus, relative age differences are more precise than absolute ages.

The significantly different ages yielded from two different sericite samples (**Figure 3.16** points 2 and 3) seemingly indicate two episodes of sericitic alteration: one associated with pluton crystallization and a younger one associated with skarn formation. Alternatively, these two different ages indicate much greater uncertainties than are shown by the error bars.

Finally, the skarn scapolite sample, with the lowest age retention temperature ought to yield the youngest age. Instead, it gives the oldest age (**Figure 3.16**), much older than the oldest igneous age and 5 Ma older than the skarn phlogopite ages. Based on the high $^{40}Ar/^{36}Ar$ ratio I believe that this mineral gained Ar from the surrounding minerals while it was still open to Ar diffusion and that the age has no geologic meaning.

Most of the skarn mineral ages are considerably more robust than the intrusion ages (**Figure 3.16**, **Table 3.1**) and seem consistently younger, but there is overlap at the 2 sigma uncertainty. Apparent uncertainties in the igneous dates make the apparently younger skarn ages uncertain.

If taken at face value, the most important implications of these dates are (1) some quartz-sericite-pyrite alteration is approximately contemporaneous with the NF pluton and (2) the NF skarn is significantly (at the 1-sigma level) younger than—hence, genetically unrelated to—the adjacent pluton. The first point indicates that the NF QM—similar to other late Cretaceous 'quartz alkalic' bodies in SW Alaska—contains 'intrinsic' Au-As mineralization, but that this mineralization is older than, and unrelated to the skarn. The

second point indicates that since the exposed pluton isn't the source of skarn-forming fluids, an unexposed pluton below the skarns, Whalen Prospect included, must be responsible. Further, the principal direction of fluid flow must have been 'up' from the responsible pluton, rather than outward from the NF pluton. This inference is consistent with the relative scarcity of skarn and other meta-sediment-hosted mineralization around the NF pluton, and the restriction of most mineralization to the area W and SW of the pluton.

4 Structure

4.1 Introduction

In this section I address two major questions: (1) what structures are present that potentially disrupted the skarn and (2) what structures are responsible for the initial formation and pipe-like shape of the skarn?

With regard to the first question, I hypothesize that the structures present at the Nixon Fork deposit can be directly or indirectly related to the nearby Iditarod-Nixon Fork fault. In order to test this hypothesis I analyzed the orientations of mapped structures and grouped them into compatible structural sets. I examined thin sections to assess whether breccias at Nixon Fork were tectonic or sedimentary in origin. Previous underground mapping revealed that breccias are present, although their origin was unknown. Breccias are possible hosts of skarn mineralization and knowing the timing of faulting and the orientation of principal stress axes during deformation are useful for understanding the orientations of the breccias and their internal fabrics at the time of mineralization.

With regard to the second question, I hypothesize that the pipe shape represents the intersection of two recognizable planar structures. In order to test this hypothesis I used Vulcan 3d modeling software to construct a detailed 3d model to determine the spatial relationship between the skarn and the intrusive rocks at Nixon Fork and to better model the pipe shape.

4.2 Map derived and measured structures

4.2.1 Introduction

It should be possible to use sets of structural orientation data from previous underground mapping to constrain the deformational history of the Nixon Fork area and determine relationships of structures to the Iditarod-Nixon Fork fault. To analyze the orientation of structures, I mostly used data from previous maps (**Appendix 1**), but also a few measurements that Wes Wallace and I made (**Table 4.1**, **Appendix 2**).

Ideally, if all the structures formed as a result of a strain field related to strike-slip faulting, they would possess orientations as depicted in **Figure 1.10**. However, the structural setting at Nixon Fork may have changed over time requiring a more complex model.

I plotted all structural measurements in lower hemisphere stereographic projections (stereonets). I separated groups of possibly related structures. Previous workers assigned general structure types to each attitude (e.g., reverse fault, joint), but I don't know what criteria were used to identify each structure type. Further, in an area of complex structural history, faults may have been reactivated under different conditions. The latest fault movement won't necessarily reflect original movement; fault orientation is more likely to reflect original sense of movement.

4.2.2 Dikes and folds

The felsic and mafic dikes are everywhere mapped as near vertical, so I plotted them on rose diagrams. Based on 101 measurements (**Figure 4.1**), the mean felsic dike strike is

34° ± 9° (95 percent confidence interval). Based on 44 measurements (**Figure 4.1**), the mean mafic dike strike is 13° ± 10° (95 percent confidence interval). The orientations of the two types of dikes are significantly different and indicate different stress orientations at the times of felsic (ca. 70 Ma) and mafic (ca. 60 Ma) dike emplacement. Furthermore, the dikes provide a direct indication of extension direction (~103° for felsic and ~124° for mafic dikes).

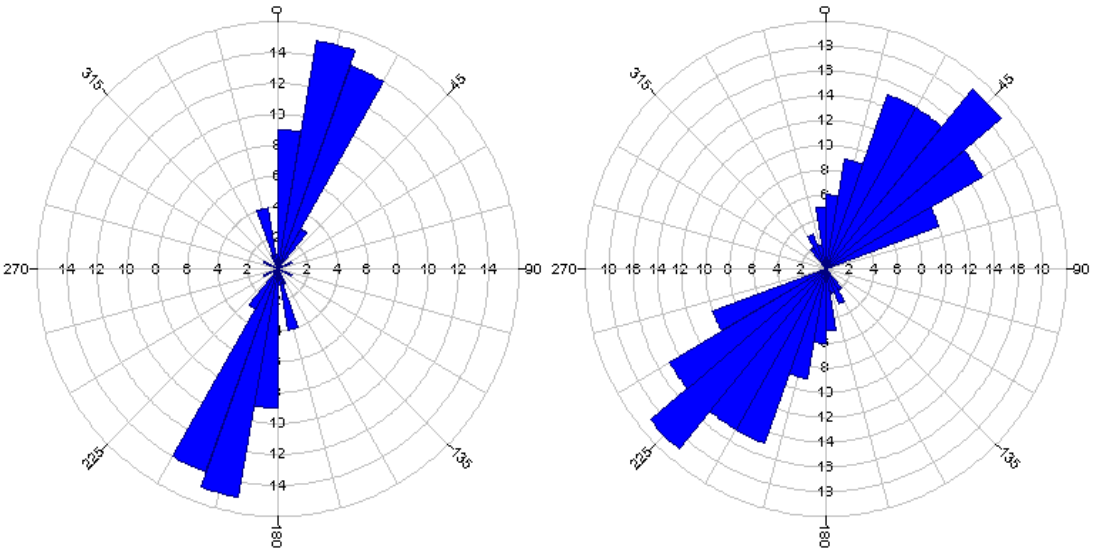

Figure 4.1 Rose diagrams of mafic (left, n = 44) and felsic (right, n = 101) dike orientations at Nixon Fork.

Minor folds in the carbonate rocks are common underground. Based on 82 measurements, their mean trend and plunge is 176°/57° with a 95% confidence interval of 6°. The mean pole to bedding planes in carbonate rocks has a trend and plunge of $2^{o}/6^{o}$ (**Figure 4.3**). The poles to bedding define a diffuse girdle, suggesting folding about an axis roughly indicated by the pole to the best-fit great circle through the girdle. This

pole is oriented 178°/40°, similar to that of the mean minor fold axis. The differences are not significant, given the poorly defined girdle.

The relatively tight clustering of the minor fold axes (**Figure 4.2**) suggests that they formed in a single deformational episode, involving E-W contraction (Bauer, 1980; Wintzer, 2009). This contraction direction is nearly parallel to the extension direction indicated by the mafic dikes (**Figure 4.1**) and indicates radically different stress orientations at the times of folding versus mafic dike emplacement (ca. 60 Ma). Mafic dikes cut across all rock types, including folded carbonate rocks (e.g., **Figure 1.7**)

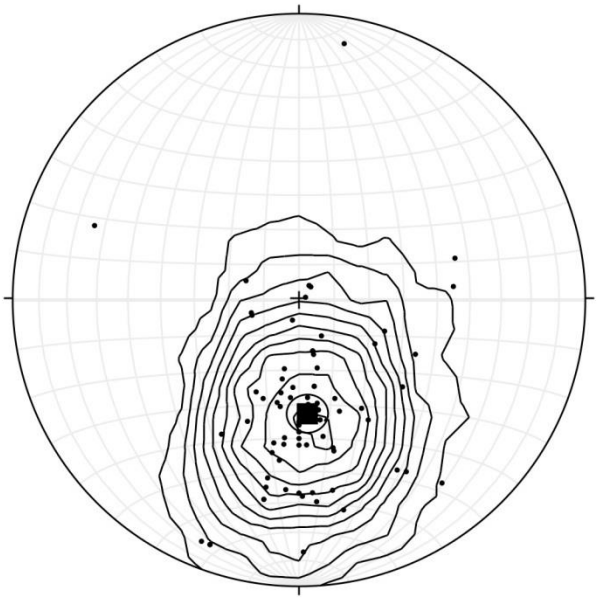

Figure 4.2 Contoured lower hemisphere stereographic projection of minor fold axes (black dots) at Nixon Fork. N=82, with a mean orientation (black square) of 176^{o}/ 57^{o} and 95% confidence interval of 6^{o} following the method of Kamb (1959). Contour interval is 1% of points per 1% area.

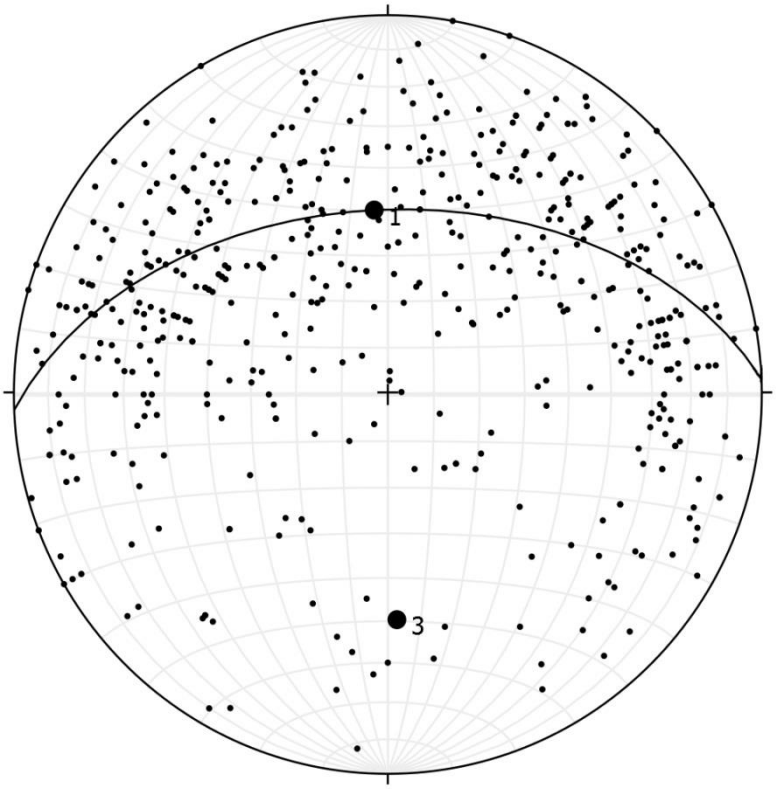

Figure 4.3 Lower hemisphere stereographic projection of poles (black dots) to bedding planes at Nixon Fork, N=505. The pole to the best-fit great circle to bedding poles defines the fold axis and is oriented 178°/40°.

4.2.3 Faults, veins and joints

Faults are visible underground at Nixon Fork, but very few have discernible slickenlines, other kinematic indicators, or clearly observable offsets that can be used to determine last direction of fault movement and thus fault type. **Figure 4.4** and **Figure 4.5** show stereographic projections of structures identified as normal faults, reverse faults and strike-slip faults on underground maps (**Appendix 1)**. I employed measurements for 20 normal, 14 reverse, and 18 strike-slip faults. Although this is a small sample size, the distributions show potentially meaningful patterns. Where there is more than one

significant population of a structure type I assigned them to alphabetically labeled groups to help differentiate between them.

Normal faults (**Figure 4.4**) include six (Group A) that strike at 80°-110° and nine (Group B) that strike at 40°-50°. The orientations of these two sets are significantly different, and thus, cannot have formed simultaneously. Group A faults are consistent with strain related to the Nixon Fork-Iditarod fault (**Figure 1.11**); Group B must represent a completely different event.

Mapped reverse faults (**Figure 4.5)** include eight (Group C) with strikes of 350°-020° and another five (Group D) with strikes of 100°-110°. Because reverse faults usually have dips of 30°-45° (Davis and Reynolds, 1996) and all of these have dips >80°, they are too steep for the original motion to have been reverse. Only the two faults with orientations of approximately 0°/45° are likely to have original reverse motion. However, the orientations of these two are consistent with movement on the Nixon Fork-Iditarod fault (**Figure 1.11**).

Faults mapped as sinistral (**Figure 4.5**) and dextral (**Figure 4.5**) exhibit a variety of orientations, with few obvious patterns. Sinistral faults include three (Group E) with strikes of 120°-140°, three (Group F) with nearly perpendicular strikes of 060°-080°, and three more with other orientations. Group E is consistent with strain related to the Nixon Fork-Iditarod fault (**Figure 1.11**). One dextral fault (Group G) has a strike of about 050° and a nearly vertical dip, sub-parallel to the present Nixon Fork-Iditarod fault. Four faults (Group H) have strikes of 120°-140° and steep dips, nearly perpendicular to the

050^{o} strike of the Nixon Fork-Iditarod fault. The remaining dextral faults possess a variety of orientations.

In sum, some of the previously mapped underground faults are consistent with formation accompanying or related to the Nixon Fork-Iditarod fault. The majority of the mapped reverse faults must be reactivated non-reverse faults and the majority of the strike-slip faults cannot be easily related to the Nixon Fork-Iditarod fault. However, the previously mapped faults are too scattered in orientation to clearly determine any local patterns.

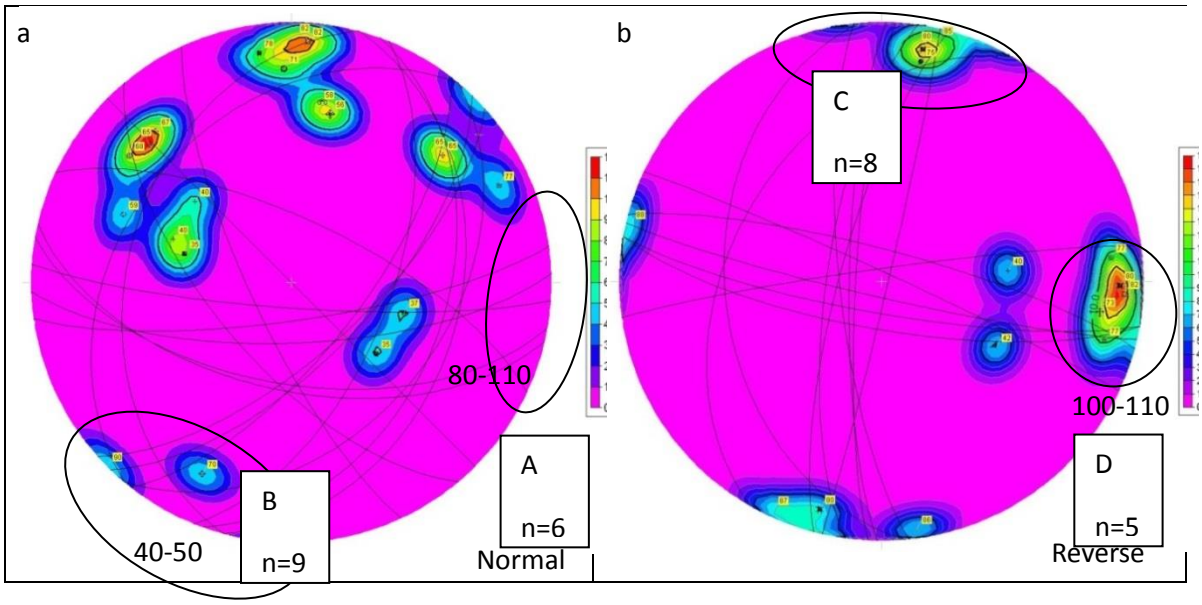

Figure 4.4 Lower hemisphere stereographic projections of planes and poles to (a) 20 normal faults and (b) 14 reverse faults identified in previous mapping at Nixon Fork. Ovals define strike of faults discussed in text, pole numbers are dips of respective planes. Boxes label groups of measurements as well as giving the number of measurements in each oval. Contours are 1% of points per 1% area.

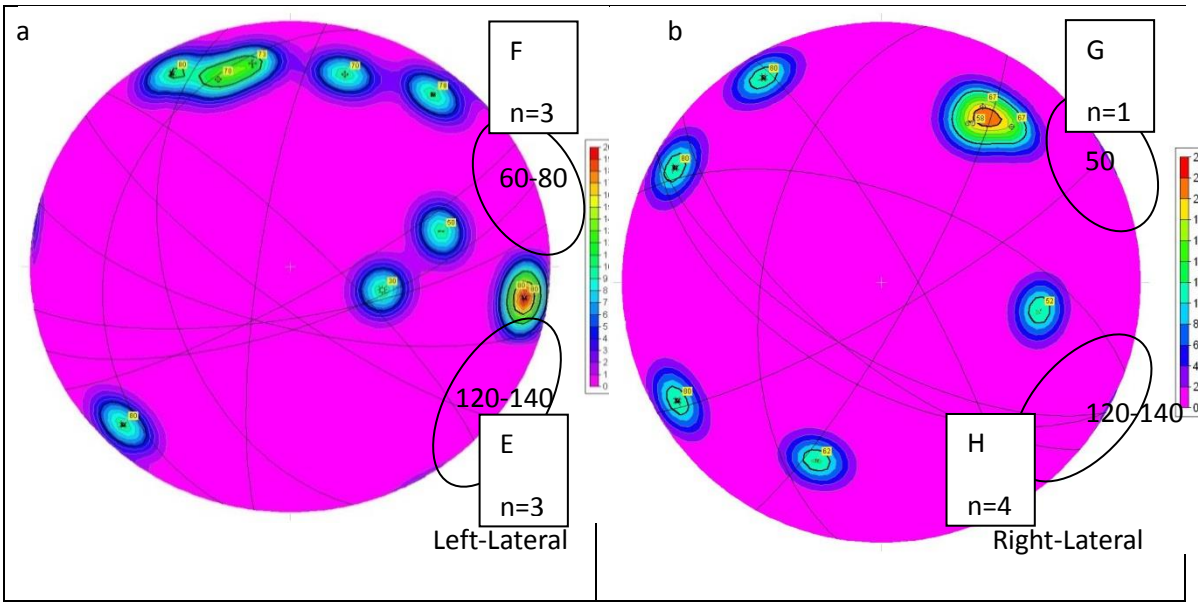

Figure 4.5 Lower hemisphere stereographic projections of planes and poles to 10 sinistral (a) and 8 dextral (b) strike-slip faults at Nixon Fork. Ovals define strike of faults discussed in text, boxes have a reference letter which is used to help identify each group of faults as well as number of measurements in each oval, pole numbers are dips of respective planes. Contours are 1% of points per 1% area.

Many vein and joint attitudes were recorded (**Appendix 1**) on the underground maps. Veins commonly form along fault planes, and mapped joints could possibly be faults that lack kinematic indicators or shear fractures that share the attitude of related faults. More importantly, joints and veins that originated as extension fractures provide a direct indication of extension direction.

The strongest maximum defined by the veins (Group I, red) (**Figure 4.6**) has a mean orientation of 211°/82^{o} (n=12). An additional maximum (Group J, green) has a mean

orientation of 97°/ 57^{o} (n=3). This latter group is consistent with extension associated with the Nixon Fork-Iditarod fault (**Figure 1.11**); the former group is not but is oriented the same as the felsic dikes (**Figure 4.1**).

Of the many joints measured, three groups (**Figure 4.8)** stand out: K (19^{o}/86^{o}, n=10), L (251^{o}/30^{o}, n=20), and M (131^{o}/73^{o}, n=11). Of these, the Group K joints are suspiciously similar in orientation to the mafic dikes (average 13^{o}/steep), suggesting a common origin.

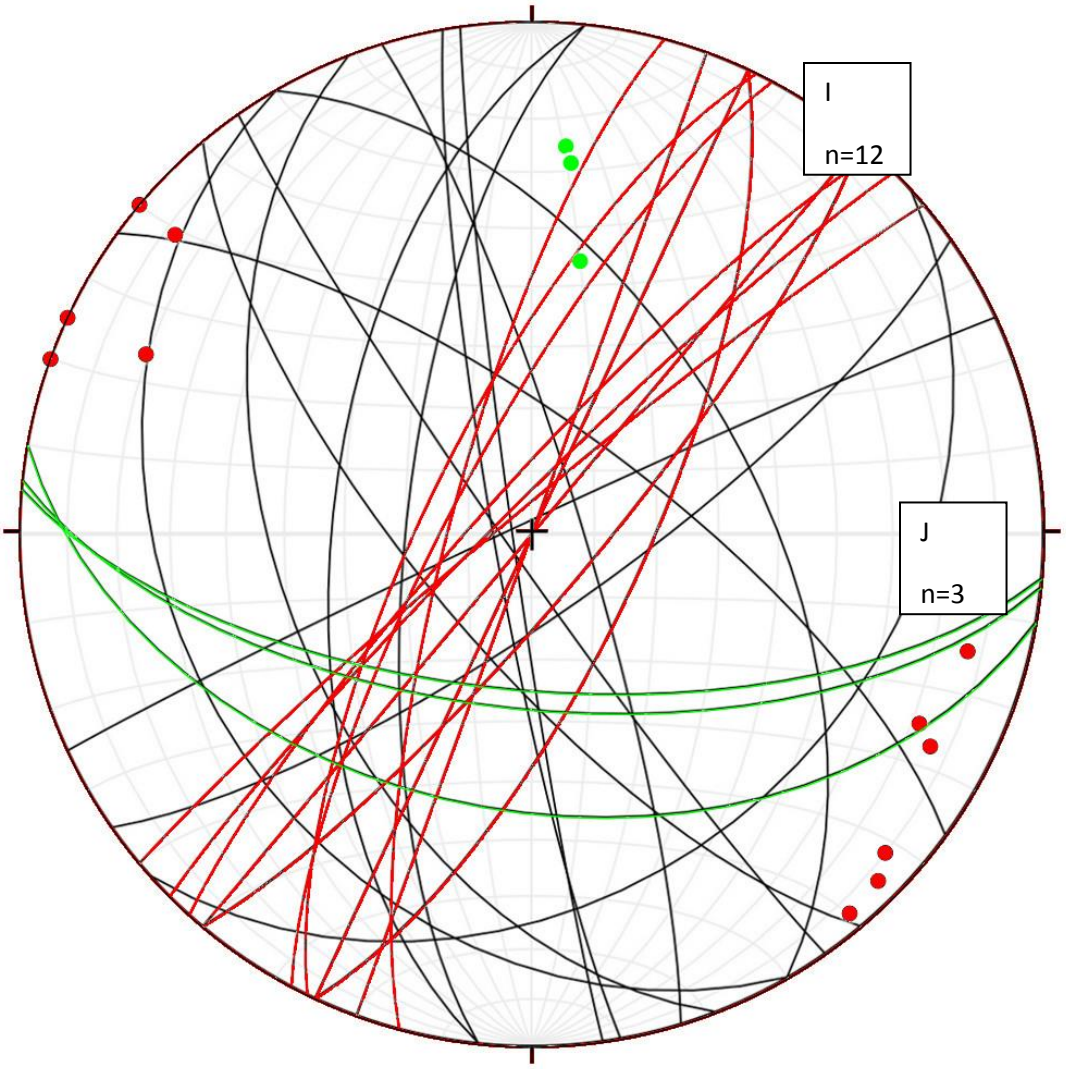

Figure 4.6 Lower hemisphere stereographic projection of veins and their poles at Nixon Fork, N=29. Maxima are defined by 12 red planes with mean orientation of 211°/82°and 3 green planes with mean orientation of 97°/57°.

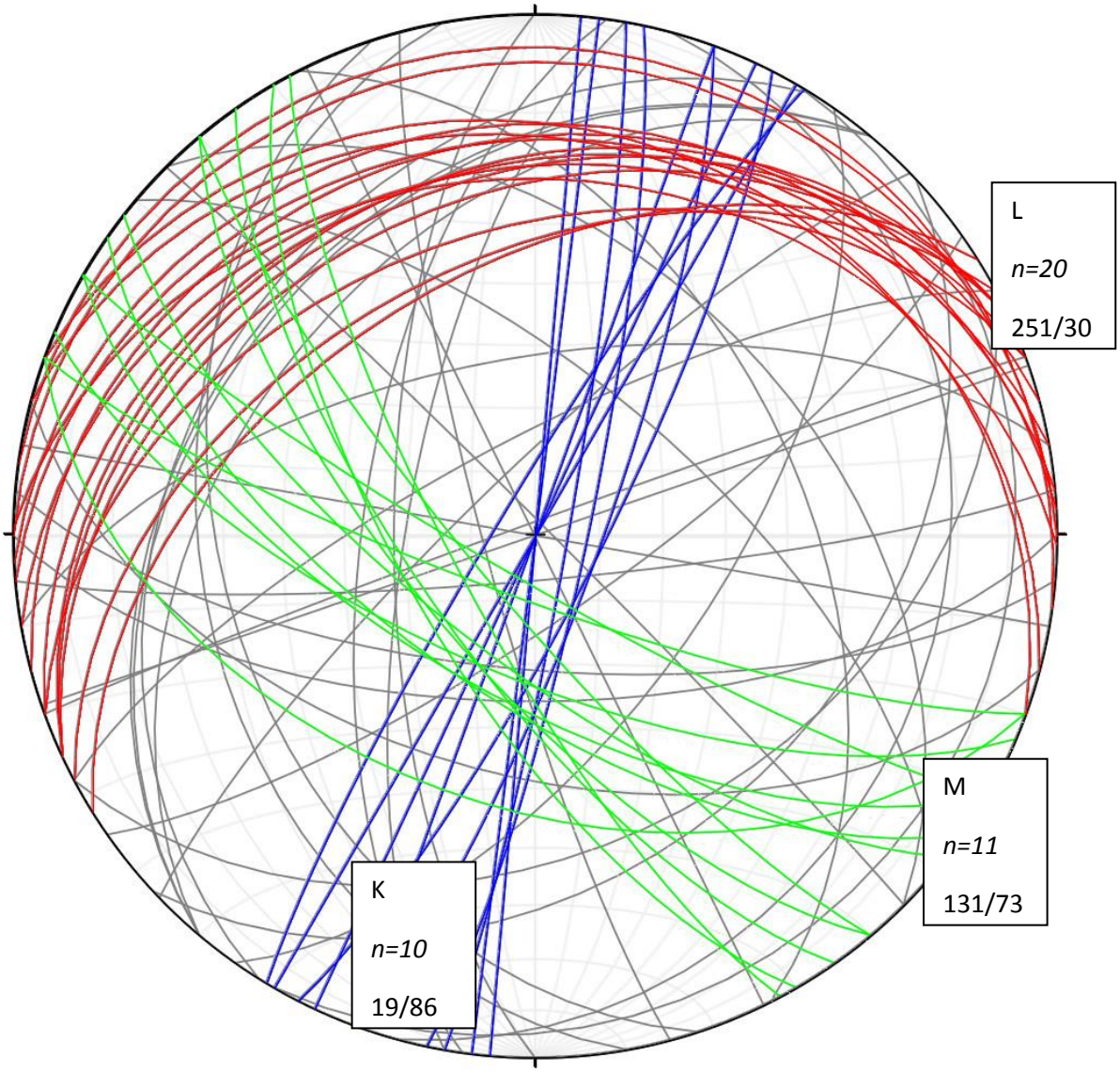

Figure 4.7 Lower hemisphere stereographic projection of joints at Nixon Fork, N=69. Maxima defined by 20 red planes (mean 251°/30°), 11 green planes (mean 131°/73°), 10 blue planes (mean 19°/ 86°).

Wes Wallace measured (**Table 4.1**) two sets of minor thrust faults (**Figure 4.8**). The average orientation of one set (Group N) is 256°/30°; the other, less well-defined Group O is 118°/32°, consistent with a contraction direction of ~004°. Of these thrust faults, one

(number 6, **Table 4.1**) is approximately the same orientation as the two reverse faults with moderate dips (**Figure. 4.4**) identified on previous maps. Although fault 6 is grouped with three other faults of Group O, its strike is approximately half-way between those of Group O and Group N and may represent a separate family. Removing it from Group O gives that group an average orientation of 101°/32°**.**

Table 4.1 Fault and related attitudes measured on the 360 m level at the Nixon Fork mine by Wes Wallace.

Fault #	Attitudes[1]	Comments[2]
1	218/42 FP	Set 2 conjugate thrust, cuts OT acl
2	358/31 FP	Set 1 conjugate thrust
3	333/26 FP; 307/25 Slns	Set 1 conjugate thrust
4	346/30 FP	Set 1 conjugate thrust
4	187/55 FP	Set 2 conjugate thrust
5	325/43 FP; 10/23 Slns	Set 1 conjugate thrust
6	278/48 FP; 227/48 Slns	Set 3 thrust, cuts set 1 above
7	167/26 FP	Set 2 conjugate thrust w/ CC vein

[1] attitudes of planes recorded as dip azimuth/dip inclination; lines as trend/ plunge. [2]acl = anticline, scl = syncline, FA = fold axis, OT = overturned, FP = fault plane, Slns = slickenlines, CC = calcite

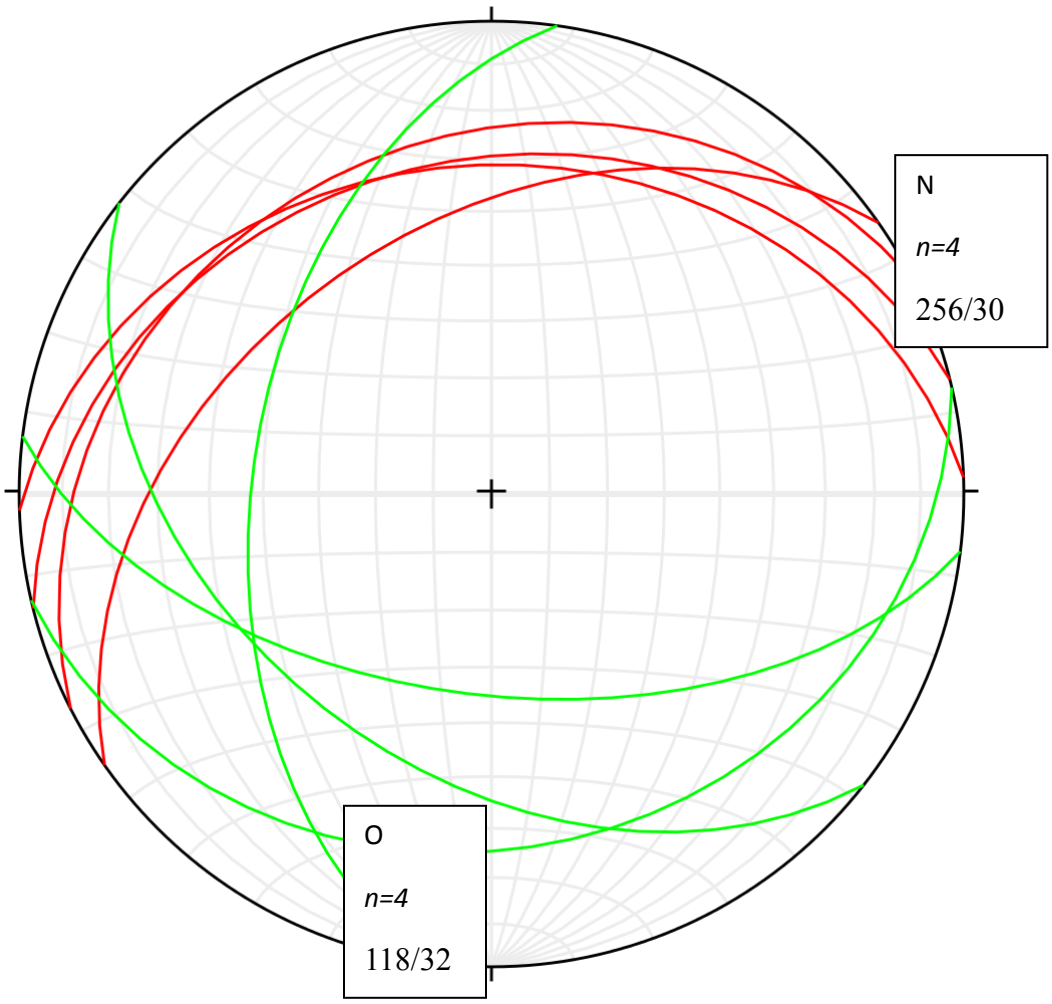

Figure 4.8 Lower hemisphere stereographic projection of conjugate thrust faults measured by Wes Wallace at Nixon Fork, n=8. Groups are defined by 4 red planes (mean 256°/30°), and 4 green planes (mean 118°/32°).

4.2.4 Discussion

I hypothesized that faults at the Nixon Fork mine could be related to the Iditarod-Nixon Fork fault. My analysis, however, indicates that only two out of six compatible structure sets are consistent with that major fault.

The limited structural data make it possible to identify different sets of structures that are compatible with each other assuming a simple strain model (**Figure 1.11**). Compatible

structure sets are those that preferentially form in the same regional strain field. My interpretations are summarized in **Table 4.2** and **Figure 4.9**.

Dike orientations at Nixon Fork provide the most useful structural information. The two dike types have consistent orientation, known geochronology, and directly indicate extension direction normal to their propagation direction, with extension directions of ~124° for felsic and ~103° for mafic dikes.

The extension direction obtained from the felsic dikes is almost perfectly parallel to the strongest maximum defined by the Group I vein measurements (~121° extension). Application of the simple strain model **(Figure 1.11)** to this orientation (~124° extension) also accounts for the Group B set of southeast-dipping (~124° extension) normal faults and two northwest-dipping (~115° extension) normal faults that are likely Group B conjugates (**Table 4.1**; **Figure 4.1; Figure 4.4;Figure 4.6**).

In contrast, the 013°-striking, steeply dipping mafic dikes are close to parallel with the Group K joints, with average orientations of $19^{o}/86^{o}$ (**Table 4.2**, **Figure 4.7**). This is approximately the same orientation as Group C reverse faults, 006°/80°. If these steeply dipping faults originated as joints or normal faults, then they and the Group K joints could all be associated with the mafic dike emplacement.

Ironically, neither set of dikes and associated structures is consistent with right lateral motion on the Iditarod-Nixon Fork fault. According to the simple strain model (**Figure 1.11**) dikes associated with right lateral motion would be oriented approximately 45^{o} clockwise from the right lateral fault. This is clearly not the case.

A maximum indicated by 11 Group M joints (**Figure 4.7**) as well as two southeast-striking normal faults (**Figure 4.4**) would form with an extension direction ~41° and are consistent with the secondary orientation of the ideal model.

Another maximum, the Group L joint set, is practically identical in orientation to the Group N thrust faults mapped by Wes Wallace (**Figure 4.7).** It is consequently reasonable to assume that these are in fact thrust faults. The average fault orientations suggest contraction directions of 341° (L joints), 346° (N thrusts) and 011° (O thrusts). (**Table 4.2,Figure 4.9**).

Another set of extensional (and reactivated extensional?) structures forms a compatible structure set with an extensional direction of 004°-025° (**Table 4.2**). This direction is consistent with right-lateral strike-slip on the Iditarod-Nixon Fork fault. This set (**Table 4.2**,**Figure 4.9**) contains Group A normal faults (n=5 southwest dip, n=1 northeast dip conjugate), Group J veins (n=3), and the anomalously steep Group D "reverse faults" (n=4). I hypothesize that Group D faults represent reactivated normal faults or normal faults misinterpreted as reverse faults.

Fold axes recorded in the metasedimentary rocks vary considerably (**Figure 4.2**) both in trend and plunge. The bulk of axes trend 150°-210° (average 176^{o}), but plunges range from 5° to 90° (average 57°). The contraction direction indicated by average fold axis trend is 86^{o}. Steep plunge could possibly be explained by the Mystery pluton intruding into the hinge of a local syncline (Patton and others, 1980) or by tilt related to the previously mentioned down-to-southeast normal faults (**Table 4.2**, **Figure 4.9**).

Faults identified by previous workers as dextral or sinistral define no clear pattern and very few of them are near vertical, suggesting that whatever kinematic indicators were used to identify these as strike-slip are likely either the result of reactivation and are not indicative of fault origin or that they originated as oblique-slip faults.

In sum, my interpretations suggest two contraction events and four extension events (**Figure 4.9, Table 4.2**). The first contraction (C1) event is defined by plunging fold axes, and occurred prior to pluton intrusion, as the pluton cuts plunging fold axes and steeply dipping bedding. The first extension (E1) event is defined by felsic dikes, normal faults and a set of veins, and most likely corresponds to felsic dike intrusion. The second extension (E2) event is defined by mafic dikes and a set of joints, and most likely corresponds to mafic dike intrusion. A set of faults previously identified as reverse faults, but that are more likely to be extension fractures based on their near-vertical orientation, may also have formed during this event. The third extension (E3) event is defined by normal faults, veins, and a set of faults previously identified as reverse faults, but that are more likely to be normal faults based on their orientation. This event doesn't have well constrained timing, but the orientation of the structures suggests that they could have formed contemporaneous with movement on the Iditarod-Nixon Fork fault. The fourth extension (E4) event is defined by a set of joints and does not have well constrained timing, but the orientation of the joints suggests that they may be secondary structures related to the Iditarod-Nixon Fork fault. The second contraction (C2) event is defined by conjugate thrust faults and a set of structures previously identified as joints, but that are more likely to be thrust faults based on their orientation. This event has unknown timing.

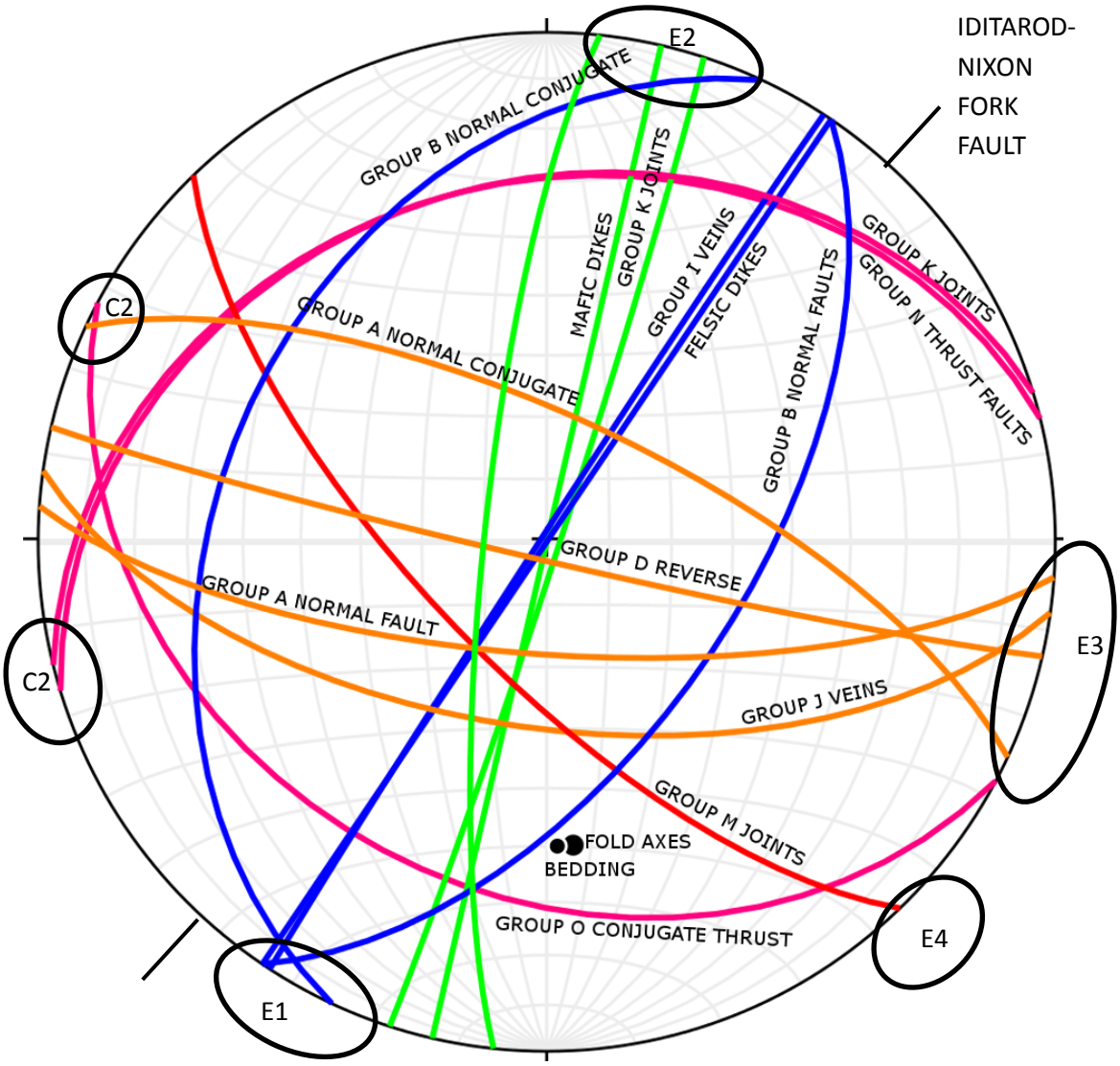

Figure 4.9 Approximate orientations of sets of structures grouped by color into compatible composite sets. Black pole = Contraction 1, blue planes = Extension 1, green planes = Extension 2, orange planes = Extension 3, red planes = Extension 4, fuchsia = Contraction 2.

Table 4.2 Possible compatible sets of structures at Nixon Fork

Set	Orientation[1]	Number	Type	Extension (E) or contraction (C) direction
Contraction 1 (before pluton intrusion)				
Fold axes	176/57	N=82	contraction	C86
Fold axis from poles to bedding	178/40	N=505 (beds)	contraction	C88
Extension 1 (felsic dike intrusion)				
Felsic dikes	34/~90	N=101	extension	E124
Group I veins	211/82NW	N=12	extension	E121
Group B normal faults	34/58SE	N=7	normal	E124
Group B normal faults	205/36NW	N=2	normal conjugate	E115
Extension 2 (mafic dike intrusion)				
Mafic dikes	13/~90	N=44	extension	E103
Group C reverse faults	186/80NW	N=6	extension?	E096
Group K joints	19/86SE	N=10	extension	E109
Extension 3 (possibly primary with respect to Nixon Fork fault)				
Group A normal faults	94/72SW	N=5	normal	E004
Group J veins	97/57SW	N=3	normal?	E008
Group A normal faults	295/70NE	N=1	normal conjugate	E025
Group D reverse faults	103/87SW	N=5	extension?	E013
Extension 4 (possibly secondary with respect to Nixon Fork fault)				
Group M joints	131/73SW	N=11	extension	E041
Contraction 2 (timing unknown)				
Group L joints	251/30NW	N=20	thrust?	C341
Group N, O conjugate thrusts (WKW)	256/30NW (N) 101/32SW (O)	N=4 (N) N=3 (O)	conjugate thrusts	C346 C011

[1]planes given as strike/dip; lines as trend/plunge

4.3 Breccias

4.3.1 Introduction

In order to fully assess deformation of the Nixon Fork skarn I needed to identify the origin of breccias such as those in Figure 1.6. Breccia bodies have been identified (**Chapter 1**, **Figure 1.6**) both underground and in drill core. They were traditionally interpreted as solution collapse features (Jasper, 1961), but more recent Nixon Fork internal documents have speculated that they are fault related (Power and others, 2003). Breccias at Nixon Fork rarely contain ore-grade metal values. Their main importance is that: if they are sedimentary, they represent an important stratigraphic marker; if they are tectonic, they represent shear zones that potentially deform ore bodies and intrusive contacts

4.3.2 Breccia

I have recognized three main breccia types at Nixon Fork. All are typically poorly sorted, but fine-grained samples can be well-sorted. Large clasts are typically angular; smaller clasts are sub-angular to rounded.

The most common breccias (~60% estimated) contain carbonate matrix and clasts. Carbonate clasts are meter to millimeter scale; centimeter sized clasts are most common. Also common (~25%) are variably altered Nixon Fork pluton clasts in a matrix of finely milled plutonic rock or carbonate. Plutonic clasts are tens of centimeters to millimeters in diameter; with millimeter sized clasts being most common. The least common type

(~15%) contains skarn clasts in a carbonate matrix. Skarn clasts are centimeters to millimeters in diameter; centimeter sized clasts are most common.

Underground mapping (**Figure 4.10**), core examination (**Figure 4.11**), and thin-section petrography (**Figure 4.12**,**Figure 4.13**,**Figure 4.14**,**Figure 4.15**, **Figure 4.16**) indicate that the breccias are commonly polymictic and matrix-supported, with matrix compositions reflecting clast compositions.

Figure 4.10 Underground photo showing outcrop view of carbonate breccia. Clasts composed of layered limestone are surrounded by a fine-grained, brown, carbonate-rich matrix.

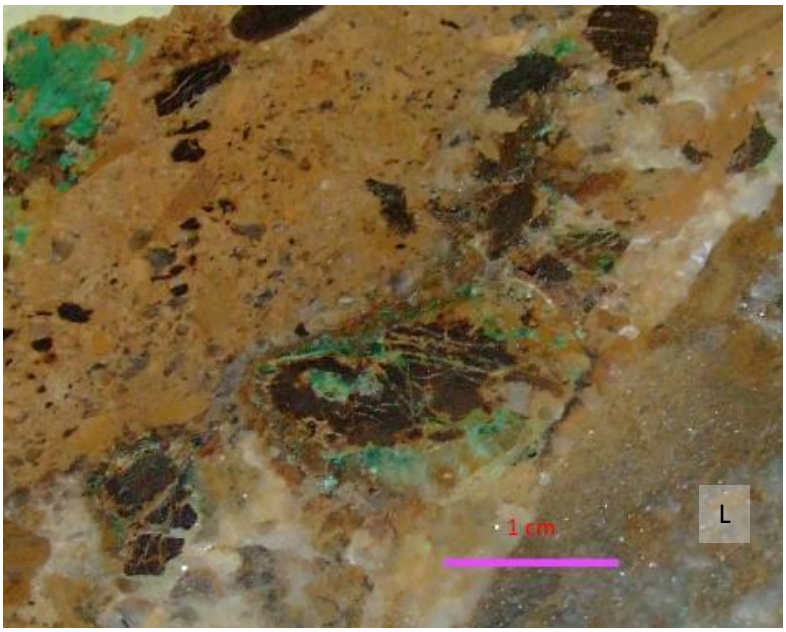

Figure 4.11 Hand sample photograph of Nixon Fork carbonate breccia with weathered sulfide clasts. A large limestone clast (L) is present in lower right. Light brown in upper left half of photo is lightly FeOx stained carbonate. Darker brown and green are secondary Fe and Cu minerals.

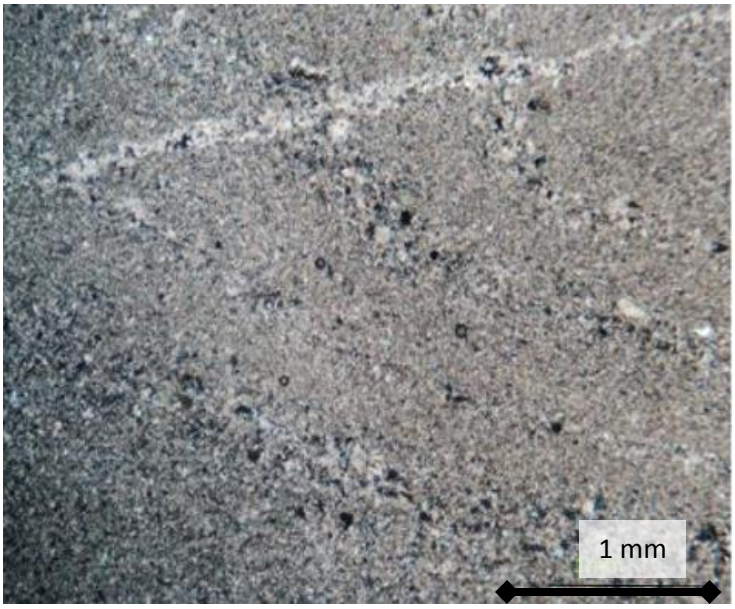

Figure 4.12 Altered plutonic breccia. Laminations reflect systematic grain size variations. Crossed polars.

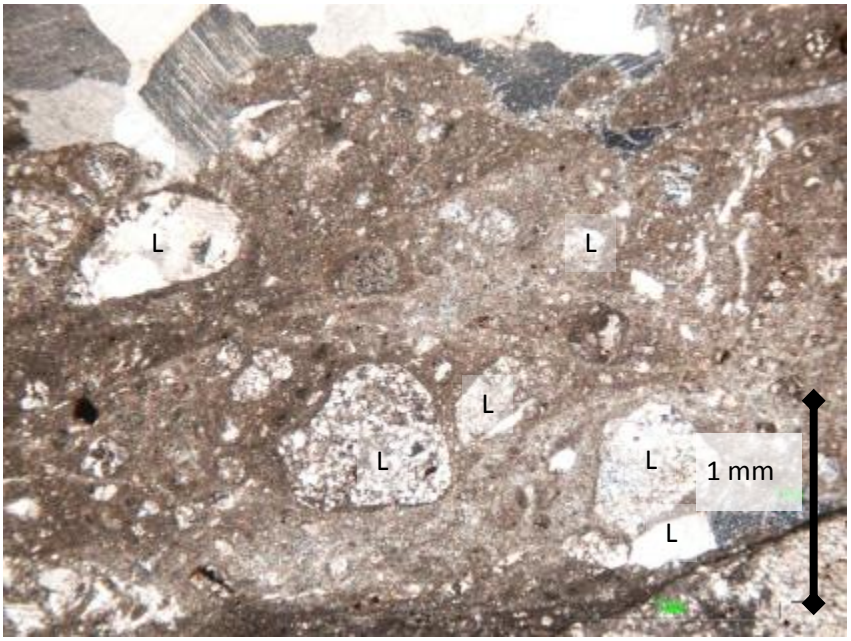

Figure 4.13 Photomicrograph of brecciated Nixon Fork limestone; matrix displays FeOx staining. Large white and grey patches (L) are fragments tectonically plucked from the edges of an intact limestone clast. Plane polarized light.

Tectonic fabrics present in thin section include rolled grains (**Figure 4.11**, **Figure 4.12**), brecciated ore (**Figure 4.13**), brittle quartz deformation (**Figure 4.14**), and stress cracking in cataclastic deformation (**Figure 4.15**).

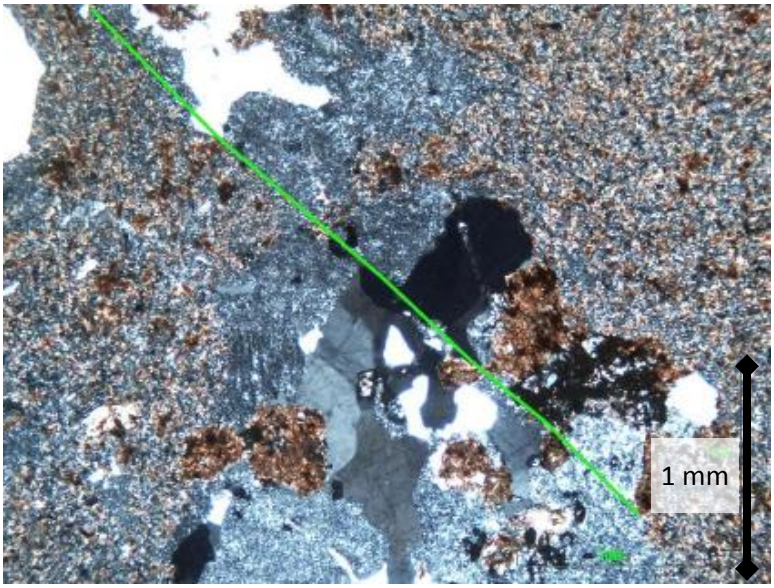

Figure 4.14 Photomicrograph of altered and broken Nixon Fork plutonic breccia. Carbonate is the ubiquitous brown mineral and kaolinite is the smaller silver-blue mineral scattered throughout. A quartz grain (black) in the center is tectonically split (green line). Crossed polars.

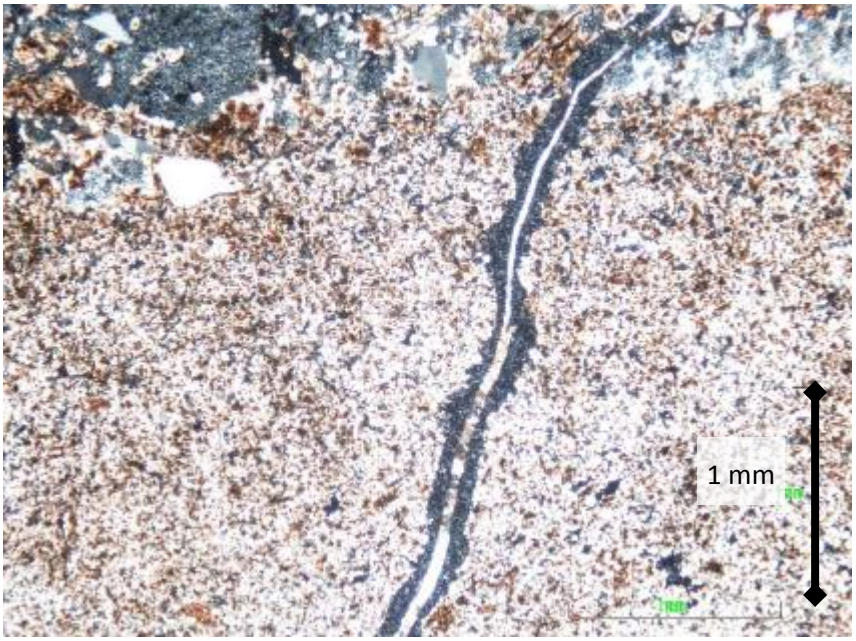

Figure 4.15 Photomicrograph of a transverse crack through carbonate breccia matrix adjacent to an altered plutonic clast. The crack is filled with calcite inside a kaolinite envelope. Crossed polars.

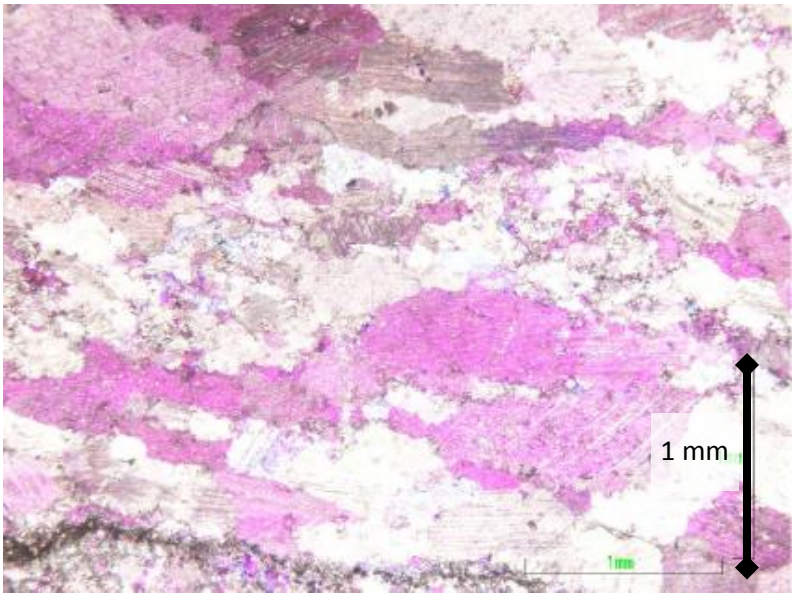

Figure 4.16 Photomicrograph of a marble clast in a Nixon Fork carbonate breccia. The clast shows bands of calcite in crystallographic alignment that I interpret as tectonic creep. Crossed polars with wave plate.

Aligned calcite grains (**Figure 4.16**) are not necessarily due to tectonism, but may represent original sedimentary alignment. **Figure 4.16** is a photomicrograph of a single clast displaying ductile deformation in the midst of brittlely deformed rock. Other clasts of Nixon Fork marble do not contain aligned grains.

Some of the breccias contain variably-weathered sulfide clasts. **Figure 4.13** shows clasts of secondary FeOx in what would otherwise be a typical Nixon Fork carbonate breccia. Due to the high pH caused by abundant calcite, secondary iron oxide and copper carbonate minerals were precipitated near the primary sulfide grains.

4.3.3 Discussion

I interpret the breccias at Nixon Fork to be fault related, thus their distribution might be a useful tool to identify major faults at Nixon Fork. **Figure 4.13** shows brecciated sulfide, which indicates that tectonism has affected the skarn. Additionally, **Figure 1.6** shows skarn surrounded by breccia that might be interpreted as breccia forming around a skarn pipe, given the abrupt contacts on either side. Altered plutonic rocks commonly occur in the breccias, indicating that these formed after the pluton (and skarn). However, I have not been able to connect breccia bodies underground and do not know if they are related to a particular fault type.

4.4 3-D Modeling

4.4.1 Introduction

In order to test my hypothesis of a strong structural control responsible for the pipe-shaped skarn body, I needed to model the shapes of the deposit in 3 dimensions. Newberry and others (1997) claimed that the orebodies at Nixon Fork were steeply plunging pipes, necessitating as-yet unidentified structural control. In this section I test my hypothesis via examining relationships between skarn and igneous units as well as attempting to assess post-skarn deformation by a 3 dimensional examination of the orebodies.

I simplified the Nixon Fork GEMCOM mine model by combining rock units. For example, I combined multiple carbonate units into one carbonate unit. I combined suspected and mapped breccia units, but they’re too few to be useful. I re-classified

igneous units as Mystery pluton, felsic dikes (insufficient occurrences), and mafic dikes. I re-classified skarn into pyroxene-dominant and garnet-dominant skarn. Much of the skarn, especially in the upper mine levels, is too weathered to reliably distinguish original mineralogy. Such undifferentiated skarn I combined with garnet-dominant skarn.

Connecting units between levels was problematic, as I did not incorporate drill hole data and serious geologic changes occurred between mapped mine levels. Connecting the skarn units was particularly problematic. I had to choose between several possibilities with insufficient data. Consequently, skarn body shapes are typically conjectural.

4.4.2 Modeling

The skarn body can be mapped as a semi-continuous pipe (**Figure 4.17**) from 160 level up to 230 level. It then appears to jog north 20 m and is present adjacent to the decline again at 250 level. From there it continues upward to the 400 level. At the 290 level another skarn body is present 30 m northeast of the main skarn. It is not reencountered until the 330 level, where a pyroxene skarn body is mapped 10 m east of the main skarn body. The northeastern skarn body isn't reencountered on any other levels. A garnet skarn body is located approximately 10 m north of the main ore pipe on the 340 level. This apparently grades into a garnet skarn surrounded by oxidation on level 350, and both bodies are co-linear with a garnet body surrounded by limestone breccia on the 370 level and an oxidized skarn body on the 400 level. Skarn on the various level maps can be modeled as a single pipe, but this pipe does not exhibit a simple zoning and appears to splinter into segments as one approaches the surface.

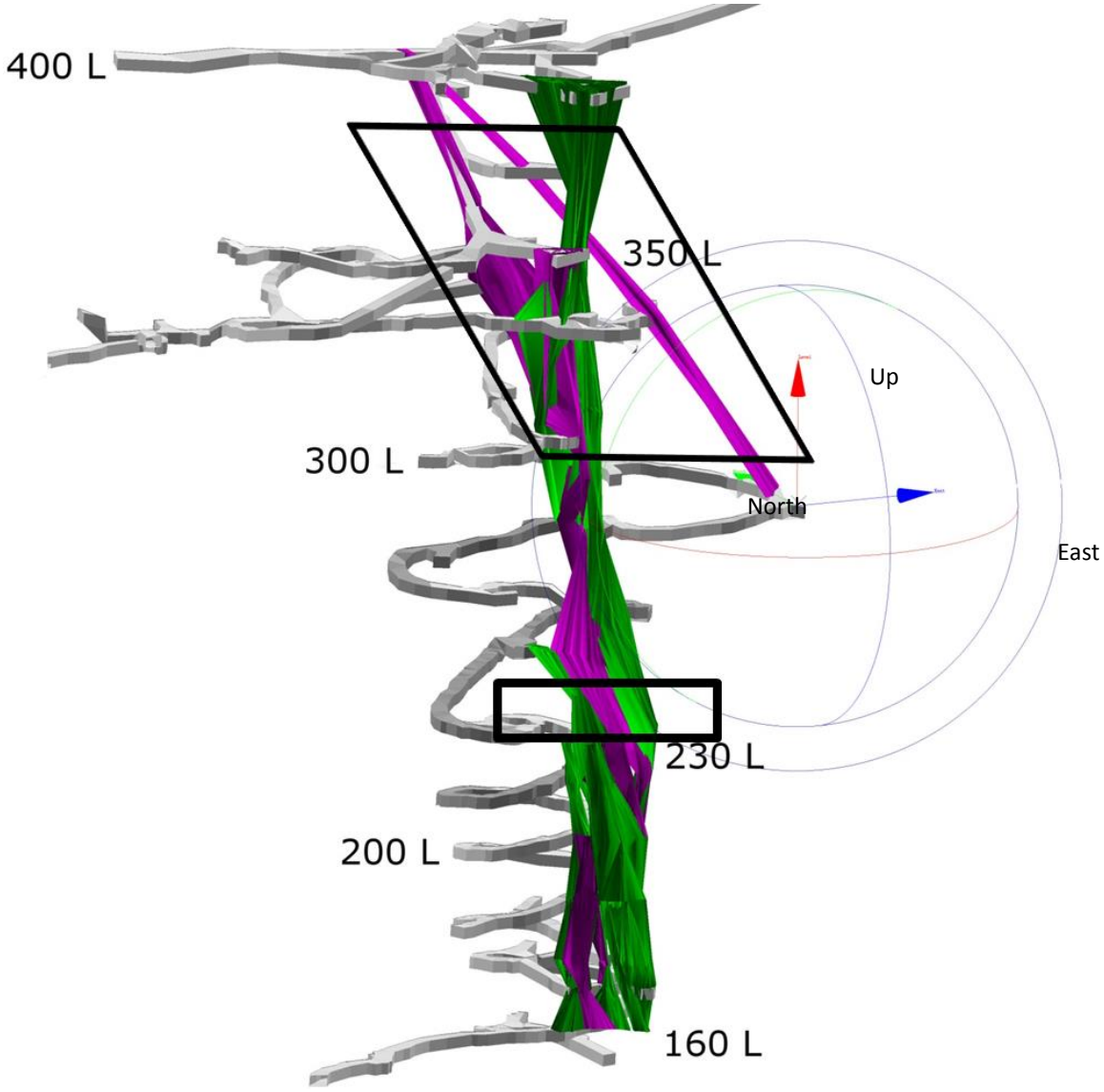

Figure 4.17 View to the northeast of the Crystal Garnet decline, with the modeled continuous skarn body. Fuchsia is garnet bearing (and undifferentiated) skarn, and green is pyroxene skarn.

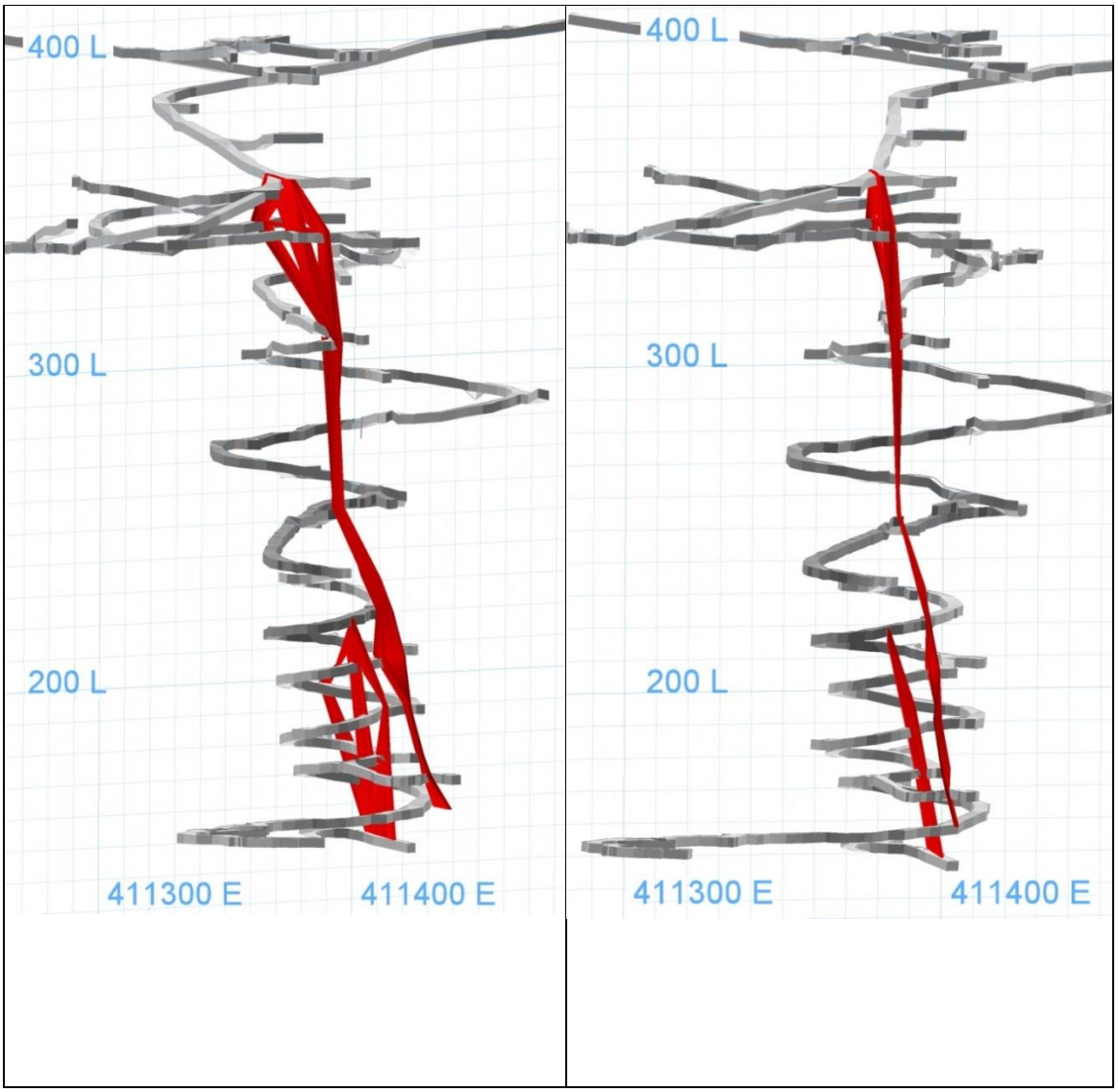

Figure 4.18 View to the northeast (a) and north (b) of the Crystal Garnet decline, with the modeled mafic dike bodies. Mafic dikes are modeled as red solids that link occurrences between levels. Triangular holes in the mafic dikes (a) are plotting artifacts from lack of horizontal control on some levels the dike crosses.

Two different mafic dikes (**Figure 4.18**) cut the skarn at Nixon Fork. One, farther east, is more vertically extensive in the underground workings. It strikes 010 and is nearly vertical. The other is located approximately 10 m to the west. It has a strike of 015 and a

steep east dip. Plan maps show small fault offsets of the dikes, too small to be visible at the scale of **Figure 4.18**. Mafic dikes are not mapped above the 350 level, the same level where there is a major discontinuity in the skarn (**Figure 4.17**, **Figure 4.18**, **Figure 4.19**).

A fin of the Mystery pluton is discontinuously modeled next to the skarn pipe (**Figure 4.19**). Occurrences of this unit appear and disappear between levels. Notably a branch appears on the west side of the skarn from the 160 to 230 levels, another on the east side of the skarn from the 200 to 240 levels, and a third on the south side of the skarn from the 260 to 380 levels.

Previous Nixon Fork exploration (Power and others, 2003) has shown that the pluton in this area is a series of embayments and disconnected bodies sporadically in contact with the skarn and curving away at depth. While the main body of the Mystery pluton is to the southeast of the mine workings (toward the viewer in **Figure 4.17**), the embayments are part of a larger projection that juts past the skarn pipe to the south and projects toward the skarn from the southwest.

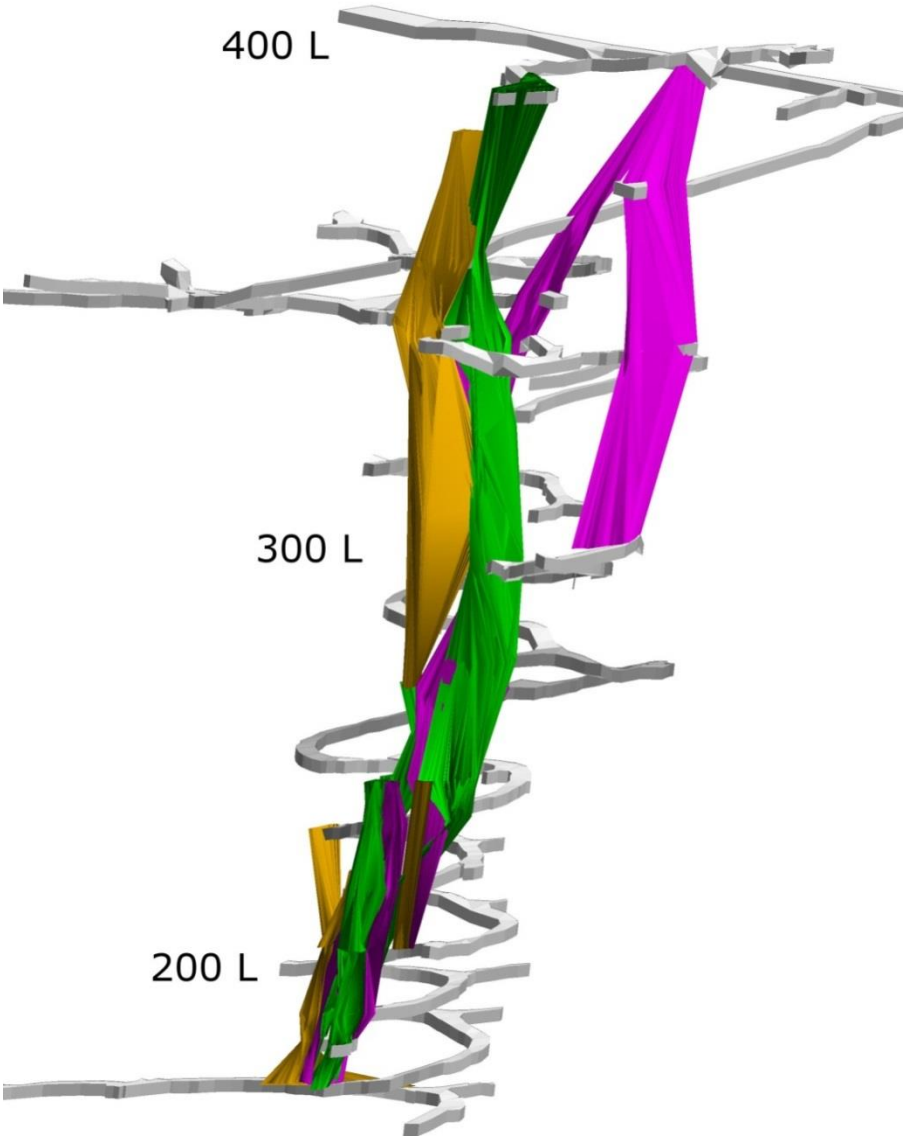

Figure 4.19 Oblique view to the west of the Crystal Garnet decline, with modeled pyroxene (green) and garnet bearing (fuchsia) skarn with Mystery pluton (yellow). Mystery pluton is mapped adjacent to skarn through multiple levels, but is not vertically continuous.

4.4.3 Discussion

The Mystery pluton is present adjacent to the skarn sporadically from the base of the mine up to approximately the 240 level and upwards from the 260 level. However, there doesn't appear to be a consistent association between pluton and skarn. The upper garnet segment doesn't have associated igneous rocks, but it also appears to be surrounded by breccias or is faulted. The lack of consistent spatial association argues against a genetic association between Mystery pluton and skarn. I don't have enough data to determine if the upper skarn is a faulted segment.

The three-dimensional modeling indicates that the skarn does form a steeply south-plunging (45°-90°, 65° over most of its length) pipe, although there are complications. I model at least two faults disrupting the skarn, from the 230 to the 250 level and above the 350 level. Both jog to the north as the pipe ascends, away from the Mystery pluton.

The skarn pipe lies along a line with an approximate orientation of 210°/65°. This trend is very close to the average strike of felsic dikes (34°/90° = 214°/90°) and group I veins (210°/84°). That is, the skarn pipe lies in the plane defined by dikes that predated skarn formation, but only by 1-2 My. Two different sets of structures are nearly perpendicular to the felsic dikes and intersect them at approximately the same orientation as the skarn pipe. Group A normal faults and group J veins define one set and group M joints define another. That is, the orientation of the skarn pipe coincides approximately with the intersection of planes defined by felsic dikes and by faults possibly related to the

Iditarod-Nixon fault. This is consistent with the skarn-forming fluids having exploited the intersection of two existing structures, the felsic dikes and faults cutting them at a high angle.

Due to the lack of data between levels, I cannot say if the mafic dikes are cut by additional faults between levels, nor what relationship the western dike has to the eastern one. The western dike might join the eastern one above the 200 level or it might veer to the west and not be exposed in the upper mapped mine levels. Mafic dikes as mapped cannot be continuously modeled above the 350 level, the same level where there is a major discontinuity in the skarn. This suggests that an unidentified fault in this area cuts both the dikes and skarn. Alternatively, extensive rock oxidation in the upper levels might make it impossible to recognize a mafic dike. The breccia envelope surrounding the skarn in **Figure 1.6** occurs at the 210 level, and is possibly related to the nearby 230-250 discontinuity. The 230-250 discontinuity presumably took place before the intrusion of the mafic dikes, as they do not show any appreciable offset at that level.

It is hard to discern a genetic relationship between the skarn and the nearby pluton, as the spatial relationship is unclear. Further, lack of skarn zoning away from mapped plutonic rock makes a connection unlikely. However, because felsic magma is unlikely to form discontinuous intrusions, the apparently discontinuous bodies suggest tectonic disruption of an originally continuous body under ductile conditions.

4.5 Conclusion

The two sets of dikes possess contrasting orientations that are consistent with contrasting compositions and ages. The extension direction associated with felsic dike emplacement was approximately 124°; that associated with mafic dike emplacement was 103°. The overall orientation of the skarn pipe (~ 210°/65°) lies within the plane defined by the felsic dike trend, suggesting that skarn-forming fluids utilized a fault or fracture formed during felsic dike emplacement.

Sometime after the skarn formed it was disrupted by numerous mapped faults (**Appendix 1**), two of which are large enough to show on the model: one between the 230 and 250 level and another at approximately the 350 level.

Mafic dikes intruded with a north-south (13° ± 10°) vertical orientation, indicating the extension direction at the time. Due to the somewhat undulatory nature of the mafic dikes, I cannot say for sure if they are cut by additional faults between levels, nor what relation the western dike has to the eastern one, although they do not appear to have any significant displacement. Mafic dikes, as mapped, cannot be continuously modeled above the 350 level, the same level where there is a major discontinuity in the skarn. This suggests an unidentified fault at this level which either cuts or acts as a barrier for the dikes and skarn. **Figure 4.13**, which shows brecciated sulfide, indicates tectonism has affected the skarn. The sulfide clasts could have been brecciated any time after formation, as the oxidation of ore is pervasive up to 200 m underground.

5 Conclusions

The Nixon Fork skarn has an extensive history of deformation and, somewhat surprisingly, most of it is unrelated to the Iditarod-Nixon Fork fault. Based on a variety of evidence, the Mystery pluton isn't the source of the Nixon Fork skarn.

The timing of mineralization is well constrained via $^{40}Ar/^{39}Ar$ dating of the pluton (~69.4 $\pm$ 0.6 Ma), felsic dikes and pluton alteration (~68.4 $\pm$ 0.4 Ma), skarn (~67.6 $\pm$ 0.5 Ma) and mafic dikes (~62 $\pm$ 0.2 Ma), as well as cross-cutting relationships with the mafic dikes. Based on these data, the Mystery pluton likely cooled to biotite argon retention temperature at about 69 Ma. Slightly afterward (~68 Ma) felsic dikes intruded and cut the pluton, indicating extension oriented ~125°. Veins and normal faults were likely formed with the felsic dikes. (**Figure 5.1**).

The anomalously young ages (~68 Ma) for skarn minerals suggest that an intrusive body at depth was responsible for the skarn and not the nearby Mystery pluton. Three-dimensional modeling from level maps shows Mystery pluton discontinuously adjacent to skarn through several levels (**Figure 4.19**). Such is consistent with $^{40}Ar/^{39}Ar$ dating suggesting that the Mystery pluton is older than the skarn. Additionally, the skarn is not zoned outward from the pluton (**Figure 4.19**), which would be the case if the pluton was responsible for the skarn.

The main skarn pipe is approximately a line with the orientation 210°/65°. This orientation is approximately the line defined by the intersection of two planes: (a) felsic dikes (and group I veins) and (b) group A normal faults, group J veins, and group M

joints. These structural pathways are likely avenues for additional skarn-forming fluids in the area.

The felsic dikes and the mafic dikes are likely unrelated. The felsic dikes are not only about 6 million years older than the mafic dikes, but also of significantly different orientation. Mafic dikes possess a north-south orientation, indicating extension oriented ~108°. This extension direction was also likely associated with an extensive set of joints (**Figure 5.1**). Mafic dikes display only minor structural offsets. However, they do not appear on maps above the 350 level, where there is a discontinuity in the skarn, indicating a possible post-mafic dike offset.

Breccias contain clasts of pluton, skarn, mineralized rocks and clasts with fault fabric (**Section 4.3)**. Consequently, brecciation took place after skarn formation and possibly before mafic dike emplacement.

Right-lateral motion on the Nixon Fork-Iditarod fault probably occurred discontinuously throughout Tertiary time. This strike-slip motion may have been accompanied by southwest-dipping normal faults (**Figure 5.1**). Relatively little structural deformation could be linked to the Iditarod-Nixon Fork fault (**Figure 5.1**) compared to the overall volume of structures.

Further study of the structures could benefit from incorporating drill hole data into the three-dimensional models I presented. Based on this thesis, skarn researchers are cautioned not to assume that a pluton near a skarn is necessarily responsible for the skarn.

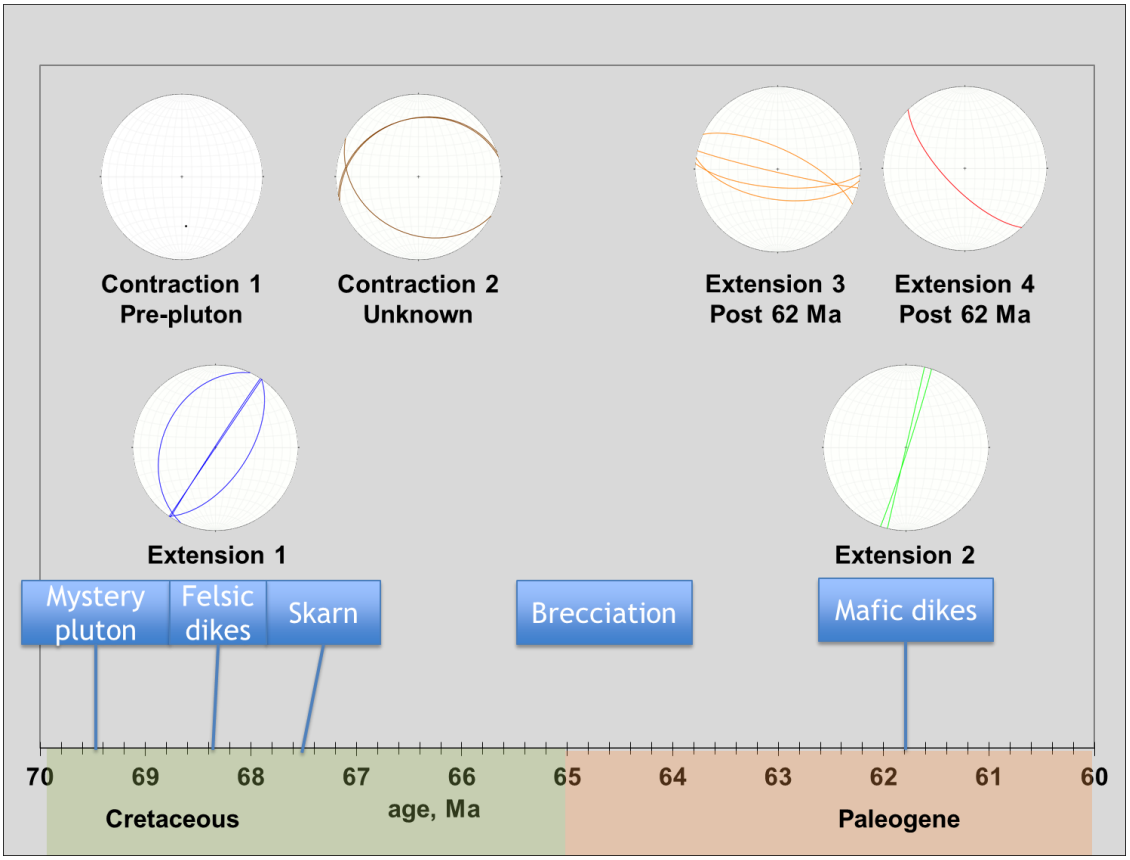

Figure 5.1 Diagram depicting timing of different strain field orientations associated with the Nixon Fork deposit. Contraction 1 occurred prior to intrusion of the Mystery pluton and Contraction 2 has no identified time of formation. Extension 1 is at roughly 69 Ma, coincident with the intrusion of felsic dikes. Extension 2 is at roughly 62 Ma, coincident with intrusion of mafic dikes. Extensions 3 & 4 are possibly related to each other and likely occurred in conjunction with right lateral motion on the Iditarod-Nixon Fork fault.

6 References

Bateman, P., Dudek, A., Keller, J., Lameyre, J., Le Bas, M.J., Sabine, P.A., Schmid, R., Sorensen, H., Streckeisen, A., Woolley, A.R., and Zanettin, B., 1989, A Classification of Igneous Rocks and Glossary of Terms: Recommendations of the International Union of Geological Sciences Subcommission on the Systematics of Igneous Rocks. (R. W. Le Maitre, Ed.): Blackwell Scientific Publications, Oxford.

Bauer, R.L., 1980, Multiphase deformation in the Granite Falls-Montevideo area, Minnesota River Valley, in: Selected Studies of Archean Gneisses and Lower Proterozoic Rocks, Southern Canadian Shield, eds. Morey, G.B. Hanson, G.N.: Geological Society of America Special Papers, v. 182, p. 1–18.

Blodgett, R.B., 1998, Emsian (Late Early Devonian) fossils indicate a Siberian origin for the Farewell Terrane, p. 53-61 in Clough, J.G., and Larson, Frank, eds., Short notes on Alaska geology 1997: Alaska Division of Geological & Geophysical Surveys Professional Report 118:.

Brooks, A.H., and Martin, G.C., 1921, The Alaskan mining industry in 1919, p. 59-95, in U.S. Geological Survey, Mineral resources of Alaska, report on progress of investigations in 1919: U.S. Geological Survey Bulletin 714:.

Brown, J.S., 1925, The Nixon Fork country, p. 97-144, in U.S. Geological Survey, Mineral resources of Alaska, report on progress of investigations in 1924: U.S. Geological Survey Bulletin 783:.

Bundtzen, T.K., and Miller, M.L., 1997, Precious metals associated with Late Cretaceous-Early Tertiary igneous rocks of southwestern Alaska: Economic Geology, v. Monograph , p. 242–286.

Burnett, W.J., and Grady, J.C., 2005, Whalen Glory Hole 2005 Exploration report, unpublished report for Mystery Creek Resources, Inc.: p. 27.

Coe, R.S., Globerman, B.R., Plumley, P.W., and Thrupp, G.A., 1985, Paleomagnetic results from Alaska and their tectonic implications, in Howell, D.G., ed., Tectonostratigraphic terranes of the Circum-Pacific region: American Association of Petroleum Geologists, v. Circum-Pac, p. 85–108.

Cutler, S.E., 1994, Geology and Mineralization of the Nixon Fork Skarn: Unpublished M.S. thesis, University of Alaska Fairbanks, p. 133.

Davis, G.H., and Reynolds, S., 1996, Structural Geology of Rocks and Regions: John Wiley & Sons, Inc.

De la Roche, H. De, Leterrier, J., Grandclaude, P., and Marchal, M., 1980, A classification of volcanic and plutonic rocks using R1R2-diagram and major-element analyses — Its relationships with current nomenclature: Chemical Geology, v. 29, p. 183–210.

Deal, M., 2012, Origins and Zoning of the Buckhorn Gold Skarn, NE Washington: M.S. Thesis, University of Alaska Fairbanks, p. 176.

Decker, J., Bergman, S.C., Blodgett, R.B., Box, S.E., Bundtzen, T.K., Clough, J.G., Coonrad, W.L., Gilbert, W.G., Miller, M.L., Murphy, J.M., Robinson, M.S., and Wallace, W.K., 1994, Geology of southwestern Alaska, in Plafker, George, and Berg, H.C., The Geology of Alaska: Geological Society of America:.

Dickin, A.P., 2005, Radiogenic Isotope Geology: Cambridge University Press, p. 512.

Einaudi, M.T., and Burt, D.M., 1982, Introduction; terminology, classification, and composition of skarn deposits: Economic Geology, v. 77, p. 745–754.

Freeman, C.J., and Giroux, G.H., 2012, GEOLOGIC REPORT NF-12-1 Technical Report on the Nixon Fork Mine Project, Medfra Quadrangle, Alaska: Avalon Development Corporation, Faribanks, Alaska, p. 135.

Gaber, L.J., Foland, K.A., and Corbato, C.E., 1988, On the significance of Ar release from biotite and amphibole during $^{40}Ar/^{39}Ar$ vacuum heating: Geochimica et Cosmochimica Acta, v. 52, p. 2457–2465.

Hamilton, T.D., 1994, Late Cenozoic glaciation of Alaska: the geology of Alaska., *in* Plafker, G. and Berg, H.C. eds., The Geology of North America, Vol. G-1, Geological Society of America, Boulder, CO, p. 813–844.

Harrison, T.M., 1981, Diffusion of ^{40}Ar in hornblende: Contributions to Mineralogy and Petrology, v. 78, p. 324–331.

Herreid, G.H., 1966, Geology and geochemistry of the Nixon Fork area, Medfra Quadrangle: Alaska Division of Mines and Minerals Geologic Report 22: p. 29.

Jasper, M.W., 1961, Report on mespelt mine operation of Strandberg Mines, Inc., Nixon Fork district, Medfra quadrangle, Alaska: p. 9.

Kamb, W.B., 1959, Ice petrofabric observations from Blue Glacier, Washington in relation to theory and experiment.: Journal of Geophysical Research, v. 64, p. 1891–1909.

Kendrick, M.A., and Phillips, D., 2009, New constraints on the release of noble gases during in vacuo crushing and application to scapolite Br–Cl–I and $^{40}Ar/^{39}Ar$ age determinations: Geochimica et Cosmochimica Acta, v. 73, p. 5673–5692.

Lanphere, M.A., and Dalrymple, G.B., 2000, First-principles calibration of ^{38}Ar tracers: Implications for the ages of $^{40}Ar/^{39}Ar$ fluence monitors, U.S. Geological Survey Professional Paper 1621: p. 10.

Layer, P., 2000, Argon-40/Argon-39 age of the El'gygytgyn impact event, Chukotka, Russia: Meteroitics and Planetary Science, v. 35, p. 591–599.

LeBas, M.J., Le Maître, R.W.L., Streckeisen, A., and Zanettin, B., 1986, A Chemical Classification of Volcanic-Rocks Based on the Total Alkali Silica Diagram: Journal of Petrology, v. 27, p. 745–750.

Martin, G.C., 1922, Gold lodes in the upper Kuskokwim region, Alaska, in U.S. Geological Survey, Mineral resources of Alaska, report on progress of investigations in 1920: U.S. Geological Survey Bulletin 722: p. 149–161.

McDougall, I., and Harrison, T.M., 1999, Geochronology and Thermochronology by the 40Ar/39Ar method-2nd ed: Oxford University Press, p. 269, New York.

Merrihue, C., and Turner, G., 1966, Potassium-argon dating by activation with fast neutrons: Journal of Geophysical Research, v. 71, p. 2852–2857.

Mertie, J.B., 1936, Mineral deposits of the Ruby-Kuskokwim region, Alaska: U.S. Geological Survey Bulletin 864-C: p. 115–245.

Meschede, M., 1986, A method of discriminating between different types of mid-ocean ridge basalts and continental tholeiites with the Nb-Zr-Y diagram: Chemical Geology, v. 56, p. 207–218.

Miller, M., Bradley, D., Bundtzen, T., and McClelland, W., 2002, Late Cretaceous through Cenozoic strike-slip tectonics of southwestern Alaska: The Journal of Geology, v. 110, p. 247–270.

Mitchell, J., 1968, The argon -40/ argon -39 method for potassium-argon age determination: Geochimica et Cosmochimica Acta, v. 32, p. 781–790.

Moll, E.J., Silberman, L., and Patton, W.W., 1981, Chemistry, mineralogy, and K-Ar ages of igneous and metamorphic rocks of the Medfra quadrangle, Alaska: U.S. Geological Survey Open-File Report 80-811C: p. 1.

Mrozek, S., 2012, Geology and the Origin of the Mike Lake Au-Cu Skarn Deposit, Yukon Territory, Canda:.

Newberry, R.J., Allegro, G.L., Cutler, S.E., Hagen-Levelle, D.D., Adams, D.D., Nicholson, L.C., Weglarz, T.B., Bakke, A.A., Clautice, K.H., Coulter, G.A., Ford, M.J., Myers, G.L., and Szumigala, D., 1997, Skarn deposits of Alaska, in Goldfarb, R.J., and Miller, L.D., eds., Mineral Deposits of Alaska: Economic Geology Monograph 9: p. 355–395.

Nokleberg, W., Bundtzen, T., Berg, H., Andersen, G.L., Chipp, E.R., Gaard, D.R., Burton, P.J., Dunbier, J., Scherkenbach, D.A., Foley, J.Y., Thurow, G., Warner, J.D., Freeman, C.J., Gamble, B.M., and others, 1994, Metallogeny and major mineral deposits of Alaska, in Plafker, George, and Berg, H.C., The Geology of Alaska: Geological Society of America: p. 1.

Patton, W.W., Box, S.E., Moll-Stalcup, E.J., and Miller, T.P., 1994, Geology of west-central Alaska: U.S. Geological Survey Open-File Report 89-554: p. 54.

Patton, W.W., Moll, E.J., Dutro, J.T., Silberman, L., and Chapman, R.M., 1980, Preliminary geologic map of Medfra quadrangle, Alaska: U.S. Geological Survey Open-File Report 80-811-A: p. 1.

Patton, W.W., Moll, E.J., and King, H.D., 1984, The Alaskan Mineral Resources Assessment Program : Guide to Information Contained in the Folio of Geologic and Mineral-Resource Maps of the Medfra Quadrangle , Alaska: p. 11.

Pearce, J.A., and Cann, J.R., 1973, Tectonic setting of basic volcanic rocks determined using trace element analyses: Earth and Planetary Science Letters, v. 19, p. 290–300.

Pearce, J.A., Harris, N.B.W., and Tindle, A.G., 1984, Trace element discrimination diagrams for the tectonic interpretation of granitic rocks: Journal of Petrology, v. 25, p. 956–983.

Power, W., Burnett, W., Stapleton, P., Peden, R., Stuart, R., Wilson, P., Kirby, L., Robertson, S., Panizza, N., and Holden, D., 2003, Geological Data Audit and modeling, Nixon Fork Mining Region, Vicinity Medfra, Alaska: p. 125.

Reiners, P.W., and Brandon, M.T., 2006, Using thermochronology to understand orogenic erosion: Annual Reviews of Earth and Planetary Science, v. 34, p. 219–266.

Reiners, P.W., Ehlers, T.A., and Zeitler, P.K., 2005, Past, present, and future of thermochronology. in: Low-Temperature Thermochronology: Techniques, Interpretations, and Applications, edited by P. W. Reiners & T. A. Ehlers: Rev. Mineral. Geochem., v. 58, p. 1–18.

Samson, S.D., and Alexander, E.C., 1987, Calibration of the interlaboratory $^{40}Ar/^{39}Ar$ dating standard MMhbl.: Chemical Geology, v. 66, p. 27–34.

Silberling, N.J., Jones, D.L., Monger, J.W.H., Coney, P.J., Berg, H.C., and Plafker, G., 1994, Lithotectonic terrane map of Alaska and adjacent parts of Canada, in Plafker, George, and Berg, H.C., The Geology of Alaska: Geological Society of America: p. 1 sheet.

Streckeisen, A., and Le Maitre, R.W., 1979, A chemical approximation to the modal QAPF classification of the igneous rocks: Neues Jahrbuch f{ü}r Mineralogie, Abhandlungen, v. 136, p. 169–206.

Szumigala, D., 1993, Gold mineralization related to Cretaceous-Tertiary magmatism in the Kuskokwim Mountains of west-central and southwestern Alaska: University of California, p. 310.

Szumigala, D., 1996, Gold mineralization related to Cretaceous-Tertiary magmatism in west-central Alaska-A geochemical model and prospecting guide for the Kuskokwim region: Geological Society of Nevada Symposium Proceedings, *in* Geology and Ore Deposits of the American Cordillera,, p. 1317–1340.

Wallace, W., Hanks, C., and Rogers, J., 1989, The southern Kahiltna terrane: Implications for the tectonic evolution of southwestern Alaska: Geological Society of America Bulletin, v. 101, p. 1389–1407.

Wallis, C.S., Rennie, D.W., and Hendry, J.W., 2003, Report on the Nixon Fork Project, Alaska: Roscoe Postle Associates Inc., Toronto, Ontario, p. 61.

Winchester, J.A., and Floyd, P.A., 1977, Geochemical discrimination of different magma series and their differentiation products using immobile elements: Chemical Geology, v. 20, p. 325–343.

Wintzer, N.E., 2009, Structure of the Skagit Gneiss Complex in Diablo Lake area, North Cascades, WA: San Jose State University, Master's Thesis, p. 84.

Appendix

Mystery Creek Resources, Inc underground mapping of the Nixon Fork mine.

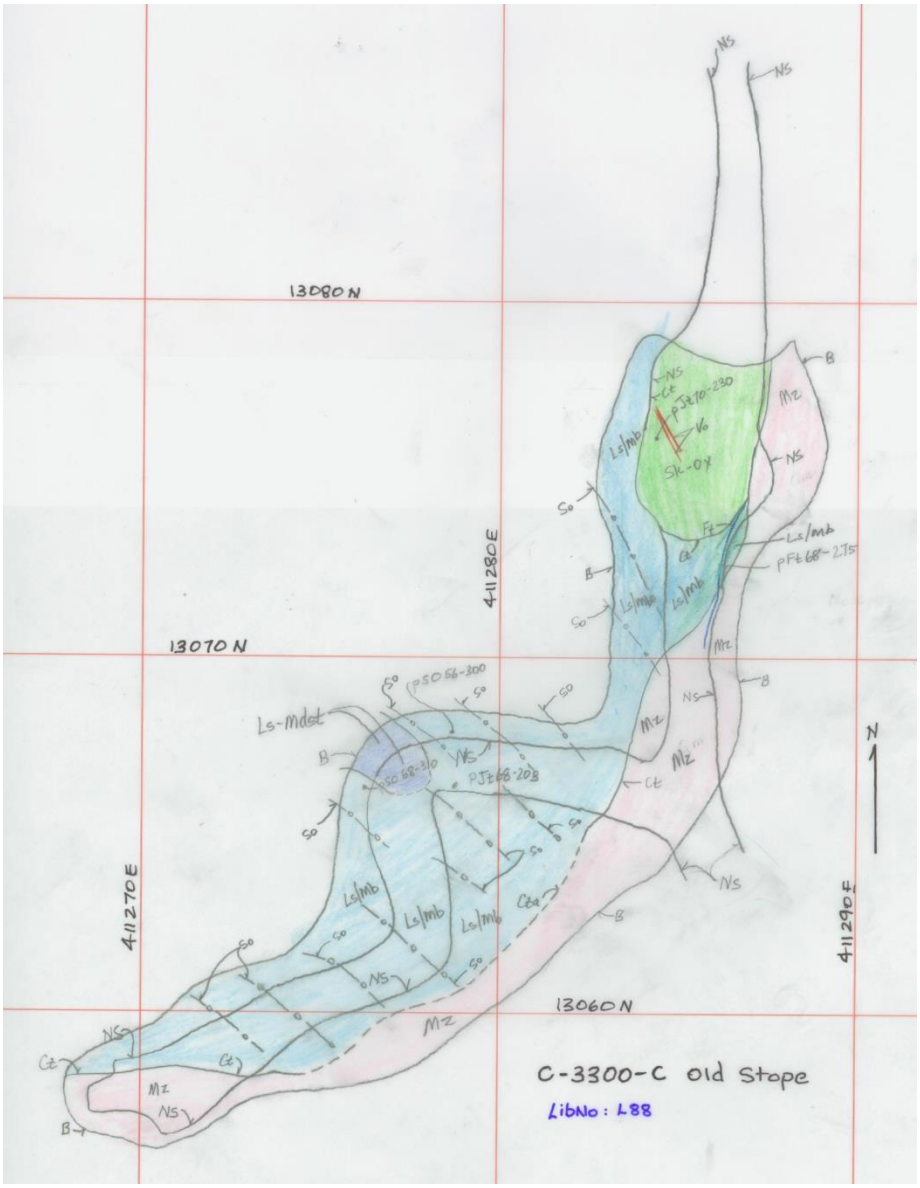

Figure A-1 Geologic map of 3300C stope 342 m elevation underground workings. Green is oxidized skarn, orange is Mystery pluton, light blue is limestone/marble, dark blue is limestone/mudstone. Purple line is CAD outline of the level. pSø = layering, pJt = joint plane, pFa = fold axis, pFaa = fold axis-anticline, pFas = fold axis-syncline, pSl = slickenlines, pFtN = normal fault, pFt = fault plane, pVc = calcite vein, pCt = contact plane, Ct = contact, Ft = minor fault, Fr = minor fracture. Map image created by Mystery Creek Resources, Inc.

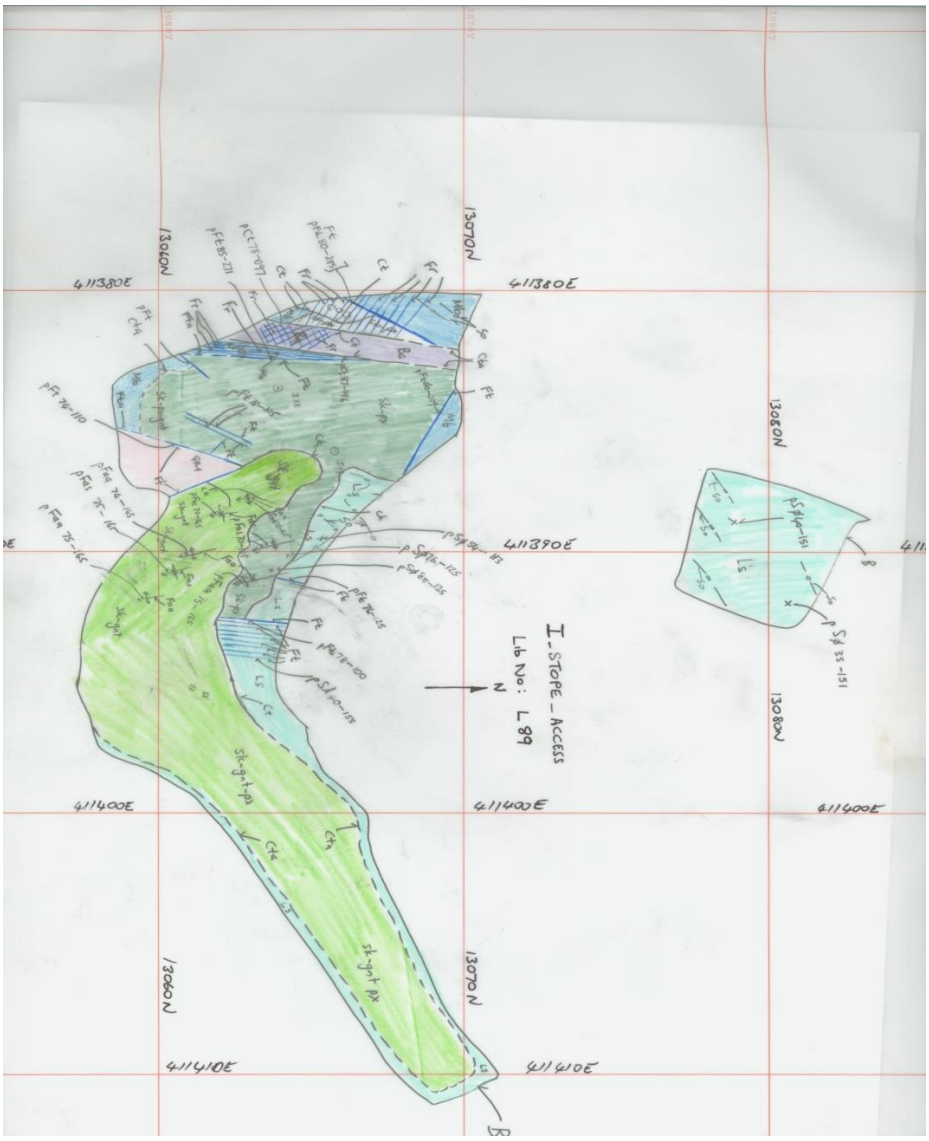

Figure A-2 Geologic map of I stope access 245 m to 255 m elevation underground workings. Light green is garnet pyroxene skarn, dark green is pyroxene skarn, orange is Mystery pluton, light blue is limestone, dark blue is marble, purple is mafic dike. Red line is CAD outline of the level. pSø = layering, pJt = joint plane, pFa = fold axis, pFaa = fold axis-anticline, pFas = fold axis-syncline, pSl = slickenlines, pFtN = normal fault, pFt = fault plane, pVc = calcite vein, pCt = contact plane, Ct = contact, Ft = minor fault, Fr = minor fracture. Map image created by Mystery Creek Resources, Inc.

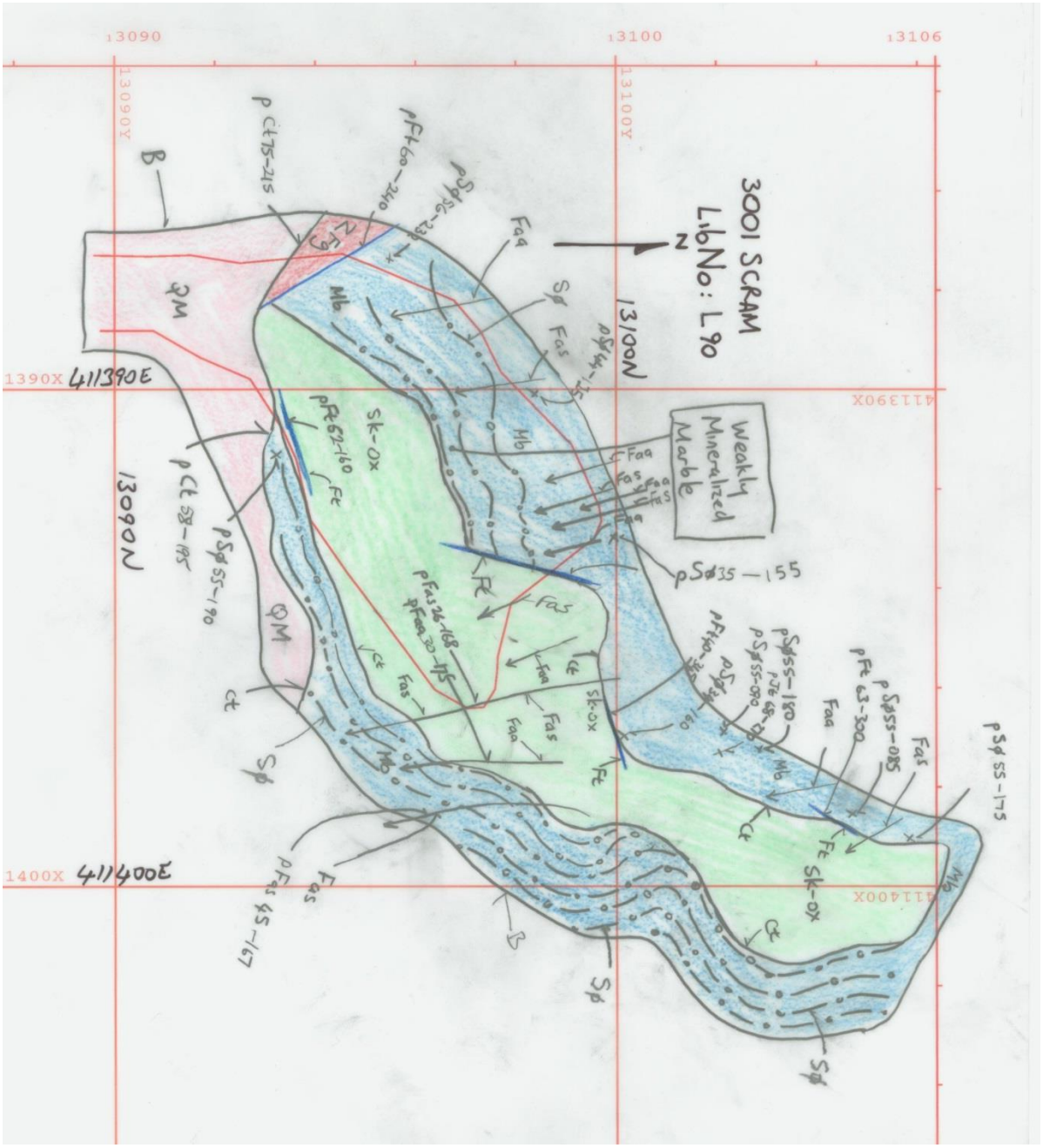

Figure A-3 Geologic map of 3001 SCRAM 385 m elevation underground workings. Light green is oxidized skarn, light orange is Mystery pluton, dark orange is felsic dike, blue is marble. Red line is CAD outline of the level. pSø = layering, pJt = joint plane, pFa = fold axis, pFaa = fold axis-anticline, pFas = fold axis-syncline, pSl = slickenlines, pFtN = normal fault, pFt = fault plane, pVc = calcite vein, pCt = contact plane, Ct = contact, Ft = minor fault, Fr = minor fracture. Map image created by Mystery Creek Resources, Inc.

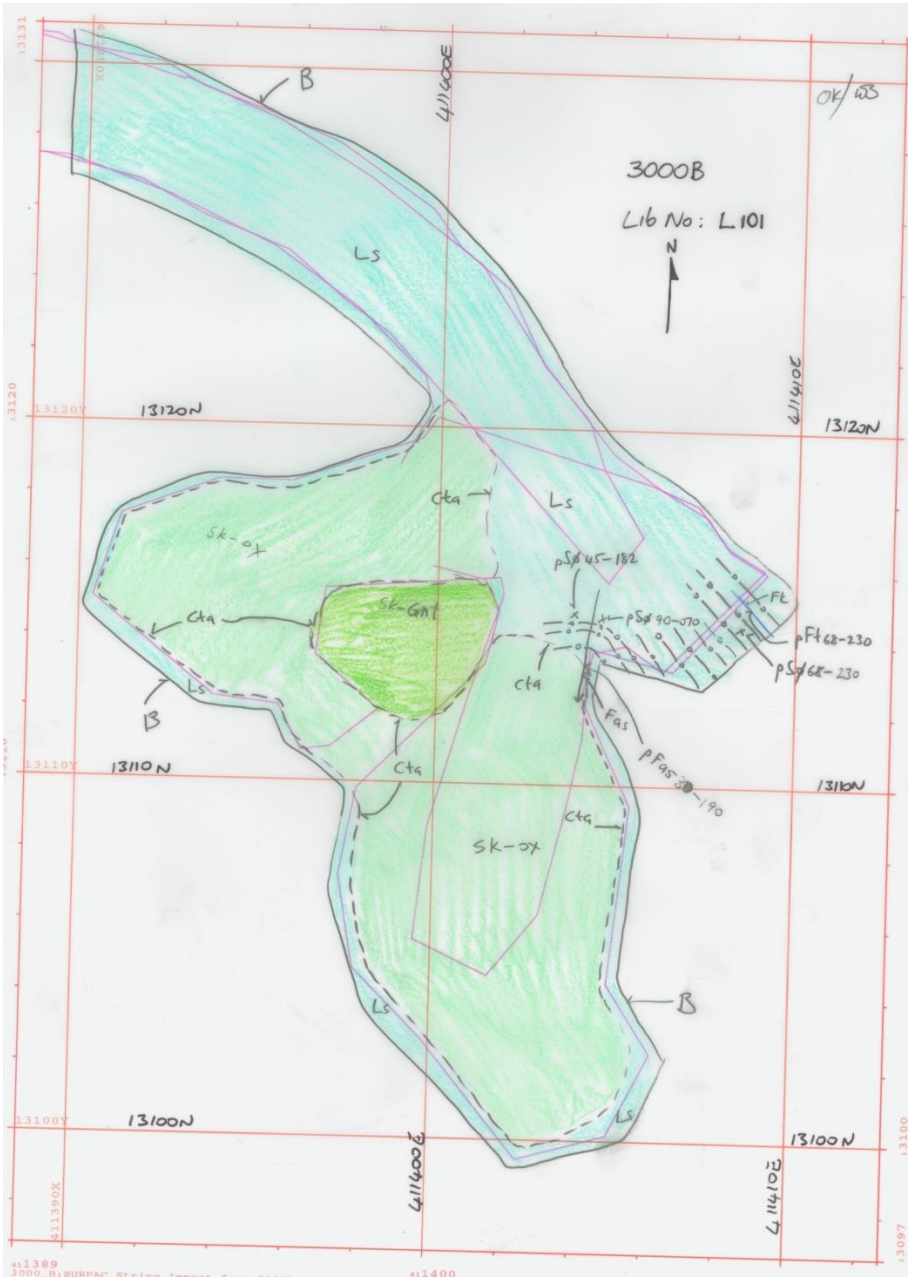

Figure A-4 Geologic map of 3000B stope 346 m to 352 m elevation underground workings. Light green is oxidized skarn, dark green is garnet skarn, blue is limestone. Red line is CAD outline of the level. pSø = layering, pJt = joint plane, pFa = fold axis, pFaa = fold axis-anticline, pFas = fold axis-syncline, pSl = slickenlines, pFtN = normal fault, pFt = fault plane, pVc = calcite vein, pCt = contact plane, Ct = contact, Ft = minor fault, Fr = minor fracture. Map image created by Mystery Creek Resources, Inc.

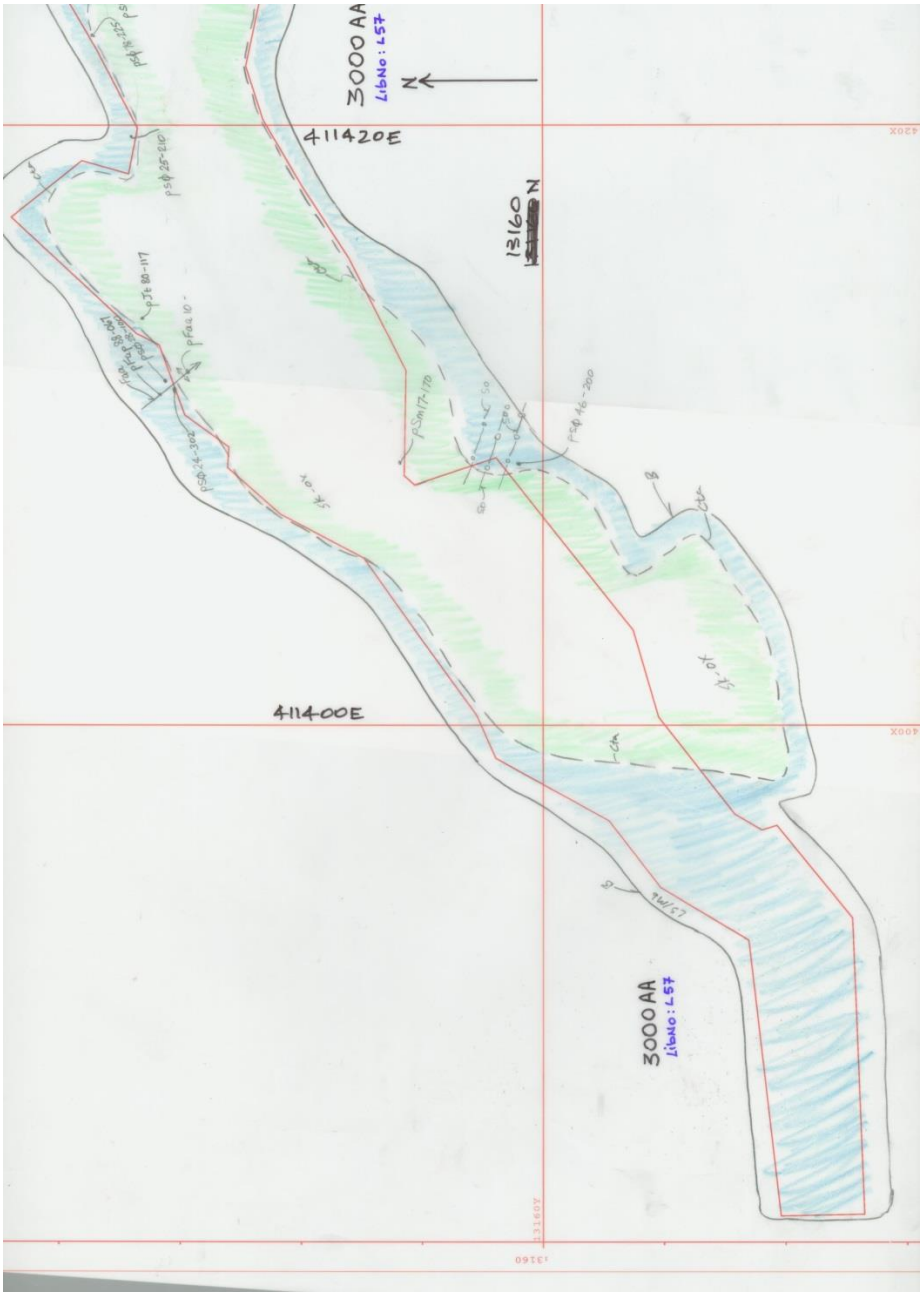

Figure A-5 Geologic map of 3000AA 395 m to 400 m elevation underground workings. Light green is oxidized skarn, light blue is limestone/marble. Red line is CAD outline of the level. pSø = layering, pJt = joint plane, pFa = fold axis, pFaa = fold axis-anticline, pFas = fold axis-syncline, pSl = slickenlines, pFtN = normal fault, pFt = fault plane, pVc = calcite vein, pCt = contact plane, Ct = contact, Ft = minor fault, Fr = minor fracture. Map image created by Mystery Creek Resources, Inc.

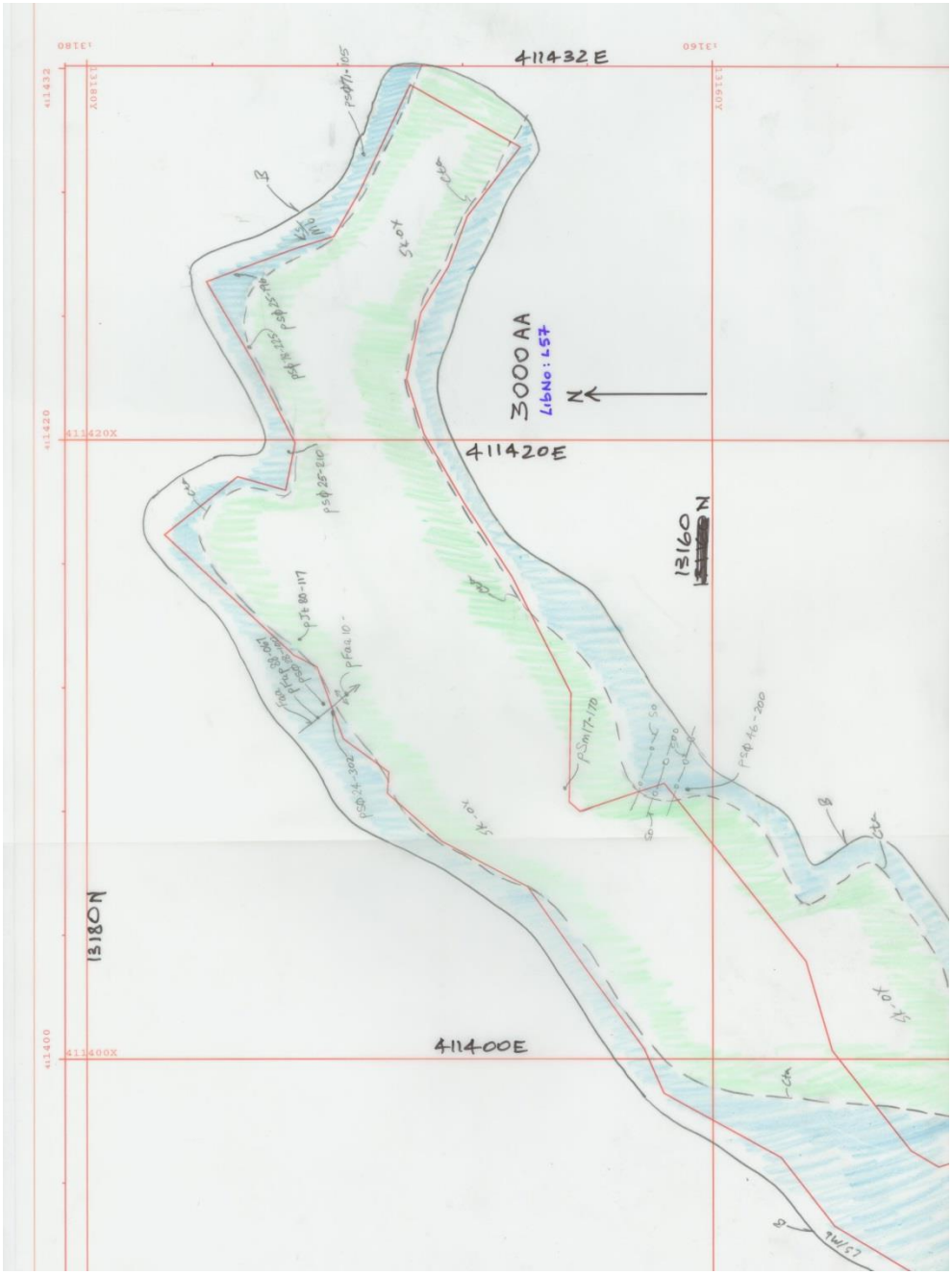

Figure A-6 Geologic map of 3000AA 395 m to 400 m elevation underground workings. Light green is oxidized skarn, light blue is limestone/marble. Red line is CAD outline of the level. pSø = layering, pJt = joint plane, pFa = fold axis, pFaa = fold axis-anticline, pFas = fold axis-syncline, pSl = slickenlines, pFtN = normal fault, pFt = fault plane, pVc = calcite vein, pCt = contact plane, Ct = contact, Ft = minor fault, Fr = minor fracture. Map image created by Mystery Creek Resources, Inc.

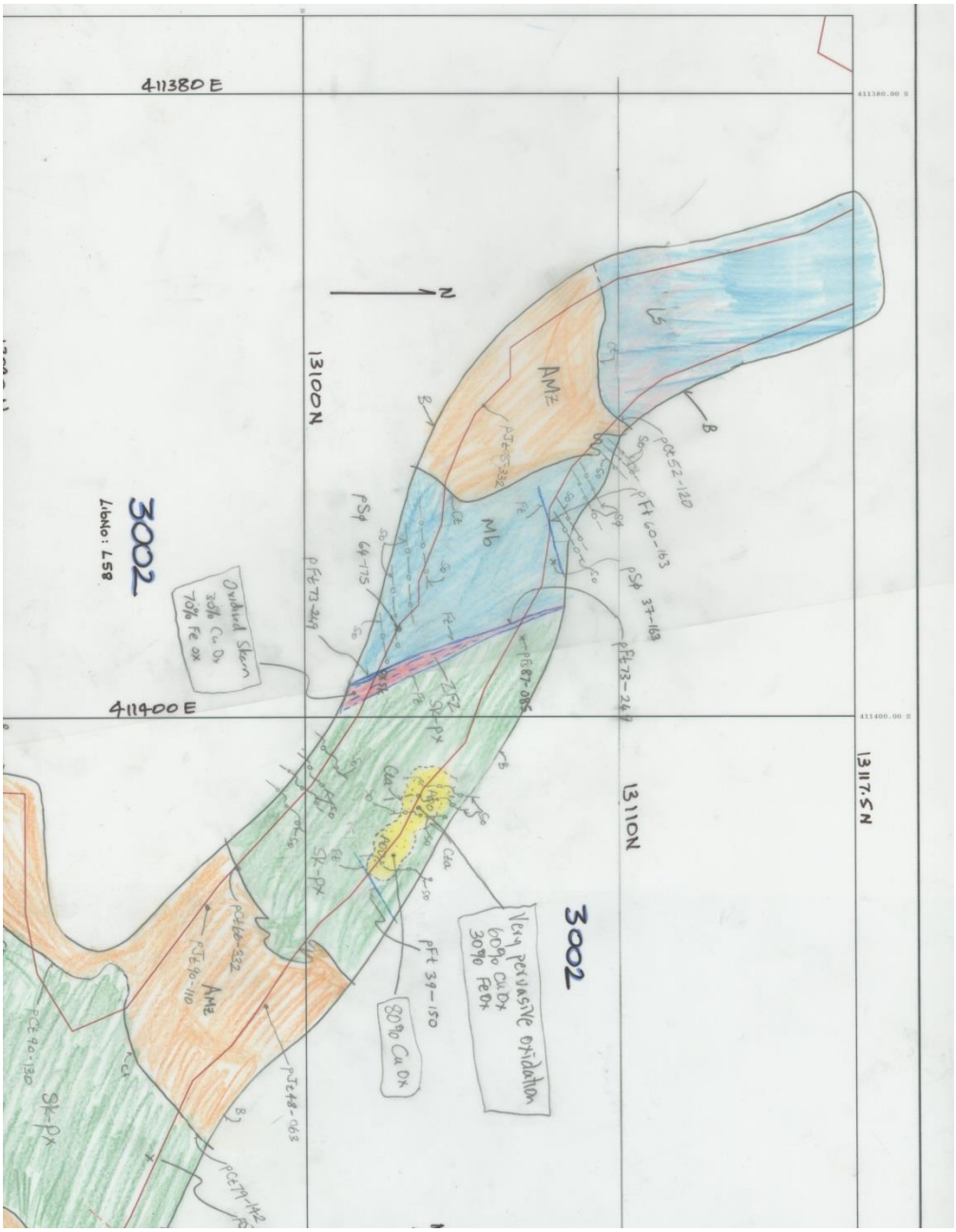

Figure A-7 Geologic map of 3002/3002A 394 m to 400 m underground workings. Red is oxidized skarn, dark green is pyroxene skarn, yellow is oxidation, orange is Mystery pluton, blue is limestone/marble. Red line is CAD outline of the level. pSø = layering, pJt = joint plane, pFa = fold axis, pFaa = fold axis-anticline, pFas = fold axis-syncline, pSl = slickenlines, pFtN = normal fault, pFt = fault plane, pVc = calcite vein, pCt = contact plane, Ct = contact, Ft = minor fault, Fr = minor fracture. Map image created by Mystery Creek Resources, Inc.

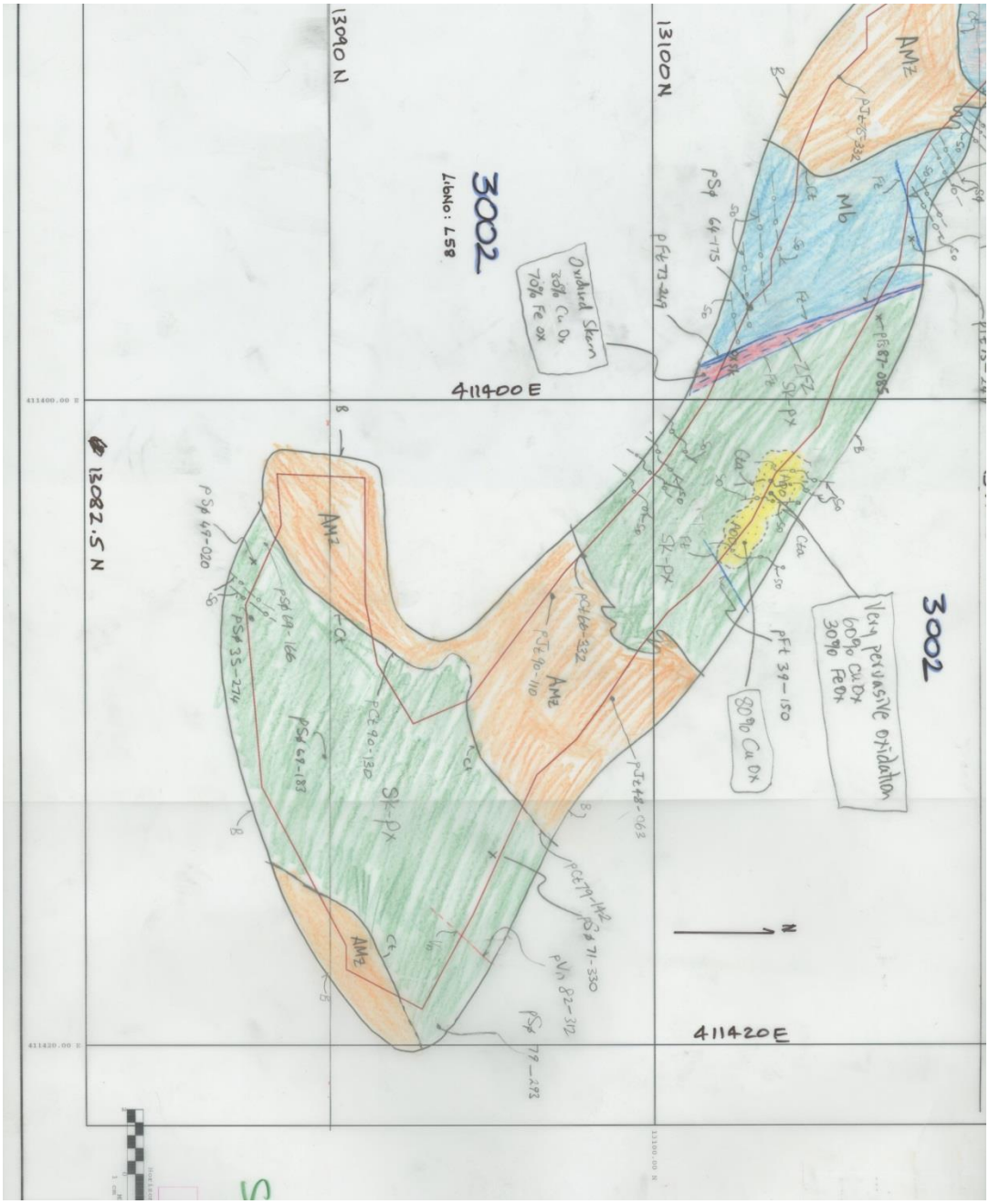

Figure A-8 Geologic map of 3002/3002A 394 m to 400 m underground workings. Red is oxidized skarn, dark green is pyroxene skarn, yellow is oxidation, orange is Mystery pluton, blue is limestone/marble. Red line is CAD outline of the level. pSø = layering, pJt = joint plane, pFa = fold axis, pFaa = fold axis-anticline, pFas = fold axis-syncline, pSl = slickenlines, pFtN = normal fault, pFt = fault plane, pVc = calcite vein, pCt = contact plane, Ct = contact, Ft = minor fault, Fr = minor fracture. Map image created by Mystery Creek Resources, Inc.

Figure A-9 Geologic map of 3004 D 330 m to 333 m elevation underground workings. Light green is garnet magnetite skarn/garnet skarn, red is Mystery pluton, light blue is limestone/ marble. Red line is CAD outline of the level. pSø = layering, pJt = joint plane, pFa = fold axis, pFaa = fold axis-anticline, pFas = fold axis-syncline, pSl = slickenlines, pFtN = normal fault, pFt = fault plane, pVc = calcite vein, pCt = contact plane, Ct = contact, Ft = minor fault, Fr = minor fracture. Map image created by Mystery Creek Resources, Inc.

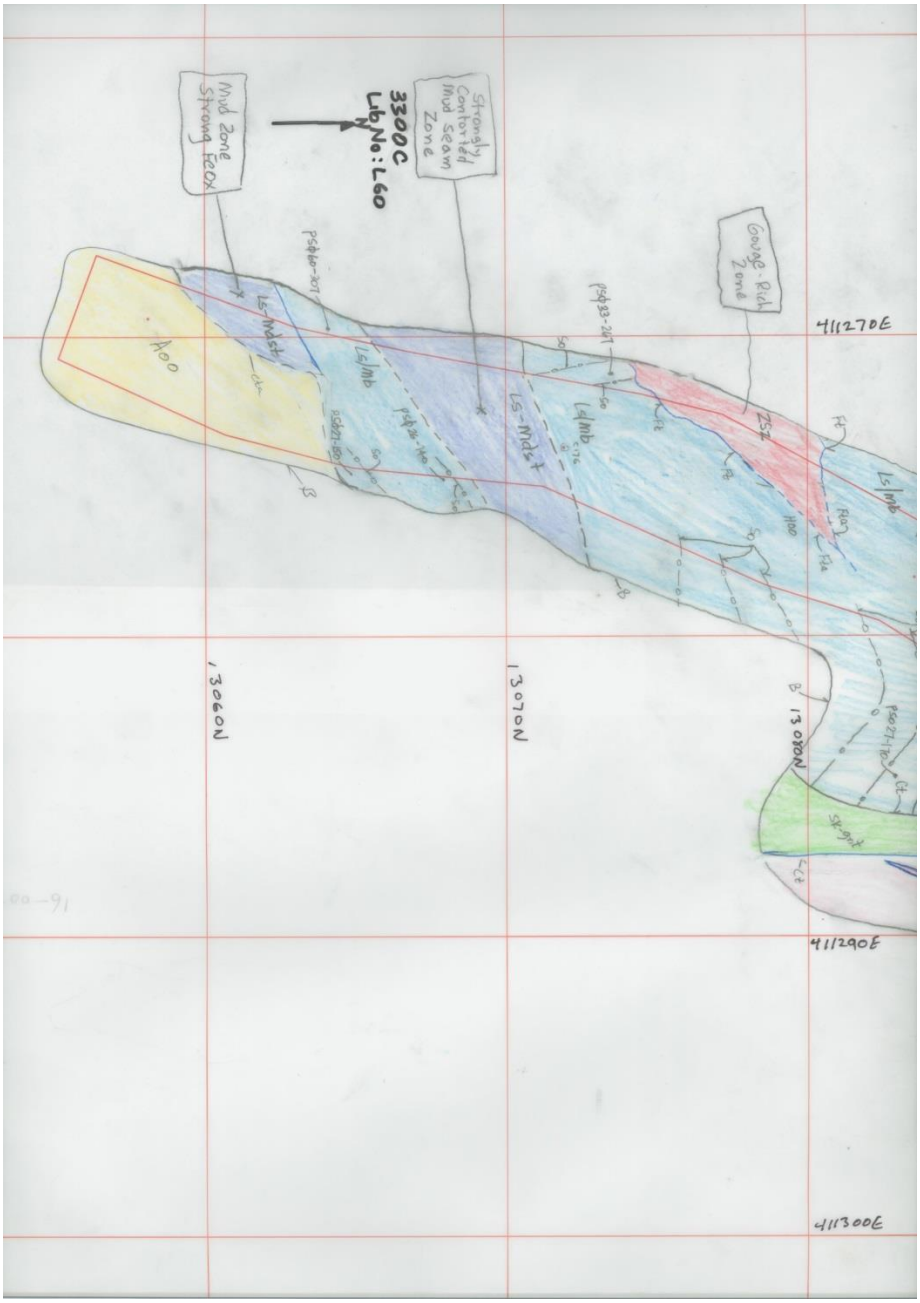

Figure A-10 Geologic map of 3300 C 335 m to 351 m elevation underground workings. Light green is garnet skarn, orange is Mystery pluton, light blue is limestone/marble, dark blue is limestone/mudstone, red is fault gouge. Red line is CAD outline of the level. pSø = layering, pJt = joint plane, pFa = fold axis, pFaa = fold axis-anticline, pFas = fold axis-syncline, pSl = slickenlines, pFtN = normal fault, pFt = fault plane, pVc = calcite vein, pCt = contact plane, Ct = contact, Ft = minor fault, Fr = minor fracture. Map image created by Mystery Creek Resources, Inc.

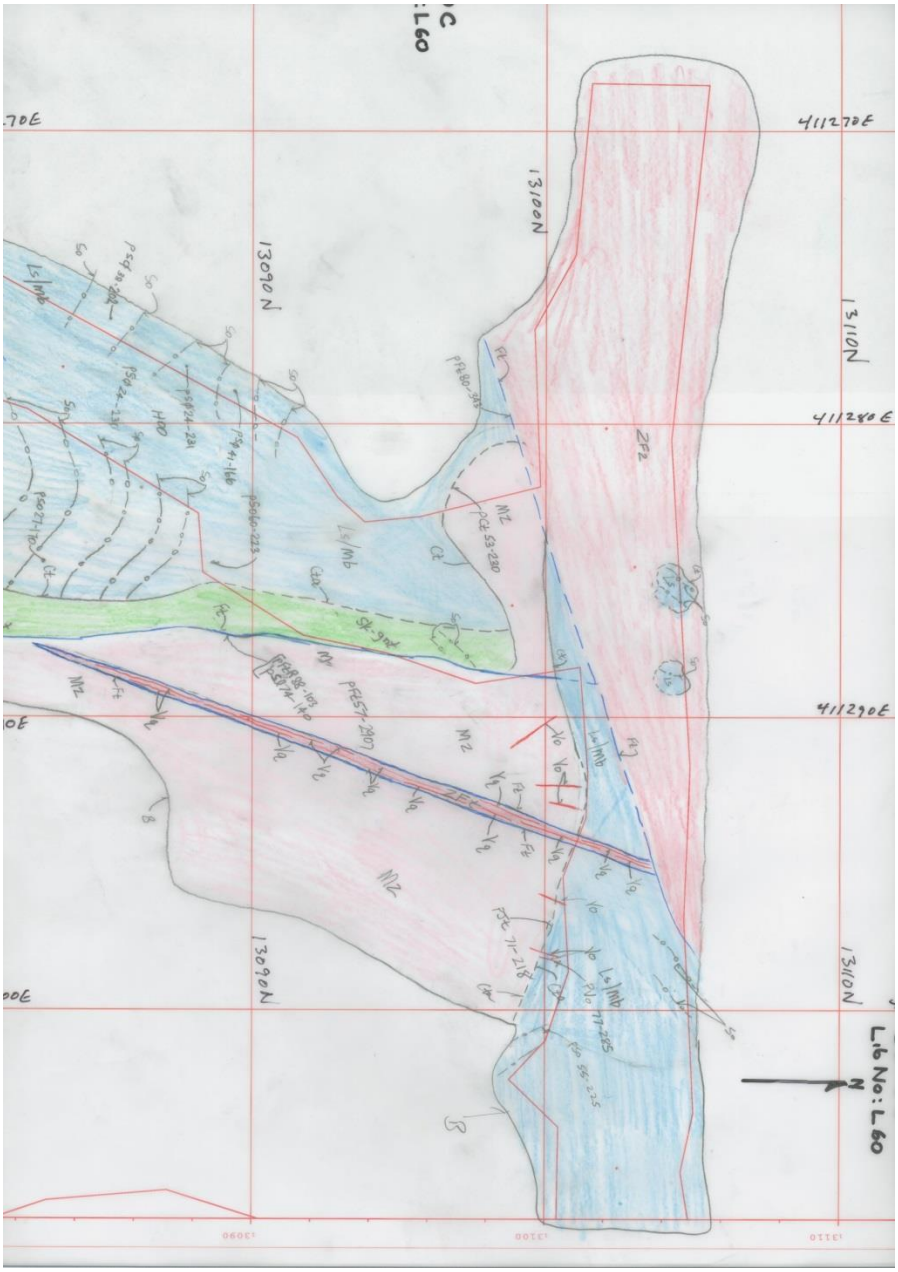

Figure A-11 Geologic map of 3300 C 335 m to 351 m elevation underground workings. Light green is garnet skarn, orange is Mystery pluton, light blue is limestone/marble, red is fault gouge. Red line is CAD outline of the level. pSø = layering, pJt = joint plane, pFa = fold axis, pFaa = fold axis-anticline, pFas = fold axis-syncline, pSl = slickenlines, pFtN = normal fault, pFt = fault plane, pVc = calcite vein, pCt = contact plane, Ct = contact, Ft = minor fault, Fr = minor fracture. Map image created by Mystery Creek Resources, Inc.

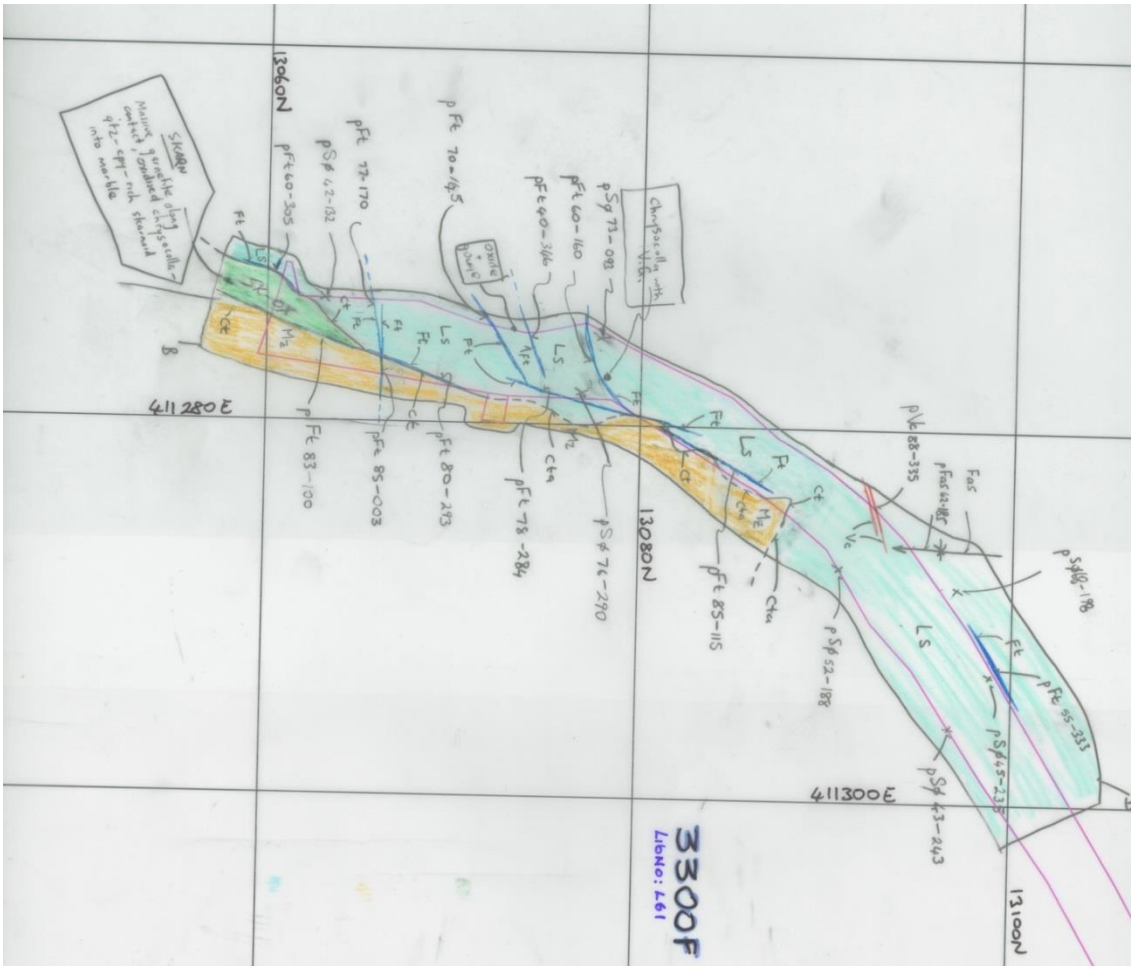

Figure A-12 Geologic map of 3300 F 304 m to 309 m elevation underground workings. Light green is oxidized skarn, yellow is Mystery pluton, light blue is limestone. Red line is CAD outline of the level. pSø = layering, pJt = joint plane, pFa = fold axis, pFaa = fold axis-anticline, pFas = fold axis-syncline, pSl = slickenlines, pFtN = normal fault, pFt = fault plane, pVc = calcite vein, pCt = contact plane, Ct = contact, Ft = minor fault, Fr = minor fracture. Map image created by Mystery Creek Resources, Inc.

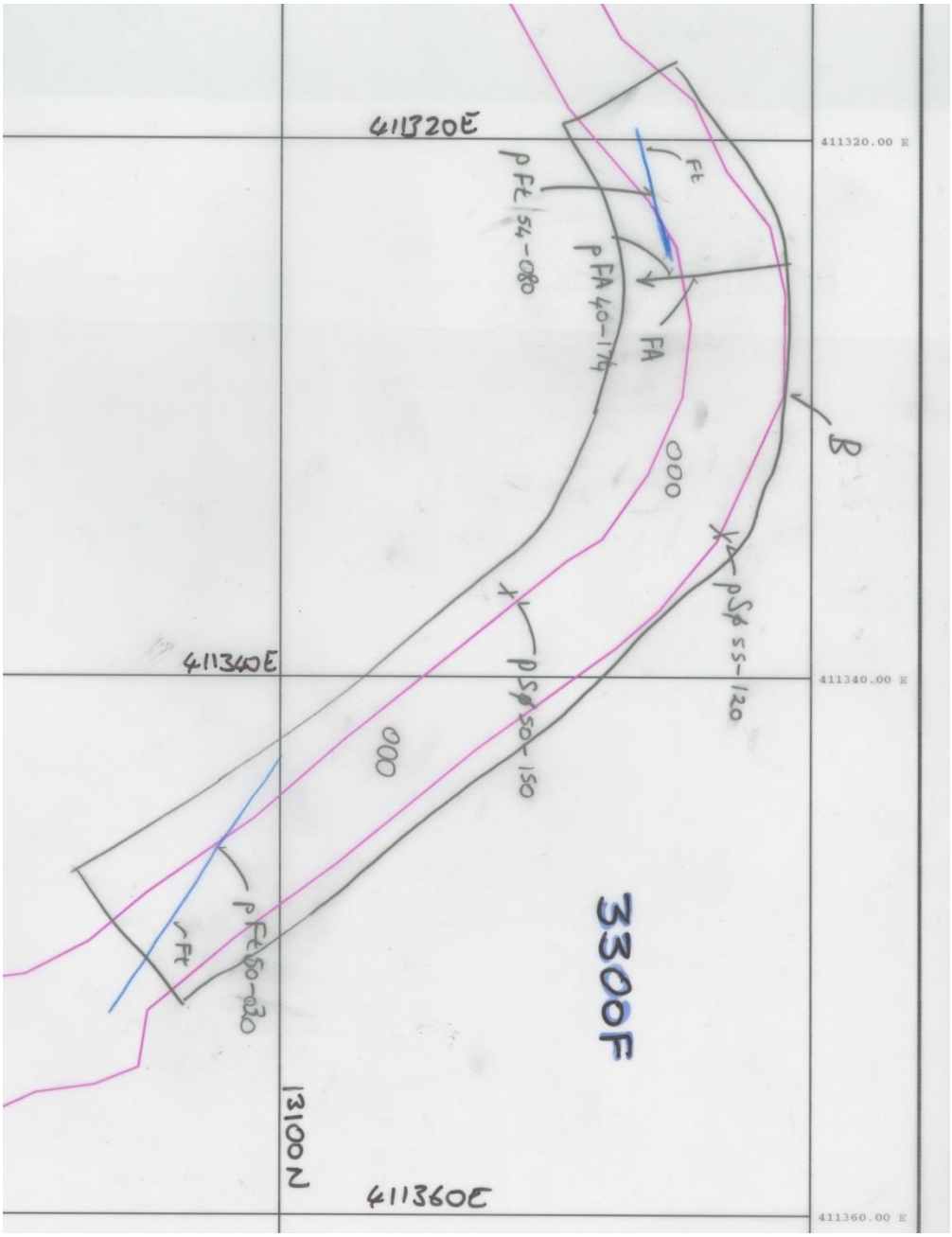

Figure A-13 Geologic map of 3300 F 304 m to 309 m elevation underground workings. 000 designation indicates unidentified rock/void. Red line is CAD outline of the level. pSø = layering, pJt = joint plane, pFa = fold axis, pFaa = fold axis-anticline, pFas = fold axis-syncline, pSl = slickenlines, pFtN = normal fault, pFt = fault plane, pVc = calcite vein, pCt = contact plane, Ct = contact, Ft = minor fault, Fr = minor fracture. Map image created by Mystery Creek Resources, Inc.

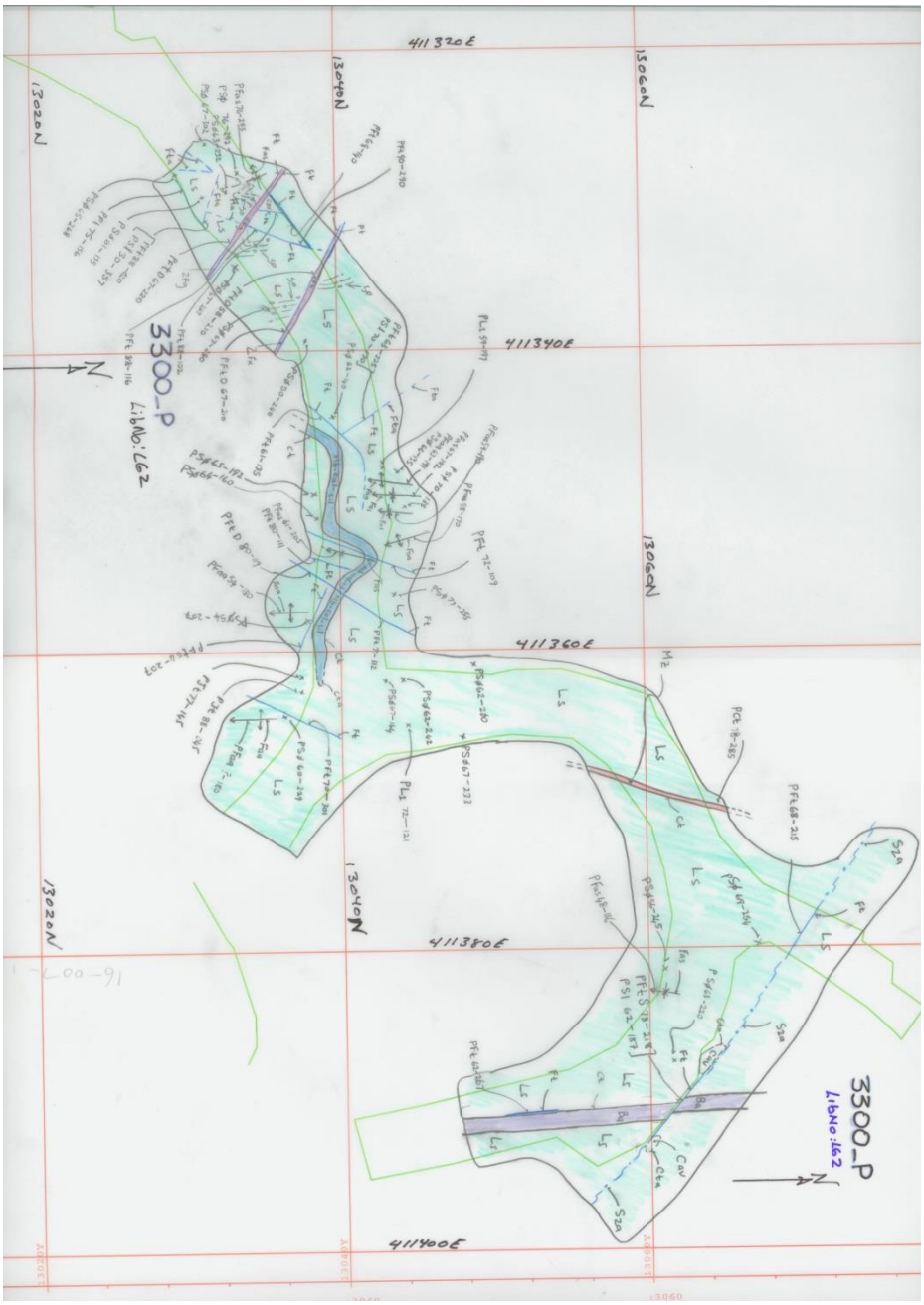

Figure A-14 Geologic map of 3300 P 150 m to 170 m elevation underground workings. Orange is Mystery pluton, light blue is limestone, dark blue is marble/siltstone, purple is mafic dike, red is fault gouge. Red line is CAD outline of the level. pSø = layering, pJt = joint plane, pFa = fold axis, pFaa = fold axis-anticline, pFas = fold axis-syncline, pSl = slickenlines, pFtN = normal fault, pFt = fault plane, pVc = calcite vein, pCt = contact plane, Ct = contact, Ft = minor fault, Fr = minor fracture. Map image created by Mystery Creek Resources, Inc.

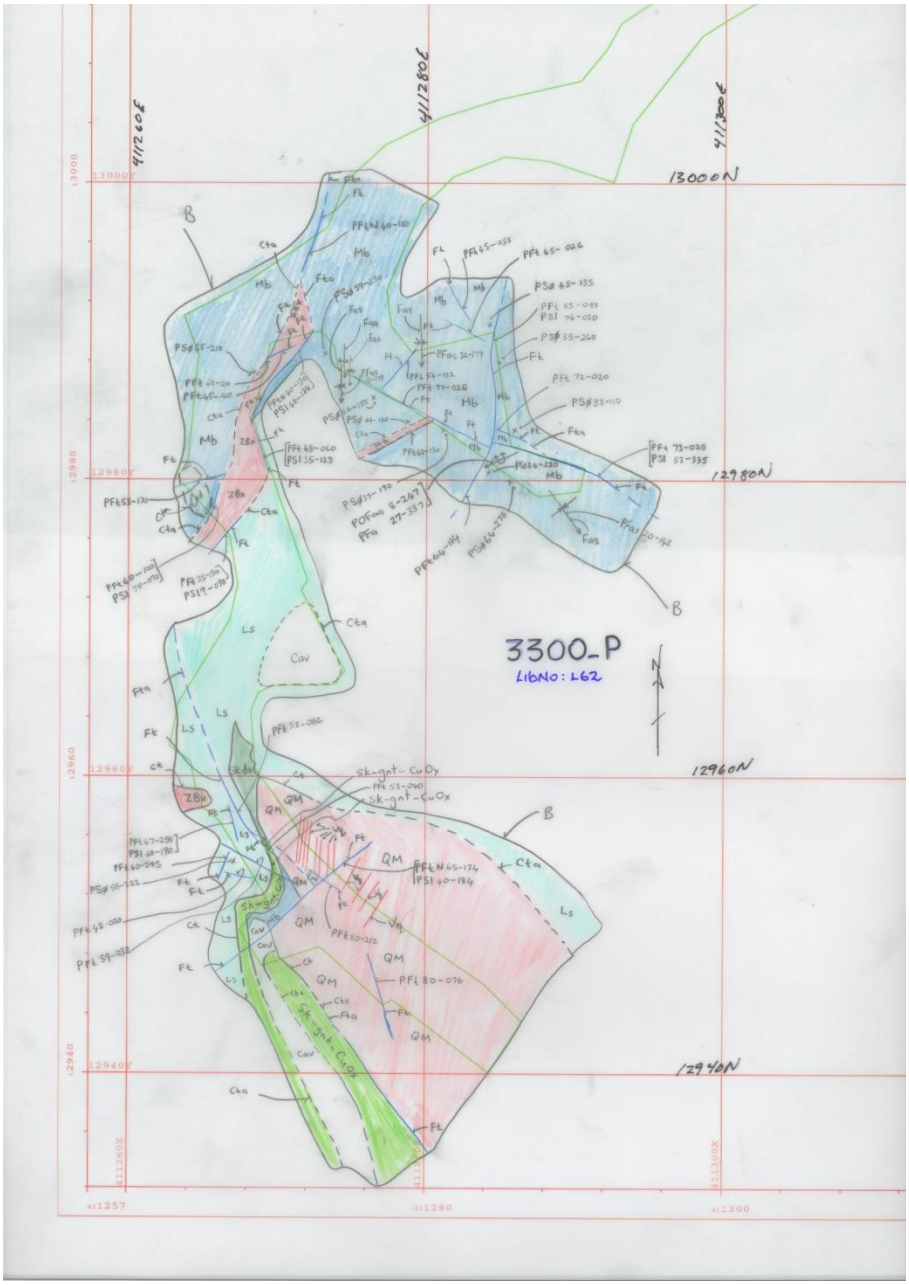

Figure A-15 Geologic map of 3300 P 150 m to 170 m elevation underground workings. Light green is garnet oxidized copper skarn, dark green is pyroxene skarn, orange is Mystery pluton, light blue is limestone, dark blue is marble, red is breccia. Red line is CAD outline of the level. Cav = void, pSø = layering, pJt = joint plane, pFa = fold axis, pFaa = fold axis-anticline, pFas = fold axis-syncline, pSl = slickenlines, pFtN = normal fault, pFt = fault plane, pVc = calcite vein, pCt = contact plane, Ct = contact, Ft = minor fault, Fr = minor fracture. Map image created by Mystery Creek Resources, Inc.

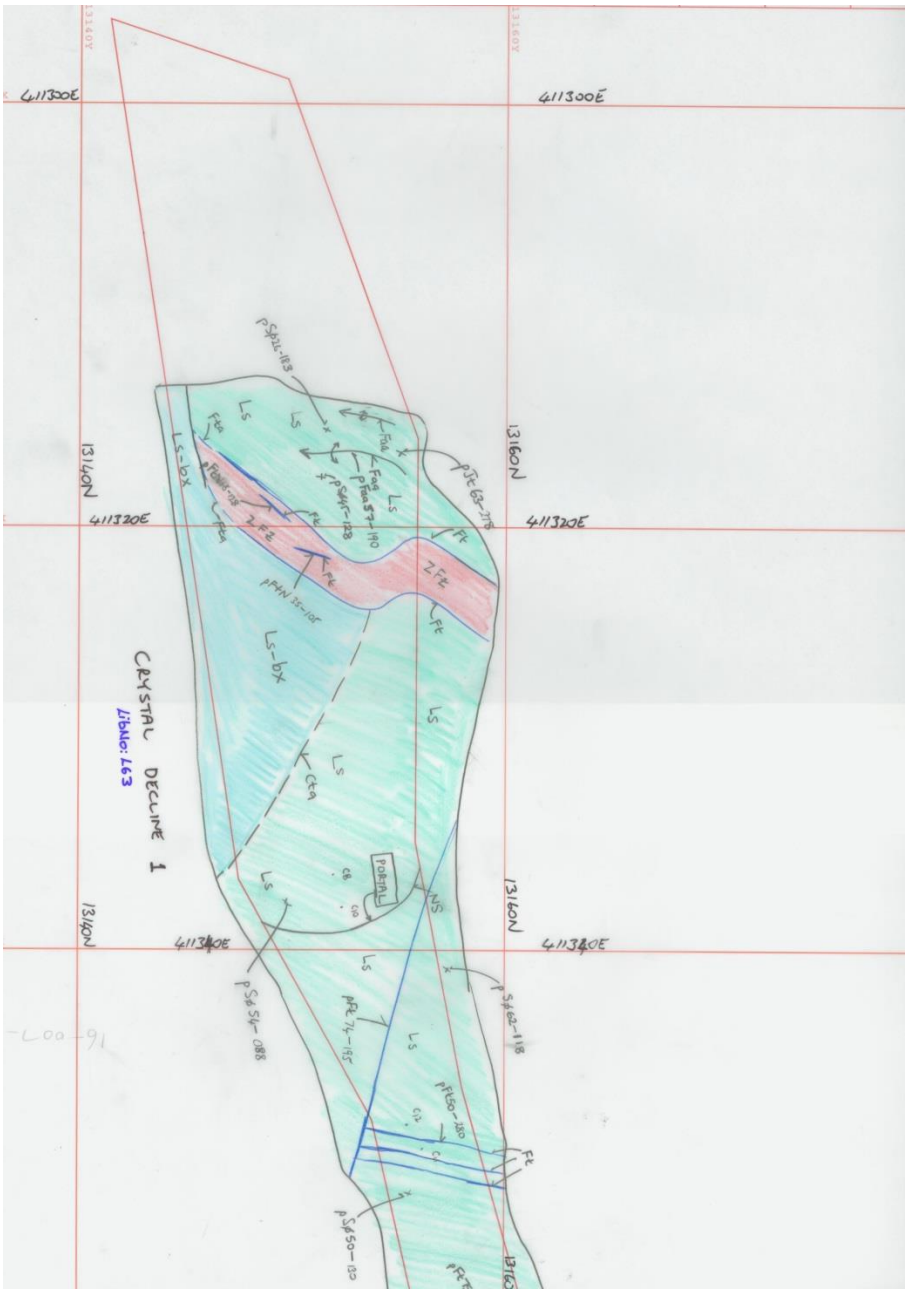

Figure A-16 Geologic map of Portal/C3002 Access 375 m to 404 m elevation underground workings. Light blue is limestone, dark blue is limestone breccia, red is fault zone. Red line is CAD outline of the level. pSø = layering, pJt = joint plane, pFa = fold axis, pFaa = fold axis-anticline, pFas = fold axis-syncline, pSl = slickenlines, pFtN = normal fault, pFt = fault plane, pVc = calcite vein, pCt = contact plane, Ct = contact, Ft = minor fault, Fr = minor fracture. Map image created by Mystery Creek Resources, Inc.

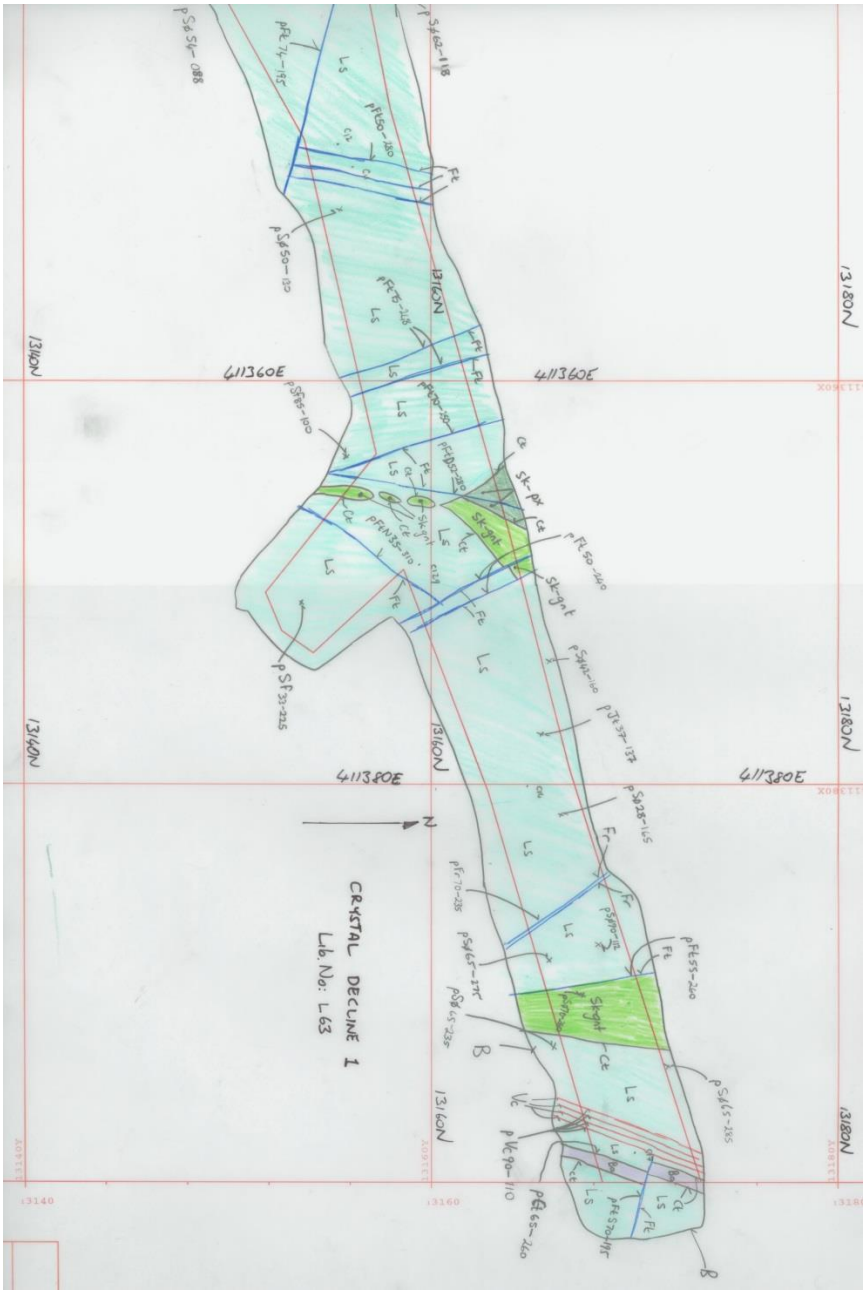

Figure A-17 Geologic map of Portal/C3002 Access 375 m to 404 m elevation underground workings. Light green is garnet skarn, dark green is pyroxene skarn, light blue is limestone, purple is mafic dike. Red line is CAD outline of the level. pSø = layering, pJt = joint plane, pFa = fold axis, pFaa = fold axis-anticline, pFas = fold axis-syncline, pSl = slickenlines, pFtN = normal fault, pFt = fault plane, pVc = calcite vein, pCt = contact plane, Ct = contact, Ft = minor fault, Fr = minor fracture. Map image created by Mystery Creek Resources, Inc.

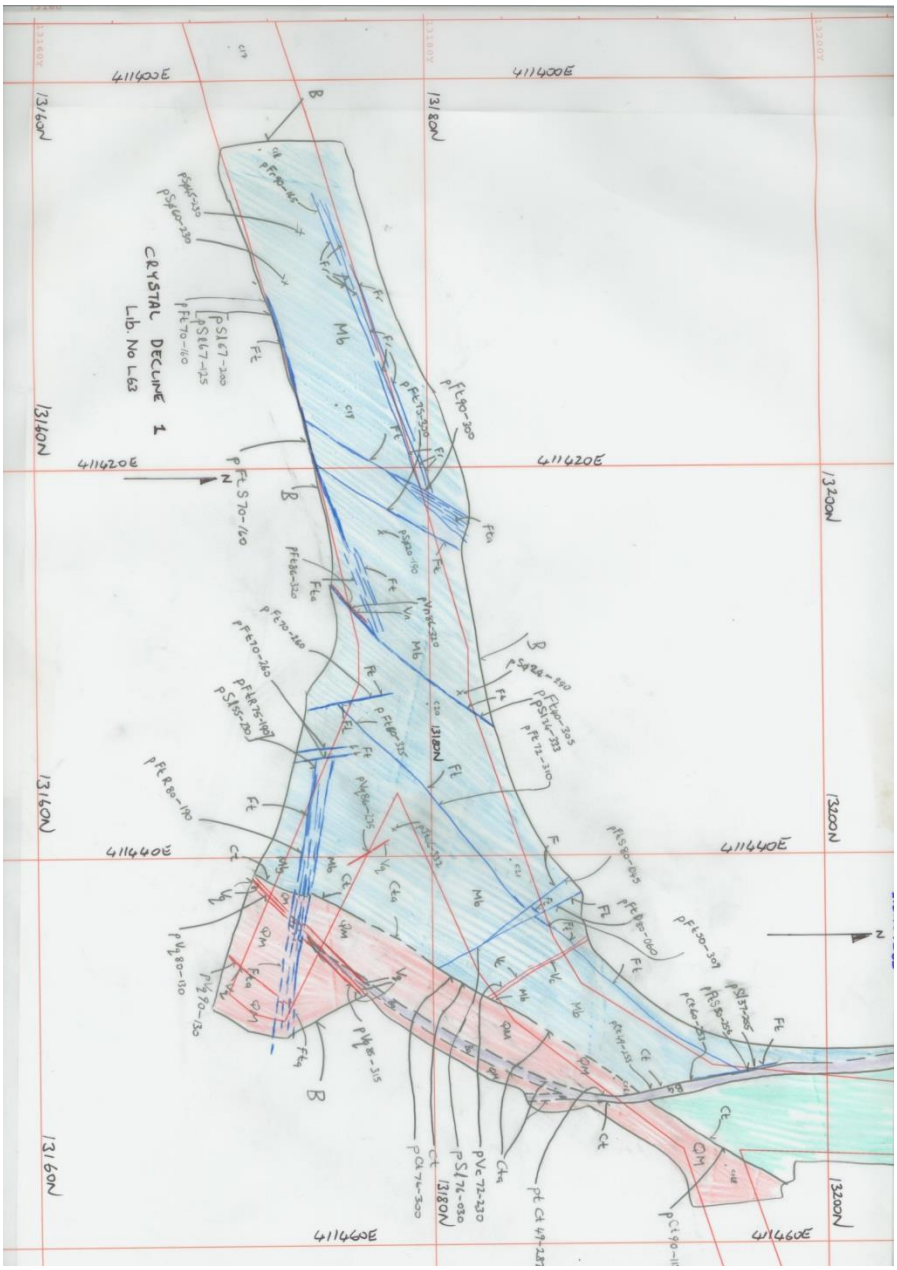

Figure A-18 Geologic map of Portal/C3002 Access 375 m to 404 m elevation underground workings. Orange is Mystery pluton, light blue is limestone, dark blue is marble, purple is mafic dike. Red line is CAD outline of the level. pSø = layering, pJt = joint plane, pFa = fold axis, pFaa = fold axis-anticline, pFas = fold axis-syncline, pSl = slickenlines, pFtN = normal fault, pFt = fault plane, pVc = calcite vein, pCt = contact plane, Ct = contact, Ft = minor fault, Fr = minor fracture. Map image created by Mystery Creek Resources, Inc.

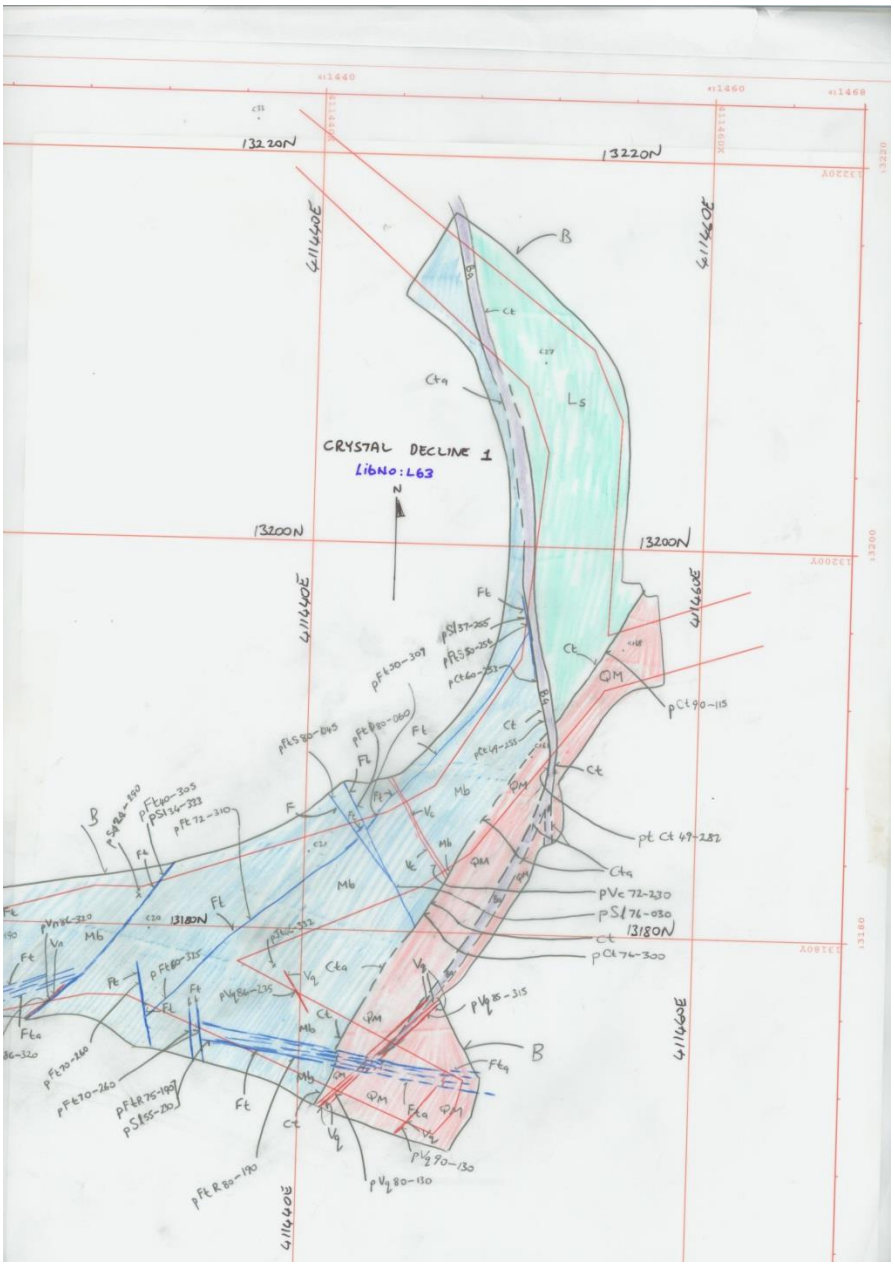

Figure A-19 Geologic map of Portal/C3002 Access 375 m to 404 m elevation underground workings. Orange is Mystery pluton, light blue is limestone, dark blue is marble, purple is mafic dike. Red line is CAD outline of the level. pSø = layering, pJt = joint plane, pFa = fold axis, pFaa = fold axis-anticline, pFas = fold axis-syncline, pSl = slickenlines, pFtN = normal fault, pFt = fault plane, pVc = calcite vein, pCt = contact plane, Ct = contact, Ft = minor fault, Fr = minor fracture. Map image created by Mystery Creek Resources, Inc.

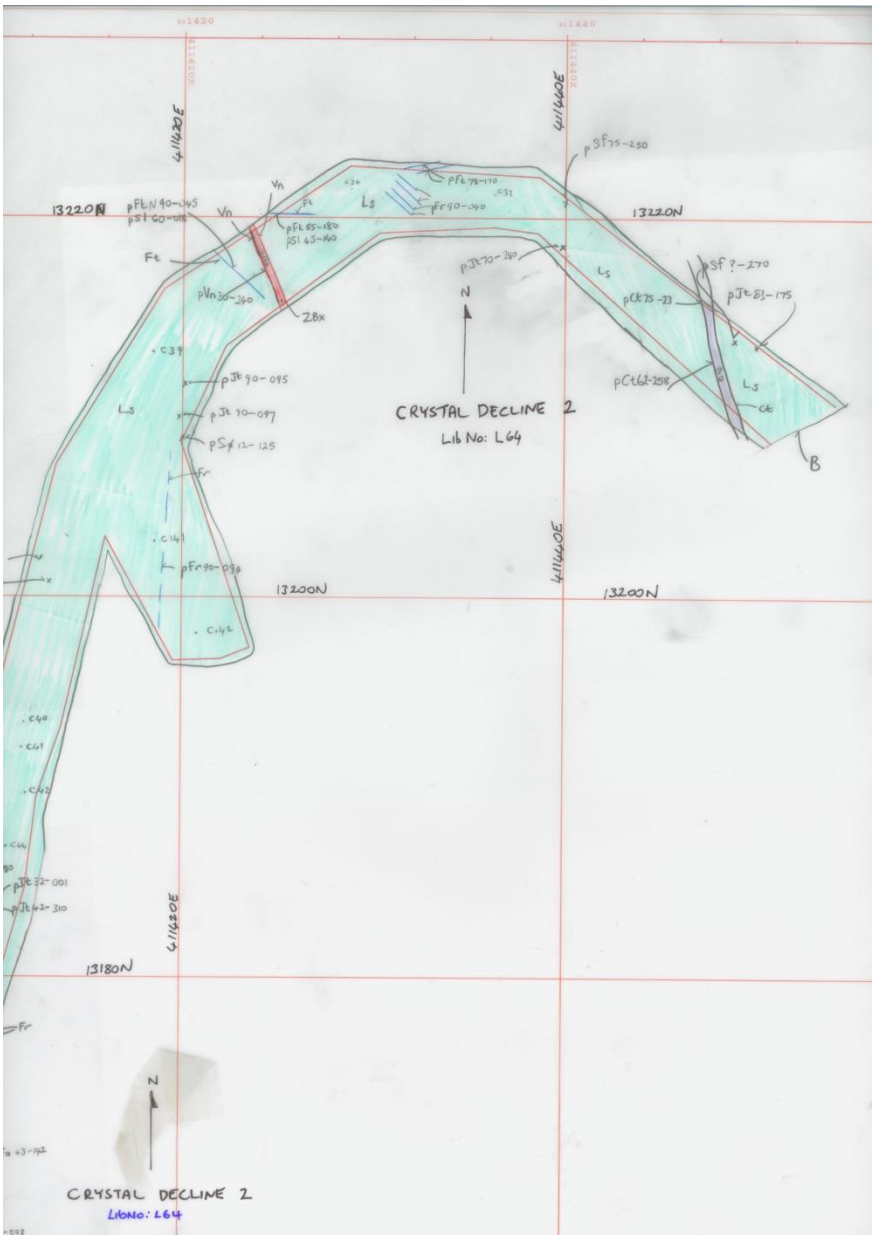

Figure A-20 Geologic map of C3003/C3000 Upper Access/C3003 Crosscut/3001 Crosscut/3001 Access 346 m to 380 m elevation underground workings. Light blue is limestone, purple is mafic dike, red is breccia. Red line is CAD outline of the level. pSø = layering, pJt = joint plane, pFa = fold axis, pFaa = fold axis-anticline, pFas = fold axis-syncline, pSl = slickenlines, pFtN = normal fault, pFt = fault plane, pVc = calcite vein, pCt = contact plane, Ct = contact, Ft = minor fault, Fr = minor fracture. Map image created by Mystery Creek Resources, Inc.

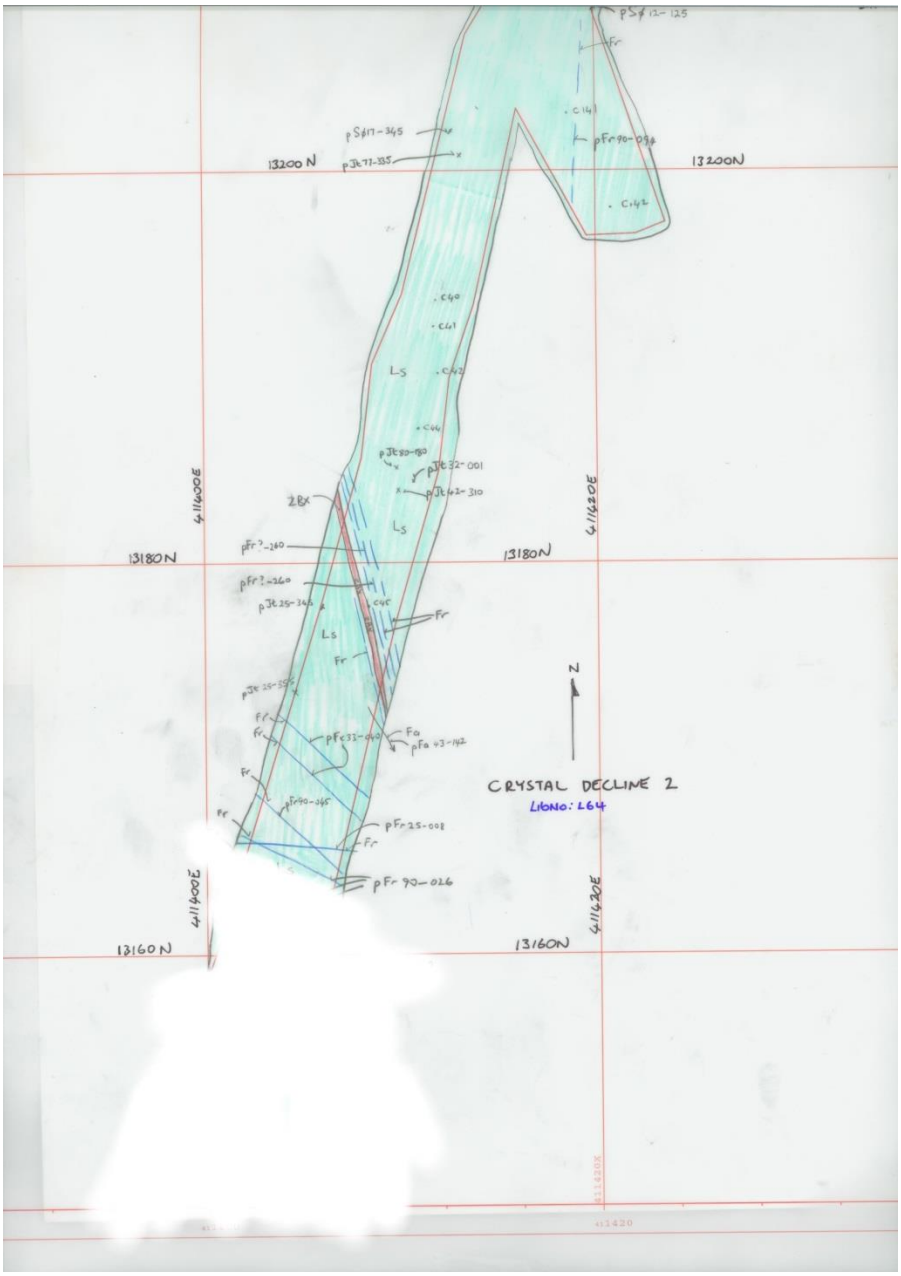

Figure A-21 Geologic map of C3003/C3000 Upper Access/C3003 Crosscut/3001 Crosscut/3001 Access 346 m to 380 m elevation underground workings. Light blue is limestone, red is breccia. Red line is CAD outline of the level. pSø = layering, pJt = joint plane, pFa = fold axis, pFaa = fold axis-anticline, pFas = fold axis-syncline, pSl = slickenlines, pFtN = normal fault, pFt = fault plane, pVc = calcite vein, pCt = contact plane, Ct = contact, Ft = minor fault, Fr = minor fracture. Map image created by Mystery Creek Resources, Inc.

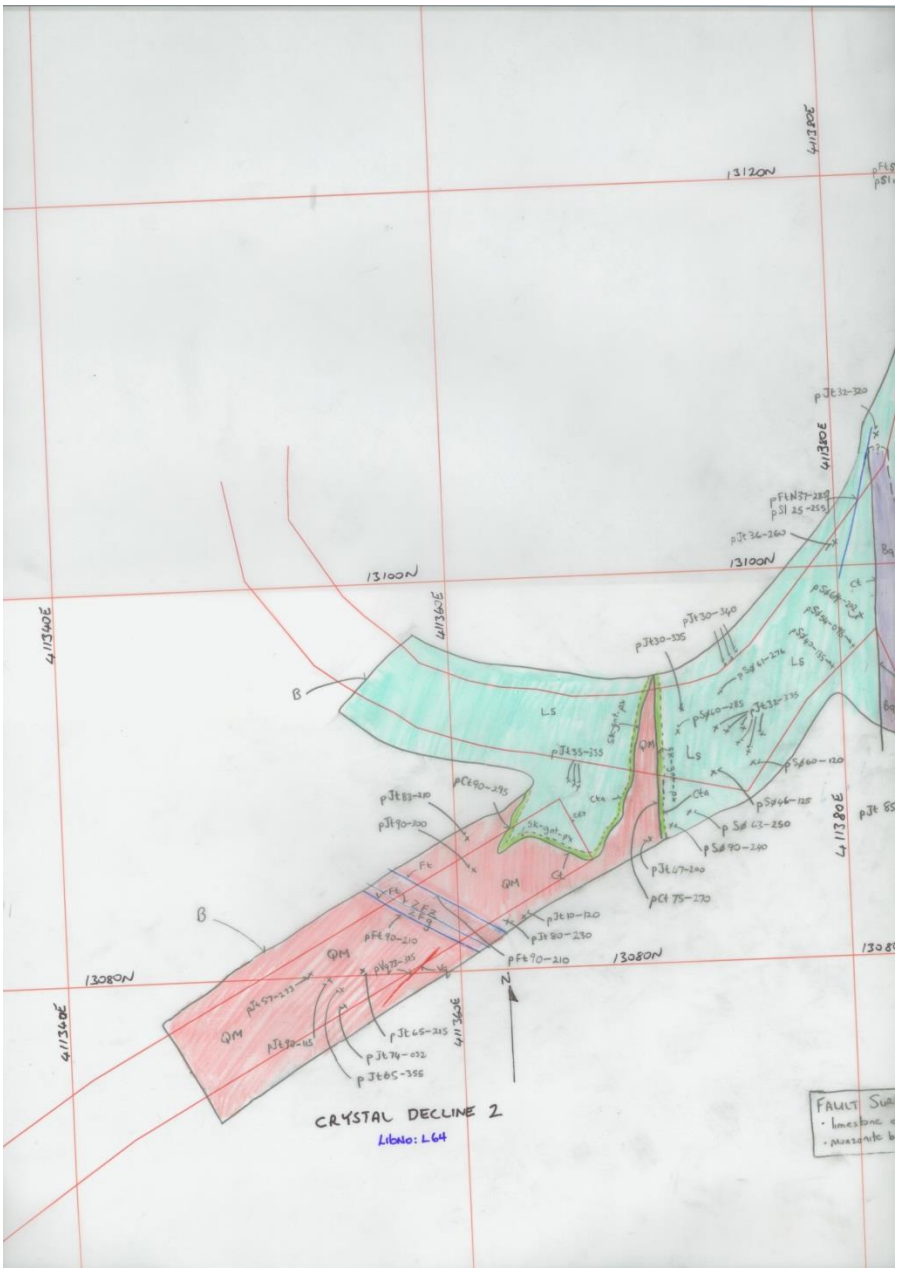

Figure A-22 Geologic map of C3003/C3000 Upper Access/C3003 Crosscut/3001 Crosscut/3001 Access 346 m to 380 m elevation underground workings. Light green is garnet pyroxene skarn, orange is Mystery pluton, light blue is limestone, purple is mafic dike. Red line is CAD outline of the level. pSø = layering, pJt = joint plane, pFa = fold axis, pFaa = fold axis-anticline, pFas = fold axis-syncline, pSl = slickenlines, pFtN = normal fault, pFt = fault plane, pVc = calcite vein, pCt = contact plane, Ct = contact, Ft = minor fault, Fr = minor fracture. Map image created by Mystery Creek Resources, Inc.

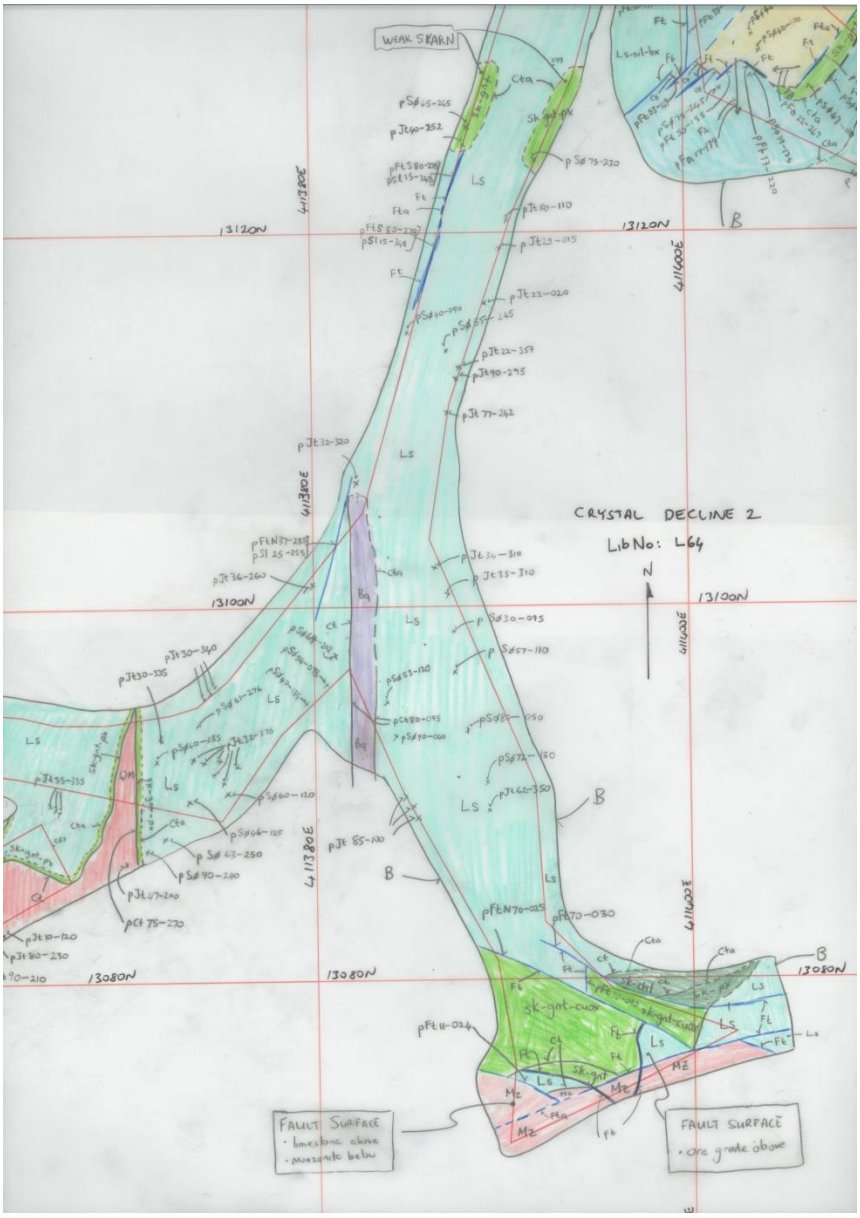

Figure A-23 Geologic map of C3003/C3000 Upper Access/C3003 Crosscut/3001 Crosscut/3001 Access 346 m to 380 m elevation underground workings. Light green is garnet pyroxene skarn/garnet skarn/garnet copper oxide skarn, dark green is pyroxene skarn/chlorite skarn, orange is Mystery pluton, light blue is limestone, lighter blue is limestone breccia/limestone siltstone breccia, yellow is oxidized sulfides, purple is mafic dike. Red line is CAD outline of the level. pSø = layering, pJt = joint plane, pFa = fold axis, pFaa = fold axis-anticline, pFas = fold axis-syncline, pSl = slickenlines, pFtN = normal fault, pFt = fault plane, pVc = calcite vein, pCt = contact plane, Ct = contact, Ft = minor fault, Fr = minor fracture. Map image created by Mystery Creek Resources, Inc.

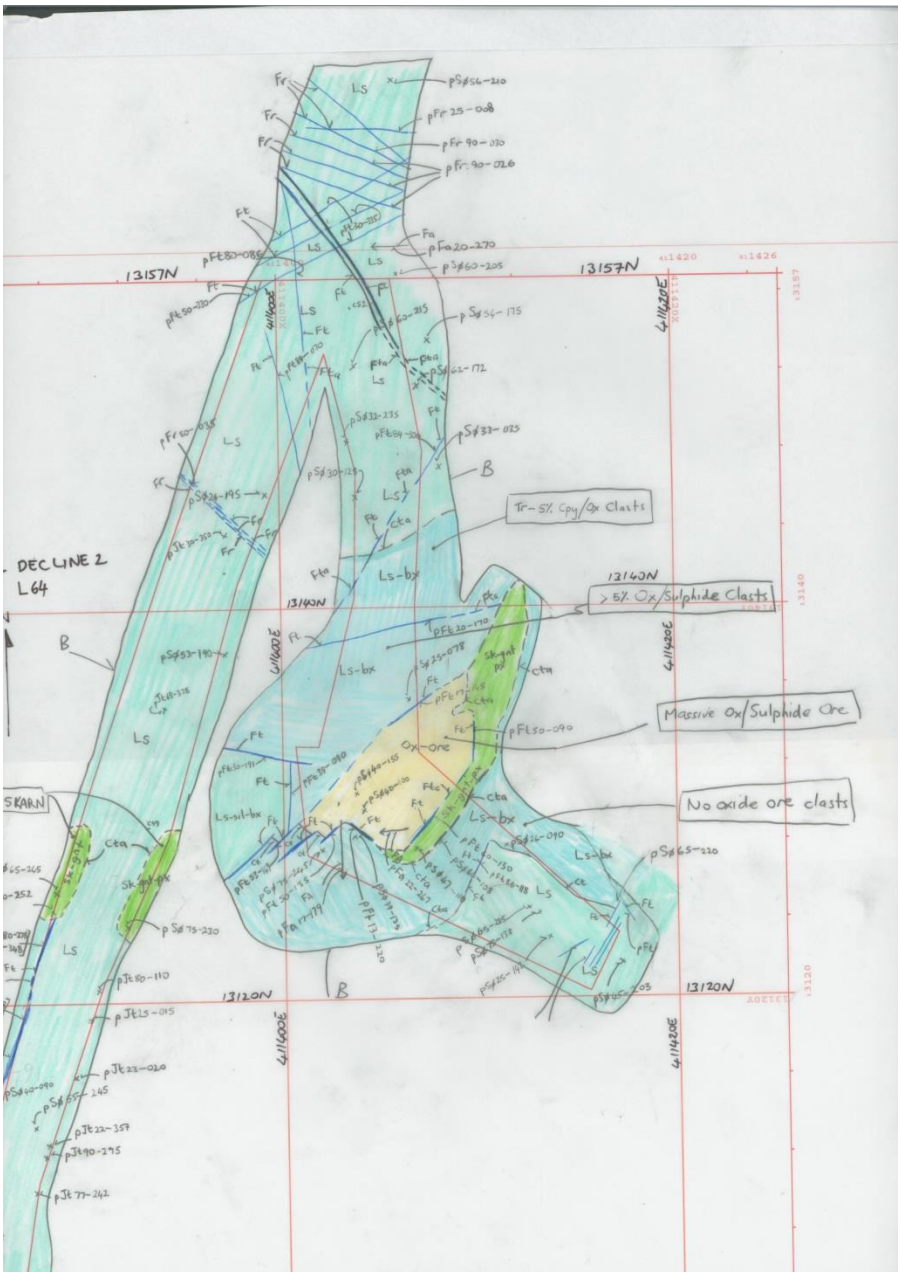

Figure A-24 Geologic map of C3003/C3000 Upper Access/C3003 Crosscut/3001 Crosscut/3001 Access 346 m to 380 m elevation underground workings. Light green is garnet pyroxene skarn/garnet skarn, light blue is limestone, lighter blue is limestone breccia/limestone siltstone breccia, yellow is oxidized sulfides. Red line is CAD outline of the level. pSø = layering, pJt = joint plane, pFa = fold axis, pFaa = fold axis-anticline, pFas = fold axis-syncline, pSl = slickenlines, pFtN = normal fault, pFt = fault plane, pVc = calcite vein, pCt = contact plane, Ct = contact, Ft = minor fault, Fr = minor fracture. Map image created by Mystery Creek Resources, Inc.

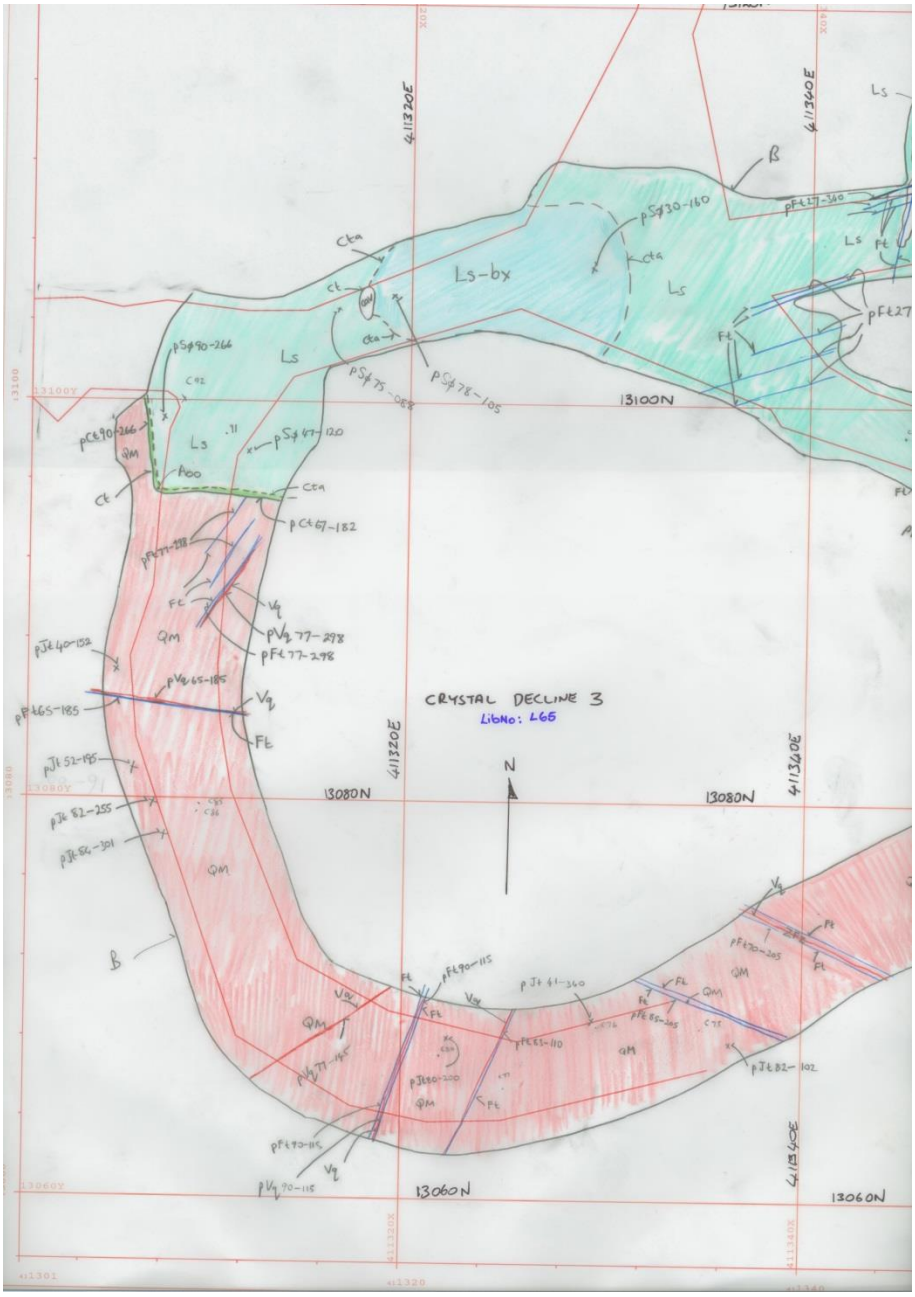

Figure A-25 Geologic map of Crystal Decline 340 m to 356 m elevation underground workings. Light green is mineralized zone, orange is Mystery pluton, light blue is limestone, lighter blue is limestone breccia, red is fault zone/veins. Red line is CAD outline of the level. Cav = void, pSø = layering, pJt = joint plane, pFa = fold axis, pFaa = fold axis-anticline, pFas = fold axis-syncline, pSl = slickenlines, pFtN = normal fault, pFt = fault plane, pVc = calcite vein, pCt = contact plane, Ct = contact, Ft = minor fault, Fr = minor fracture. Map image created by Mystery Creek Resources, Inc.

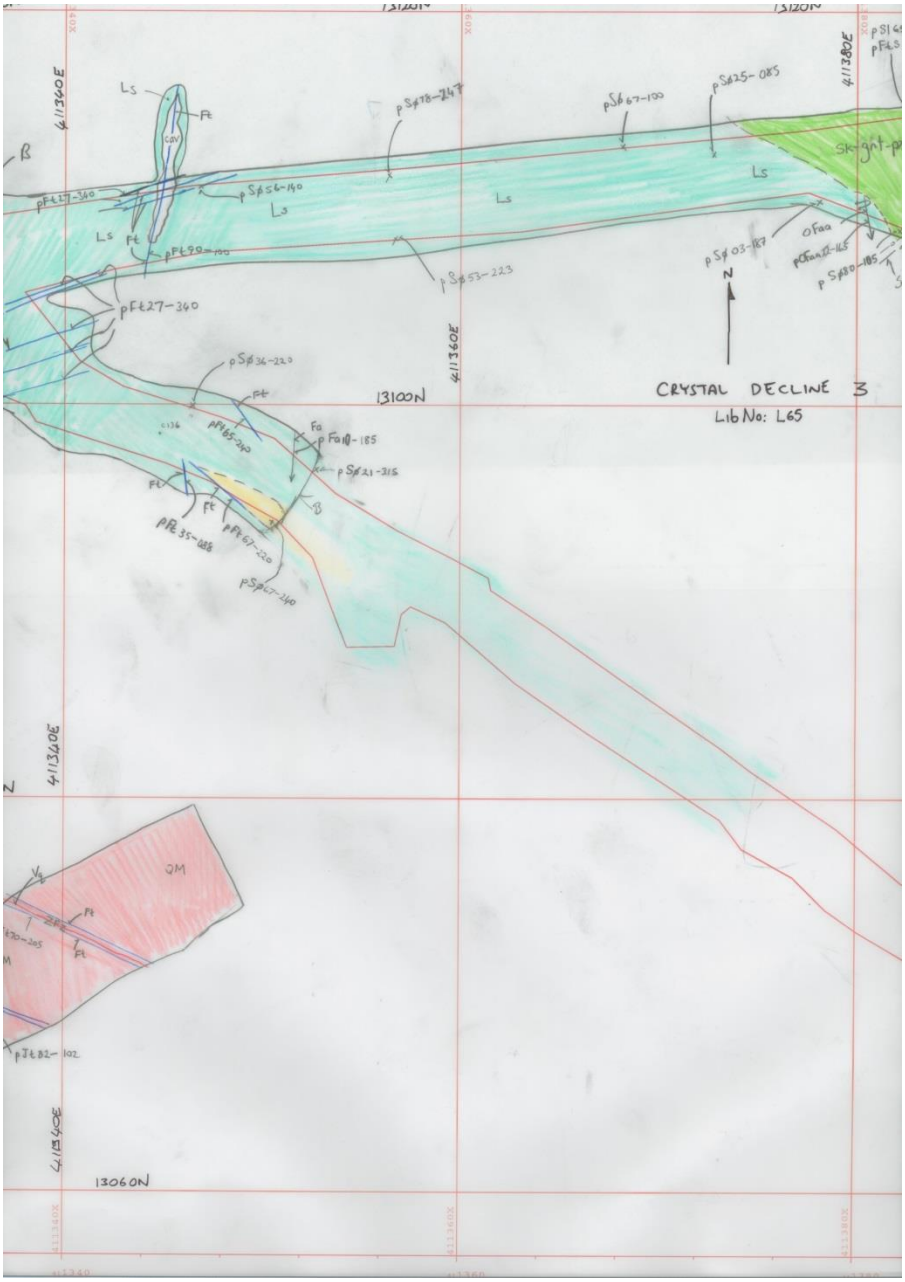

Figure A-26 Crystal Decline 340 m to 356 m elevation underground workings. Light green is garnet pyroxene skarn, orange is Mystery pluton, light blue is limestone, red is fault zone/veins, yellow is oxidation. Red line is CAD outline of the level. Cav = void, pSø = layering, pJt = joint plane, pFa = fold axis, pFaa = fold axis-anticline, pFas = fold axis-syncline, pSl = slickenlines, pFtN = normal fault, pFt = fault plane, pVc = calcite vein, pCt = contact plane, Ct = contact, Ft = minor fault, Fr = minor fracture. Map image created by Mystery Creek Resources, Inc.

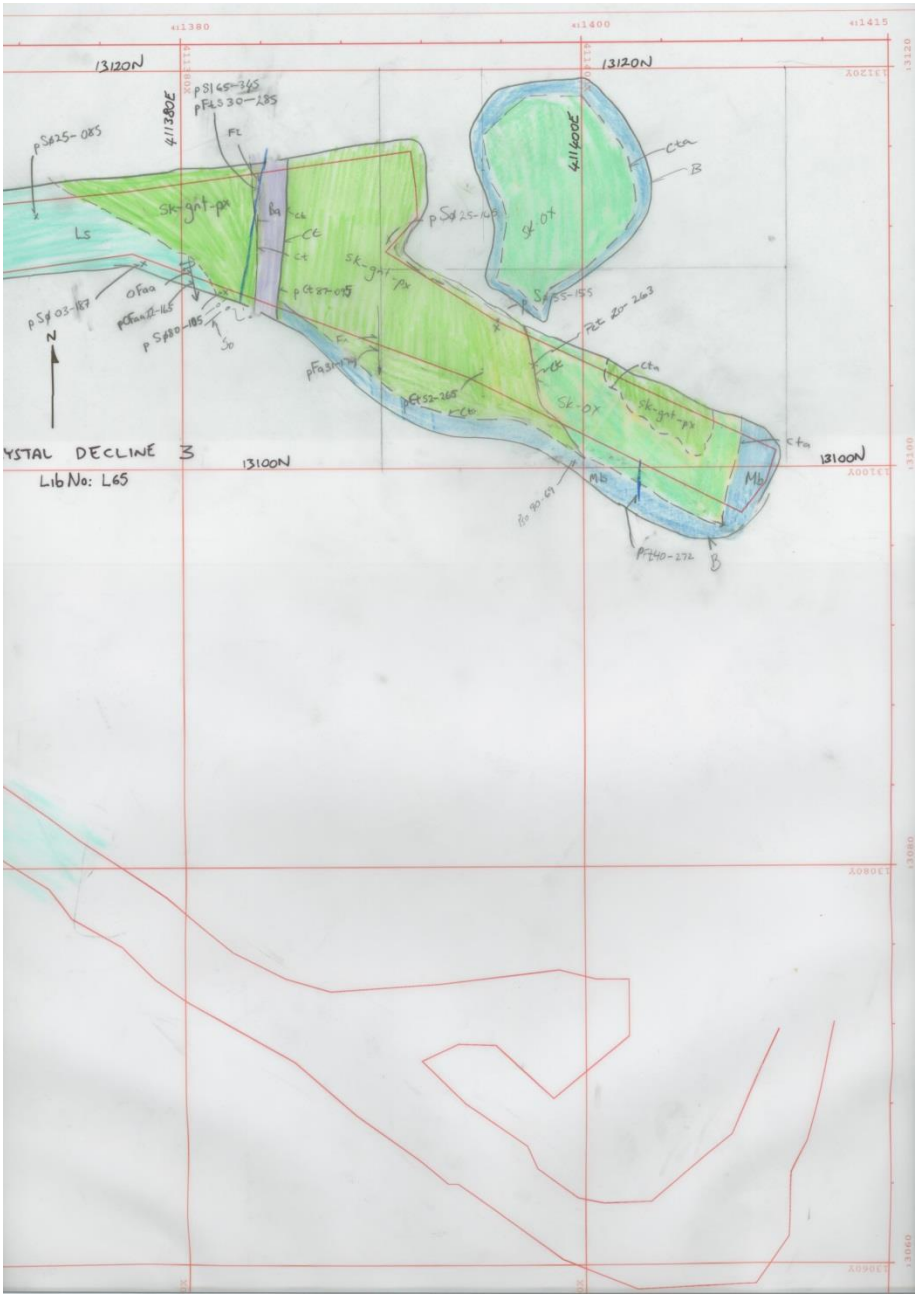

Figure A-27 Geologic map of Crystal Decline 340 m to 356 m elevation underground workings. Light green is garnet pyroxene skarn, blue-green is oxidized skarn, light blue is limestone, dark blue is marble, purple is mafic dike. Red line is CAD outline of the level. pSø = layering, pJt = joint plane, pFa = fold axis, pFaa = fold axis-anticline, pFas = fold axis-syncline, pSl = slickenlines, pFtN = normal fault, pFt = fault plane, pVc = calcite vein, pCt = contact plane, Ct = contact, Ft = minor fault, Fr = minor fracture. Map image created by Mystery Creek Resources, Inc.

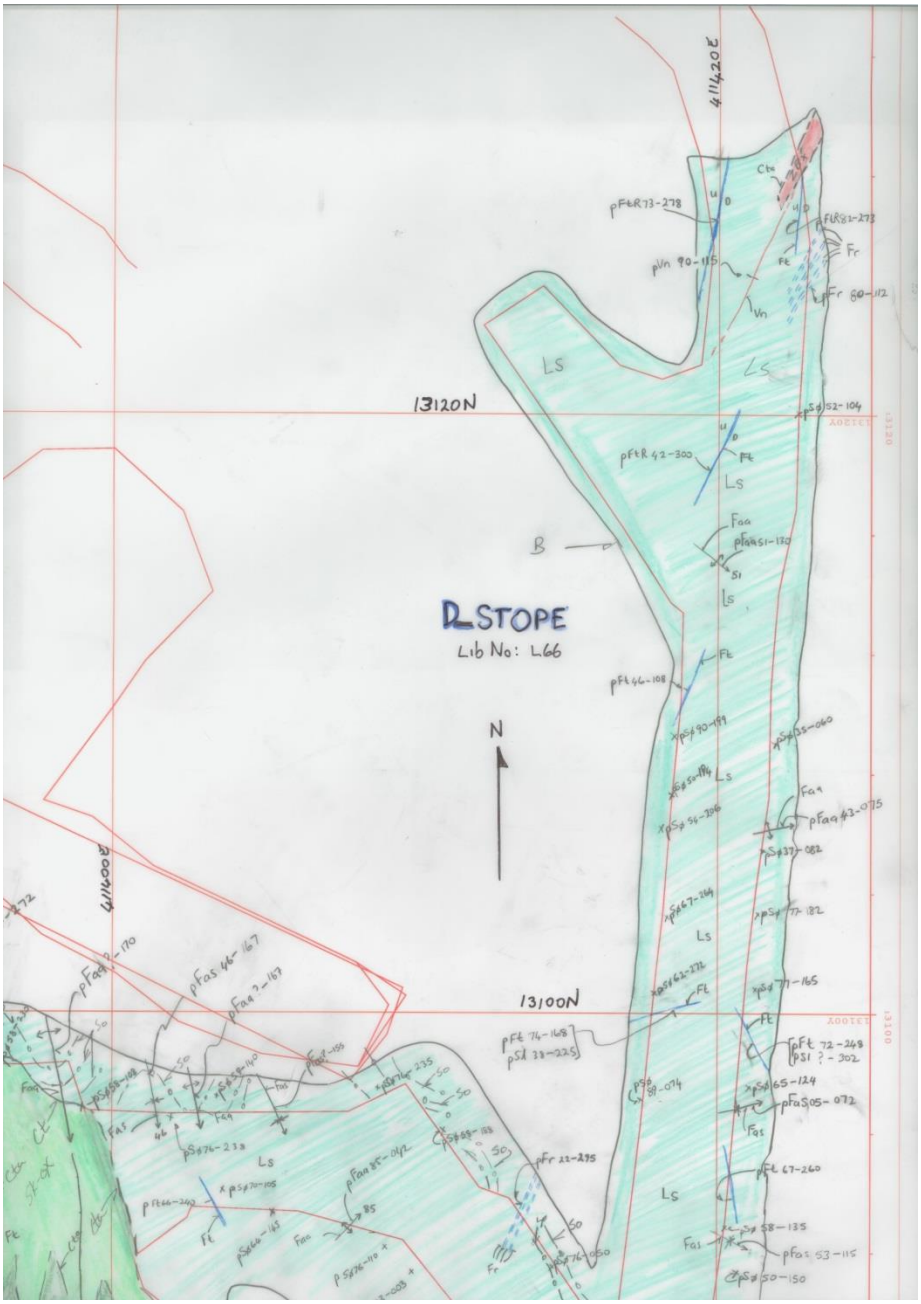

Figure A-28 Geologic map of D Stope/D Decline 324 m to 350 m elevation underground workings. Light green is oxidized skarn, dark green is pyroxene skarn, red is breccia, light blue is limestone. Red line is CAD outline of the level. pSø = layering, pJt = joint plane, pFa = fold axis, pFaa = fold axis-anticline, pFas = fold axis-syncline, pSl = slickenlines, pFtN = normal fault, pFt = fault plane, pVc = calcite vein, pCt = contact plane, Ct = contact, Ft = minor fault, Fr = minor fracture. Map image created by Mystery Creek Resources, Inc.

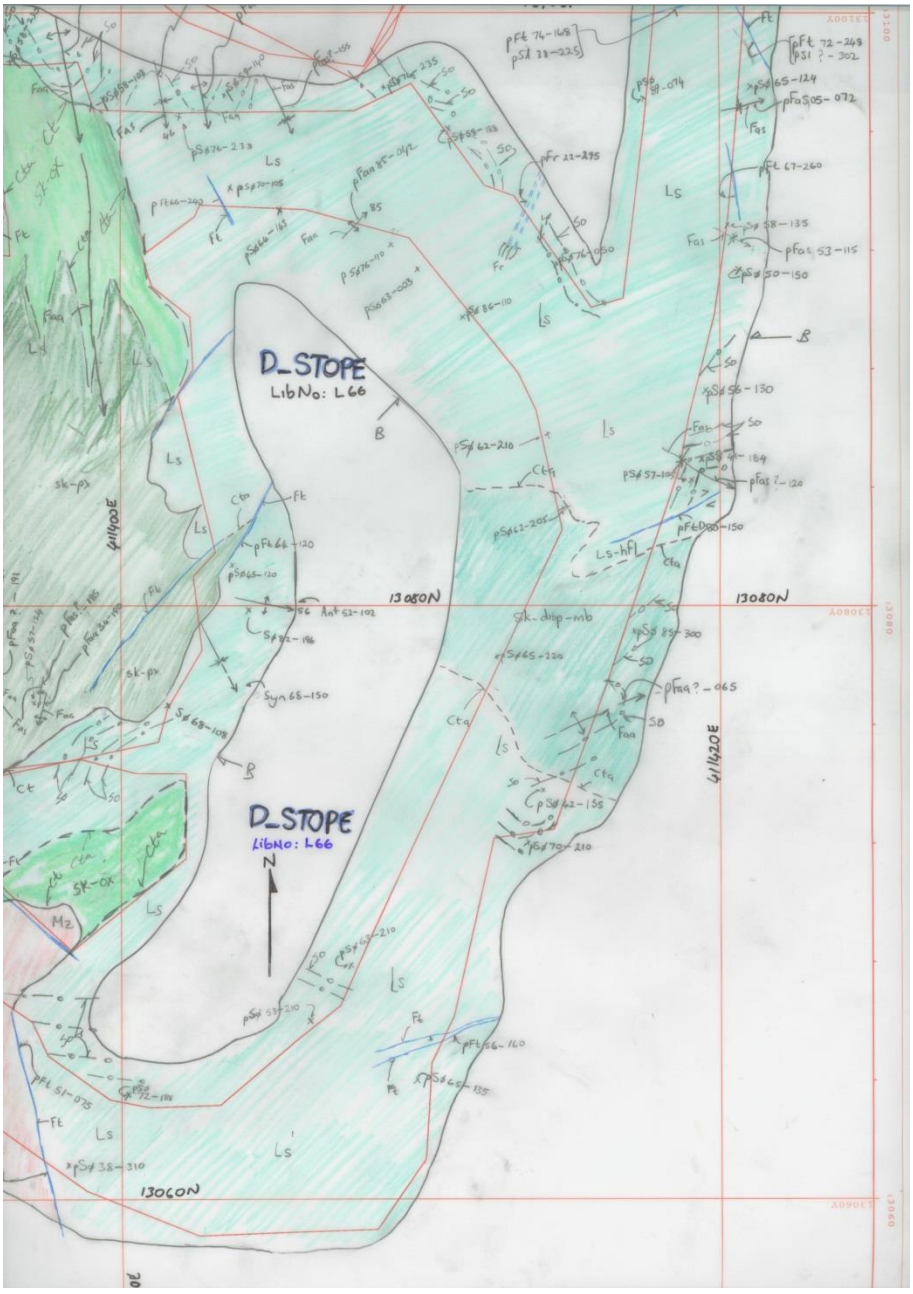

Figure A-29 Geologic map of D Stope/D Decline 324 m to 350 m elevation underground workings. Light green is oxidized skarn, dark green is pyroxene skarn, red is breccia, light blue is limestone, dark blue is marble and diopside skarn, orange is Mystery pluton. Red line is CAD outline of the level. pSø = layering, pJt = joint plane, pFa = fold axis, pFaa = fold axis-anticline, pFas = fold axis-syncline, pSl = slickenlines, pFtN = normal fault, pFt = fault plane, pVc = calcite vein, pCt = contact plane, Ct = contact, Ft = minor fault, Fr = minor fracture. Map image created by Mystery Creek Resources, Inc.

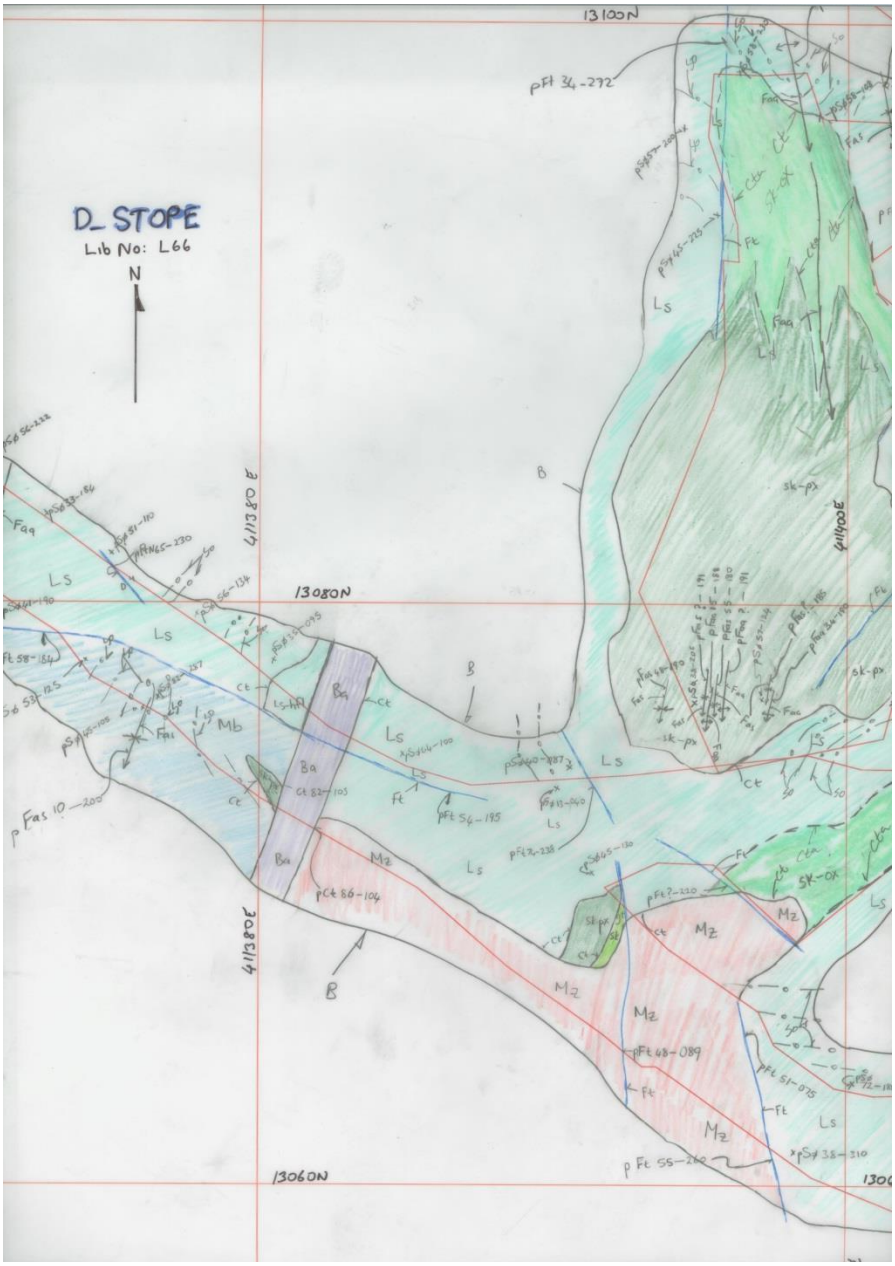

Figure A-30 Geologic map of D Stope/D Decline 324 m to 350 m elevation underground workings. Blue green is oxidized skarn, light green is garnet skarn, dark green is pyroxene skarn, light blue is limestone, dark blue is marble, orange is Mystery pluton, purple is mafic dike. Red line is CAD outline of the level. pSø = layering, pJt = joint plane, pFa = fold axis, pFaa = fold axis-anticline, pFas = fold axis-syncline, pSl = slickenlines, pFtN = normal fault, pFt = fault plane, pVc = calcite vein, pCt = contact plane, Ct = contact, Ft = minor fault, Fr = minor fracture. Map image created by Mystery Creek Resources, Inc.

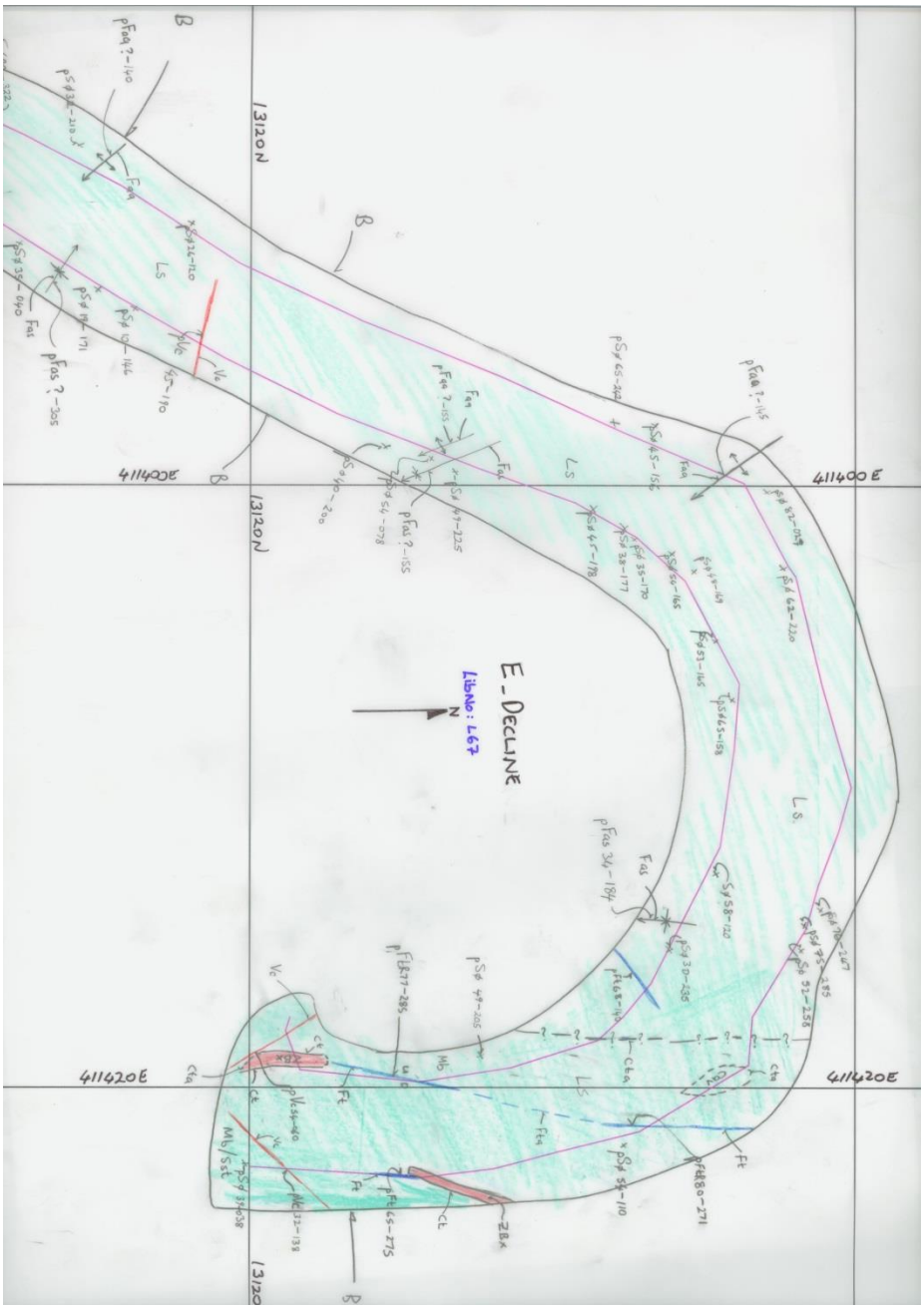

Figure A-31 Geologic map of E Decline/E Stope 308 m to 328 m elevation underground workings. Light blue is limestone, dark blue is marble/siltstone, red is breccia. Red line is CAD outline of the level. pSø = layering, pJt = joint plane, pFa = fold axis, pFaa = fold axis-anticline, pFas = fold axis-syncline, pSl = slickenlines, pFtN = normal fault, pFt = fault plane, pVc = calcite vein, pCt = contact plane, Ct = contact, Ft = minor fault, Fr = minor fracture. Map image created by Mystery Creek Resources, Inc.

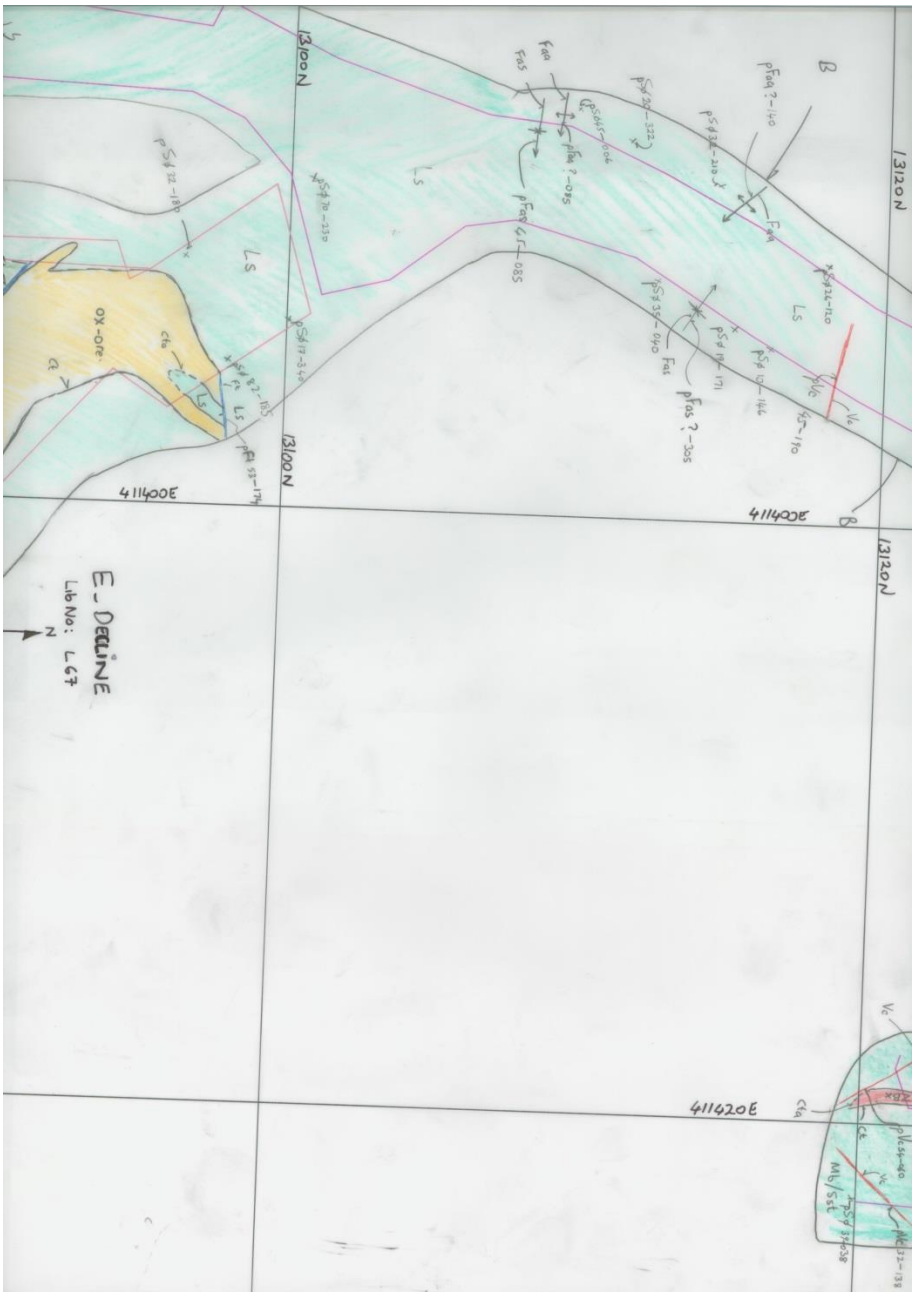

Figure A-32 Geologic map of E Decline/E Stope 308 m to 328 m elevation underground workings. Dark green is pyroxene skarn, yellow is oxidized sulfides, light blue is limestone, dark blue is marble/siltstone, red is breccia. Red line is CAD outline of the level. pSø = layering, pJt = joint plane, pFa = fold axis, pFaa = fold axis-anticline, pFas = fold axis-syncline, pSl = slickenlines, pFtN = normal fault, pFt = fault plane, pVc = calcite vein, pCt = contact plane, Ct = contact, Ft = minor fault, Fr = minor fracture. Map image created by Mystery Creek Resources, Inc.

Figure A-33 Geologic map of E Decline/E Stope 308 m to 328 m elevation underground workings. Light green is garnet skarn, dark green is pyroxene skarn, yellow is oxidized sulfides, light blue is limestone, dark blue is marble. Red line is CAD outline of the level. pSø = layering, pJt = joint plane, pFa = fold axis, pFaa = fold axis-anticline, pFas = fold axis-syncline, pSl = slickenlines, pFtN = normal fault, pFt = fault plane, pVc = calcite vein, pCt = contact plane, Ct = contact, Ft = minor fault, Fr = minor fracture. Map image created by Mystery Creek Resources, Inc.

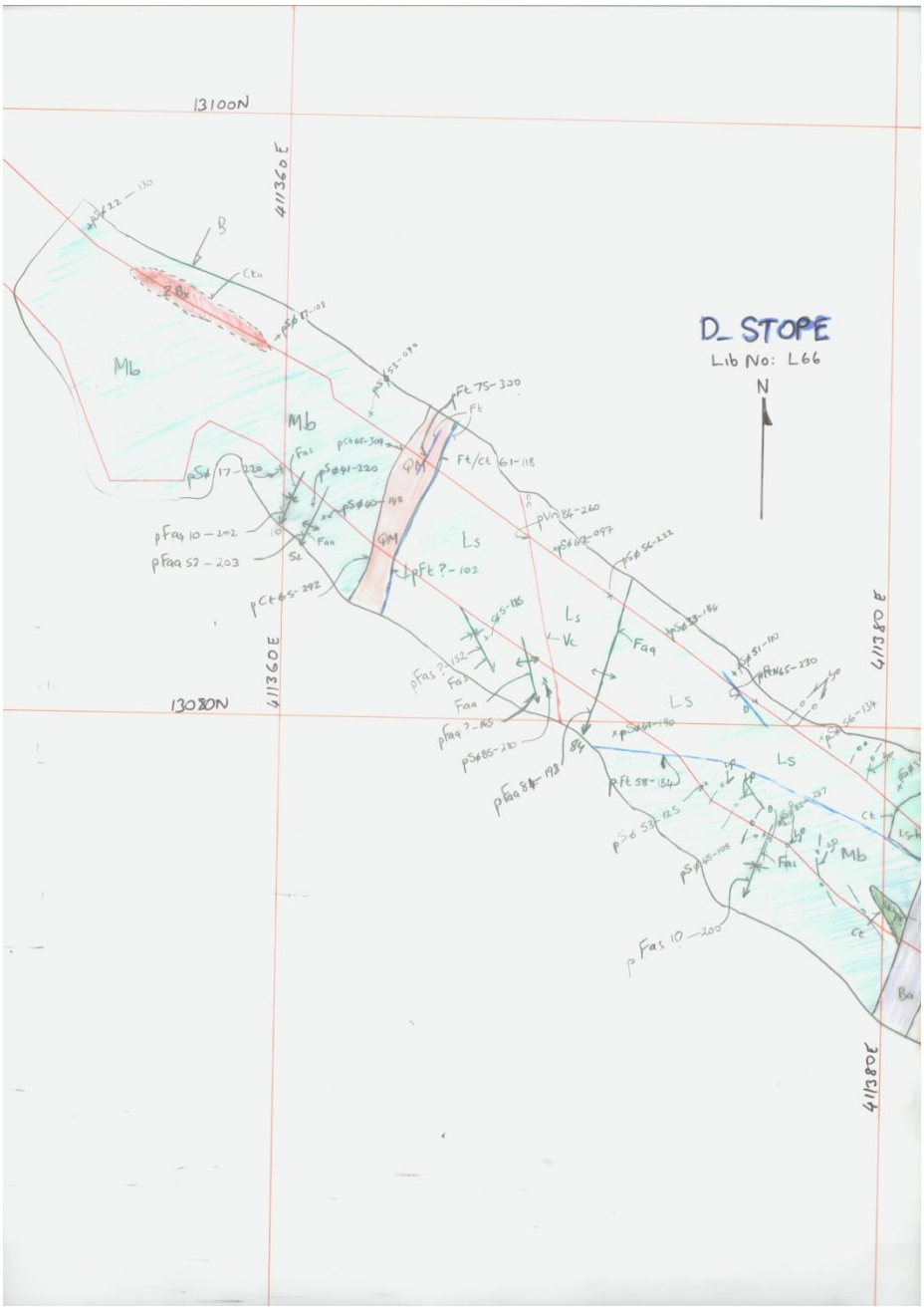

Figure A-34 Geologic map of D Stope/D Decline 324 m to 350 m elevation underground workings. Dark green is pyroxene skarn, orange is Mystery pluton, light blue is limestone, dark blue is marble, purple is mafic dike, red is breccia. Red line is CAD outline of the level. pSø = layering, pJt = joint plane, pFa = fold axis, pFaa = fold axis-anticline, pFas = fold axis-syncline, pSl = slickenlines, pFtN = normal fault, pFt = fault plane, pVc = calcite vein, pCt = contact plane, Ct = contact, Ft = minor fault, Fr = minor fracture. Map image created by Mystery Creek Resources, Inc.

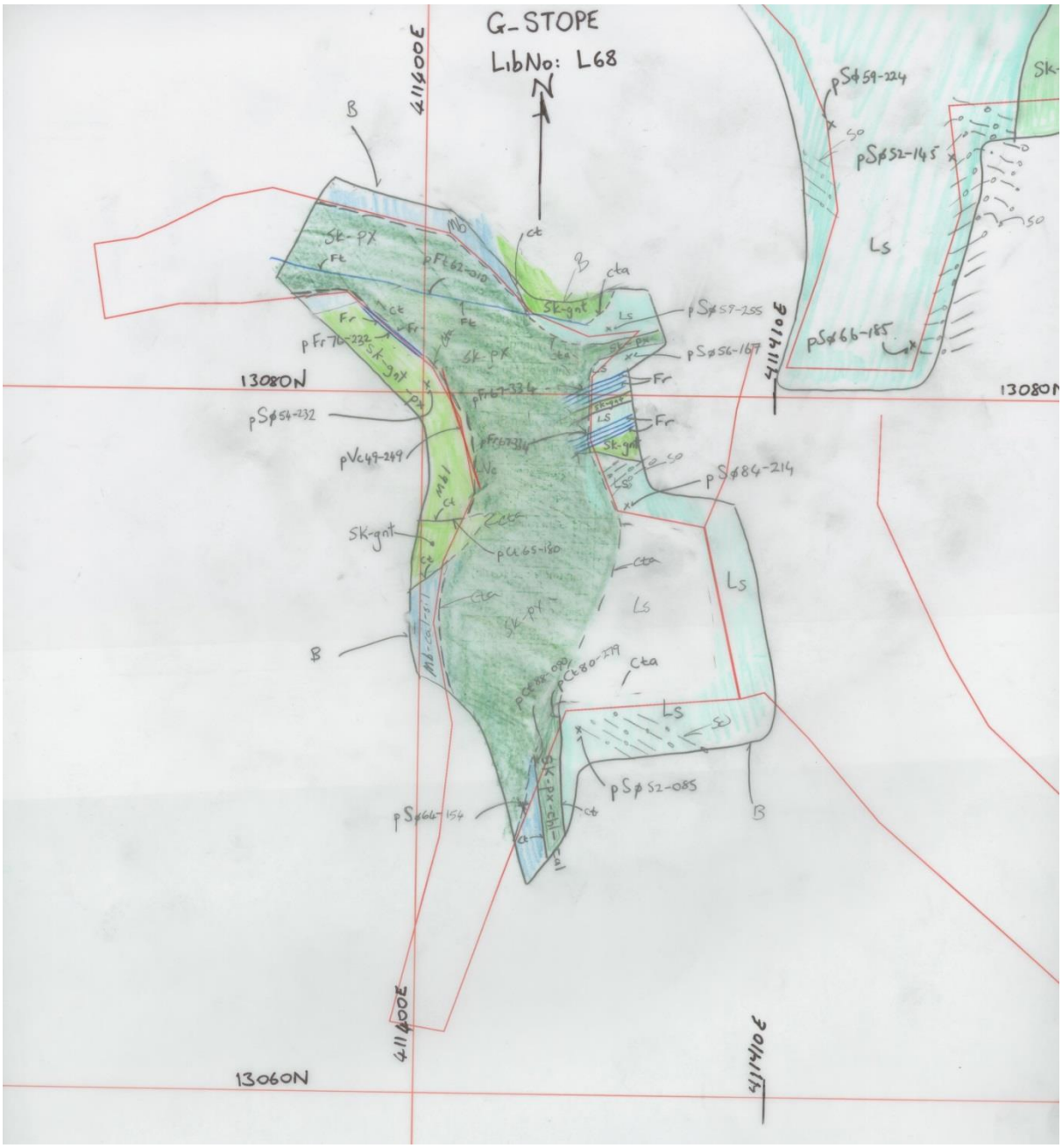

Figure A-35 Geologic map of G Stope/G Decline 282 m to 300 m elevation underground workings. Light green is garnet pyroxene skarn/garnet skarn, dark green is pyroxene skarn/pyroxene chlorite calcite skarn, light blue is limestone, dark blue is marble/siltstone. Red line is CAD outline of the level. pSø = layering, pJt = joint plane, pFa = fold axis, pFaa = fold axis-anticline, pFas = fold axis-syncline, pSl = slickenlines, pFtN = normal fault, pFt = fault plane, pVc = calcite vein, pCt = contact plane, Ct = contact, Ft = minor fault, Fr = minor fracture. Map image created by Mystery Creek Resources, Inc.

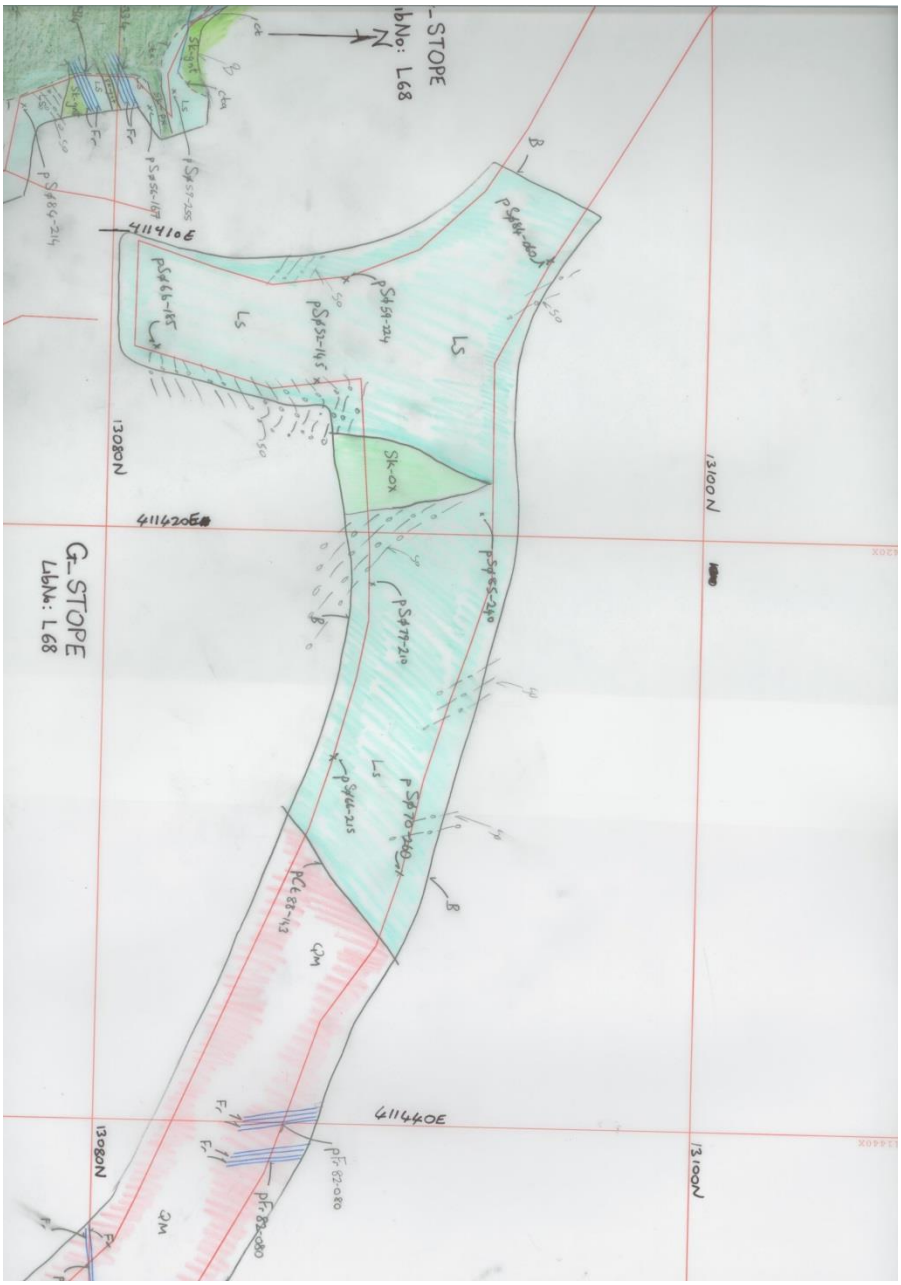

Figure A-36 Geologic map of G Stope/G Decline 282 m to 300 m elevation underground workings. Light green is oxidized skarn, orange is Mystery pluton, light blue is limestone. Red line is CAD outline of the level. pSø = layering, pJt = joint plane, pFa = fold axis, pFaa = fold axis-anticline, pFas = fold axis-syncline, pSl = slickenlines, pFtN = normal fault, pFt = fault plane, pVc = calcite vein, pCt = contact plane, Ct = contact, Ft = minor fault, Fr = minor fracture. Map image created by Mystery Creek Resources, Inc.

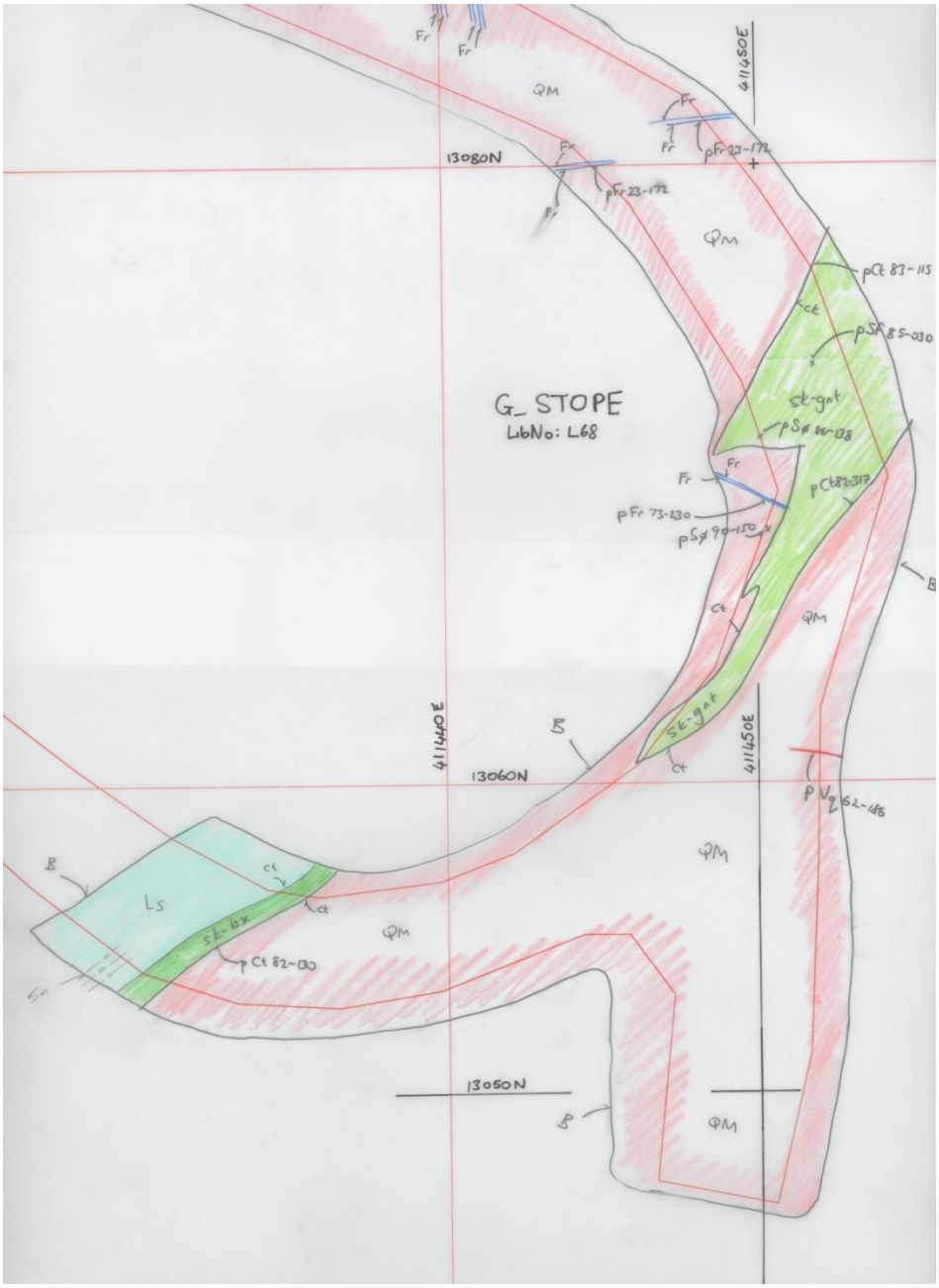

Figure A-37 Geologic map of G Stope/G Decline 282 m to 300 m elevation underground workings. Light green is garnet skarn, dark green is brecciated skarn, orange is Mystery pluton, light blue is limestone. Red line is CAD outline of the level. pSø = layering, pJt = joint plane, pFa = fold axis, pFaa = fold axis-anticline, pFas = fold axis-syncline, pSl = slickenlines, pFtN = normal fault, pFt = fault plane, pVc = calcite vein, pCt = contact plane, Ct = contact, Ft = minor fault, Fr = minor fracture. Map image created by Mystery Creek Resources, Inc.

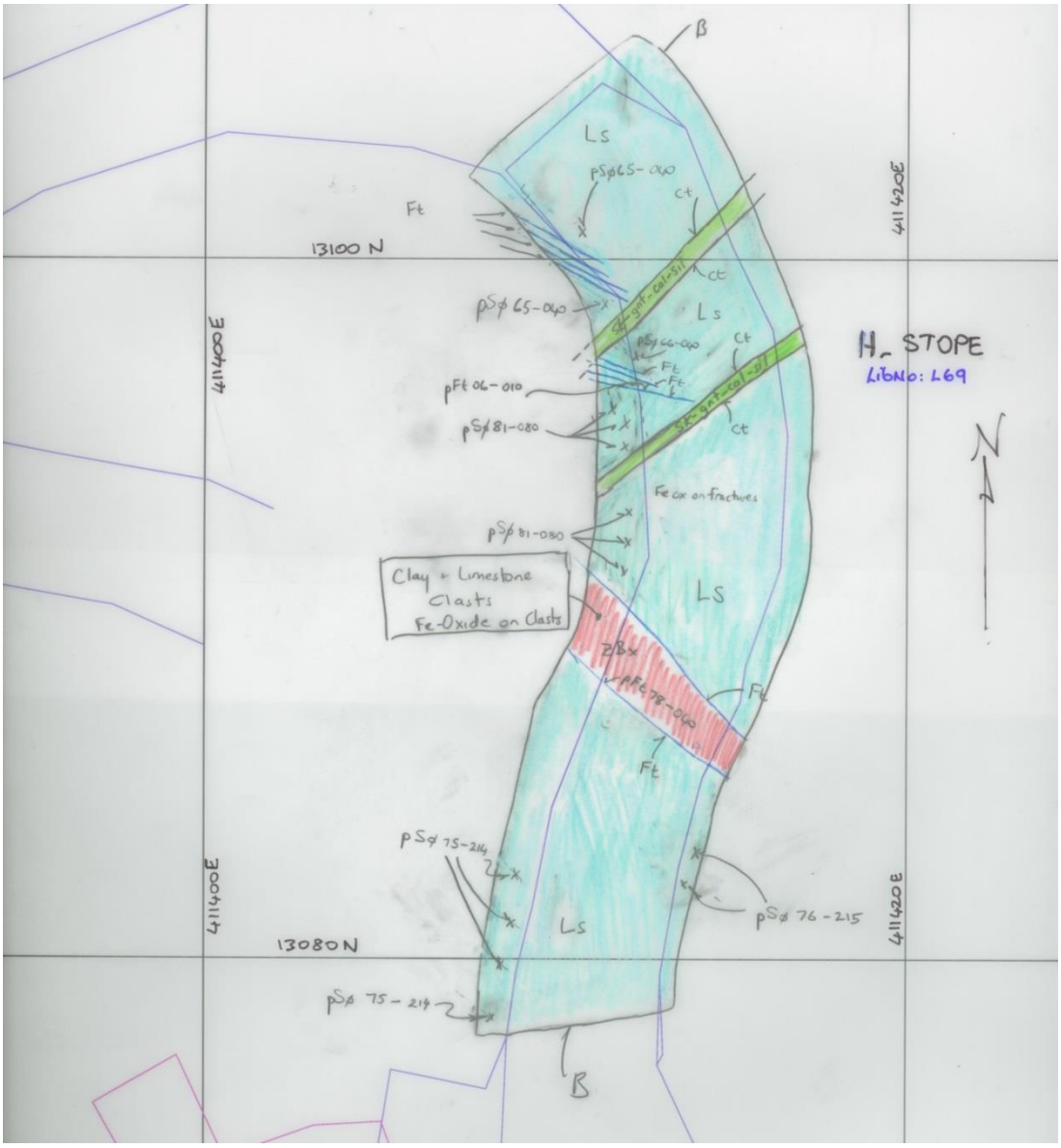

Figure A-38 Geologic map of H Stope/H Decline 260 m to 286 m elevation underground workings. Light green is garnet calcite skarn, light blue is limestone, red is breccia. Red line is CAD outline of the level. pSø = layering, pJt = joint plane, pFa = fold axis, pFaa = fold axis-anticline, pFas = fold axis-syncline, pSl = slickenlines, pFtN = normal fault, pFt = fault plane, pVc = calcite vein, pCt = contact plane, Ct = contact, Ft = minor fault, Fr = minor fracture. Map image created by Mystery Creek Resources, Inc.

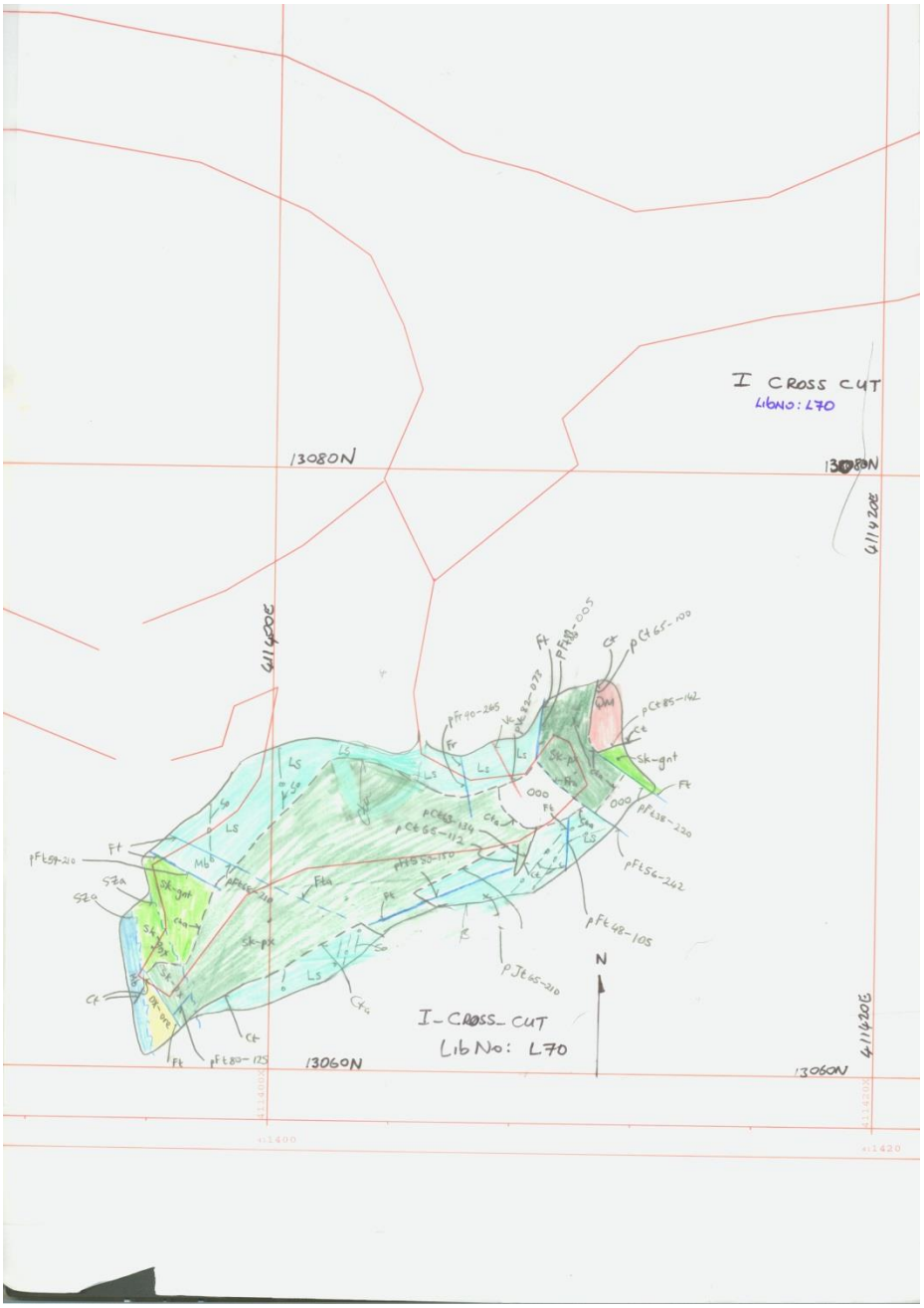

Figure A-39 Geologic map of I Cross Cut/I Stope 254 m to 271 m elevation underground workings. Light green is garnet skarn, dark green is pyroxene skarn, orange is Mystery pluton, light blue is limestone, dark blue is marble, yellow is oxidized sulfides. Red line is CAD outline of the level. pSø = layering, pJt = joint plane, pFa = fold axis, pFaa = fold axis-anticline, pFas = fold axis-syncline, pSl = slickenlines, pFtN = normal fault, pFt = fault plane, pVc = calcite vein, pCt = contact plane, Ct = contact, Ft = minor fault, Fr = minor fracture. Map image created by Mystery Creek Resources, Inc.

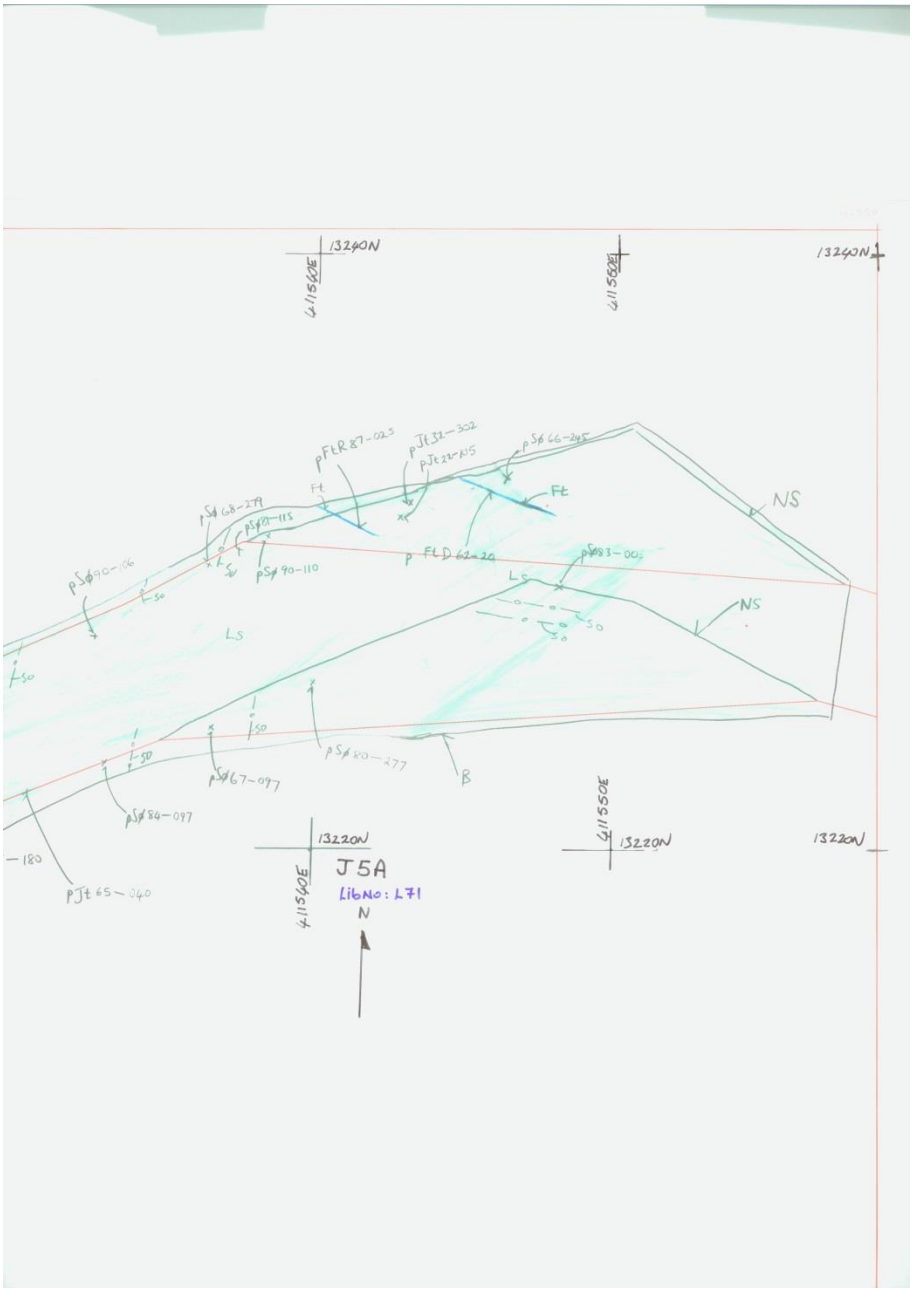

Figure A-40 Geologic map of J5A 380 m to 397 m elevation underground workings. Light blue is limestone. Red line is CAD outline of the level. pSø = layering, pJt = joint plane, pFa = fold axis, pFaa = fold axis-anticline, pFas = fold axis-syncline, pSl = slickenlines, pFtN = normal fault, pFt = fault plane, pVc = calcite vein, pCt = contact plane, Ct = contact, Ft = minor fault, Fr = minor fracture. Map image created by Mystery Creek Resources, Inc.

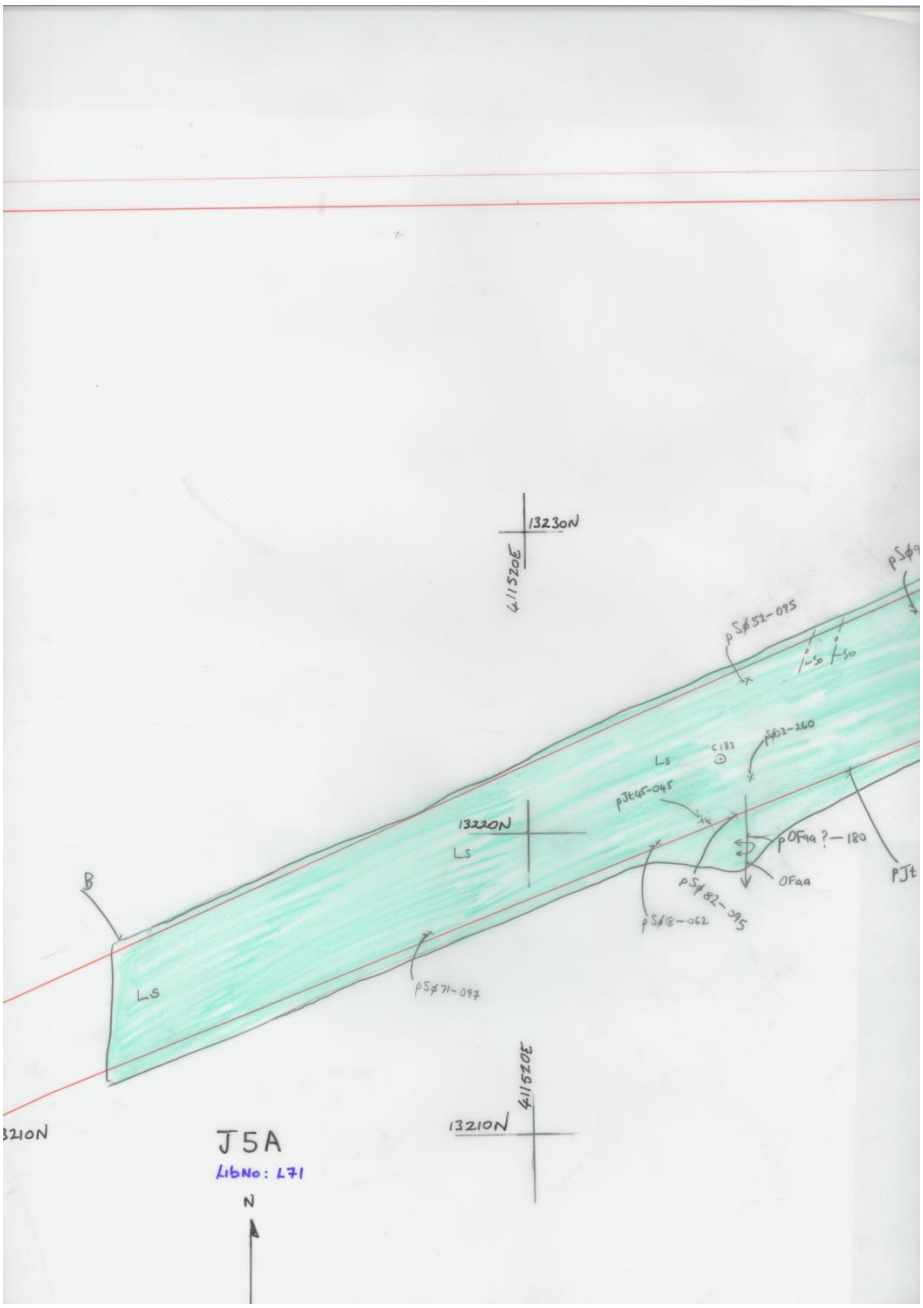

Figure A-41 Geologic map of J5A 380 m to 397 m elevation underground workings. Light blue is limestone. Red line is CAD outline of the level. pSø = layering, pJt = joint plane, pFa = fold axis, pFaa = fold axis-anticline, pFas = fold axis-syncline, pSl = slickenlines, pFtN = normal fault, pFt = fault plane, pVc = calcite vein, pCt = contact plane, Ct = contact, Ft = minor fault, Fr = minor fracture. Map image created by Mystery Creek Resources, Inc.

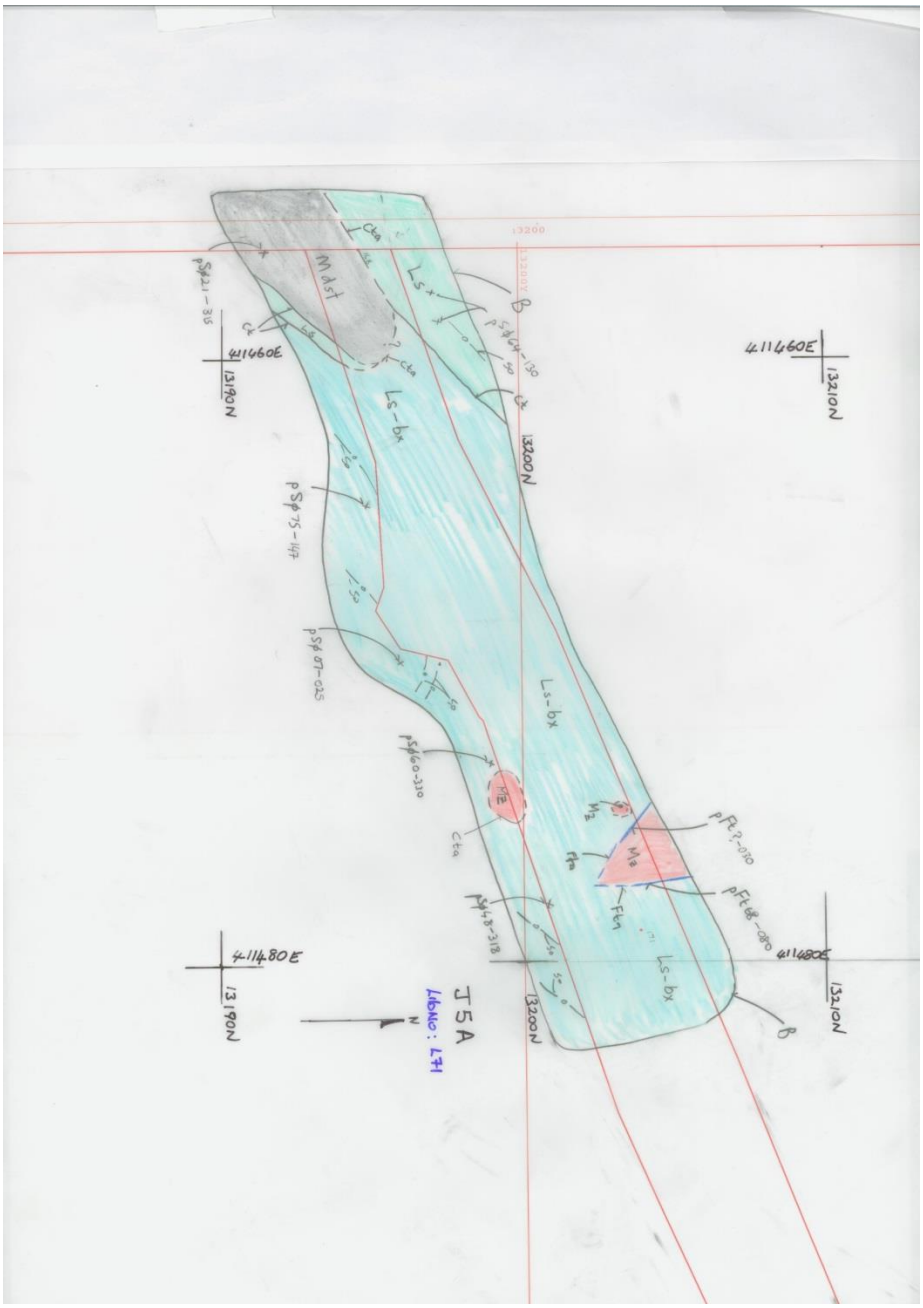

Figure A-42 Geologic map of J5A 380 m to 397 m elevation underground workings. Orange is Mystery pluton, light blue is limestone, lighter blue is limestone breccia, grey is mudstone. Red line is CAD outline of the level. pSø = layering, pJt = joint plane, pFa = fold axis, pFaa = fold axis-anticline, pFas = fold axis-syncline, pSl = slickenlines, pFtN = normal fault, pFt = fault plane, pVc = calcite vein, pCt = contact plane, Ct = contact, Ft = minor fault, Fr = minor fracture. Map image created by Mystery Creek Resources, Inc.

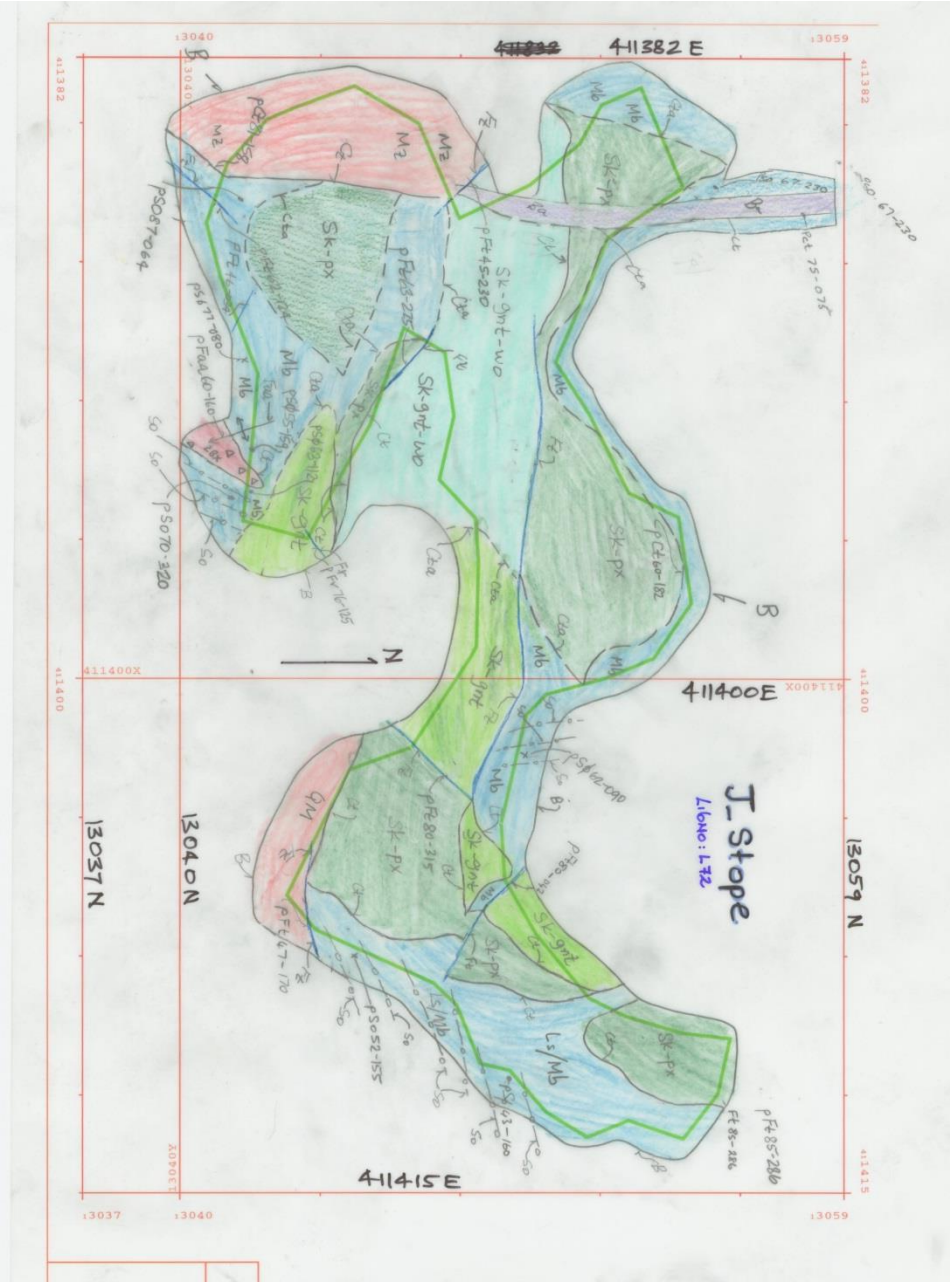

Figure A-43 Geologic map of J Stope underground workings. Light green is garnet pyroxene skarn, dark green is pyroxene skarn, orange is Mystery pluton, light blue is limestone/marble, lighter blue is garnet wollastonite skarn, dark blue is marble, purple is mafic dike, red is breccia. Red line is CAD outline of the level. pSø = layering, pJt = joint plane, pFa = fold axis, pFaa = fold axis-anticline, pFas = fold axis-syncline, pSl = slickenlines, pFtN = normal fault, pFt = fault plane, pVc = calcite vein, pCt = contact plane, Ct = contact, Ft = minor fault, Fr = minor fracture. Map image created by Mystery Creek Resources, Inc.

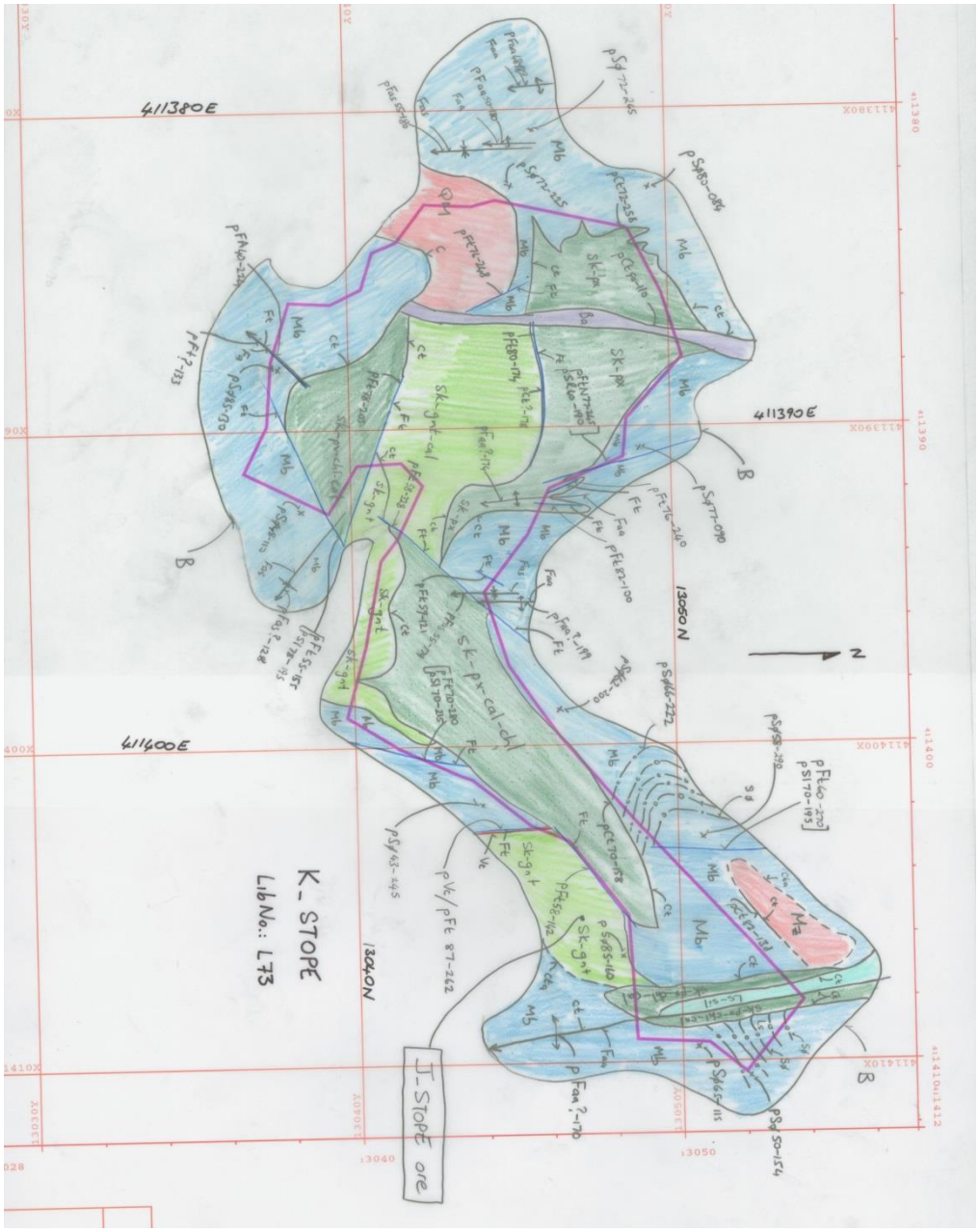

Figure A-44 Geologic map of K Stope underground workings. Light green is garnet skarn/calcite garnet skarn, dark green is pyroxene skarn/chlorite calcite pyroxene skarn, orange is Mystery pluton, light blue is limestone/siltstone, dark blue is marble, purple is mafic dike. Red line is CAD outline of the level. pSø = layering, pJt = joint plane, pFa = fold axis, pFaa = fold axis-anticline, pFas = fold axis-syncline, pSl = slickenlines, pFtN = normal fault, pFt = fault plane, pVc = calcite vein, pCt = contact plane, Ct = contact, Ft = minor fault, Fr = minor fracture. Map image created by Mystery Creek Resources, Inc.

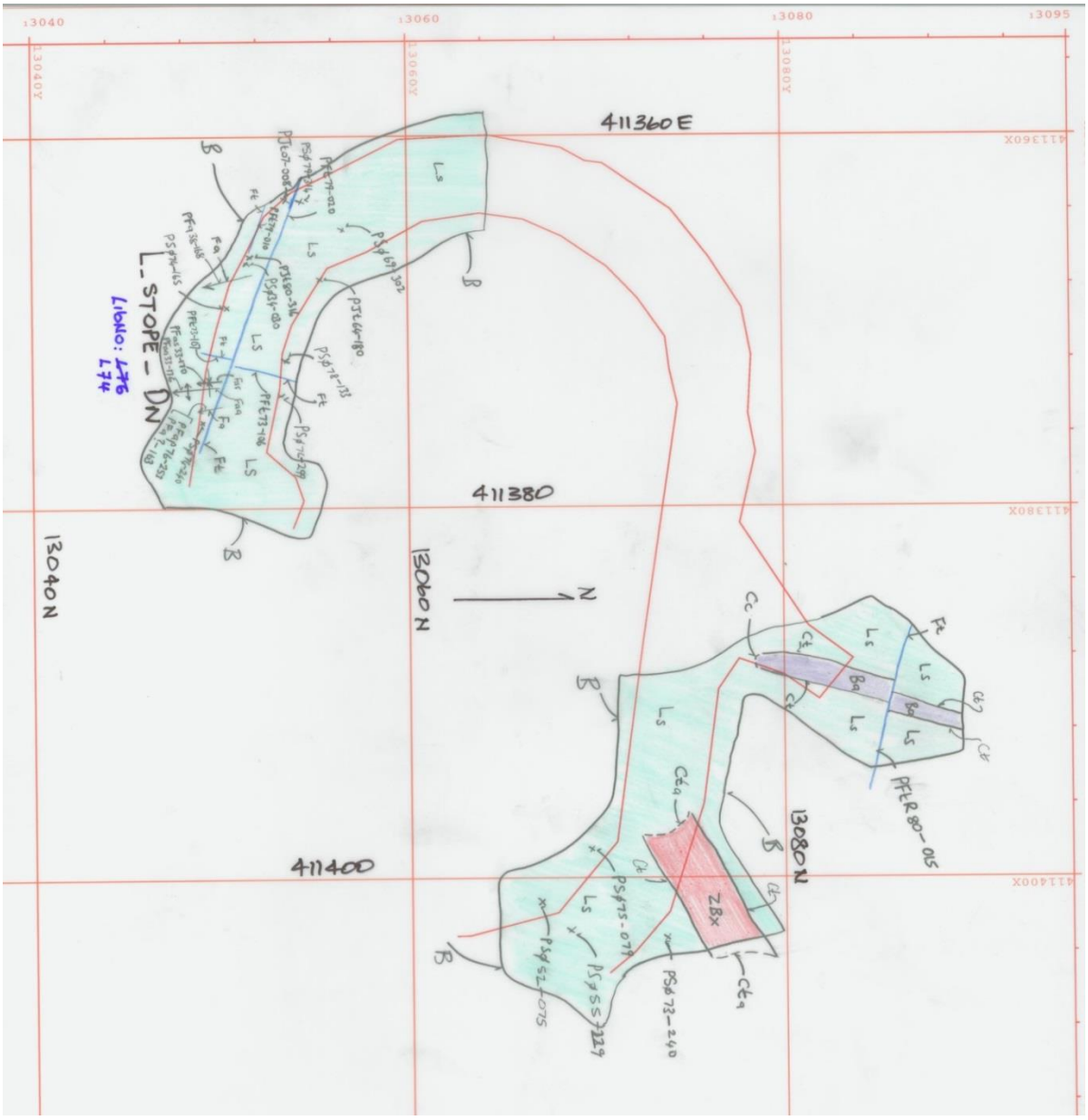

Figure A-45 Geologic map of L Stope 195 m to 207 m elevation underground workings. Light blue is limestone, purple is mafic dike, red is breccia. Red line is CAD outline of the level. pSø = layering, pJt = joint plane, pFa = fold axis, pFaa = fold axis-anticline, pFas = fold axis-syncline, pSl = slickenlines, pFtN = normal fault, pFt = fault plane, pVc = calcite vein, pCt = contact plane, Ct = contact, Ft = minor fault, Fr = minor fracture. Map image created by Mystery Creek Resources, Inc.

Figure A-46 Geologic map of L Stope 195 m to 207 m elevation underground workings. Light green is garnet skarn, dark green is pyroxene skarn, orange is Mystery pluton, light blue is limestone, purple is mafic dike. Red line is CAD outline of the level. pSø = layering, pJt = joint plane, pFa = fold axis, pFaa = fold axis-anticline, pFas = fold axis-syncline, pSl = slickenlines, pFtN = normal fault, pFt = fault plane, pVc = calcite vein, pCt = contact plane, Ct = contact, Ft = minor fault, Fr = minor fracture. Map image created by Mystery Creek Resources, Inc.

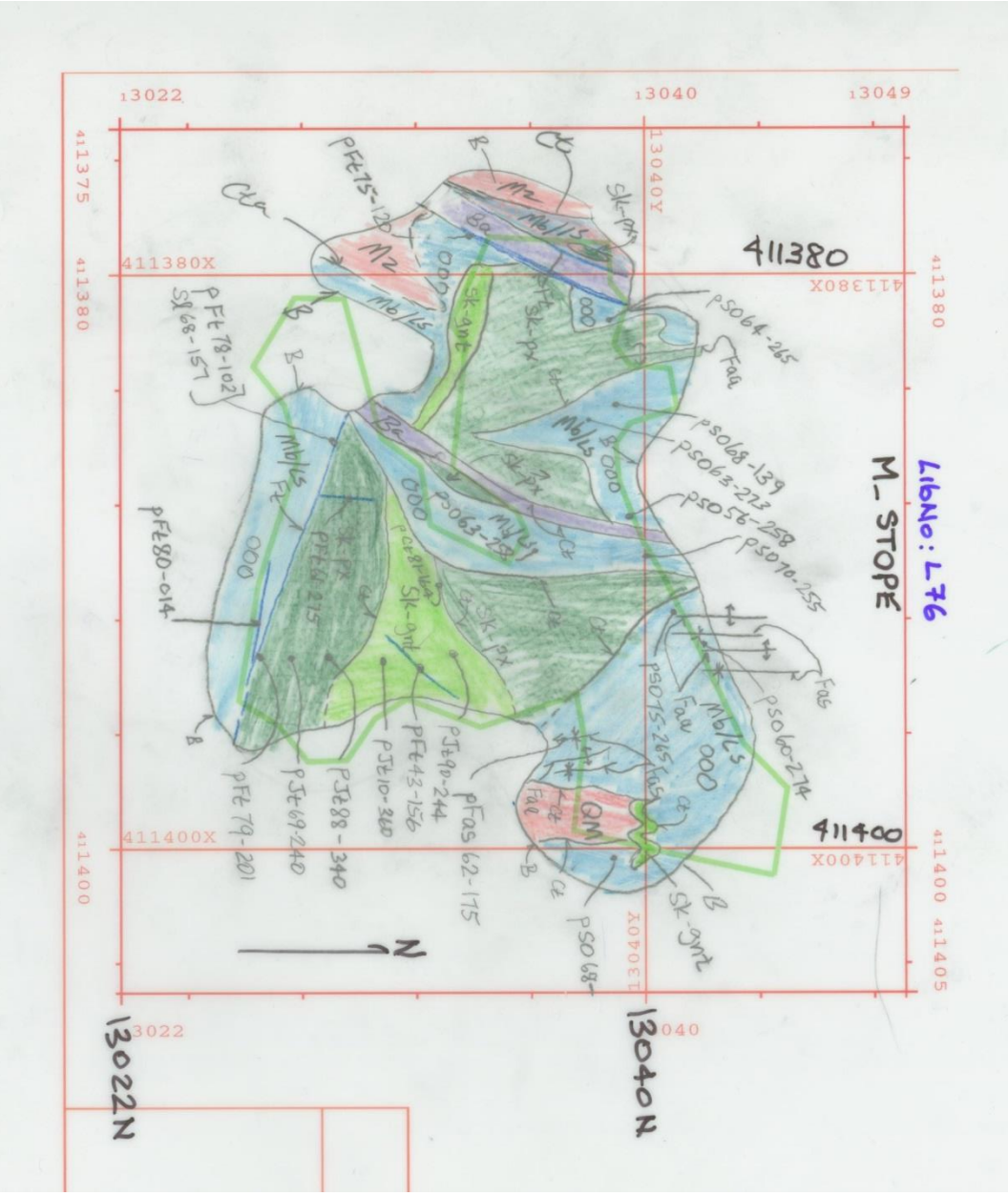

Figure A-47 Geologic map of M Stope 192 m to 200 m elevation underground workings. Light green is garnet skarn, dark green is pyroxene skarn, orange is Mystery pluton, light blue is marble/limestone, purple is mafic dike. Red line is CAD outline of the level. pSø = layering, pJt = joint plane, pFa = fold axis, pFaa = fold axis-anticline, pFas = fold axis-syncline, pSl = slickenlines, pFtN = normal fault, pFt = fault plane, pVc = calcite vein, pCt = contact plane, Ct = contact, Ft = minor fault, Fr = minor fracture. Map image created by Mystery Creek Resources, Inc.

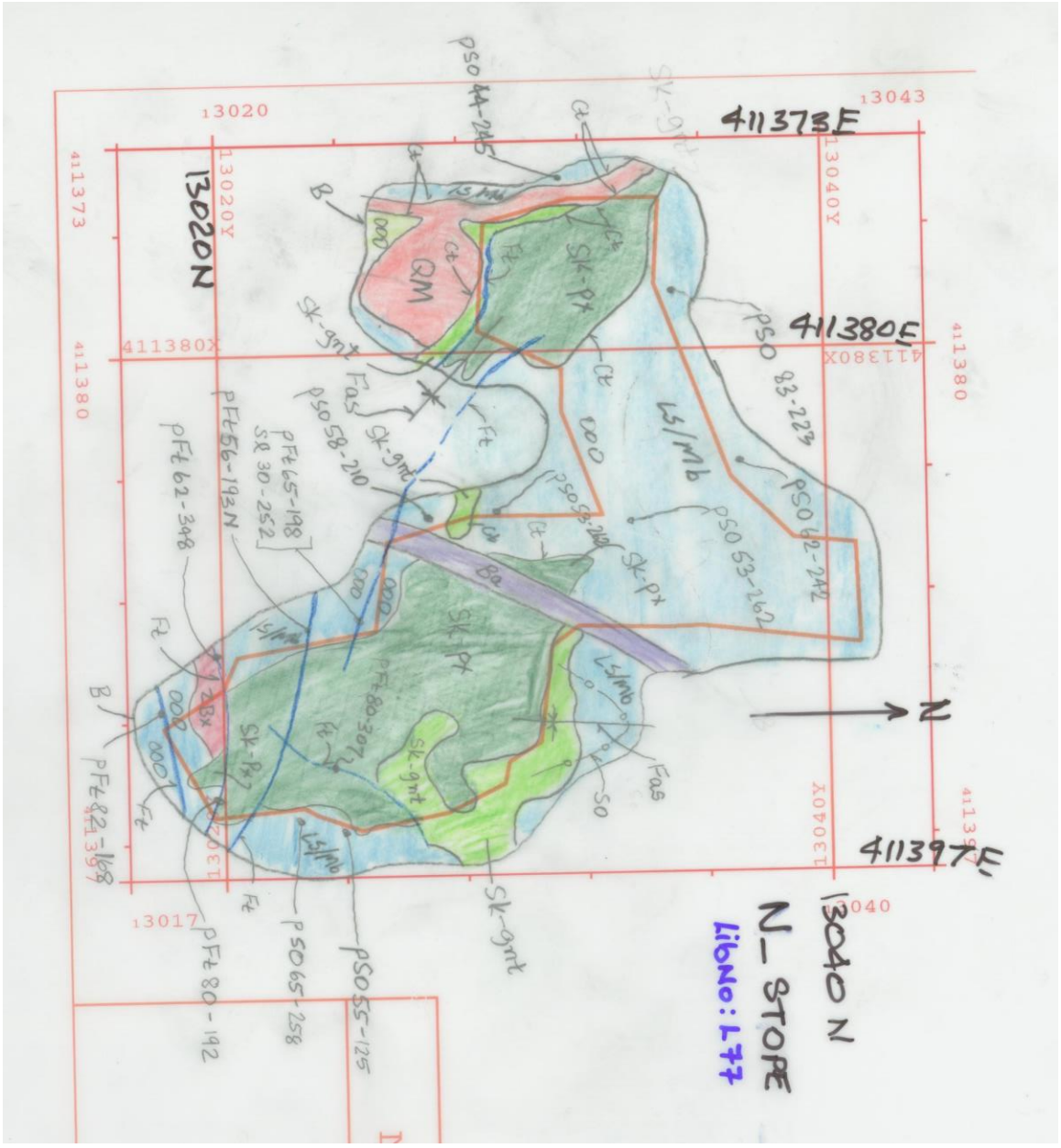

Figure A-48 Geologic map of N Stope 175 m to 182 m elevation underground workings. Light green is garnet skarn, dark green is pyroxene skarn, orange is Mystery pluton, light blue is marble/limestone, purple is mafic dike, red is breccia. Red line is CAD outline of the level. pSø = layering, pJt = joint plane, pFa = fold axis, pFaa = fold axis-anticline, pFas = fold axis-syncline, pSl = slickenlines, pFtN = normal fault, pFt = fault plane, pVc = calcite vein, pCt = contact plane, Ct = contact, Ft = minor fault, Fr = minor fracture. Map image created by Mystery Creek Resources, Inc.

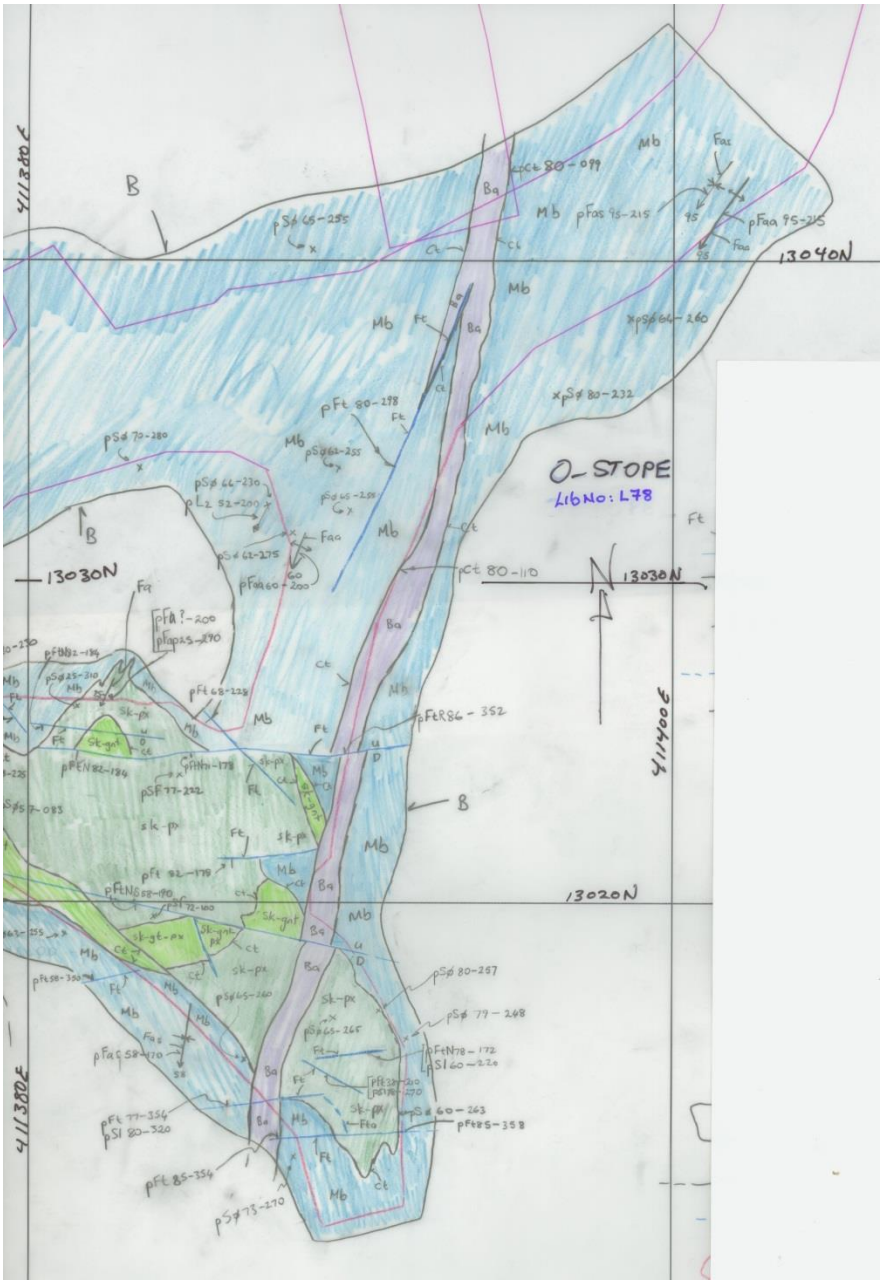

Figure A-49 Geologic map of O Stope 171 m to 180 m elevation underground workings. Light green is garnet pyroxene skarn/garnet skarn, dark green is pyroxene skarn, blue is marble, dark blue is marble, purple is mafic dike. Red line is CAD outline of the level. pSø = layering, pJt = joint plane, pFa = fold axis, pFaa = fold axis-anticline, pFas = fold axis-syncline, pSl = slickenlines, pFtN = normal fault, pFt = fault plane, pVc = calcite vein, pCt = contact plane, Ct = contact, Ft = minor fault, Fr = minor fracture. Map image created by Mystery Creek Resources, Inc.

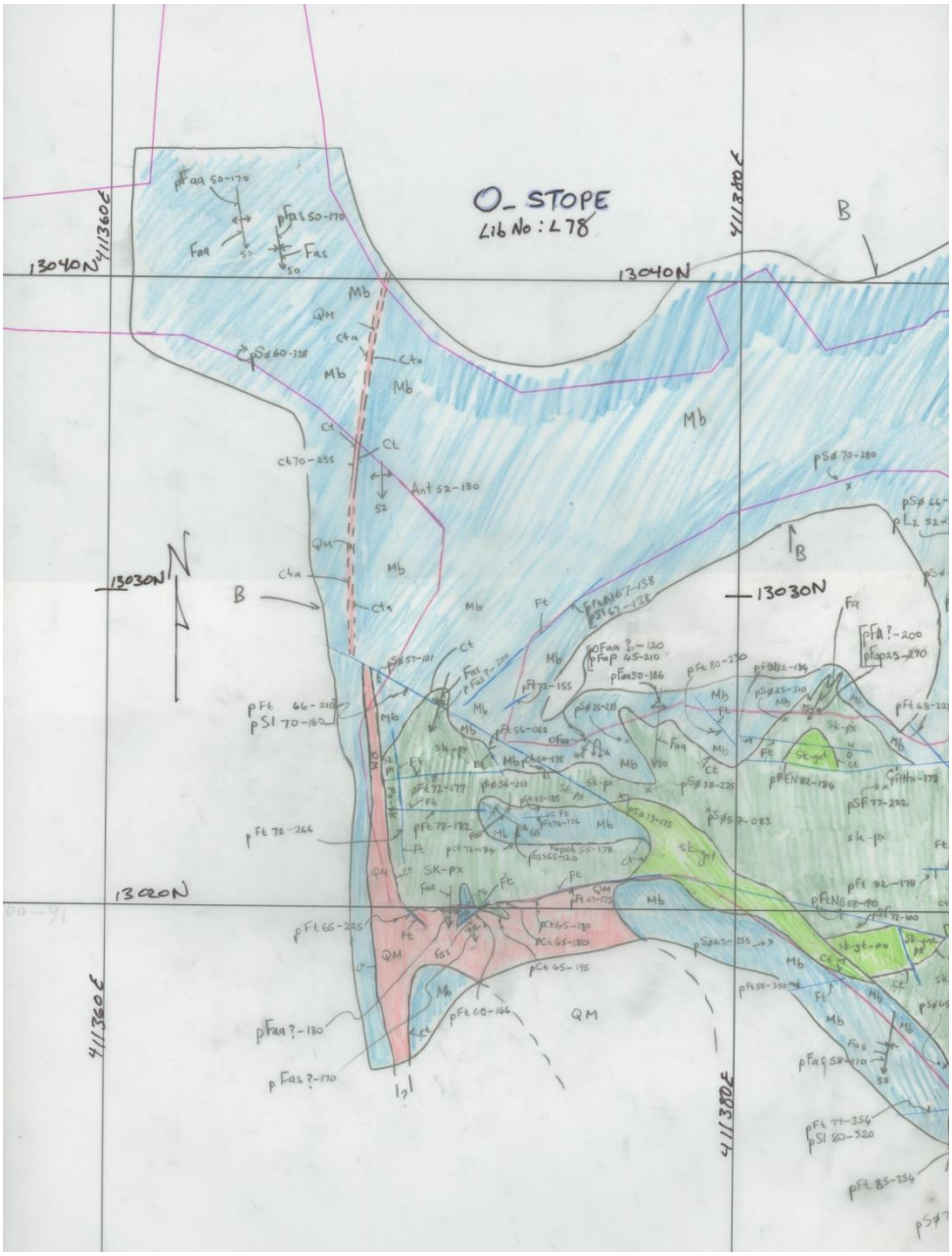

Figure A-50 Geologic map of O Stope 171 m to 180 m elevation underground workings. Light green is garnet pyroxene skarn/garnet skarn, dark green is pyroxene skarn, orange is Mystery pluton, blue is marble. Red line is CAD outline of the level. pSø = layering, pJt = joint plane, pFa = fold axis, pFaa = fold axis-anticline, pFas = fold axis-syncline, pSl = slickenlines, pFtN = normal fault, pFt = fault plane, pVc = calcite vein, pCt = contact plane, Ct = contact, Ft = minor fault, Fr = minor fracture. Map image created by Mystery Creek Resources, Inc.

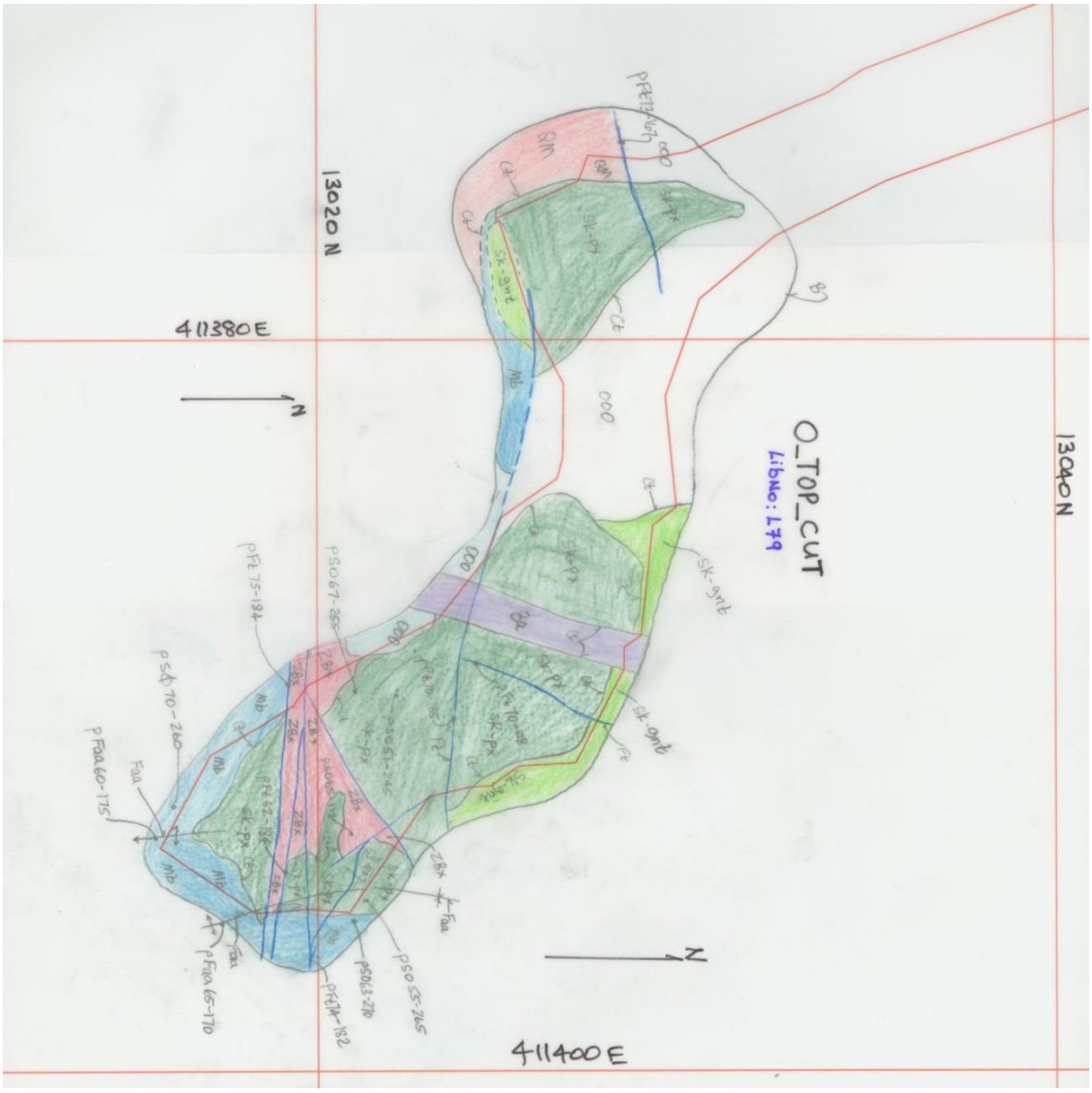

Figure A-51 Geologic map of O Top Cut 171 m to 177 m elevation underground workings. Light green is garnet skarn, dark green is pyroxene skarn, orange is Mystery pluton, light blue is limestone, dark blue is marble, purple is mafic dike, red is breccia. Red line is CAD outline of the level. pSø = layering, pJt = joint plane, pFa = fold axis, pFaa = fold axis-anticline, pFas = fold axis-syncline, pSl = slickenlines, pFtN = normal fault, pFt = fault plane, pVc = calcite vein, pCt = contact plane, Ct = contact, Ft = minor fault, Fr = minor fracture. Map image created by Mystery Creek Resources, Inc.

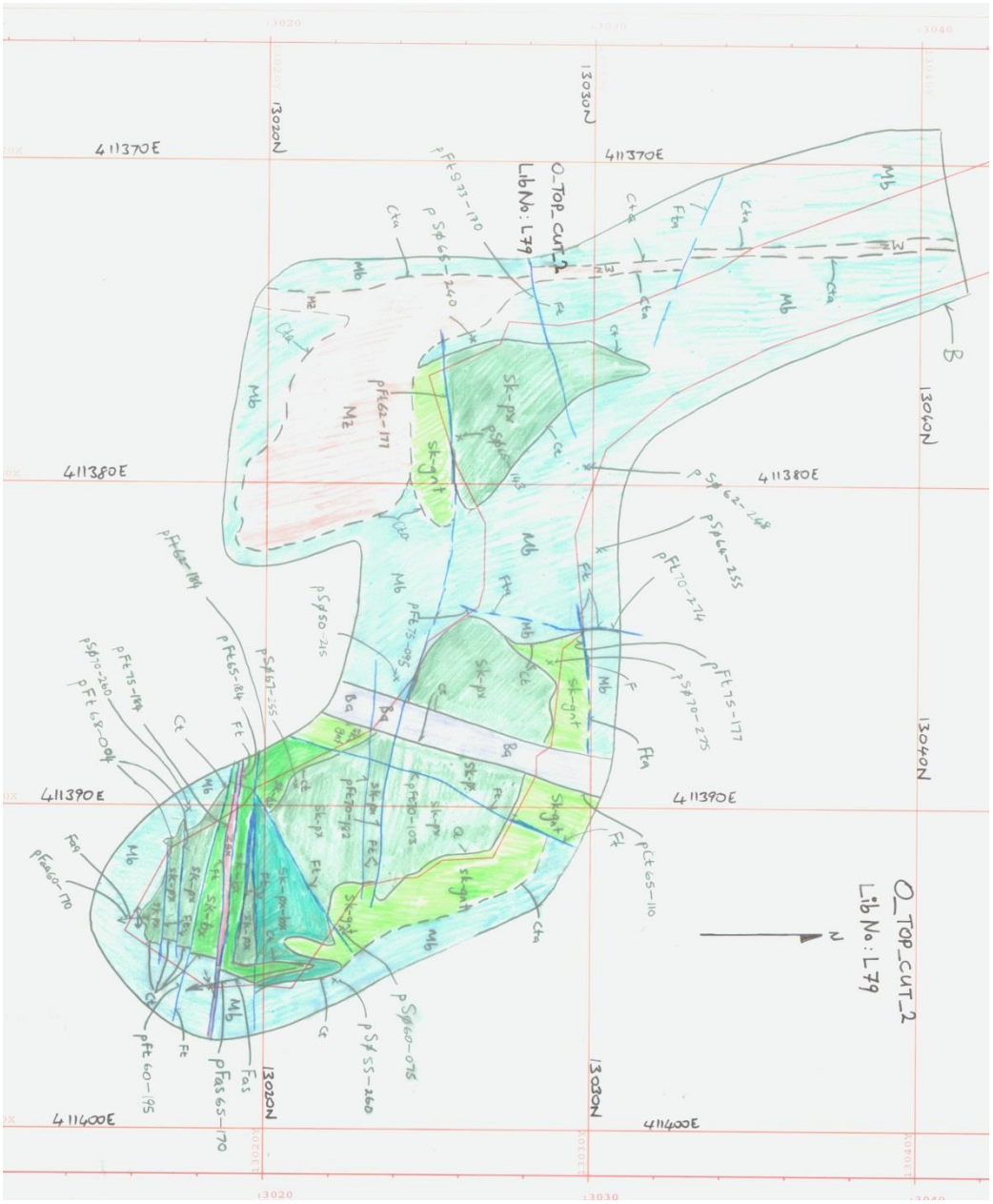

Figure A-52 Geologic map of O Top Cut 171 m to 177 m elevation underground workings. Yellow-green is garnet skarn, green is brecciated skarn, blue-green is brecciated pyroxene skarn, dark green is pyroxene skarn, blue is marble, purple is mafic dike. Red line is CAD outline of the level. pSø = layering, pJt = joint plane, pFa = fold axis, pFaa = fold axis-anticline, pFas = fold axis-syncline, pSl = slickenlines, pFtN = normal fault, pFt = fault plane, pVc = calcite vein, pCt = contact plane, Ct = contact, Ft = minor fault, Fr = minor fracture. Map image created by Mystery Creek Resources, Inc.

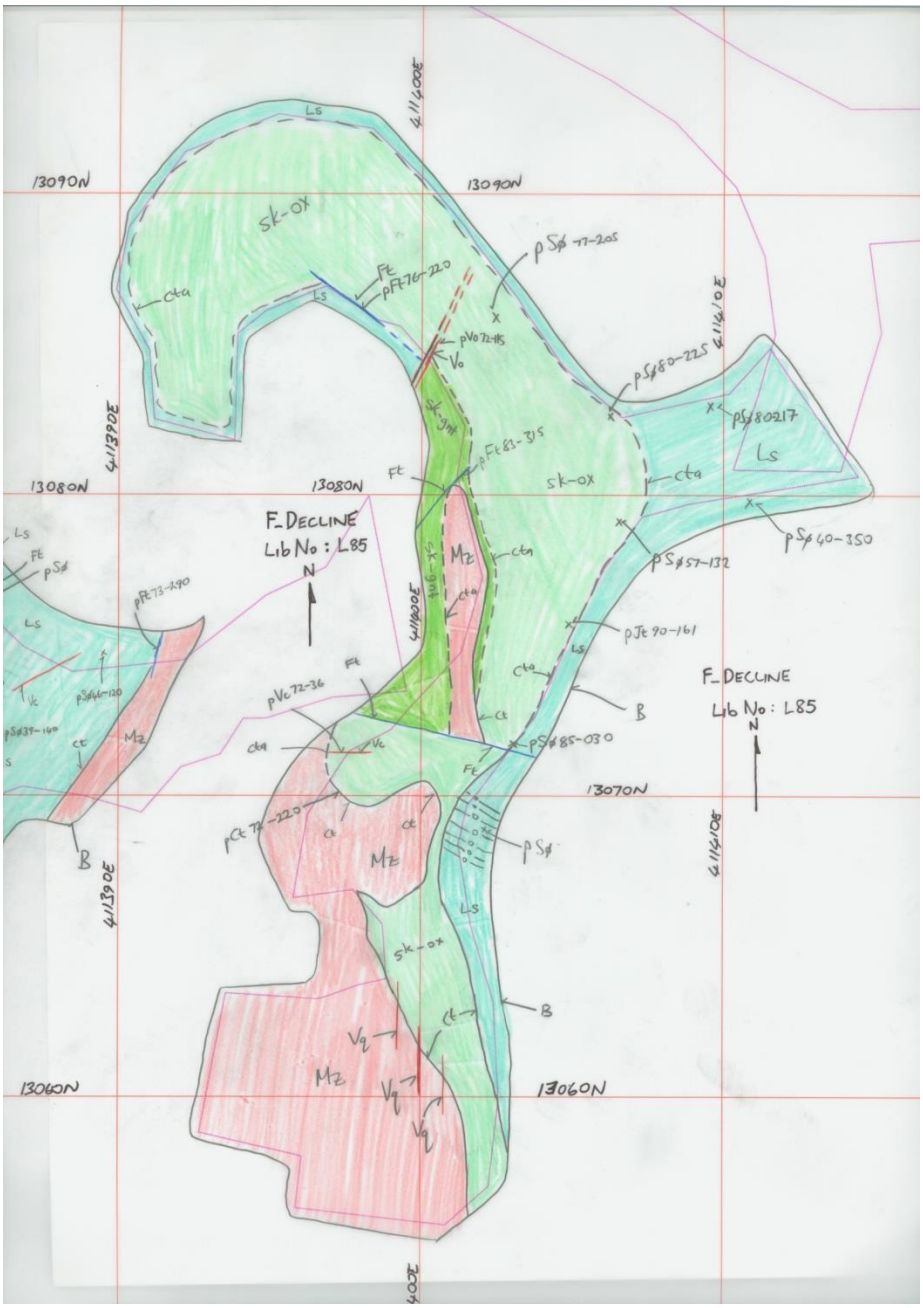

Figure A-53 Geologic map of F Decline/F Stope underground workings. Light green is garnet skarn, blue-green is oxidized skarn, orange is Mystery pluton, light blue is limestone. Red line is CAD outline of the level. pSø = layering, pJt = joint plane, pFa = fold axis, pFaa = fold axis-anticline, pFas = fold axis-syncline, pSl = slickenlines, pFtN = normal fault, pFt = fault plane, pVc = calcite vein, pCt = contact plane, Ct = contact, Ft = minor fault, Fr = minor fracture. Map image created by Mystery Creek Resources, Inc.

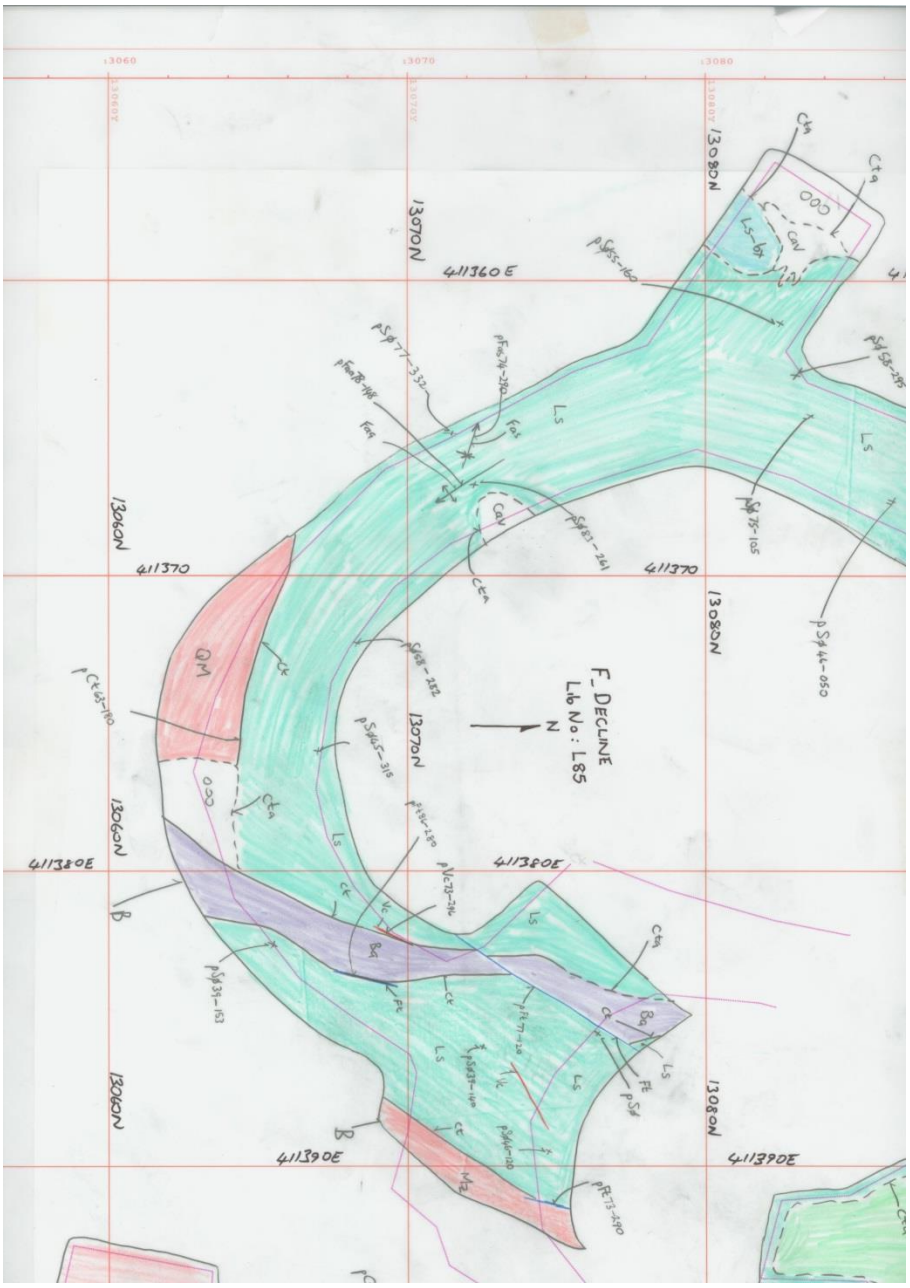

Figure A-54 Geologic map of F Decline/F Stope underground workings. Orange is Mystery pluton, light blue is limestone, lighter blue is limestone breccia, purple is mafic dike. Red line is CAD outline of the level. Cav = void, pSø = layering, pJt = joint plane, pFa = fold axis, pFaa = fold axis-anticline, pFas = fold axis-syncline, pSl = slickenlines, pFtN = normal fault, pFt = fault plane, pVc = calcite vein, pCt = contact plane, Ct = contact, Ft = minor fault, Fr = minor fracture. Map image created by Mystery Creek Resources, Inc.

Figure A-55 Geologic map of F Decline/F Stope underground workings. Light blue is limestone, lighter blue is limestone breccia, purple is mafic dike, red is fault gouge. Red line is CAD outline of the level. pSø = layering, pJt = joint plane, pFa = fold axis, pFaa = fold axis-anticline, pFas = fold axis-syncline, pSl = slickenlines, pFtN = normal fault, pFt = fault plane, pVc = calcite vein, pCt = contact plane, Ct = contact, Ft = minor fault, Fr = minor fracture. Map image created by Mystery Creek Resources, Inc.

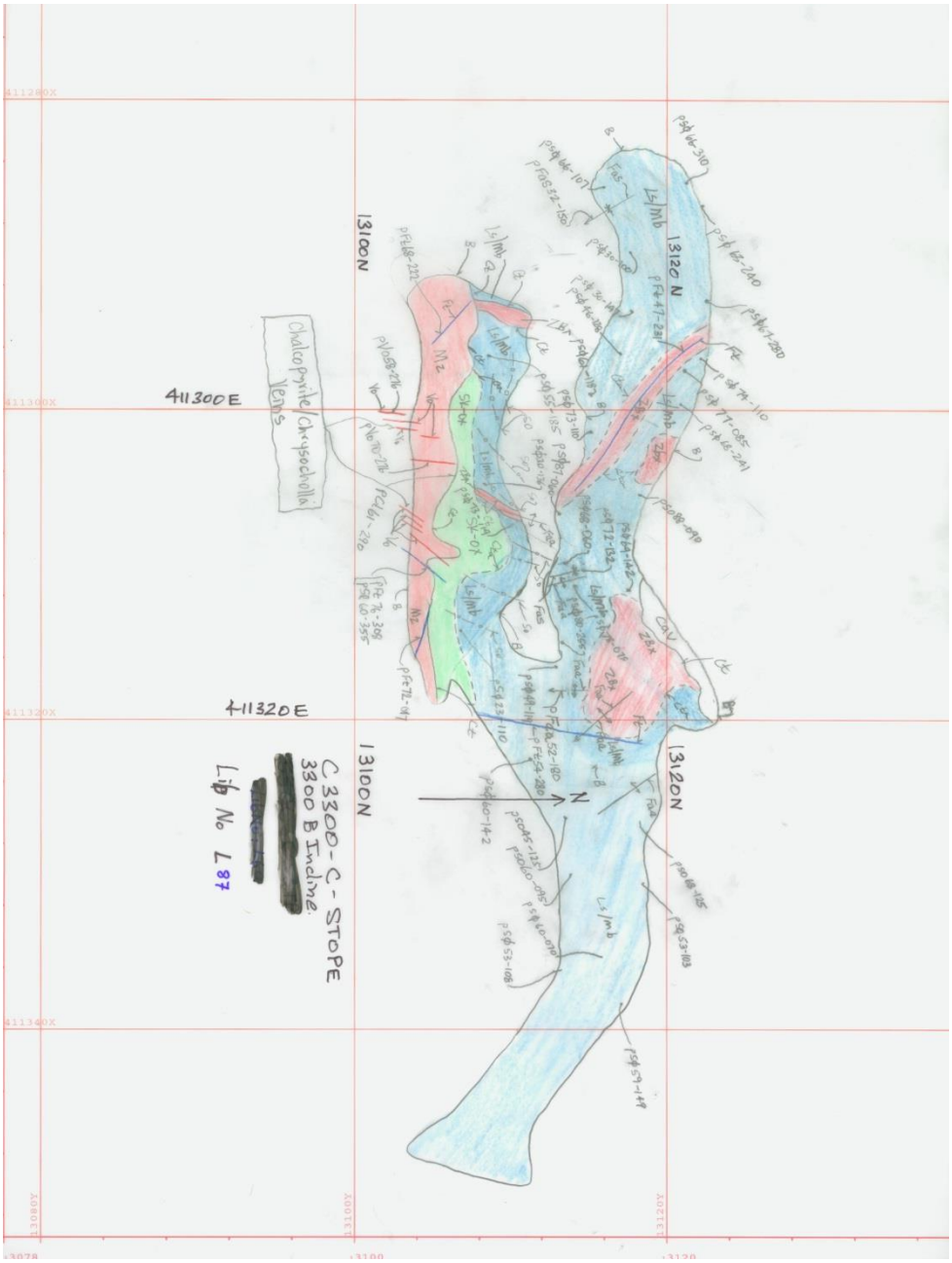

Figure A-56 Geologic map of 3300 C Stope/3300 B Incline 351 m to 365 m elevation underground workings. Light green is oxidized skarn, orange is Mystery pluton, light blue is limestone/marble, red is breccia. Red line is CAD outline of the level. pSø = layering, pJt = joint plane, pFa = fold axis, pFaa = fold axis-anticline, pFas = fold axis-syncline, pSl = slickenlines, pFtN = normal fault, pFt = fault plane, pVc = calcite vein, pCt = contact plane, Ct = contact, Ft = minor fault, Fr = minor fracture. Map image created by Mystery Creek Resources, Inc.